# ANALYSIS AND DESIGN OF BUILDING STRUCTURES WITH SUPPLEMENTAL LEAD DAMPERS UNDER EARTHQUAKE AND WIND LOADS

A thesis
submitted in partial fulfilment
of the requirements for the Degree
of
Doctor of Philosophy
in the
Department of Civil Engineering
University of Canterbury

by

Xi Lin

University of Canterbury
Christchurch, New Zealand
1999

# ABSTRACT

This research is carried out to investigate the dynamic behaviour of a 12-storey reinforced concrete framed structure with recently developed lead-shear dampers such as the Penguin Vibration Dampers under earthquake and wind loadings.

For regular framed structures under earthquake excitations, a satisfactory distribution of damper yield strengths in the storeys has been found using the criteria of minimising interstorey drift, base shear and cost of the dampers. The displacement, acceleration and the interstorey drift responses for the structure with supplemental dampers can be reduced significantly. Pushover analyses of the structure with supplemental dampers have been performed and the results have been compared with that of the structure without dampers. Equivalent SDOF system for the MDOF structure with dampers has been obtained through appropriate transformation by means of displacement shape of the structure at the target displacement. For such a distribution of the dampers, the structure with supplemental dampers will behave predominantly in its first mode. The equivalent SDOF system can be used to predict the response of the MDOF structure with dampers with good accuracy. A simplified nonlinear static method, taking into account the effect of the supplemental dampers, has been investigated to conduct the seismic analysis of the structure with dampers. While comparing with the nonlinear time history analysis method, it has been found that this simplified method can give a very good approximation to the response. By investigating the effects on the displacement and acceleration response associated with the supplemental dampers under earthquake excitations, optimal damping levels of the dampers have been found. Based on the simplified nonlinear static method and the optimal damping ratio of the dampers, a displacement-based design procedure has been established to determine the damper yield strengths in the storeys for preliminary seismic design.

Time-domain analyses of the structure with supplemental lead dampers have been performed using the artificial wind time history that was simulated by means of an equivalent wind spectrum technique. The effects of the dampers on the structural displacement response are not as significant as on the acceleration response for wind loading. For structures under the serviceability Limit State subject to wind loading, the acceleration response is the main concern. Considerable benefit can be gained by incorporating the dampers into the structures.

The simplified analytical method, a code-type frequency-domain method taking the effect of the dampers into account, has been established. A design procedure for determining the yield strength of the dampers in a structure subject to wind loading has been established.

## ACKNOWLEDGMENTS

This research was carried out in the Civil Engineering Department of the University of Canterbury.

I wish to express my sincere gratitude to Dr P.J. Moss and Dr A.J. Carr for their invaluable advice and encouragement as supervisors of the project. Their kindness, patience and cheerful hearts are greatly appreciated.

I also wish to thank Dr J.X.Q. Zhao in Institute of Geological & Nuclear Sciences Ltd and T. Kelly in Holmes Consulting Group for their providing test results of the prototype PVD, NZS4203 compatible earthquake time histories, useful information and their helpful comments.

Warm gratitude is given to my fellow postgraduates for their encouragement and constructive discussions.

The partly financial assistance provided by Penguin Engineering Ltd is gratefully acknowledged.

I wish to thank my family for their prayers, love, understanding and support.

Finally, I would like to give my deep thanks and praises to my God and my Lord – Jesus Christ. He is the very source of my strength, wisdom, ability, peace, endurance, ……, my everything. This is my story and my testimony: "for apart from Him I can do nothing" – John 15:5.

# TABLE OF CONTENTS

## 3. MODELLING OF THE INELASTIC STRUCTURE AND THE SUPPLEMENTAL LEAD DAMPERS



## 4. BRIEF INTRODUCTION TO ANALYTICAL METHODS



## 5. PLACEMENT AND DISTRIBUTION OF THE SUPPLEMENTAL DAMPERS IN THE STRUCTURE

## 6. PUSHOVER ANALYSIS OF THE STRUCTURE WITH THE SUPPLEMENTAL DAMPERS AND ITS EQUIVALENT SDOF SYSTEM



## 7. EQUIVALENT VISCOUS DAMPING RATIO

## 8. SIMPLIFIED NONLINEAR STATIC METHOD



## 9. DISPLACEMENT-BASED DESIGN PROCEDURE FOR THE STRUCTURE WITH SUPPLEMENTAL LEAD DAMPERS

# NOTATION

| | |
|---|---|
| A | = displacement amplitude |
| $a_g$ | = peak ground acceleration |
| $A_i$ | = tributary area perpendicular to wind loads for the ith floor level |
| $a_x$ | = peak acceleration |
| $a_{x,0}$ | = peak acceleration of the structure without dampers |
| $a_{x,d}$ | = peak acceleration of the structure with supplemental dampers |
| $b$ | = horizontal breadth of a vertical structure normal to the windstream |
| $B$ | = a background factor |
| $C$ | = damping coefficient of the SDOF system |
| $C$ | = a constant of proportionality |
| $[C]$ | = a damping matrix |
| $C^*$ | = generalised damping |
| $C_D$ | = drag coefficient |
| $C_h(T,1)$ | = basic seismic hazard acceleration coefficient for elastic structures |
| $C_l$ | = leeward drag coefficient |
| $C_m(z)$ | = added mass coefficient at height z |
| $Coh(r,n)$ | = square root of the coherence function |
| $c_r^*$ | = generalised damping for the rth mode |
| $C_v$ | = site-dependent factor |
| $C_w$ | = windward drag coefficient |
| $C_x$, $C_y$, $C_z$ | = exponential decay coefficients |
| $D(z,t)$ | = drag load force per unit length in a turbulent flow |
| $E$ | = spectrum of turbulence in the approaching wind stream |
| $E_d$ | = energy dissipation per cycle |
| $E_{di}$ | = energy dissipated per cycle by the dampers at the ith storey, |
| $E_d^i$ | = the energy dissipated by supplemental dampers per cycle for the *ith* vibration mode |
| $E_{di}^r$ | = energy dissipated by the dampers per cycle for the rth mode, |
| $E_s$ | = maximum elastic strain energy |
| $E_{s1}$ | = maximum elastic strain energy of the supplemental damping system |
| $E_{s2}$ | = maximum elastic strain energy of the undamped structure |
| $E_s^i$ | = strain energy of the structure with supplemental dampers for the *ith* vibration |

mode

$E_s^r$ = strain energy of the rth mode of the structure with dampers

$F(z,t)$ = drag force due to wind loads

$\{F\}$ = lateral force vector

$\{F_D(u)\}$ = supplemental damping force vector

$F$ = force

$F_d$ = damping force

$F_D'(z,t)$ = fluctuating drag due to wind loads at height z

$\overline{F}_D(z)$ = mean drag due to wind loads at height z

$F_i$ = the *ith* term of the lateral force vector $\{F\}$

$\overline{F}_i(z)$ = mean drag at the ith floor level due to wind loads

$F_i'(z,t)$ = fluctuating drag at the ith floor level due to wind loads

$F_R$ = the force factor

$F_y$ = effective first yield of the structure with dampers

$F_{y0}$ = yield base shear of the undamped MDOF structure

$F_{y0}^*$ = yield base shear of the equivalent SDOF for the undamped structure

$F_{yd}$ = yield strength of the damping system for the equivalent SDOF system

$F_{yd}^*$ = yield force of the SDOF spring representing supplemental damping system

$F_{yd1}$ = yield strength of the damper at the 1st floor level

$F_{ydi}$ = yield strength of the damper at the ith storey,

$g$ = acceleration due to gravity

$G$ = the gust factor

$g_f$ = a peak factor, the ratio of the expected peak value which occurs once per hour to the variance of the resonant part of the fluctuating response

$g_v$ = a peak factor for the upwind velocity fluctuation

$h$ = a constant for hysteretic damping

or = the height of the building structure, in metres

$H$ = height of the building structure

$H(n)$ = the mechanical admittance function

$h_1$ = $0.607h$ = the reference height

$H_i$ = height of level i relative to the ground,

$h_i$ = storey height at the ith level

$IDI_{max}$ = peak interstorey drift index

$K$ = von Karman coefficient (approximately 0.4)

or = stiffness of the structure

$K_0$ = initial elastic stiffness

$K_b$ = stiffness of a brace

$K_{bd}$ = stiffness of a brace-damper assembly in the elastic range

$K_d$ = initial stiffness of dampers

$K_{eff}$ = effective stiffness of the structure with supplemental dampers

$[K_{eff}]$ = effective secant stiffness matrix of the structure at the target displacement

$k_r^*$ = generalised stiffness for the rth mode

$K_s$ = initial elastic stiffness of the undamped structure (for the SDOF system)

$K_{s1}$ = initial storey stiffness of the undamped structure

$K_{sec,d}$ = secant stiffness of supplemental damping system

$K_{sec,s}$ = secant stiffness of the undamped structure

$K_x$, $K_z$ = nondimensional coefficients

$L^*$ = mass of the equivalent SDOF system

$L_h$ = a measure of the effective turbulence length scale, in metres

$L_u$ = limit state factor for the ultimate limit state (= 1)

$m$ = mass of the SDOF system

$\overline{m}$ = mass per unit height

$[M]$ = a diagonal mass matrix

$\overline{M}$ = mean overturning moment of the structure due to wind loads

$\hat{M}$ = expected peak overturning moment due to wind loads

$M_b$ = total building mass, kg

$m_i$ = mass at level i

$M_{ls}$ = limit state multiplier

$M_r$ = structure risk multiplier

$m_r^*$ = generalised mass for the rth mode

$M_s$ = shielding multiplier

$M_t$ = topographic multiplier

$\overline{M}_{(z,cat)}$ = site terrain/height multiplier

$N$ = an effective reduced frequency

or = number of frequency intervals

or = storey number

$n_1$ = first mode along-wind frequency of the building, in Hertz

$n_i$ = the ith mode frequency

$T$ = duration of wind time history

$p$ = load factor

$p(v)$ = probability density of v

$P$ = elastic force of the SDOF system for the undamped structure

$RPI$ = relative performance index

$P_y$ = yield force of the SDOF system for the undamped structure

$Q$ = base shear of the MDOF structure at the target displacement,

$Q_t$ = peak base shear of the MDOF structure

$r$ = constant which controls abruptness of loss of stiffness in the Ramberg-Osgood hysteresis loop model

or = a roughness factor, twice the longitudinal turbulence intensity

or = ratio of the post-yield stiffness to the initial stiffness of the undamped structure

or = distance between points 1 and 2

$r(t)$ = nonlinear restoring force of the SDOF system,

$\{r\}$ = displacement of the structure due to a unit ground displacement in the direction of earthquake excitations

$R$ = return period in years

or = risk factor for a structure

$\{R(t)\}$ = resistance vector,

$R^*$ = elastic base force of the equivalent SDOF system for the undamped structure

$r_a$ = ratio of the peak acceleration of the structure with dampers to that of the structure without dampers

$R_t^*$ = peak force of the equivalent SDOF system

$r_y$ = yield force of the equivalent SDOF system

$\{R_y(t)\}$ = yield resistance vector of the MDOF structure

$S$ = a size factor to account for the correlation of pressures over a structure

$S_a(T, \xi)$ = spectral acceleration

$S_a(T_{eff}, \xi_t)$ = spectral acceleration for the effective period $T_{eff}$ and the equivalent viscous damping ratio $\xi_t$

$S_d$ = target spectral displacement for the equivalent SDOF system

$S_d(T, \xi)$ = spectral displacement

$SEA$ = the area under the strain energy time-history for a friction damped structure

$SEA_{(0)}$ = the area under the strain energy time-history for the undamped structure

$S_F(n)$ = power spectrum of the fluctuating drag

$S_M(n)$ = power spectrum of the overturning moment

$S_p$ = structural performance factor (= 0.67)

$S_R$ = the stiffness factor

$S_v(n)$ = power spectral density function of the turbulence component

$S_v(z_1,n)$ = power spectral density function of the along-wind components of turbulence at height $z1$

$S^{cr}_{v_1v_2}(r,n)$ = the cross spectrum

$S^{*}_{veq}(n)$ = power spectral density function for the "reduced equivalent velocity fluctuation", is called the "reduced equivalent wind spectrum"

$T$ = period of structure

$T_0$ = initial period of the undamped structure

$T_b$ = natural period of the braced structure (no slippage occurring)

$T_{eff}$ = effective period of the structure with supplemental dampers

$T_g$ = the predominant ground motion period,

$u$ = relative displacement of the mass $m$ with respect to the ground

$\dot{u}$ = relative velocity of the mass $m$ with respect to the ground

$\ddot{u}$ = relative acceleration of the mass $m$ with respect to the ground

$\{u\}$ = displacement vector of the structure

$\ddot{u}_g(t)$ = ground acceleration due to a earthquake excitation

$u_i$ = lateral displacement of the structure at the ith floor level

$U_{max}$ = maximum strain energy for a friction damped structure

$U_{max(0)}$ = the maximum strain energy for the undamped structure

$\{u_r\}$ = the rth mode displacement vector of the structure

$v(z,t)$ = turbulence (fluctuating) component of wind speed at height z

$V(z,t)$ = wind speed at a height z

$\overline{V}(z)$ = mean wind speed at height z above ground,

$v_*$ = friction velocity

$V_0$ = the total optimum slip shear,

$v_1$, $v_2$ = indicate that the two records are taken at points 1 and 2

$v^{*}_{eq}(t)$ = a non-dimensional stochastic stationary Gaussian process, called the

"reduced equivalent velocity fluctuation"

$V_{eq}(z,t)$ = velocity field of an "equivalent wind structure"

$\overline{V}_G$ = mean gradient velocity

$\overline{V}_h$ = design hourly mean wind speed at height h

$w$ = a factor to account for the second order effects of the turbulence intensity

$W_i$ = seismic weight at level i,

$x(t)$ = displacement at the roof level

$\overline{x}$ = mean displacement due to wind loads

$x'(t)$ = fluctuating component of the displacement due to wind loads

$\widehat{x}$ = expected peak displacement due to wind loads

$x^*$ = displacement of the equivalent SDOF system at the target displacement

$x_r(t)$ = generalised displacement at the rth mode

$x_t^*$ = peak displacement of the equivalent SDOF system

$x_{t,r}$ = peak roof displacement of the structure at the rth mode,

$x_t$ = peak roof displacement of the MDOF structure

$x_y$ = yield roof displacement of the undamped MDOF structure

$x_y^*$ = yield displacement of the equivalent SDOF system

$Z$ = zone factor

$z_0$ = roughness length

$z_G$ = the gradient height

$\alpha$ = a constant related to the mass matrix in Rayleigh's damping model

$\alpha$ = power law exponent

$\beta$ = a constant related to the stiffness matrix in Rayleigh's damping model

$\chi^2(\frac{f\sqrt{A}}{\overline{V}})$ = aerodynamic admittance function

$\delta$ = displacement

$\delta_1$ = deformation of the damper at the 1st floor level

$\Delta_d$ = the displacement of the supplemental damping system at roof level,

$\Delta_{di}$ = damper deformation at the ith storey at the target displacement

$\Delta_i$ = deformation of the dampers at the ith floor level

$\Delta U$ = energy dissipated per cycle when the system is steadily excited by an imposed forcing function

$\Delta\xi_0$ = equivalent viscous damping due to the inelastic deformation of the structure

$\Delta^*_{y0}$ = yield roof displacement of the equivalent SDOF for the undamped structure

$\Delta_{y0}$ = yield roof displacement of the undamped MDOF structure

$\delta_{y1}$ = yield deformation of the damper at the 1st floor level

$\Delta_{yd,i}$ = yield deformation of the damper at the ith storey,

$\Delta_{yd}$ = yield deformation of the supplemental dampers

$\Delta^*_{yd}$ = yield displacement of the SDOF spring representing the supplemental damping system,

$\Delta_{yi}$ = yield deformation of the damper at the ith floor level

$\phi(z)$ = mode shape

$\{\phi\}$ = normalised deflected shape vector

$\phi_1$ = value of the normalised deflected shape vector at the 1st floor level

$\phi_i$ = the ith term of the normalised deflected shape $\{\phi\}$

$\phi_{i,r}$ = value of the rth normalised mode shape at the ith floor level

$\{\phi_r\}$ = the rth mode shape vector

$\eta$ = loss factor for hysteretic damping

or = ratio of the area enclosed in the hysteresis loop versus the area of the parallelogram $\left[4F_y\left(u_{\max}-u_y\right)\right]$

$\mu$ = ductility of structure

$\theta$ = angle of the diagonal brace relative to the horizontal

$\theta_i$ = random phase angles uniformly distributed between 0 and $2\pi$

$\nu_{eq}$ = equivalent damping coefficient ratio defined by Jacobsen

$\rho$ = air mass density

$\sigma_{BF}$ = variance (rms) of the background (non-resonant) component of the fluctuating force

$\sigma_{Bx}$ = variance (rms) of the background (non-resonant) component of the displacement

$\sigma_{DF}$ = variance (rms) of the resonant component of the fluctuating force

$\sigma_{DM}$ = variance of the resonant dynamic component of overturning moment

$\sigma_{Dx}$ = variance (rms) of the resonant component of the displacement

$\sigma_v$ = variance of the turbulence component of along-wind velocity

$\sigma_x$ = variance of the fluctuating component of the displacement

$\sigma_{\ddot{x}}$ = variance of roof acceleration

$\xi$ = fraction of critical damping

$\xi_0$ = initial viscous damping ratio of the structure

$\xi_d$ = equivalent viscous damping ratio due to supplemental dampers

$\xi_i$ = equivalent viscous damping ratio for the *ith* vibration mode

$\xi_{m1}$, $\xi_{m2}$ = two fractions of critical damping for the m1 mode and m2 mode

$\xi_t$ = total equivalent viscous damping ratio of the structure with supplemental dampers

$\{\psi\}$ = normalised lateral load vector

$\psi_i$ = the ith term of the normalised lateral load pattern vector

$\zeta$ = a constant for Coulomb damping (or frictional damping)

$\zeta_1$, $\zeta_2$ ,$\zeta_3$ ,$\zeta_4$ = four different definitions of damping capacity

$\omega^*$ = circular frequency for the equivalent SDOF system

$\omega_{m1}$, $\omega_{m2}$ = any two natural circular frequencies

$\omega_r$ = circular frequency of the rth mode

# CHAPTER 1

# INTRODUCTION

## 1.1 GENERAL

### 1.1.1 Conventional Seismic Design

The criteria for the seismic design of ductile structures set by many countries have been that buildings should be able to resist moderate earthquake without structural damage and be able to resist severe earthquake without collapse but perhaps with some structural and non-structural damage. To satisfy these design criteria, structures should be designed to have (Park, 1992):

- Adequate strength and stiffness to satisfy the serviceability limit states when responding to moderate earthquakes.
- Adequate strength, stiffness and ductility to satisfy the ultimate limit states when responding to severe earthquakes.

A basic principle in structural design against severe earthquakes is to allow the structure to absorb and dissipate energy through structural ductility. New Zealand codes (NZS4203, NZS3101) require that ductile structures be the subject of "capacity design". In the capacity design of structures, appropriate regions of the primary seismic-resisting structural systems are chosen and carefully designed and detailed for adequate strength and ductility for a severe earthquake. All other regions of the structural system, to prevent other possible failure modes, are then provided with sufficient strength to ensure that the chosen means for achieving ductility can be maintained throughout the post-elastic deformations (Park, 1992).

Sometimes, ductile structures may result in very large inelastic deformations so that they may not be used after the earthquake due to the considerations of cost and safety. For some structures, damage-control requirements may not allow them to undergo large post-elastic deformations. In recent years, more emphasis has been given to the development of cost-effective devices for dissipating seismically induced energy in the structure while keeping the structure's response as much as possible in the elastic range.

### 1.1.2 Structural Control

Structural control is to add energy dissipating devices to a structure or to isolate the structure from dynamic excitations (earthquake ground motion and wind load). There are two types of structural control systems: active control and passive control.

Active control is a type of structural protection in which the motion of a structure is controlled or modified by means of the action of a control system through some external energy supply.

The concept behind passive control is to add energy dissipating devices to a structure. The basic function of passive energy dissipation devices when incorporated into a structure is to absorb a portion of the input energy, thereby reducing energy dissipation demands on the primary structural members and minimising possible structural damage. Unlike active control systems, there is no need for an external supply of power.

There are two major passive control systems: base isolation and energy-absorbing devices (or supplemental damping devices). These are shown in Fig.1-1.

Base isolation is a seismic design strategy that reduces the level of ground motion which a structure undergoes during an earthquake by moving the period of the structure away from the predominant period of the ground motion and by increasing the equivalent damping level of the structure by hysteretic behaviour of the isolation devices. This can be achieved by introducing a flexible energy-absorbing connection, usually at the foundation level, between the structure and the ground (Skinner et al., 1993).

Many energy-absorbing devices have been proposed and studied for applications for seismic mitigation of buildings. Some of the major energy-absorbing devices in use include viscous dampers, hysteretic dampers, mass-effect dampers, etc (Fig.1-1).

## 1.2 OBJECTIVES AND SCOPE

The aims of this research project were to

- Model a recently-developed lead shear damper such as the Penguin Vibration Damper and perform time history analyses of structures with and without the dampers;

- Determine the satisfactory placement and distribution of the dampers in a structure under earthquake and wind loads;
- Determine appropriate design parameters of the dampers for the structure;
- Establish design procedures for structures with the dampers under earthquake and wind loads.

To achieve the above-mentioned objectives, the following tasks were undertaken:

- Review different types of supplemental dampers.
- Model a 12-storey reinforced concrete structure with supplemental lead dampers.
- Perform seismic time history analyses of the structure with the dampers for different placements, yield strength distributions and stiffness.
- Determine a satisfactory distribution of the dampers in the structure under earthquake excitations.
- Perform pushover analyses of the structures with the dampers, and compare the results with those of the original structure without dampers. Obtain the equivalent SDOF system for a MDOF structure with the dampers and verify such transformation.
- Estimate the effect of the dampers by means of the equivalent viscous damping and effective period of the structure with the dampers. The influence of inelastic deformations of the original structure will also be taken into account.
- Investigate the seismic simplified nonlinear static analysis method and extended its application to MDOF structures with the lead dampers.
- Establish a displacement-based design procedure for structures with the dampers for both existing and proposed structures under the design earthquake.
- Simulate artificial wind speed time history to carry out time history analyses of the structure with the dampers under wind gusts.
- Investigate placement and distribution of the dampers under wind loads.
- Investigate the simplified analysis of the structure with the dampers under wind loads.
- Establish a design procedure for the structure with the dampers under wind loads.

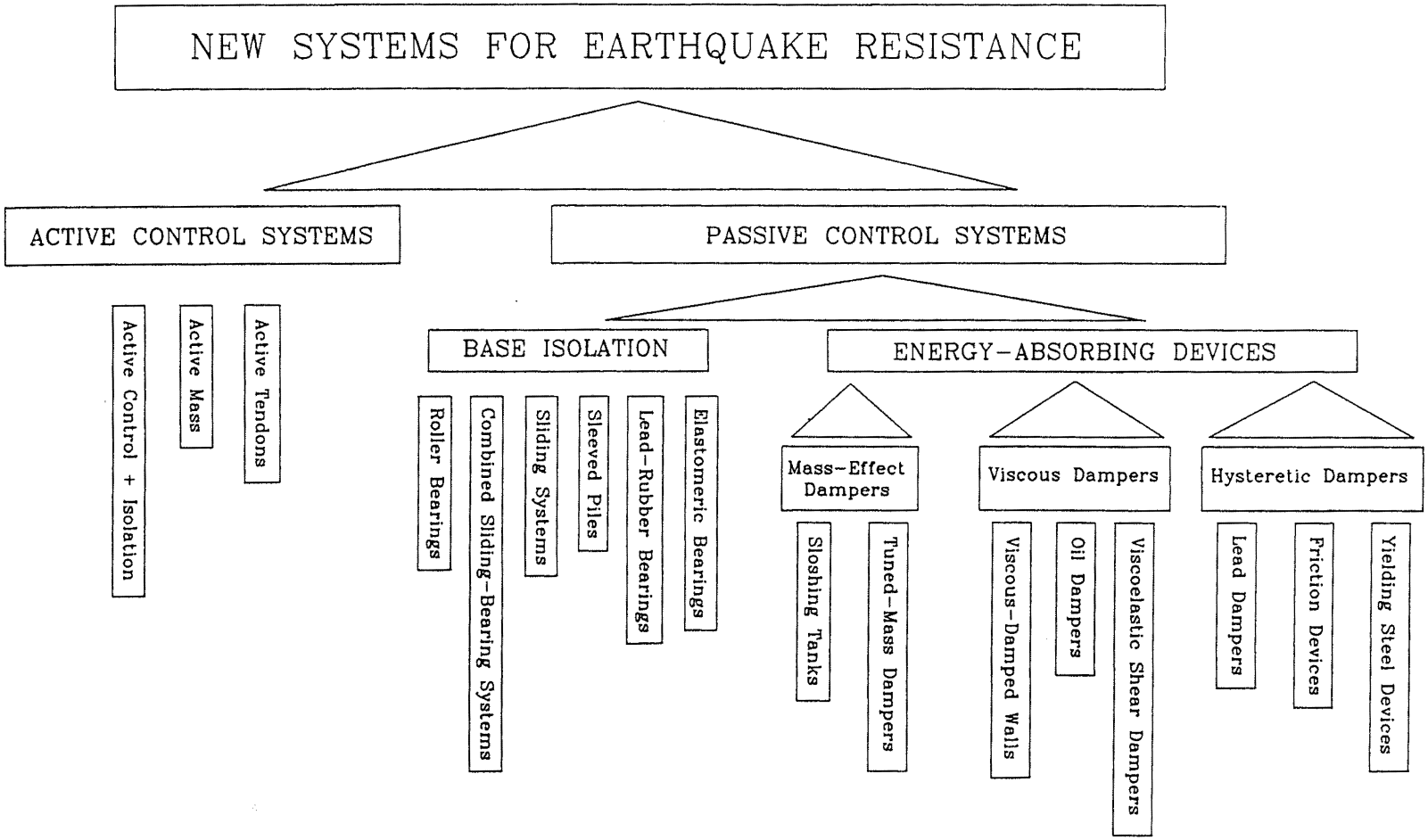


Figure 1-1. New systems for improved earthquake resistance of structures (from Aiken et al. 1990)

# CHAPTER 2

# REVIEW OF TYPES OF SUPPLEMENTAL DAMPERS

## 2.1 INTRODUCTION

Many energy-dissipating devices (supplemental dampers) have been proposed and studied for possible applications for seismic mitigation (or wind resistance) of buildings. They can be classified as either: velocity-dependent, displacement-dependent or other (ATC-33.03). Velocity-dependent devices include viscoelastic and viscous liquid devices. Displacement-dependent devices include friction devices and metallic devices. The third classification (other) includes all devices that cannot be classified as either velocity-dependent or displacement-dependent. Examples of other devices include shape-memory alloys, friction-spring assemblies with recentering capacity and tuned mass dampers.

## 2.2 VISCOELASTIC DEVICES

Viscoelastic dampers have been used in both seismic and wind applications. Mahmoodi (1969, 1986) and Keel et al. (1986) investigated the characteristics of viscoelastic dampers and their application to wind design. The characteristics and suitability of viscoelastic dampers to enhance performance of structures under earthquake excitations were studied by Lin et al. (1988), Aiken et al. (1990, 1992), Chang et al. (1991) and Lobo et al. (1993).

Viscoelastic (VE) dampers are normally made of viscoelastic layers bonded to steel plates that dissipate input energy under direct shear. Fig.2-1 shows a currently used VE damper that is comprised of two viscoelastic layers bonded to three parallel rigid surfaces.

The behaviour of viscoelastic dampers is controlled by the shear in the viscoelastic layers. The dynamic behaviour of viscoelastic materials is strongly dependent on temperature and frequency and is also affected by strain amplitude.

Viscoelastic damping materials have two components: the viscous part (energy absorbing part) and the elastic part (energy restoring part). The force in the damper can also be

expressed as having two components: the viscous force and elastic restoring force. Typical hysteresis loops of viscoelastic devices are shown in Fig.2-2

Some characteristics of viscoelastic dampers are:

(1). They have no threshold or activation force level, thus they dissipate energy for all levels of earthquake excitation and wind gust even while the structure remains elastic or at the early stages of cracking.

(2). They can be manufactured to add significant damping to building frames for improved structural response. The hysteretic characteristics of dampers are functions of shear strain level, excitation frequency, damping material type, thickness and temperature.

(3). They also make a substantial contribution to the initial stiffness of the structure. While the stiffening effect may lead to better control of lateral deformations, the same stiffening may lead to larger seismically induced forces for various ground motions.

## 2.3 VISCOUS LIQUID DEVICES

Viscous liquid devices are those dampers that depend upon the flow of fluid to achieve energy dissipation. The fluid shows viscous characteristics. These devices include viscous damping walls and fluid viscous dampers (orifice fluid dampers).

### 2.3.1 Viscous Walls

Viscous damping walls consist of a plate moving in a highly viscous fluid which is contained in a thin steel case (the wall) filled with the highly viscous fluid (Reinhorn et al., 1995b). See Fig.2-3.

The basic mechanism of a viscous wall is that it utilises an upper plate moving through a highly viscous fluid between the lower walls (viscous fluid container) and is based on Newton's Law of Viscosity. The viscous resisting force $Q_w$ and energy absorbing capacity $E_w$ can be easily adjusted to a required value by changing three factors, i.e. the viscosity of the fluid, the gap distance and the area of the wall plates. The viscosity of the fluid is dependent on temperature. This kind of damper also has a strong frequency dependency. The force in a

viscous wall is a result of the viscous resistance of the viscous fluid against movement of the upper steel plate.

### 2.3.2 Fluid Viscous Dampers

The fluid viscous damper consists of a cylinder and stainless steel piston with a bronze orifice head and an accumulator (Constantinou et al., 1992, Reinhorn et al., 1995a). The cylinder is filled with silicone oil having stable properties over a wide range of operation temperatures. The orifice flow may be compensated in a variety ways so that the mechanical characteristics of the devices are nearly unaffected by temperature. The orifice configuration and mechanical construction can be adjusted to produce various flow characteristics and complex resisting forces. The dampers show strong frequency dependence. The damper construction detail is shown in Fig.2-4.

The common characteristic of the two dampers discussed above is that the "viscous" behaviour of dampers provides the main contribution of forces that reduce the structural response. Both viscous walls and fluid viscous dampers have a strong frequency dependency.

The major distinction between these two dampers is:

The fluid viscous dampers show minor stiffening characteristics within the frequency range of interest while introducing a large amount of damping into the structure. The viscous walls show significant stiffening characteristics within the frequency range of interest while introducing a large amount of damping into the structure.

## 2.4 HYSTERETIC DEVICES

Hysteretic devices are devices that can dissipate energy through inelastic deformations of their components or friction within their parts or surfaces.

The main goals in the structural layout of a hysteretic device system are (Dorka et al., 1994):

(1) To limit the forces in the structure physically below damage levels by using the hysteretic devices as " structural fuses ".

(2) To concentrate the structural deformations in the hysteretic devices to dissipate most of the input energy.

Goal (1), in particular, distinguishes hysteretic device systems from systems that use dissipaters only to enhance damping: A hysteretic device system has a shear force envelope chosen by the designer.

There are several different dissipative mechanisms having been utilised in hysteretic devices: Friction, metal yielding and re-crystallisation (lead).

### 2.4.1 Friction Devices

There are a variety of friction devices that have been proposed for structural energy dissipation. Friction systems usually generate rectangular hysteresis loops which are characteristic of Coulomb friction. Typically these devices have very good performance characteristics, and their behaviour is not significantly affected by load amplitude, frequency or the number of applied load cycles.

Friction devices have been developed and manufactured for many years by Sumitomo Metal Ltd, Japan (Fig.2-5). A similar type of friction dampers has been manufactured by Tekton company, Arizona (Fig.2-6) (Li et al., 1995). Pall et al. (1982, 1987) proposed a friction device located at the intersection of cross bracing (Fig.2-7). Filiatrault et al. (1987) and Aiken et al. (1990) confirmed that these friction devices could enhance the seismic performance of structures.

Some characteristics of friction dampers are:

(1) The dissipated energy increases proportionally with increases in the exciting displacement. Further, the damping ratio also increases within a certain range of excitation level.

(2) The dampers show stiffening characteristics at their initial stages and show only strengthening afterwards. Stiffening and strengthening effects are almost unaffected by frequency.

(3) The period of the structure varies with the intensity of the earthquake that will shift the structural frequency away from the resonant frequency.

(4) The hysteretic behaviour of dampers provides the main contribution to the reduction of the structural response.

### 2.4.2 Metallic Devices

Metallic devices are a type of energy dissipation system that takes advantage of the hysteretic behaviour of mild steel or lead when deformed in their post-elastic range. A wide variety of different types of device utilise flexural, shear or extension deformation modes into the inelastic range (Fig.2-8). The idea of utilising separate metallic devices within a structure to absorb a large portion of seismic energy started with the work by Kelly et al. (1972) and Skinner et al. (1975). A particularly desirable feature of these systems is their stable behaviour, long term reliability and generally good resistance to environmental and temperature factors.

The resisting force of metallic energy absorbers depends on the nonlinear stress-strain characteristics and geometrical configuration of the material.

The two most commonly used materials are mild steel and lead.

#### 2.4.2.1 Yielding Steel Devices

A wide variety of devices that utilise the ability of mild steel to sustain many cycles of stable yielding behaviour have been proposed. An energy absorbing device in the form of round mild steel rod with a rectangular shape, introduced at the intersection of cross bracing, has been developed in New Zealand (Tyler, 1978, 1985, see Fig.2-9). Many of these devices making use of mild steel plates with different shapes have been proposed. For rectangular plates, the plastic deformation is limited to occurring at a finite region at the ends. For triangular or X shapes, the yielding occurs almost simultaneously throughout the entire height of the device, hence concentration of yielding and premature failure can be avoided. This characteristic is explained in Fig.2-10.

One such device that uses X-shaped steel plates is the so-called Added Damping And Stiffness (ADAS) devices (Whittaker et al., 1989, Scholl, 1990). Another device that uses triangular plates is called the Tapered-Plate Energy Absorber (TPEA, Pong et al., 1994) or T-ADAS (Tsai et al., 1993). These devices are shown in Fig.2-11 and 2-12.

Some characteristics concerning ADAS (or T-ADAS) devices are:

(1) ADAS devices installed in building frames are able to increase the stiffness, strength and energy dissipation capacity of structures. It is often desired that the ADAS devices will remain elastic under wind gusts and yield under major earthquakes.

(2) The ADAS device has excellent ductility without fatigue problems and exhibits stable behaviour without any sign of pinching or degradation.

(3) Yield forces and yield displacements of ADAS elements can be readily varied throughout the height of a structure to improve the distribution of ductility.

(4) The behaviour is not significantly affected by frequency and the number of applied load cycles.

#### 2.4.2.2 Lead Extrusion Dampers (LEDs)

The Lead-Extrusion Dampers are energy absorbing devices that convert mechanical energy to heat through the cyclic deformation of lead (Robinson, 1976, Cousins et al., 1993). Robinson (1976) found that the process of extrusion whereby a metal is forced through an orifice would be a very efficient method in that the metal is grossly deformed and the energy absorber should behave as a "plastic solid". Since lead recrystallises at room temperature thereby recovering most of its mechanical properties almost immediately after plastic deformation, lead was chosen as the metal to be extruded.

LEDs have a number of particularly desirable features: their load-deformation relationship is stable and repeatable, being largely unaffected by the number of loading cycles; they are insensitive to environmental factors; and tests have demonstrated insignificant aging effects.

There are two basic versions of the lead extrusive damper (Cousins et al., 1993). In one version, called the "constricted tube" damper, a billet of lead is forced to extrude back and forth through an orifice that is formed by an annular constriction in the surrounding tube. In the other version, the "bulged shaft" damper, the orifice is created by a bulge on a central shaft that moves back and forth through the lead billet. These two versions of the lead extrusion damper are shown in Fig.2-13. Typical load-displacement hysteresis loops for lead extrusion dampers are shown in Fig.2-14.

Some characteristics of a Lead Extrusion damper (Robinson et al., 1976) are:

(1) It is almost a pure "Coulomb damper" in that its force-displacement hysteresis loop is nearly rectangular and is practically rate-independent at earthquake-like frequencies.

(2) Because the interrelated processes of recovery, recrystallization and grain growth occur during and after the extrusion of the lead, the energy absorber is not affected by work hardening or fatigue, but instead the lead is forever returning to its original undeformed state. The extrusion damper therefore has a very long life and does not have to be replaced after an earthquake.

(3) The extrusion damper is stable in its operation and can not destroy itself by building up excessive forces.

(4) The length of stroke of the LED is limited only by the problem of buckling of the shaft during compression.

## 2.5 OTHER DEVICES

### 2.5.1 Energy Dissipating Restraint (EDR)

The Energy Dissipating Restraint is a mechanical device based on a friction mechanism in which the contact force between the friction surfaces of the device increases linearly with the deformation of the device. Fig.2-15 shows an external view and a cross section of the EDR. The device consists of a steel cylinder, a steel shaft, bronze friction wedges, steel compression wedges, a steel spring and internal stops. The deformation of the device is

defined as the relative motion of the shaft with respect to the cylinder. The resistance of the device is provided by frictional forces that develop between the bronze frictional wedges and the internal cylinder wall (Inaudi et al., 1993).

The EDR can have different configurations to provide several hysteretic behaviours. Different mechanical behaviour can be obtained by changing the pre-load of the spring and the lengths of the tension and compression gaps. Two configurations of the EDR have been studied by Inaudi et al (1993). One yields triangular hysteresis loops and the other gives flag-shaped hysteresis loops under cyclic deformation (Fig.2-16).

The overall effect of the EDR is to substantially reduce the structure deformations and interstorey drifts. Part of the change in structural response is due to the change in the stiffness of the structure when the EDRs are added and part is due to the additional damping the EDRs add to the structure. One advantage of the EDR is that it can be effective at low seismic levels or for wind loading while also being effective at high seismic levels. This is because the slip forces, and thus the energy dissipated, are proportional to the displacement of the EDR. Another advantage is that the self-centring behaviour would tend to reduce permanent offsets if the structure were deformed inelastically (Aiken et al., 1992).

### 2.5.2 Ring Spring Devices

Ring springs are frictional devices consisting of inner and outer ring elements assembled to form a spring stack. A prototype ring spring cartridge that allows bi-directional dynamic inputs to be applied to ring springs was designed and manufactured in the Department of Mechanical Engineering, University of Canterbury, New Zealand (Hill, 1995).

The ring spring cartridge primarily comprises of an outer housing and an inner shaft. The outer housing enable attachment as its end and the inner shaft locates and provides guidance for the ring spring. Pistons are used at each end of the spring to accommodate bi-directional displacements. Each piston is lined with 3mm thick rubber to cushion contacting as the cartridge undergoes displacements (Fig.17)

The ring spring cartridge can have two different pre-displacements: zero pre-displacement and the initial pre-displaced. This difference leads to two different hysteresis characteristics (see Figs.18 and 19)

An innovative pivotal rocking seismic isolation systems (PRSIS) for protecting columnar structures during earthquake has been built and tested (Hill, 1995). Configuration of the PRSIS is shown in Fig.20. Test results show that the PRSIS is effective in reducing structural loads and is able to provide significantly improved protection for structures that have fundamental periods in the range of dominant earthquake spectral acceleration.

### 2.5.3 Tuned Mass Dampers

The objective of incorporating a tuned mass damper into a structure is basically the same as those associated with other energy dissipation devices, namely, to reduce energy dissipation demand on the primary structural members under the action of external forces. This reduction, in this case, is accomplished by transferring some of the structural vibrational energy to the tuned mass damper (TMD) which, in its simplest form, consists of an auxiliary mass-spring-dashpot system anchored or attached to the main structure.

Sladek et al. (1980), motivated by published literature that reported the use of TMDs could reduce wind induced accelerations of high rise buildings by as much as 40%, investigated the possible use of vibration absorbers in reducing the seismic response of tall buildings. In their study, they considered three vibration absorbers: a tuned mass damper (TMD), a variable tuned mass damper (VTMD) and an anticipatory vibration absorber (AVA). It was found that the TMD, VTMD and AVA were ineffective in reducing the maximum seismic response of tall buildings.

Almost all TMD applications have been made towards mitigation of wind-induced motion. Seismic effectiveness of TMDs remains to be an important issue. It can be generally stated that, under earthquake-type loading, TMDs are not as effective as for wind-type loading due to the following reasons (Soong, T.T. et al., 1997):

(a) The frequency bandwidth of an earthquake excitation is not only wider than that of wind load but also richer in high frequency content so that high modes of a building structure are usually excited and the first mode representation of the structure is not adequate. Conventional TMD, tuned to the fundamental frequency of the structure, could suppress little or even amplify the dynamic response of higher modes and therefore may fail to reduce the total response under these conditions;

(b) As pointed out by a few investigators, the first peak in the response history cannot be easily reduced due to the fact that TMD passively responds to the structural movement and then reversely mitigates the response of the structure by vibrating out-of-phase with the structural movement.

There are some other energy-dissipating devices. Some of these are shape memory alloy (Witting et al., 1992), tuned liquid dampers etc. Details can be found in the textbook written by Soong et al. (1997).

## 2.6 DESCRIPTION OF A NEW LEAD-SHEAR DAMPER: PENGUIN VIBRATION DAMPER (PVD)

A new compact lead-shear damper, the PENGUIN VIBRATION DAMPER (PVD), has been developed recently by PENGUIN ENGINEERING Ltd (Monti et al., 1996). This is a compact damping device to be used as supplemental damping for tall and/or flexible structures (Fig.2-21). The damping of this device is achieved through the plastic deformation of a lead core. It is capable of sustaining thousands of cycles at any amplitude within its design range, without deterioration or requiring maintenance. This is achieved through dynamic and meta-dynamic recrystallization of lead (Monti et al., 1995).

This device is sensitive to very small displacement. Significant hysteretic damping can be achieved at displacement as low as ±2 micro metres. A standard device is sensitive to movements as small as ±2 microns such as expected in wind induced vibration, to ±10 mm as expected in a large earthquake. Larger devices have displacement capacity of up to ±1 metre. However, the sensitivity decreases as size increases. Associated damping forces range from 1KN to 1000KN (Monti et al., 1996).

The hysteresis loops of a 200KN lead-shear damper from test results are shown in Fig.2-22. All the results obtained through the testing program of this device have shown it to behave as an almost perfectly plastic device (Monti et al., 1996). The practical range of this strength-level device is from ±2 micrometers to ±10 mm. Larger displacements come with larger devices to a maximum practical displacement of ±1 meter. For example a 100-mm displacement damper will begin to give appreciable hysteretic damping at 20 micrometers, eg. this device has a dynamic range of four orders of magnitude. It has exhibited constant and reliable properties throughout extensive testing. This feature enables it to undergo many

cycles, dissipating large amounts of plastic energy while maintaining its mechanical properties. In the following chapters, this device is referred to "the supplemental lead damper".

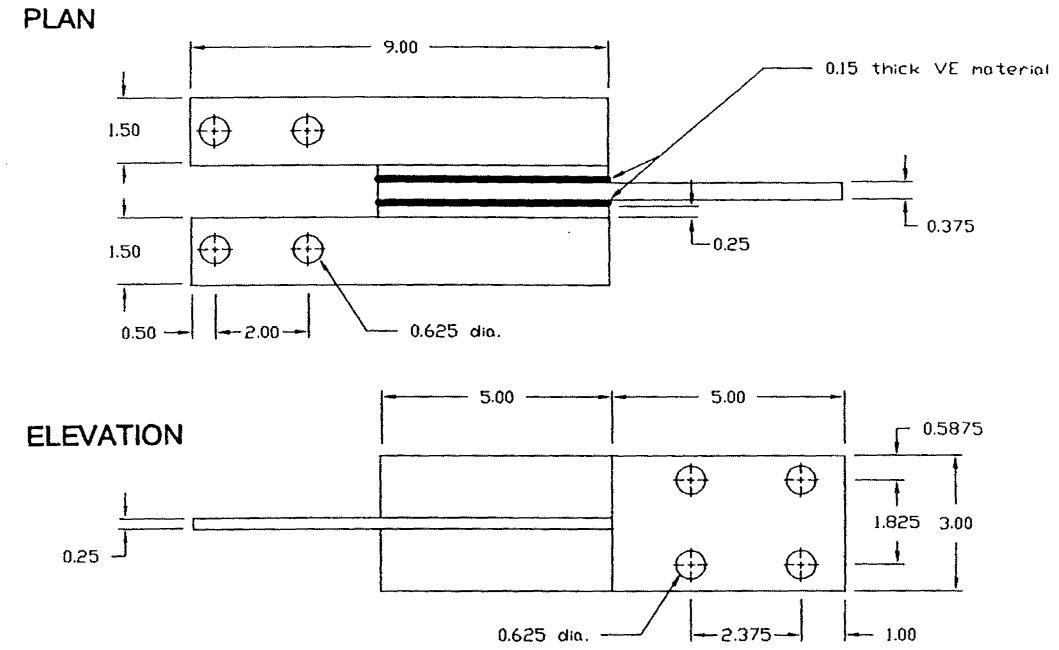


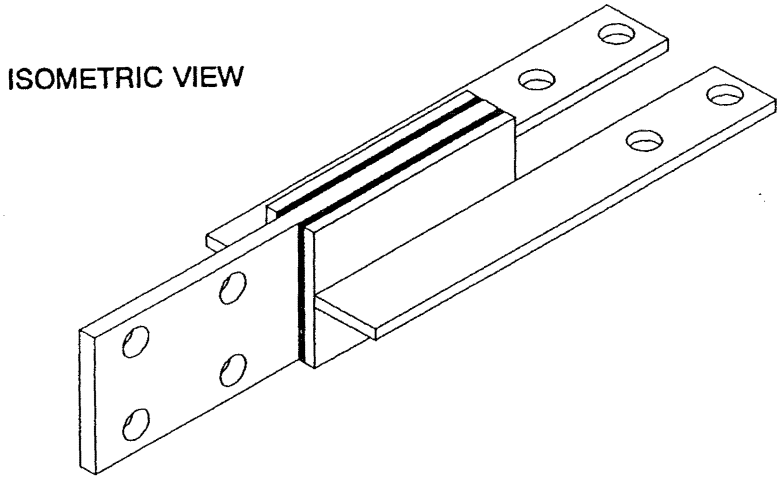


Figure 2-1. Detail of a viscoelastic (VE) damper (from Aiken et al., 1990)

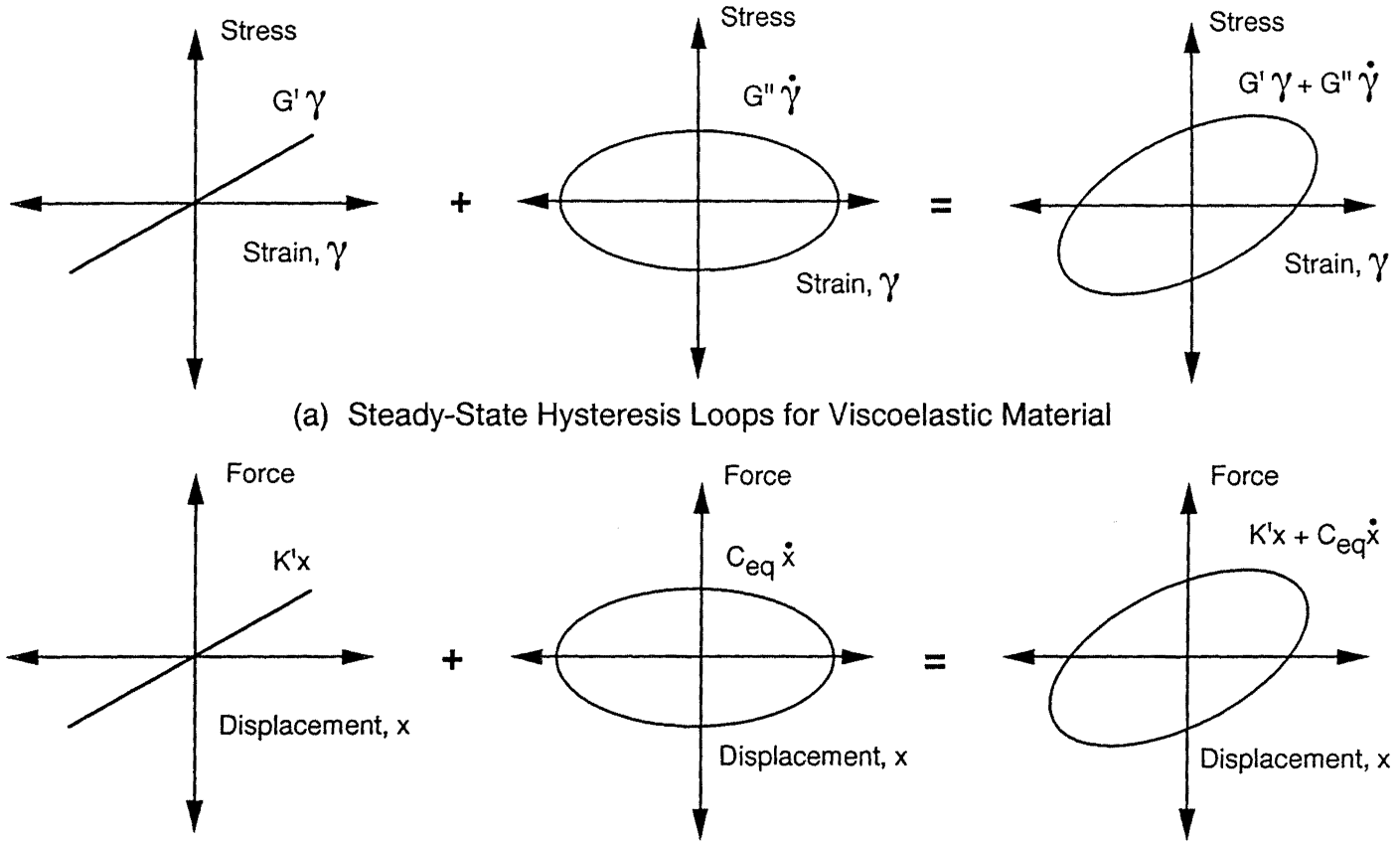


Figure 2-2. Steady-state hysteresis loops (from Bergman et al. 1993)

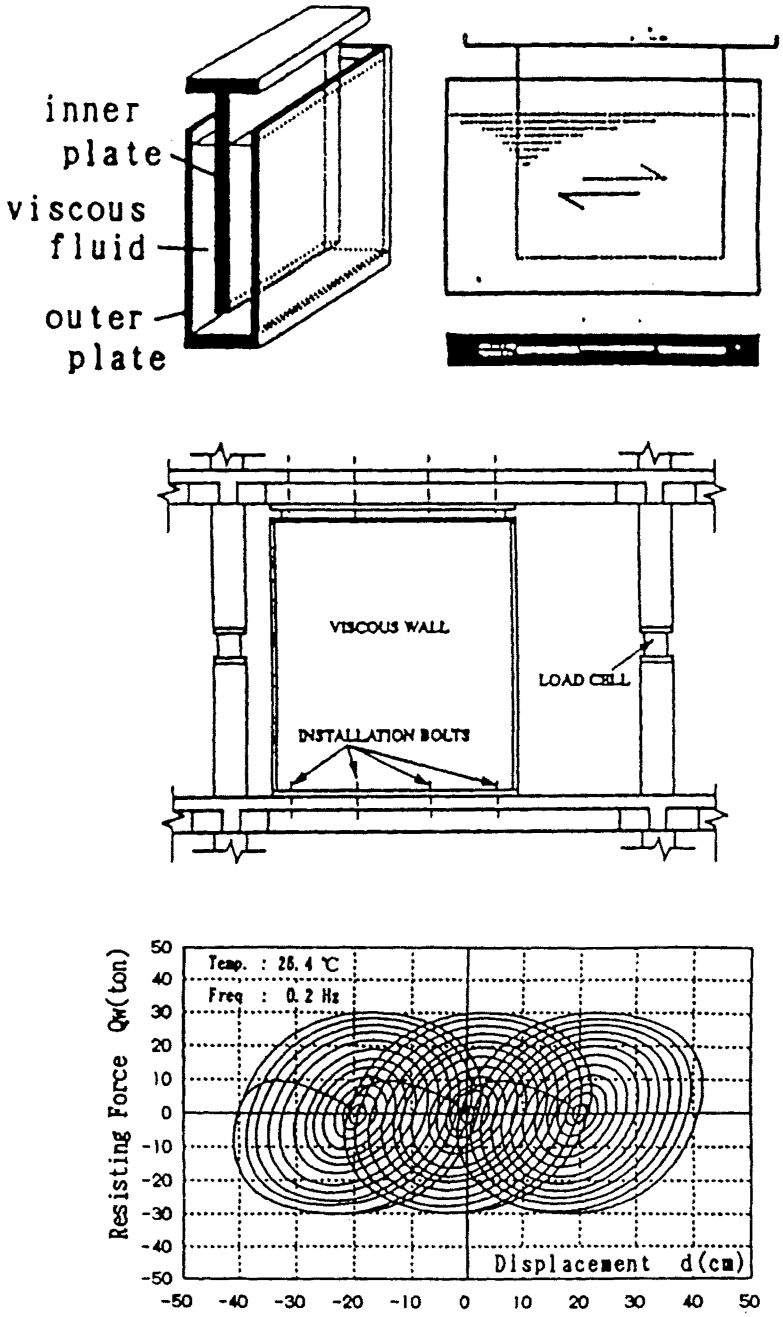


Figure 2-3.Viscous wall, installation detail and hysteresis loops
(from Miyazaki et al., 1992)

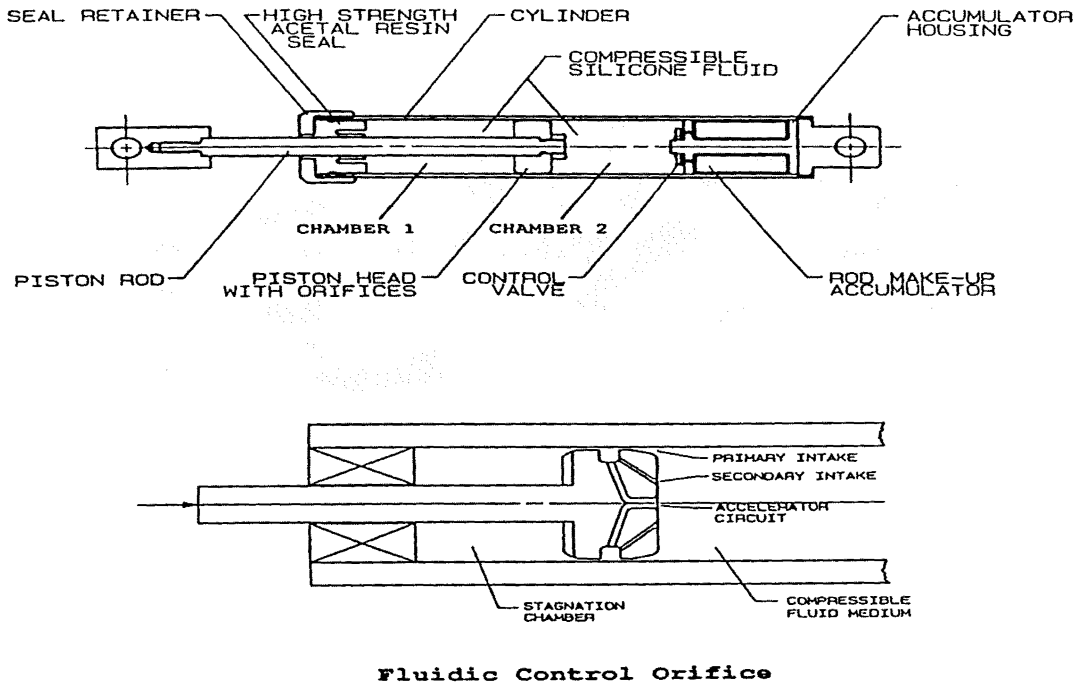


Figure 2-4. Detail of a fluid viscous damper (from Li et al., 1995)

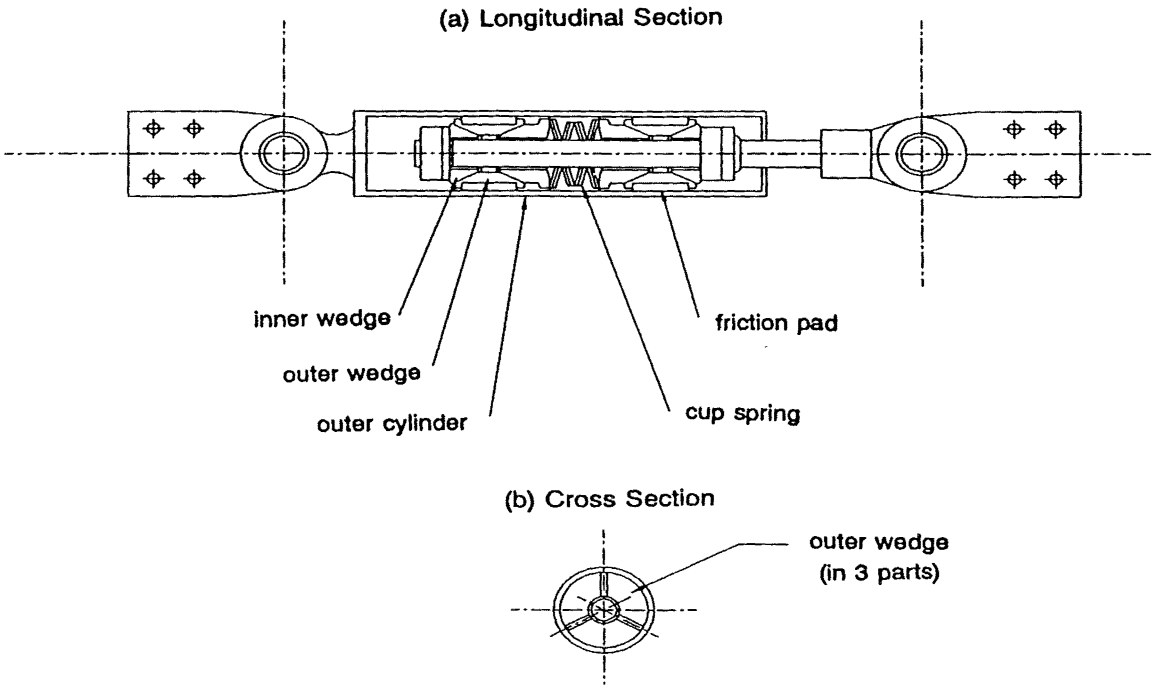


Figure 2-5. Sectional view of a Sumitomo friction damper (from Li et al., 1995)

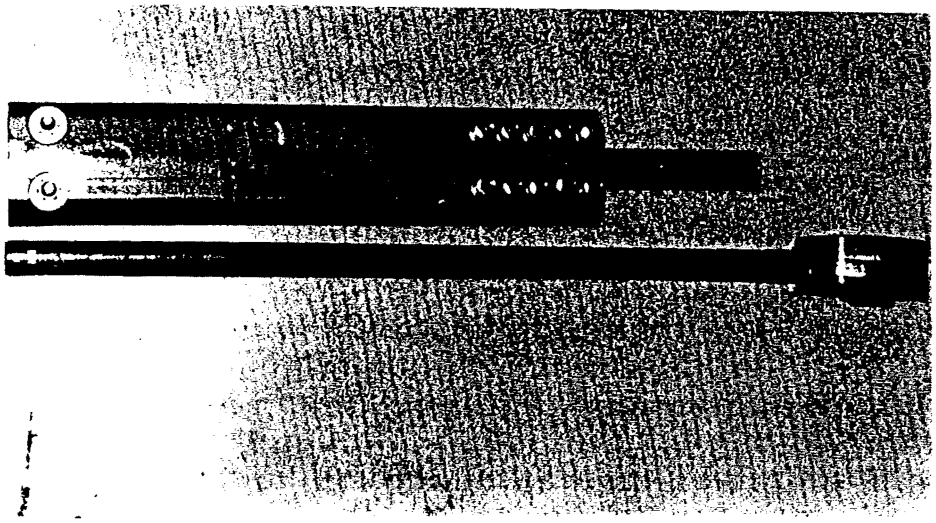

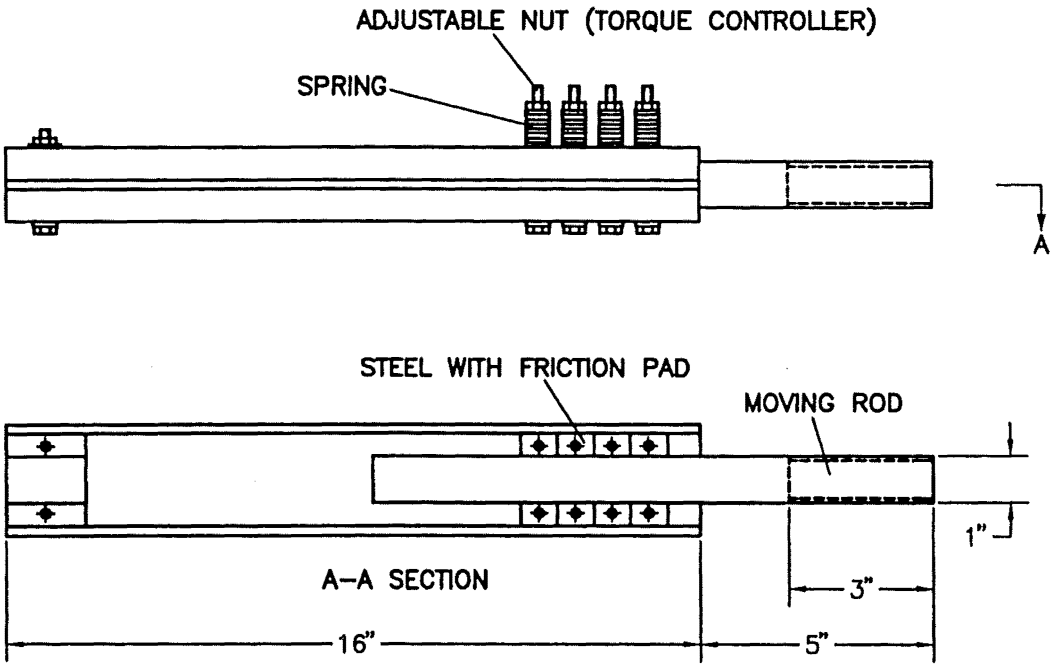


Figure 2-6. Construction of Tekton friction damper (from Li et al., 1995)

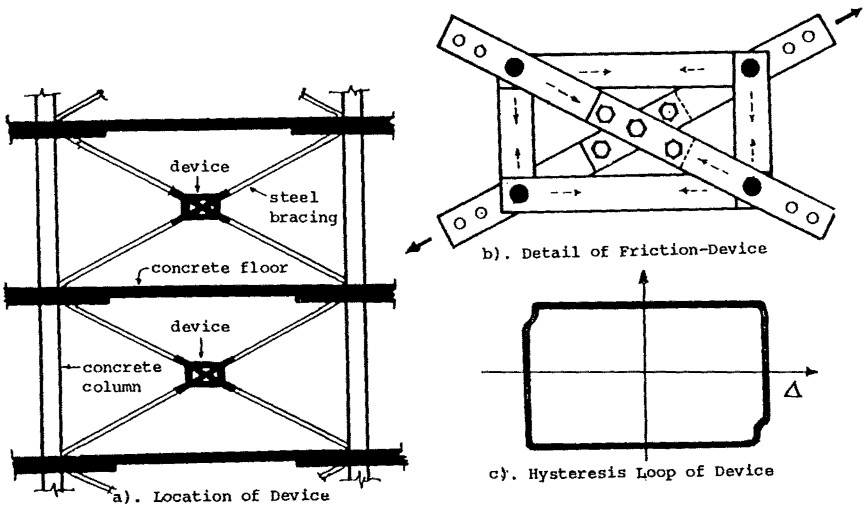


Figure 2-7. Friction device by Pall (from Pall et al., 1987)

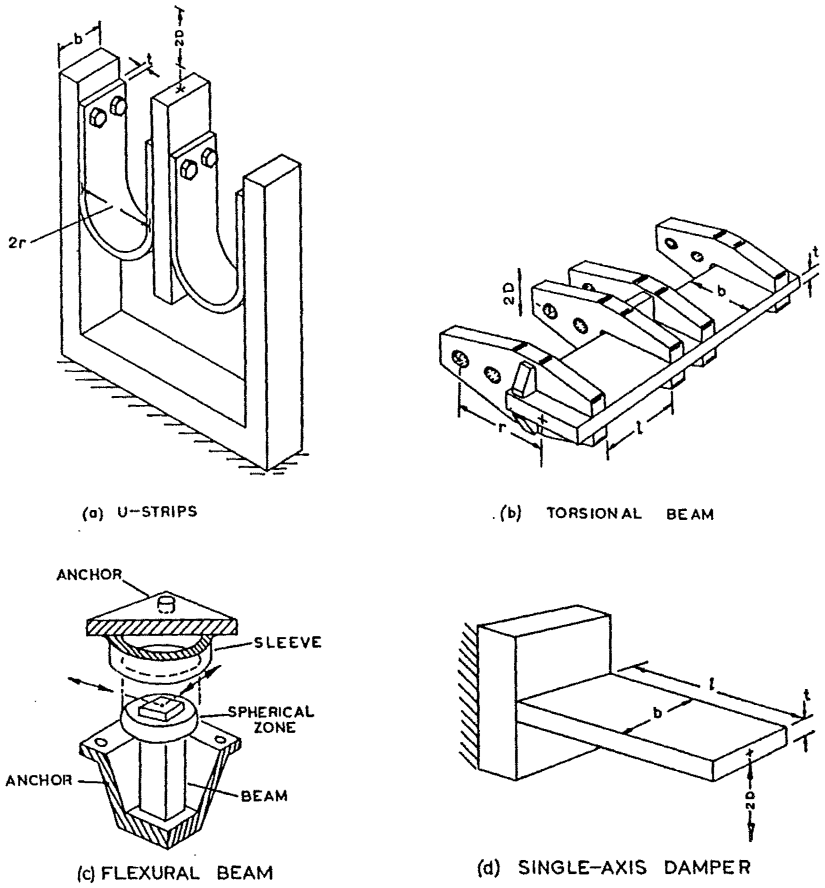


Figure 2-8. Four basic types of hysteretic damper based on the inelastic deformation of solid steel beams (from Skinner et al., 1975)

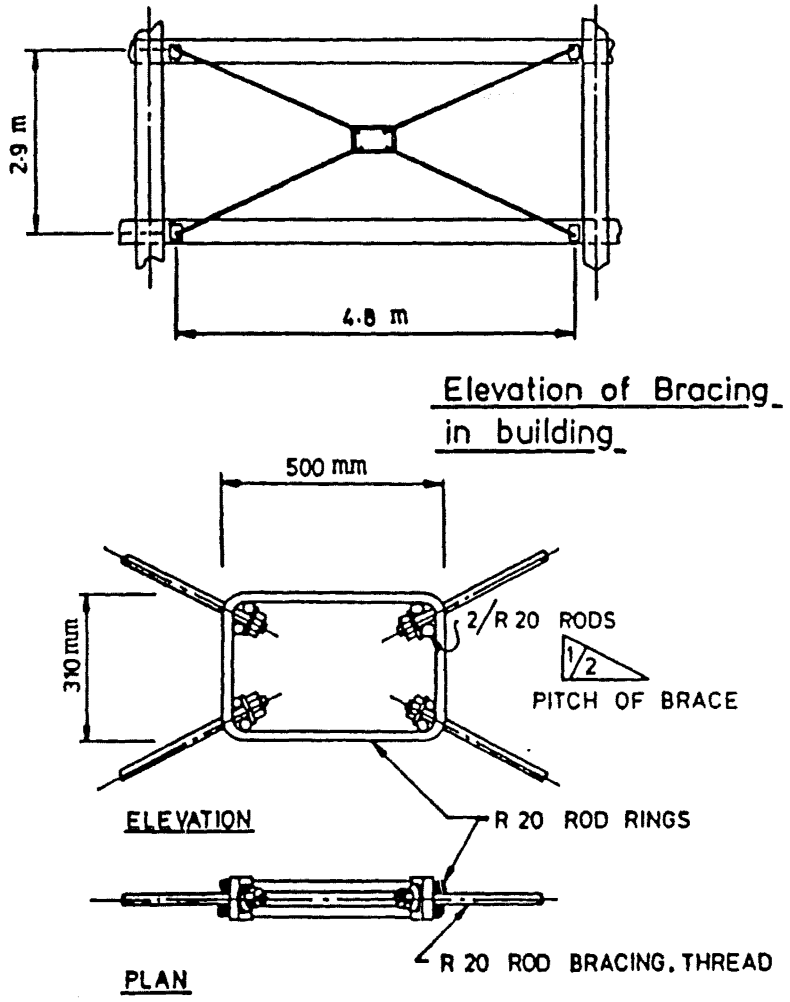


Figure 2-9. Detail of a yielding steel bracing system in a building in New Zealand (Tyler, 1985)

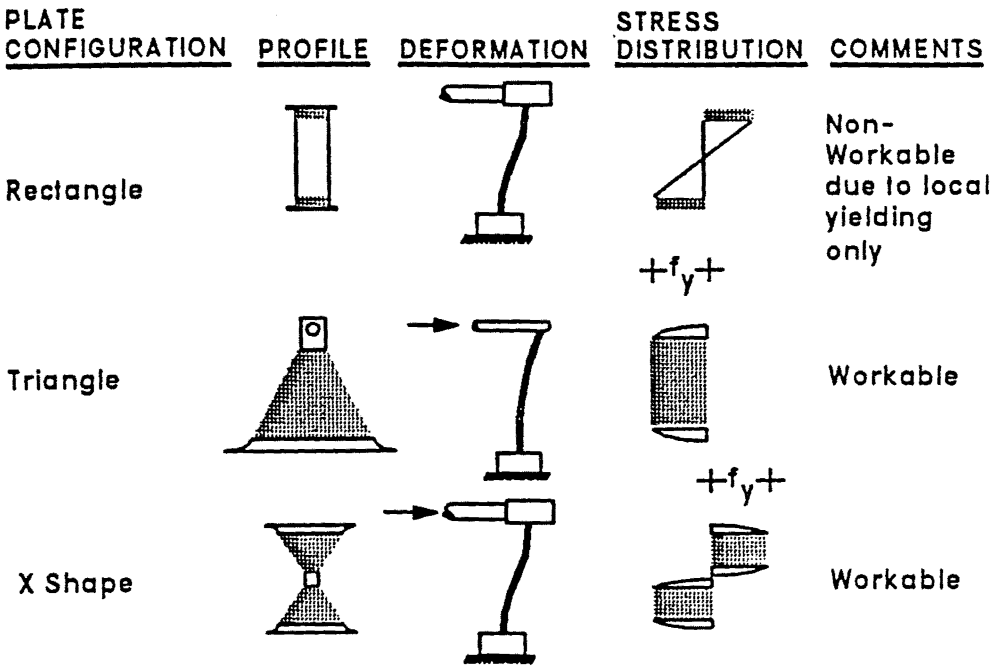


Figure 2-10. Different plate configurations of steel plate energy absorbers (from Whittaker et al., 1989)

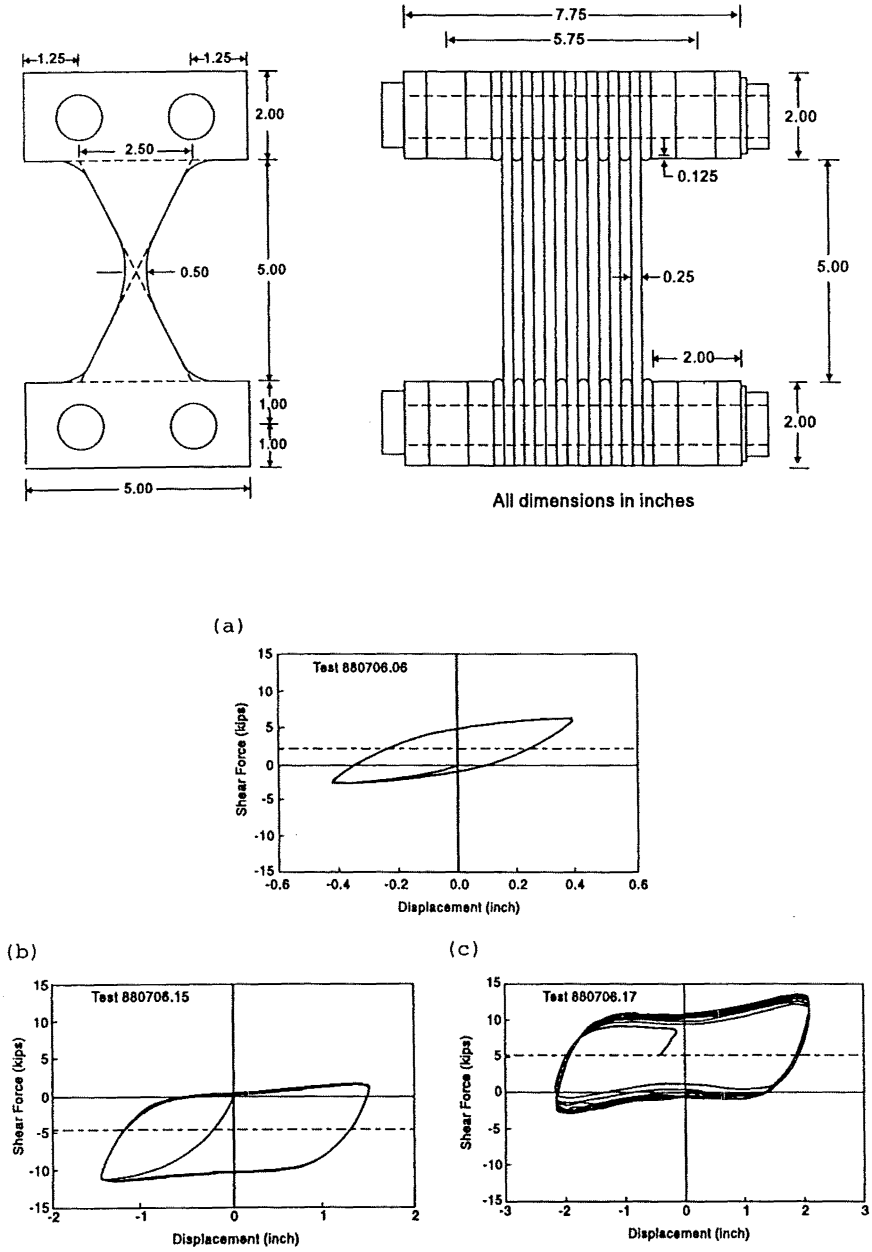


Figure 2-11. ADAS device geometry and its force-displacement response at different displacement amplitude (from Whittaker et al., 1989)

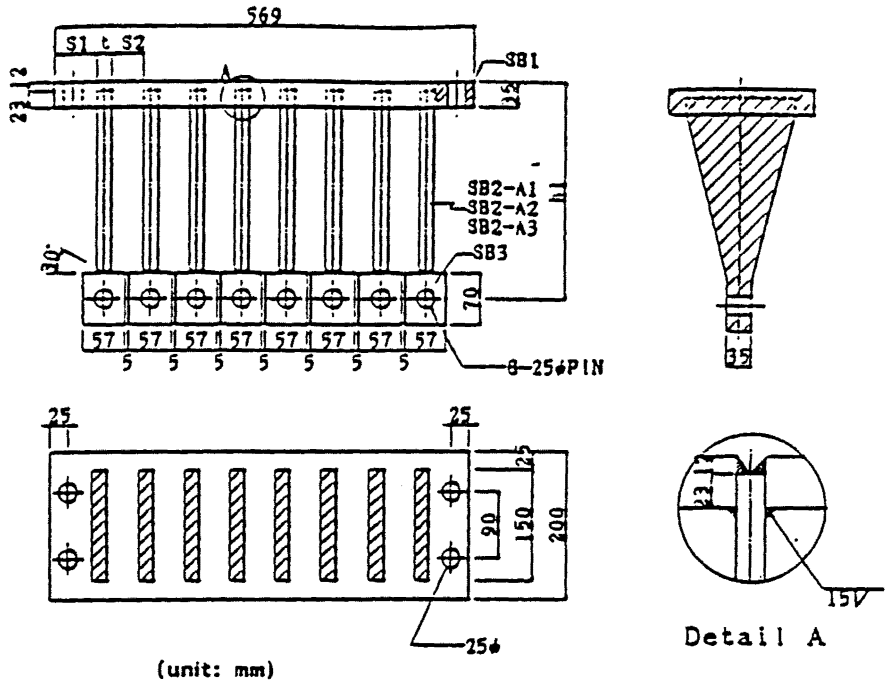


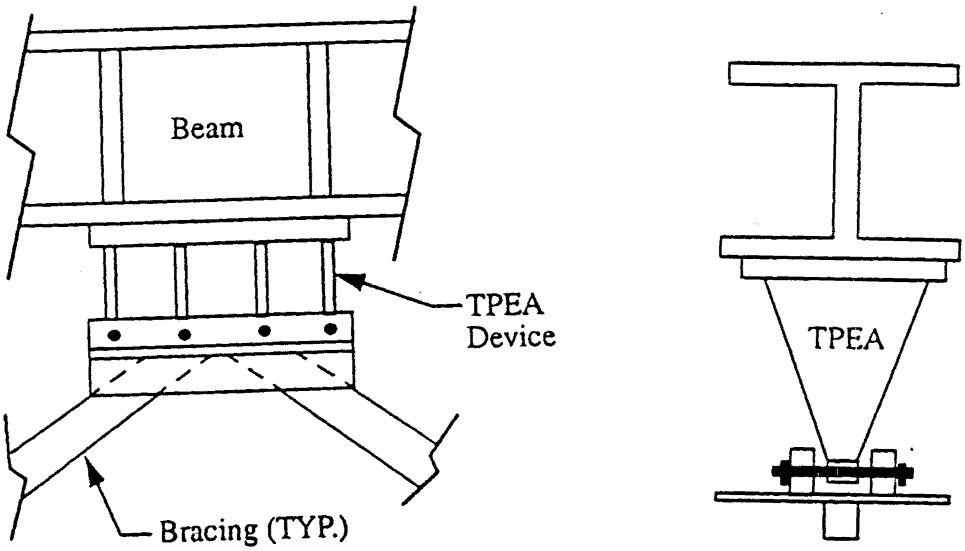


Figure 2-12. Details of TPEA specimen (from Pong et al., 1994)

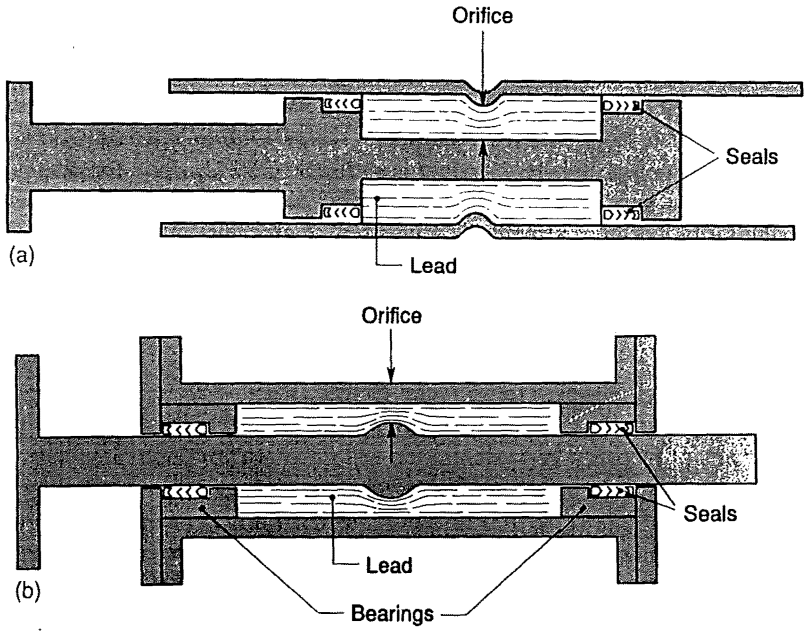


Figure 2-13. Longitudinal section of cyclic lead extrusion damper: (a) constricted-tube type (b) bulged-shaft type (from Skinner et al., 1993)

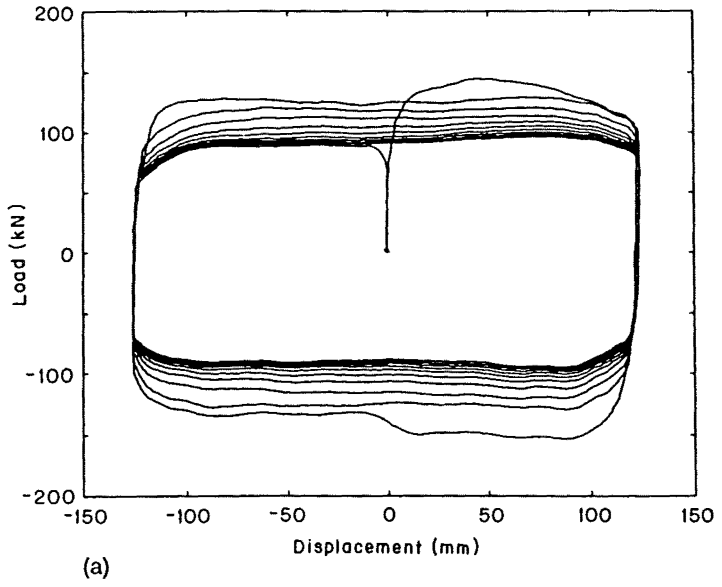


Figure 2-14. Typical load-displacement hysteresis loops for lead-extrusion dampers (from Skinner et al., 1993)

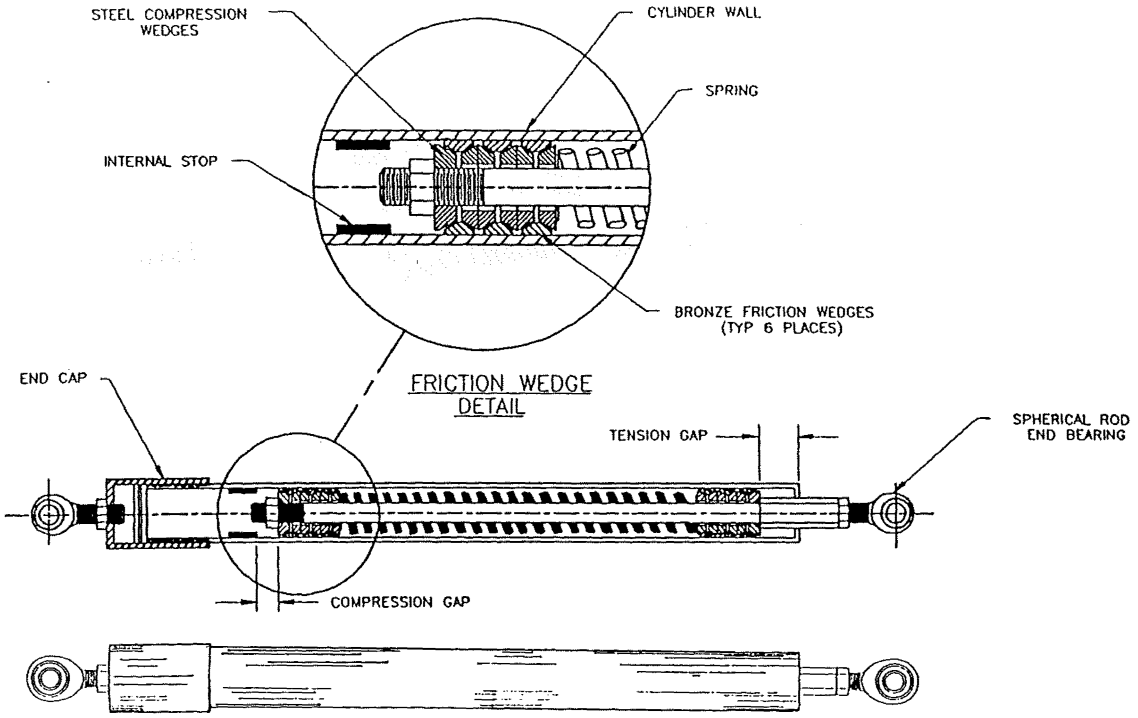


Figure 2-15. External and internal views of the Energy Dissipating Restraint (EDR) (from Inaudi et al., 1993)

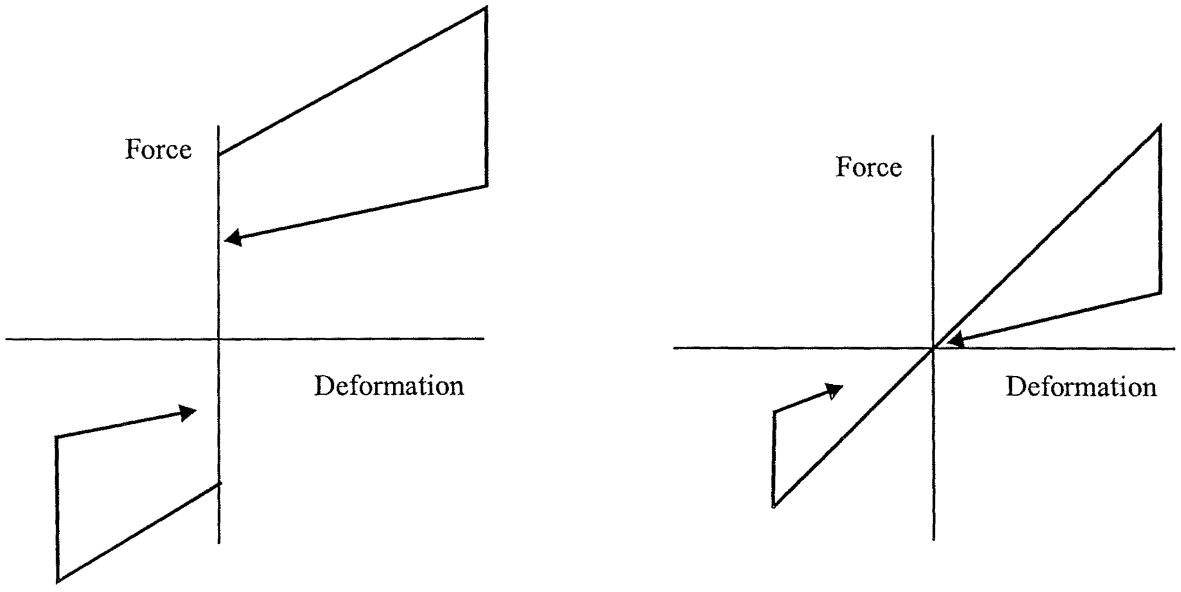


Figure 2-16. Hysteresis loops of the EDR in two different configurations: the flag and the triangular configuration (from Inaudi et al., 1993)

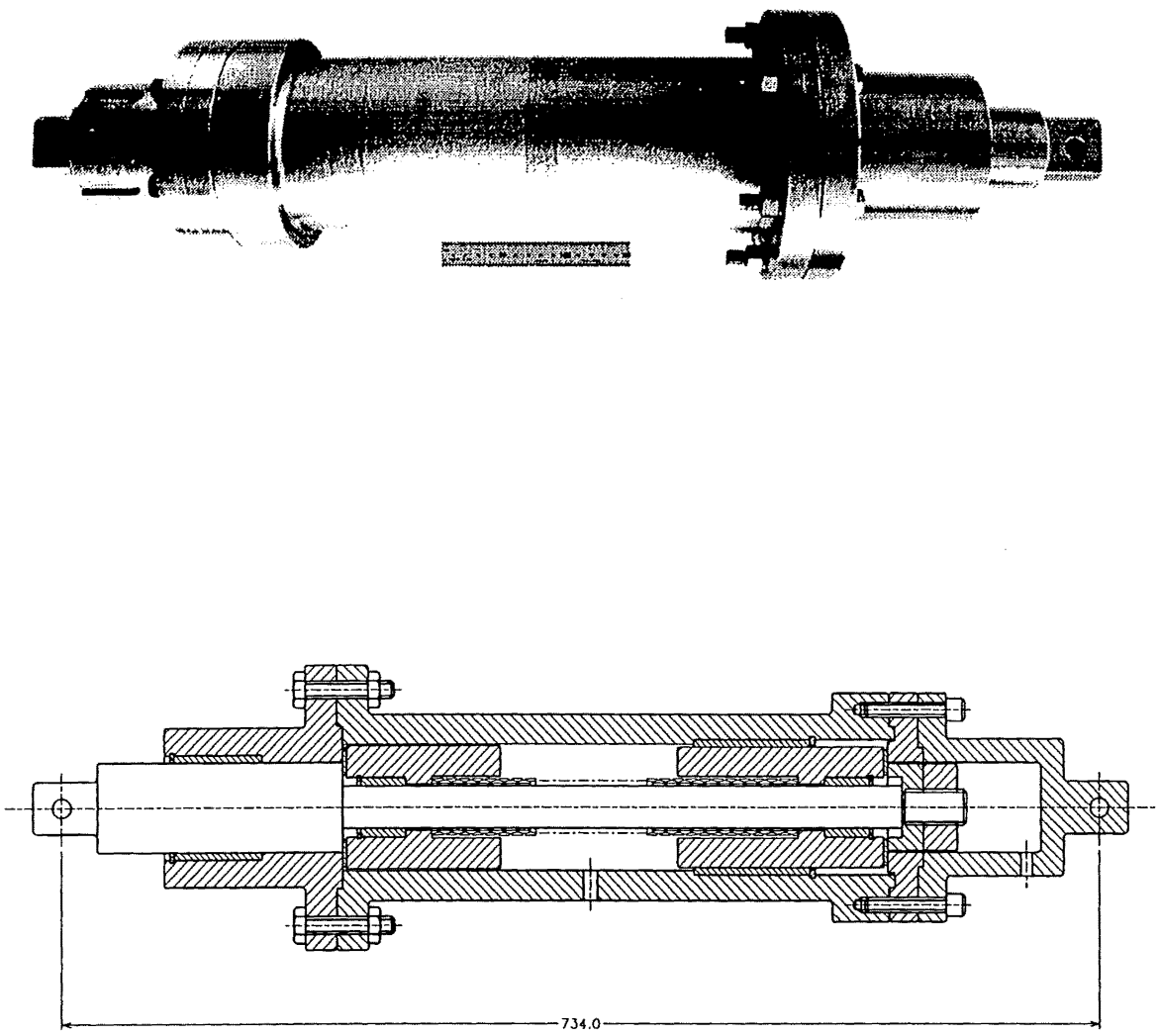


Figure 2-17. Prototype bi-directional ring spring cartridge (with 150 mm ruler)
(From Hill, 1995)

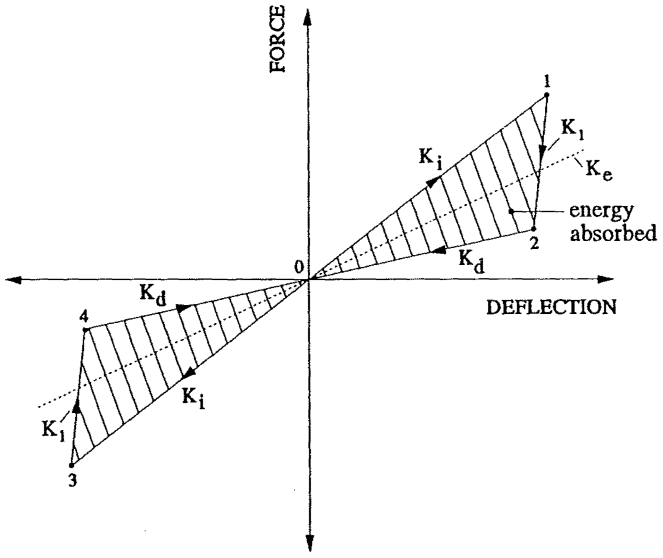


Figure 2-18. Force-deflection diagram for zero pre-displacement ring springs (From Hill, 1995)

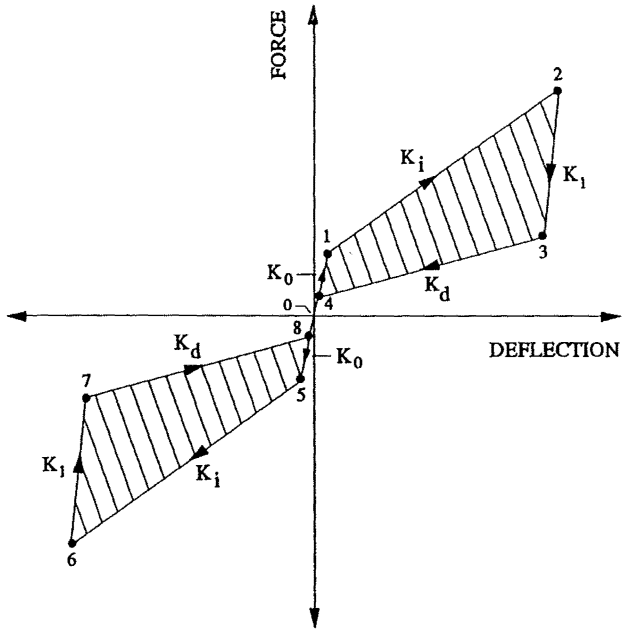


Figure 2-19. Force-deflection diagram for pre-displaced ring springs (From Hill, 1995)

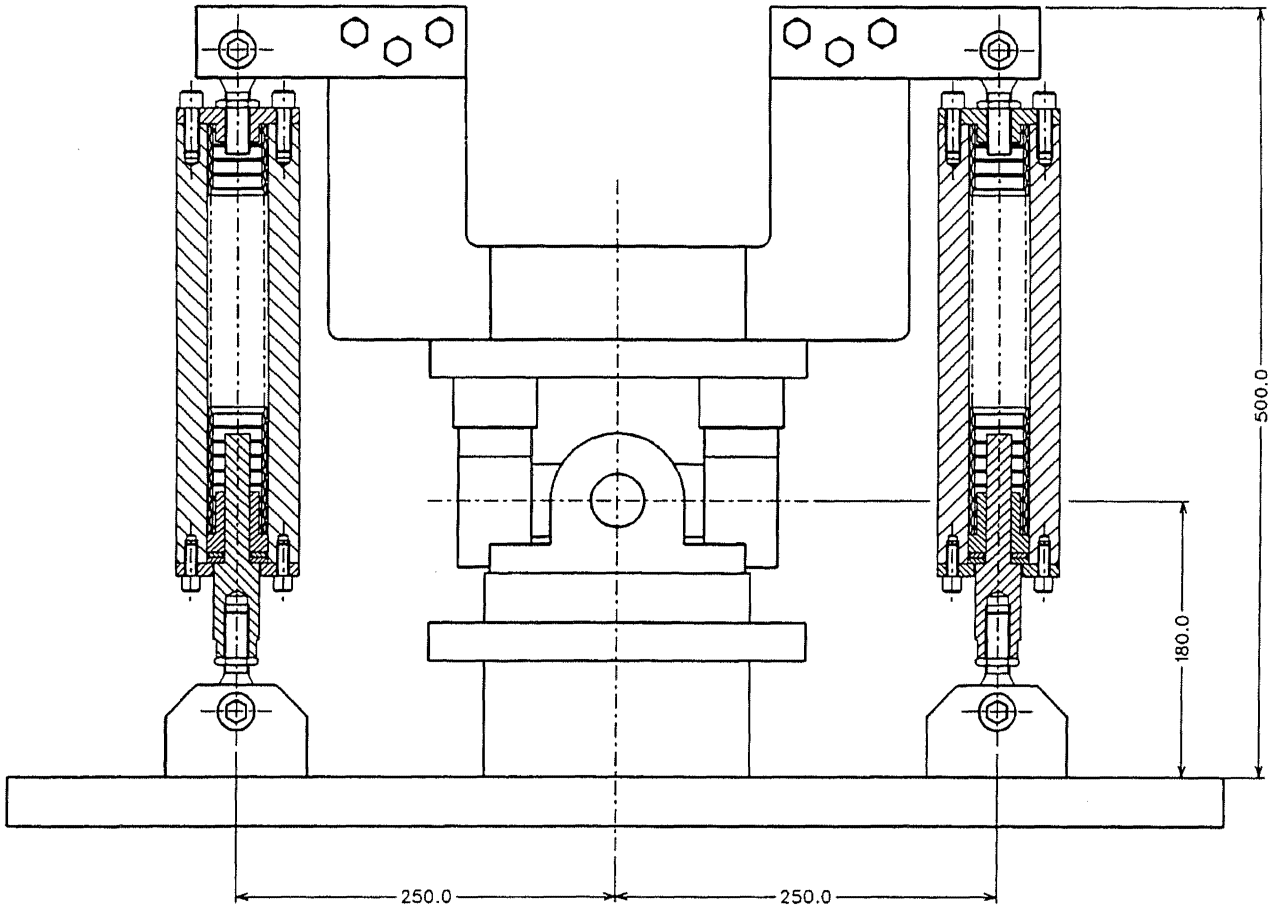


Figure 2-20 Pivotal rocking seismic isolation system (PRSIS)
(From Hill, 1995)

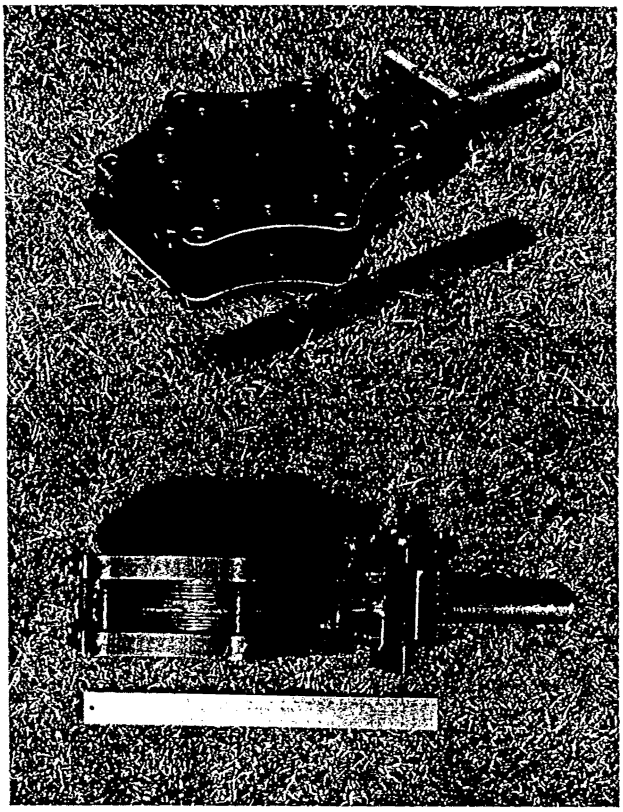

Figure 2-21. The self contained lead-shear damper (from Monti et al., 1996)

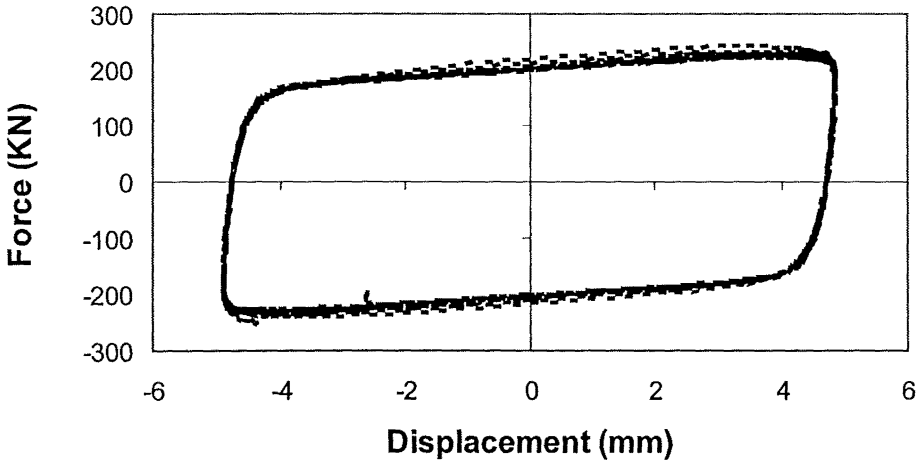


Figure 2-22. The force-displacement curves from tests
(from Penguin Engineering Ltd)

# CHAPTER 3

# MODELLING OF THE INELASTIC STRUCTURE AND THE SUPPLEMENTAL LEAD DAMPERS

## 3.1 MODELLING OF THE INELASTIC STRUCTURE

The inelastic analysis of structures subjected to earthquake loading is usually performed using step-by-step integration of the equations of motion. These equations of motion can represent the dynamic behaviour of structures with variable stiffness due to cracking, yielding, deterioration and secondary effects, etc.

The equation of motion for the structure subjected to earthquake excitations can be written as:

$$[M]\{\ddot{u}\}+[C]\{\dot{u}\}+\{R(u)\}=-[M]\{r\}\ddot{u}_g(t) \tag{3.1}$$

where $[M]$, $[C]$ are the mass and damping matrices. $\{R(u)\}$ is the nonlinear resistance vector of the structure obtained from the addition of individual component's resistance. $u, \dot{u}, \ddot{u}$ are the time dependent response, vector of displacement, velocity and acceleration respectively. $\ddot{u}_g(t)$ is the given ground acceleration due to a earthquake excitation. $\{r\}$ is the displacement of the structure due to a unit ground displacement in the direction of the earthquake excitation.

The resistance vector $\{R(u)\}$ is a function of displacement. It is based on the models adopted for analysis. The Giberson one-component model, which has a possible plastic hinge at one or both ends of the elastic central length of the member, is adopted to model the members of the structure (Sharpe, 1974). See Fig.3.1. Three types of models are used to represent the moment-curvature relationship of the frame members in the structure: modified TAKEDA model (Otani, 1974), degrading Bi-linear model (Otani, 1981) and the linear elastic model.

The modified TAKEDA model is adopted to represent all the beam members of the structure. The degrading Bi-linear model is used to represent the columns at the 1st floor level of the structure. The linear elastic model is adopted to represent all the upper columns of the structure. This is based on the capacity design concept. In the capacity design concept, a beam

sidesway mechanism for the post-elastic deformation of moment resisting frames during an earthquake excitation is chosen and the members are designed for the resulting moments and shears to ensure that other deformation mechanisms of the structure will never occur. The structure is designed in this way so that the plastic hinges can only occur at beam-ends and at the base of columns of ground floor, while the upper columns remain elastic. The modified TAKEDA model and degrading Bi-linear model are shown in Fig.3.1.

## 3.2 MODELLING OF THE SUPPLEMENTAL DAMPERS

The lead-shear damper, Penguin Vibration Damper (PVD), developed by Penguin Engineering, is a compact damping device. The damping of this device is achieved through deformation of a lead core. It provides significant hysteretic damping for a wide reliable range of displacements of four orders of magnitude. The PVD is a metallic yielding device – a type of hysteretic damper.

Two models are adopted to represent the force-displacement relationship of the lead dampers: the Ramberg-Osgood model (Kaldjian, 1967) and the elasto-plastic model.

1. Ramberg-Osgood Model

The skeleton curves of the general force-displacement relation given by the Ramberg-Osgood model are described by (see Fig.3.2)

$$\delta = \frac{F}{K_0}\left[1+\left(\frac{F}{F_y}\right)^{r-1}\right] \tag{3.2}$$

where $F$, $\delta$ = force and displacement respectively

$F_y$ = effective first yield

$K_0$ = initial elastic stiffness

$r$ = an exponent greater than or equal to 1.0

The hysteretic behaviour of the Ramberg-Osgood model with a skeleton curve given by Eq.(3.2) is described by

$$\delta - \delta_i = \left(\frac{F - F_i}{K_0}\right)\left[1 + \left|\frac{F - F_i}{2F_y}\right|^{r-1}\right] \tag{3.3}$$

where ($F_i$ , $\delta_i$ ) is the most recent point at which the direction of the loading has been reversed.

Plots of Eq (3.2) are shown in Fig.3-2 for various values of $r$ which controls the abruptness of the loss of stiffness. $r$ =1 represents the elastic case and $r = \infty$ is the elasto-plastic relation.

By trial and error, suitable parameters of the Ramberg-Osgood model ($F_y$, $K_0$ and $r$) can be determined to match the test results of the lead dampers. Parameters of $F_y$ =180KN, $K_0$ = 1944KN/mm, $r$ =15 are taken to represent this 200KN lead damper.

Comparison of the Ramberg-Osgood model and the test results is shown in Fig.3.3. It can be seen that for the parameters adopted here, they match each other quite well.

2. Elasto-Plastic Model

All the results obtained through the testing programme of this device have shown it to behave as an almost perfectly plastic device (Monti et al., 1996). For the sake of simplicity, especially for design purposes, the elasto-plastic model is also discussed here to see whether it is possible just to adopt such a simple model to carry out design studies.

For this elasto-plastic model, only two parameters are needed: yield force $F_y$ and initial stiffness $K_0$. $F_y$ = 211KN, $K_0$ =1944KN/mm. The comparison of the elasto-plastic model with the test results is shown in Fig.3.4.

Comparisons of these two models will be performed in chapter 4.

## 3.3 MODELLING OF THE INELASTIC STRUCTURES WITH SUPPLEMENTAL LEAD DAMPERS

A 12-storey 3-bay reinforced concrete frame structure was used in the following analysis. A former Ph. D student M. Tabuchi at the University of Canterbury designed this frame to the

Draft New Zealand Loadings Code, DNZ4203 (Tabuchi, 1992). The supplemental dampers are incorporated into the structure by means of diagonal braces. See Fig.3.5.

The structure with the supplemental dampers will have another dissipation term in the equation of motion for the structure. Eq(3.1) can be modified as:

$$[M]\{\ddot{u}\}+[C]\{\dot{u}\}+\{R(u)\}+\{F_D(u)\}=-[M]\{r\}\ddot{u}_g(t) \tag{3.4}$$

where $\{F_D(u)\}$ is the supplemental damping force vector obtained from a suitable transformation of bracing forces to the corresponding degrees of freedom. $\{R(u)\}$ is the nonlinear resistance vector of the original structure (not including the supplemental damping force) obtained from the addition of individual component's resistance.

The nonlinear time history analysis program RUAUMOKO (Carr, 1996a) developed in the Civil Engineering Department of University of Canterbury is used for this study. Beam members and beam-column members are adopted to represent the beams and the columns of the structure respectively. The inelastic behaviour of a beam and beam-column member follows the concept of the Giberson one-component model, which has a possible plastic hinge at one or both ends of the elastic central length of the member. A beam-column member differs from a beam member in that there is an interaction between the axial force and the moment yield states.

A damping system may consist of a diagonal brace and a damper, and is represented by a spring type member. This spring type member used here is actually a truss element — only able to resist axial force, without moment and shear force resistance. See Fig.3.6. The flexibility of the braces connecting the supplemental dampers to the structure will have influence on the effectiveness of the dampers. First it is assumed that the braces are rigid. The force-displacement relationship of this damping system is the same as that of the supplemental lead dampers. The influence of the flexibility of the braces will be investigated later.

The effect of the supplemental dampers is measured in terms of the supplemental damping force vector $\{F_D(u)\}$in Eq(3.4). There also exists the inherent damping of the original structure. This inherent damping of the structure represents a dissipation of energy due to many different mechanisms, such as internal friction, sliding friction of connections and joints

in the structure, cracking of members, the structure's environment (air and water resistance and foundations). This inherent damping can be represented in three ways: viscous damping, hysteretic damping and Coulomb damping. In most applications, the viscous damping model is often used because of its mathematical simplicity. Viscous damping has the property that there is a restoring force proportional to the velocity ($-c\dot{u}$). If a deterministic non-linear time history analysis is used, the most common model is to form the damping matrix by making it proportional to the mass and stiffness matrices, thus

$$[C]=\alpha[M]+\beta[K] \tag{3.5}$$

where $\alpha$ and $\beta$ are constants.

This model is also called the Rayleigh damping and the constants $\alpha$ and $\beta$ can be determined as:

$$\begin{aligned}\alpha &= \frac{2\omega_{m1}\omega_{m2}(\omega_{m1}\xi_{m2}-\omega_{m2}\xi_{m1})}{\omega_{m1}^2-\omega_{m2}^2}\\ \beta &= \frac{2(\omega_{m1}\xi_{m1}-\omega_{m2}\xi_{m2})}{\omega_{m1}^2-\omega_{m2}^2}\end{aligned} \tag{3.6}$$

where $\omega_{m1}$, $\omega_{m2}$ are any two natural circular frequencies and $\xi_{m1}$, $\xi_{m2}$ are their respective fractions of critical damping. By specifying the damping ratios of any two selected modes, all other modes with natural frequency $\omega_n$ subsequently have their fraction of critical damping given by

$$\xi_n = \frac{1}{2}\left(\frac{\alpha}{\omega_n}+\beta\omega_n\right) \tag{3.7}$$

as shown in Fig.3.7. In this program it is possible to form the Rayleigh damping matrix based on either the initial structural stiffness or the tangent stiffness.

It has been realised that in applying this damping model care must be exercised to avoid supercritical damped high modes that may lead to an underestimation of the structure response, especially if the contribution of these high modes is significant. Generally, the two

selected frequencies should be of the lowest and one of the highest modes that are expected to contribute significantly to the response.

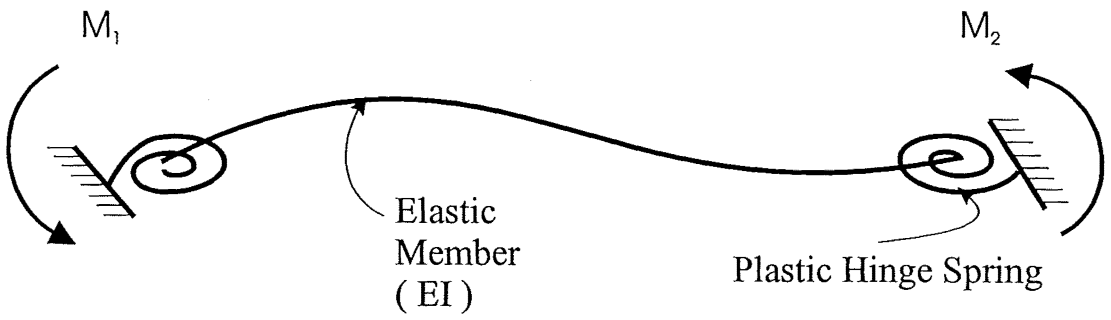


Giberson One Component Beam Column Model

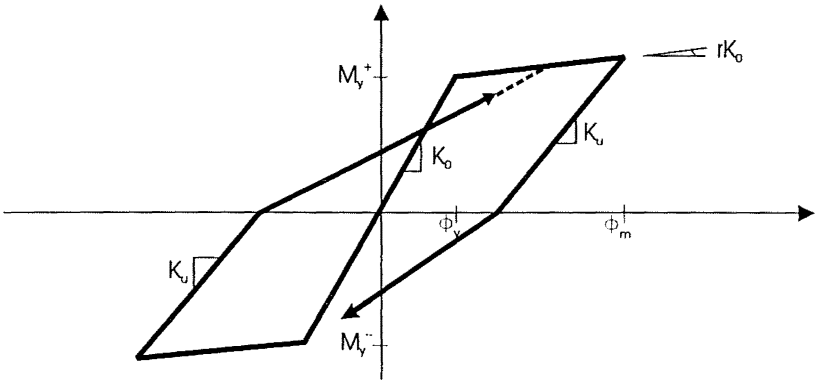


Modified Takeda Hysteresis Model

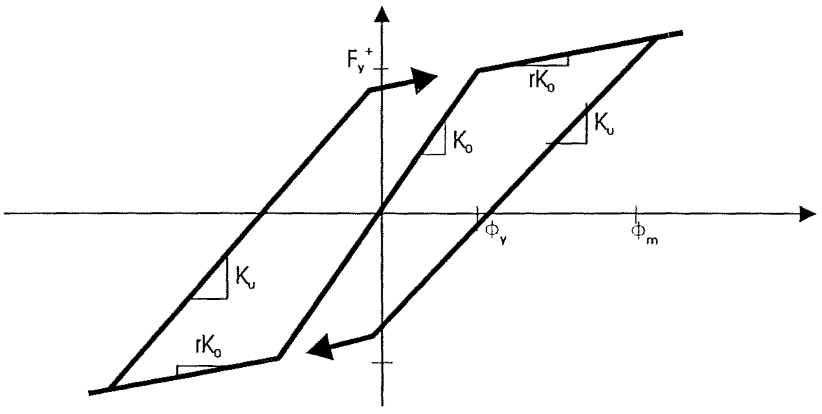


Degrading Bi-linear Hysteresis Model

Figure 3.1 Structural Beam Column Model and Hysteresis Model

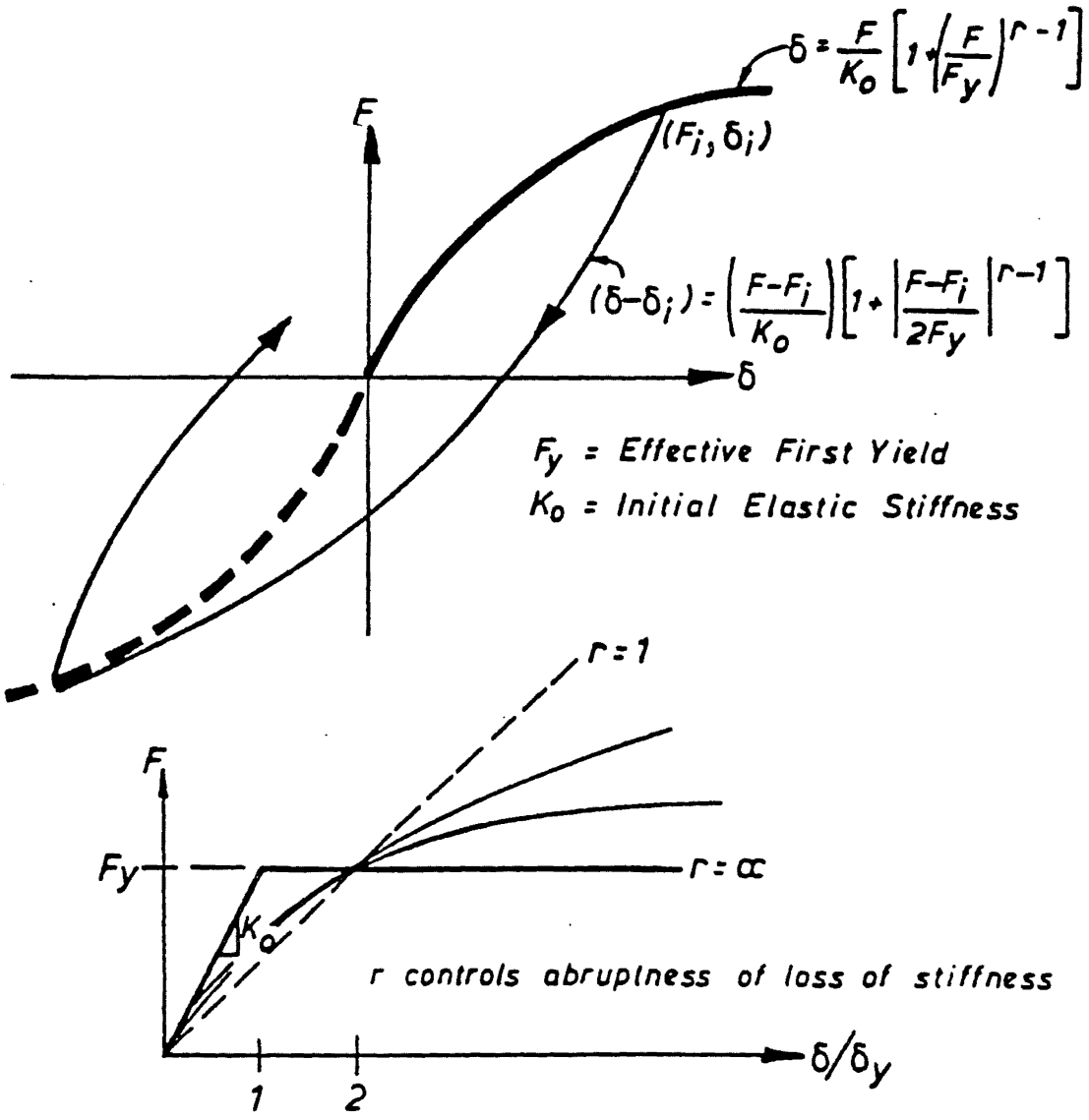


Figure 3.2 Ramberg-Osgood hysteresis loop model
(Kaldjian, 1967)

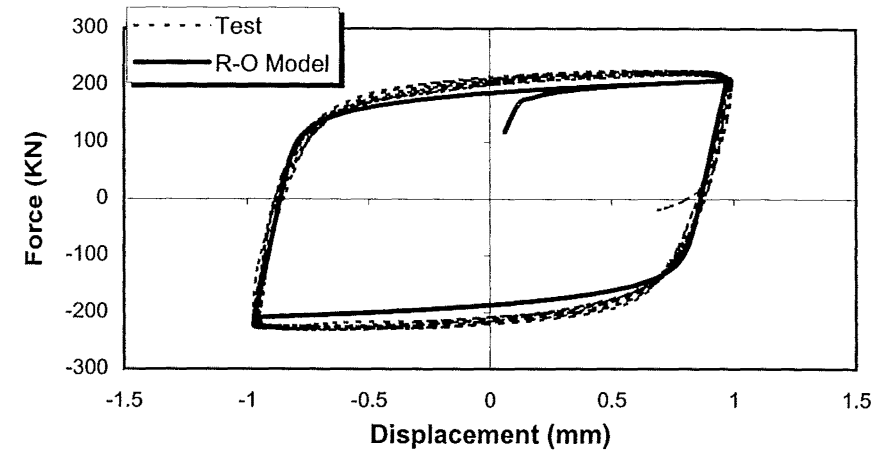


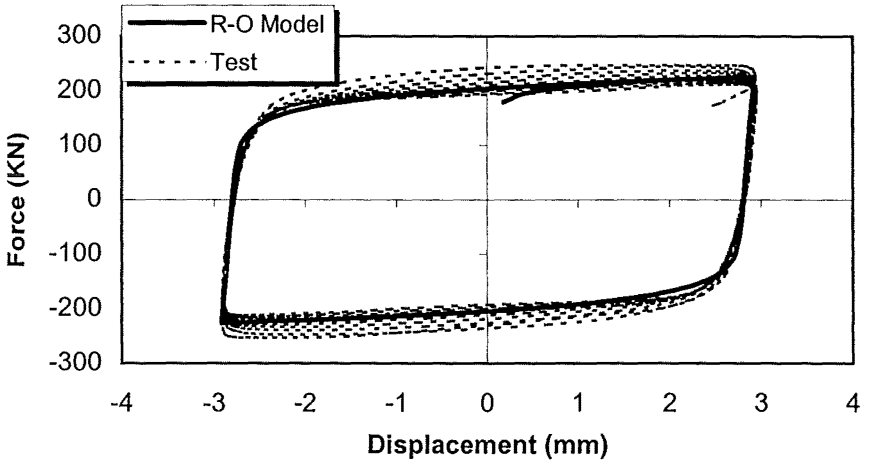


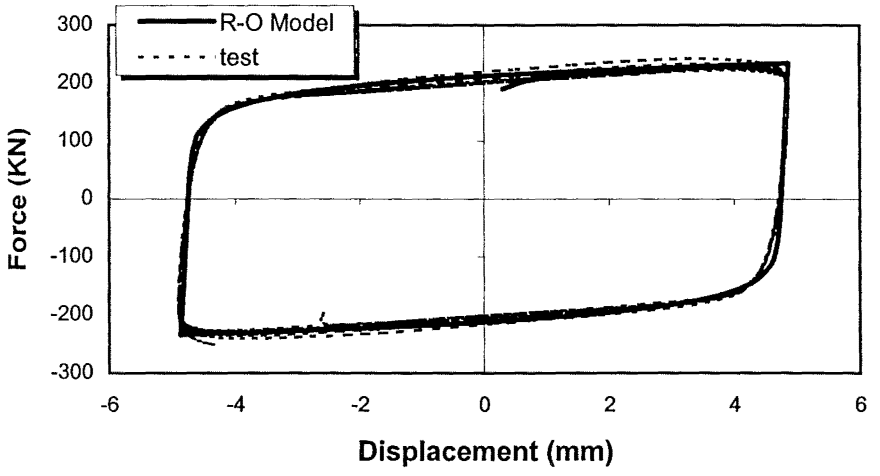


Figure 3.3 Comparison of the Ramberg-Osgood model and the test results for the 200KN lead-shear damper at different displacement amplitudes

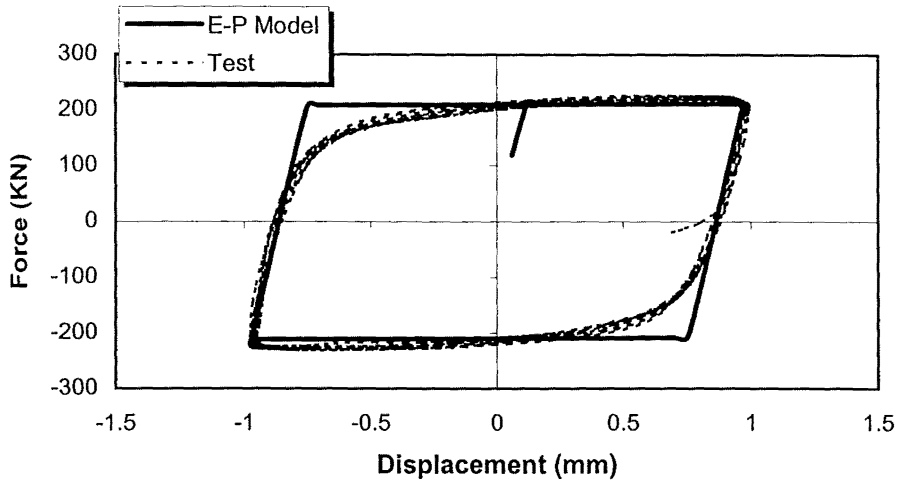


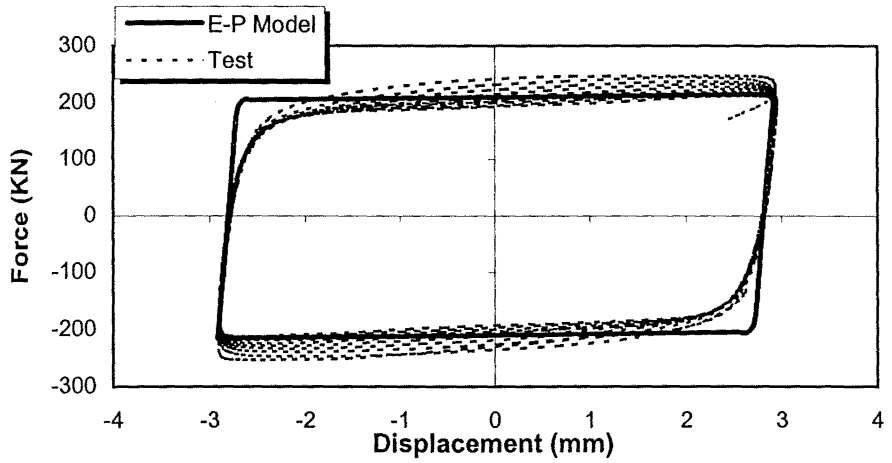


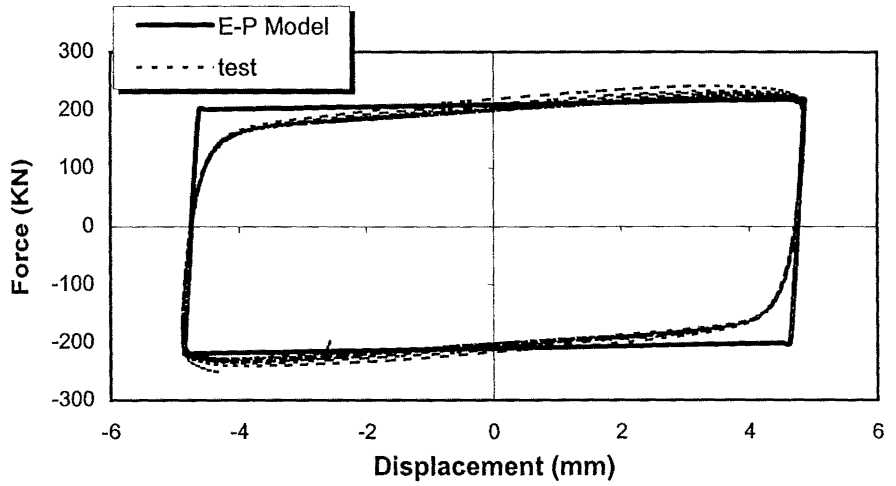


Figure 3.4 Comparison of the Elastic-Plastic model and the test result for the 200KN lead-shear damper at different displacement amplitudes

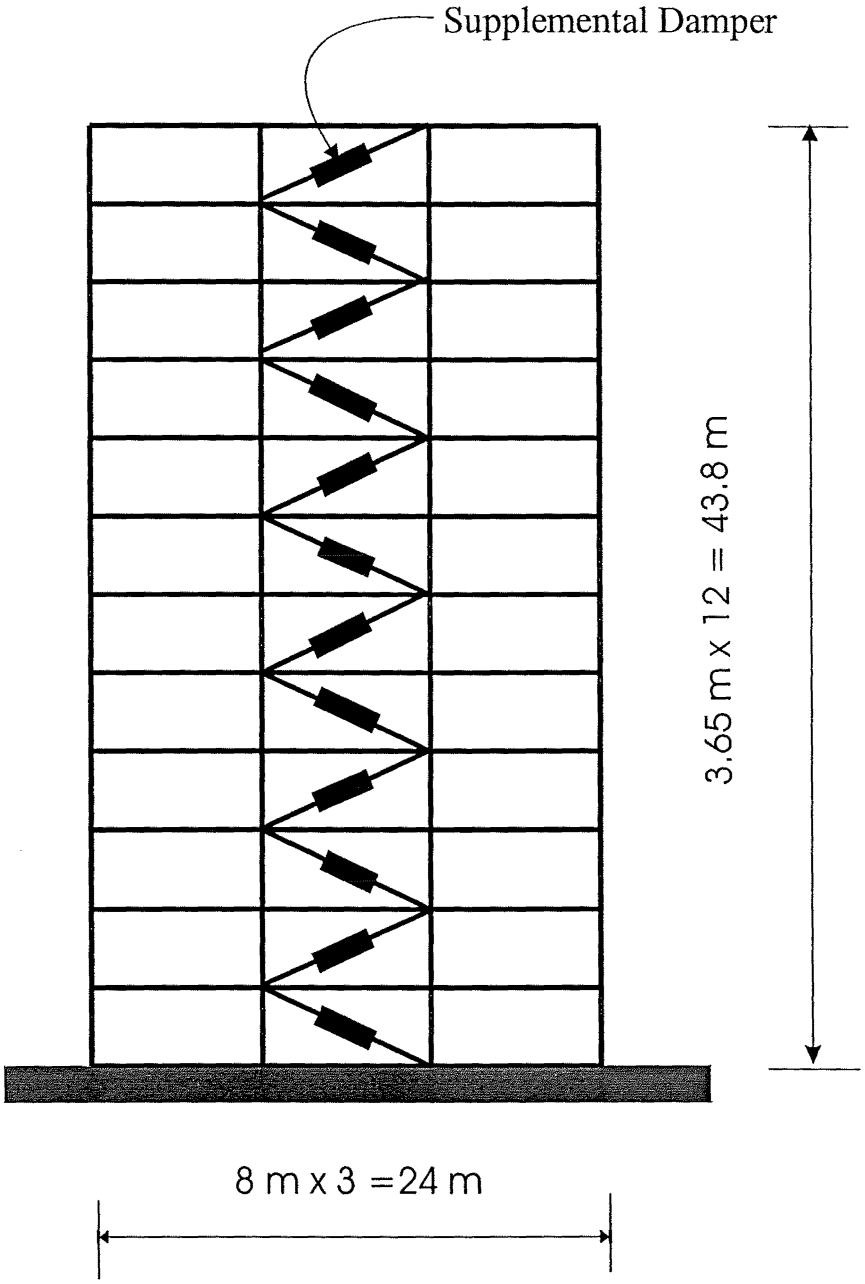


Figure 3.5 A 12-storey 3-bay Reinforced Concrete Frame Structure with the Supplemental Dampers

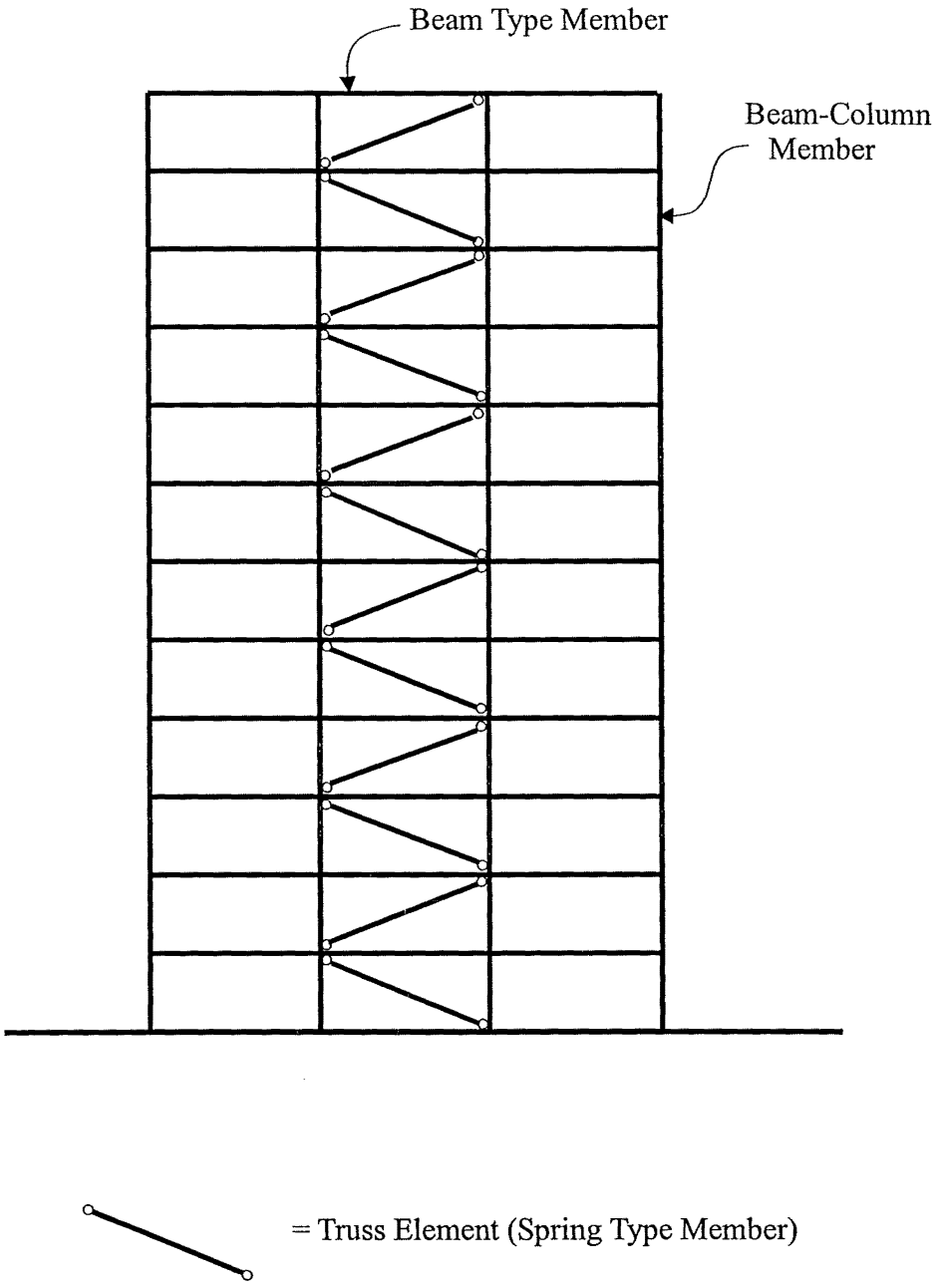


Figure 3.6 Computer Model for Analysis of the Structure with the Supplemental Dampers

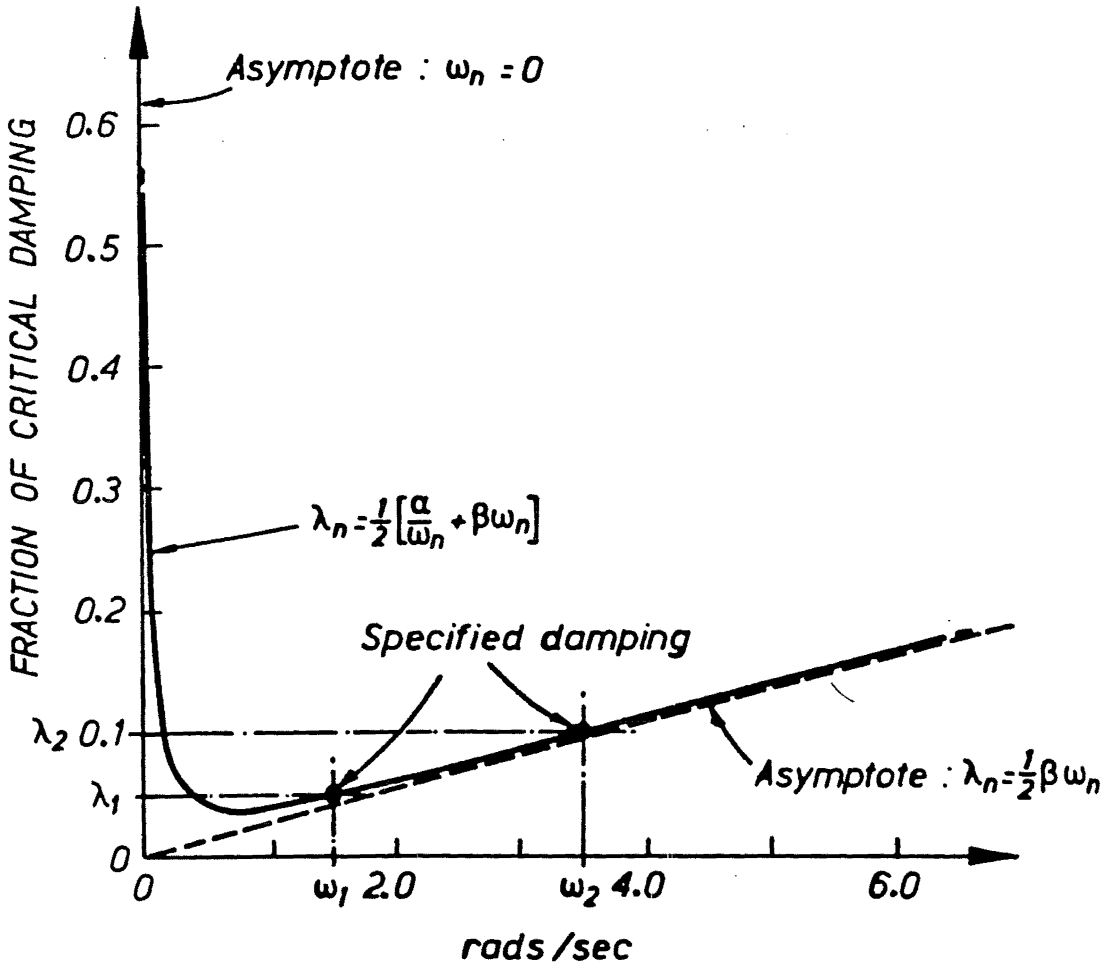


Figure 3.7 Typical Rayleigh Damping Model

# CHAPTER 4

# BRIEF INTRODUCTION TO ANALYTICAL METHODS

## 4.1 REVIEW OF ANALYTICAL METHODS USED FOR STRUCTURES WITH DIFFERENT TYPES OF SUPPLEMENTAL DAMPERS

There are four analysis methods that could be used for analysis of structures with different types of supplemental dampers under earthquake excitations. These methods are (ATC-33.03):

1. Linear static method

2. Linear dynamic time history method

3. Simplified nonlinear static method

4. Nonlinear dynamic time history method

### 4.1.1 Linear Static Method

This method applies to structures that remain essentially elastic for the design earthquake. It is based on application of a modal analysis procedure using the undamped frequencies and mode shapes of the structure, and the use of damped response spectra for the effective damping provided by the supplemental dampers. These damped response spectra are constructed from the 5%-damped response spectra using appropriate scale factors for higher damping.

Seleemah et al. (1997) and Constantinou et al. (1992) adopted this method to analyse the seismic response of structures with supplemental fluid viscous dampers. ATC-33.03 also describes this procedure.

### 4.1.2 Linear Dynamic Time History Method

The limitations on the use of this method are such that the original structures, exclusive of the supplemental damping system, must remain elastic in the design earthquake. The viscous forces developed in the seismic framing system due to supplemental dampers should be explicitly accounted for in the analysis and design of the seismic framing system (ATC-33.03).

Chang et al. (1993) used this method to analyse and design steel frame structures with added viscoelastic dampers. In his study, the force for a viscoelastic damper can be expressed as the sum of a spring force and a viscous damping force.

Reinhorn et al. (1995) analysed nonlinear complex dampers with linear viscous or viscoelastic dampers by linearizing the complex mathematical model. By this linearization, the damping force can be expressed explicitly as a viscous force and a spring force. Hence, the linear dynamic time history analysis could be performed.

Lobo et al. (1993) also gave a method for formulating the influence of an individual damper's properties on the structural properties for viscoelastic dampers. This influence is represented by a viscous damping matrix and the stiffness matrix.

In some other cases in which the structure has inelastic deformation or the effect of dampers can not be properly expressed as a viscous force, this method has limitations.

### 4.1.3 Simplified Nonlinear Static Method

This method involves a nonlinear pushover analysis of a MDOF structure to obtain the capacity curve for the structure with supplemental dampers. This capacity curve for a MDOF structure can be converted to its equivalent SDOF system using the displacement shape of the structure at the target displacement. Seismic demand of the equivalent SDOF system can be determined either from a smoothed design spectrum or a particular earthquake spectrum which is based on the 5-percent damped response and adjusted for the effective higher damping. These design spectra could be "elastic" or inelastic depending on how the effect of the inelastic deformation of the original structure is to be considered. By evaluating the demand and capacity of the equivalent SDOF system, its peak response can be estimated.

Fajfar used a nonlinear static method for the seismic damage analysis of RC buildings (Fajfar et al., 1996). It was called the N2 method in their paper. In his study, the higher mode effect was neglected.

Reinhorn introduced a nonlinear static analysis technique and its application to structures with supplemental viscoelastic dampers (Reinhorn, 1997, 1995). In his study, the higher mode effect was taken into account.

Rao also adopted this method by using inelastic demand spectra to analyse and design structures with friction dampers (Rao et al., 1995).

ATC-33.03 recommends a nonlinear static analysis procedure for the analysis of a SDOF structure with supplemental dampers.

### 4.1.4 Nonlinear Dynamic Time History Analysis

This method can be used for the analysis of all structures with all types of supplemental dampers, and has been widely used.

Due to the fact that the structure used for this study is allowed to have inelastic deformation and also that the supplemental lead dampers have strongly nonlinear characteristics, the linear analysis methods (both static and dynamic time history) may not be appropriate for this study. The simplified nonlinear static method and the nonlinear dynamic time history method were adopted for analysis of structures with supplemental lead dampers. For the simplified nonlinear static method used here, the higher mode effects were neglected.

Comparison and some limitations of these two methods are introduced in the following discussion.

## 4.2 ANALYTICAL METHODS ADOPTED FOR THIS STUDY

### 4.2.1 Time History Analysis

The performance of the structural model with the supplemental dampers was first determined analytically through time history analysis. This analysis was performed using step-by-step integration of the equations of motion shown in Eq (3-4). Models used for different types of members in the structure have been discussed in Chapter 3.

The 2-D nonlinear time history analysis program RUAUMOKO (Carr, 1996) developed in the Civil Engineering Department of University of Canterbury has been used for this analysis. The Newmark constant average acceleration method was used for the integration of the equations of motion.

This method has the advantage that all the important inelastic dynamic response characteristics of the structure can be considered explicitly in the time history analysis. However, great caution must be exercised in the selection of ground motions and in the interpretation of results. This is due to the fact that no two earthquakes are alike. This method may also be time consuming and uneconomical in most practical design cases.

### 4.2.2 Pushover Analysis

A pushover analysis is a simpler nonlinear analysis technique that can be used to estimate the dynamic demands imposed on a structure by earthquake ground motions. This procedure involves applying a predetermined lateral load pattern (a set of lateral forces) that approximately represents the relative inertia forces and pushing the structure under this load pattern. These lateral loads are incrementally increased until the deflection of the top level of the structure reaches the value expected in a design earthquake. The objective of the pushover analysis is to obtain estimates of the member forces and the global and local deformations a structure is likely to experience in a design earthquake, and to use these estimates to assess the integrity of the structural system.

For structures that behave mainly in the fundamental mode, the pushover analysis will very likely provide good estimates of global as well as local inelastic deformation demands. This analysis will also expose possible hidden design weakness that may not be found in an elastic

analysis. For structures in which higher mode effects are significant, results from the pushover analysis may be grossly inaccurate. Hence, a basic assumption for the pushover analysis is that the structure will behave primarily in its fundamental mode. Traditionally, it is also assumed that the lateral force pattern does not vary during an analysis. This assumption is not necessary when an adaptive pushover analysis is performed (Satyarno et al., 1998). The program RUAUMOKO can also be used to conduct the pushover analysis.

### 4.2.3 Simplified Nonlinear Static Analysis Method

The simplified nonlinear static method provides a means of predicting the response of the structure without having to perform a nonlinear time history analysis. This method utilises ground motion information derived from a smoothed design spectrum. These smoothed design spectra may represent the effects of different seismic events of different magnitudes and source to site distances. This method has its shortcoming in the inability to represent realistically all changes in the inelastic dynamic response characteristics of the structure caused by stiffness degradation and strength redistribution. When higher mode effects become important, this shortcoming is significant. However, recognising the limitation of nonlinear time history analysis, this method is relatively simple and in general can give rather good results concerning the peak response provided higher mode effects are not significant.

The simplified nonlinear static analytical method is based on the assumption that the response of the structure can be related to the response of an equivalent SDOF system. This assumption requires that the structural response be controlled by a single mode.

Applying this simplified nonlinear static method to the structure with the supplemental dampers, the effect of the dampers can be considered through the effective stiffness and the equivalent viscous damping due to these supplemental dampers.

The pushover analysis and simplified nonlinear static analysis method will be investigated and verified in the following chapters.

## 4.3 EARTHQUAKE EXCITATIONS

Since the simplified nonlinear static analysis method utilises ground motion information derived from smoothed design spectra, design code compatible time histories are necessary in order to be able to conduct nonlinear time history analyses and compare the results from the time history analyses with the results from the simplified nonlinear static analysis.

There are several possibilities for scaling natural earthquake records to match the design spectra. They are (Moss et al., 1999):

1. Scale the peak acceleration to about 0.4-0.45g;

2. Scale the record so as to match the spectrum in a range of period of interest;

3. Scale the record so as to match the spectrum at the first mode period of the structure;

4. Scale the record to match the spectrum at all frequencies.

In method 4, a natural earthquake record is transformed into the frequency domain and the response at every frequency is scaled so that it matches the design spectra without changing the phase characteristics. The scaled record is then transformed back into the time domain. Some different natural earthquake records can be selected as the seed records. Three different natural earthquake records are selected here: El Centro 1940 N-S component, Olympia N86E component and Taft N21E component. NZS4203 1992 design code compatible earthquake time histories based on these three natural earthquake records and their spectra are shown in Figs. 4.1, 4.2, 4.3 respectively.

## 4.4 COMPARISON OF DYNAMIC RESPONSE OF THE STRUCTURE WITH THE SUPPLEMENTAL DAMPERS USING THE RAMBERG-OSGOOD MODEL AND THE ELASTIC-PLASTIC MODEL

Two models were adopted for the hysteresis loops to match the test results of the lead dampers. They were the Ramberg-Osgood model and the elastic-plastic model. Nonlinear time history analyses of the structure with the supplemental dampers subjected to the three NZS4203 design code compatible earthquake time histories by using these two models were conducted. Three parameters were used to compare the structural dynamic response. They

were the peak roof displacement, the peak interstorey drift and the peak base shear. The results are shown in Tables 4.1, 4.2, 4.3 and Figs.4.4, 4.5, 4.6.

It can be seen both from Tables 4.1, 4.2, 4.3 and Figs.4.4, 4.5, 4.6 that the results for these two models are very similar. Only for the peak interstorey drift of the structure under Taft N21E NZS4203 code compatible earthquake, is the difference relatively greater. In general, the difference in the structural dynamic response is very small for these two models. For simplicity, the elastic-plastic model was adopted for later analyses.

| Model | Peak Roof Displacement (cm) | Peak Interstorey Drift (cm) | Peak Base Shear (KN) |
|---|---|---|---|
| Ramberg-Osgood | 15.40 | 2.079 | 1272.3 |
| Elasto-plastic | 15.26 | 1.996 | 1239.3 |
| Difference | 0.91% | 3.99% | 2.59% |

Table 4.1 Comparison of the structural dynamic response for the two different models under El Centro 1940 NZS4203 compatible earthquake

| Model | Peak Roof Displacement (cm) | Peak Interstorey Drift (cm) | Peak Base Shear (KN) |
|---|---|---|---|
| Ramberg-Osgood | 13.29 | 2.199 | 1476.7 |
| Elasto-plastic | 13.43 | 2.176 | 1435.7 |
| Difference | -1.05% | 1.05% | 2.78% |

Table 4.2 Comparison of the structural dynamic response for the two different models under Olympia N86E NZS4203 compatible earthquake

| Model | Peak Roof Displacement (cm) | Peak Interstorey Drift (cm) | Peak Base Shear (KN) |
|---|---|---|---|
| Ramberg-Osgood | 19.9 | 2.855 | 1395.4 |
| Elasto-plastic | 18.94 | 2.602 | 1365.4 |
| Difference | 4.82% | 8.86% | 2.15% |

Table 4.3 Comparison of the structural dynamic response for the two different models under Taft N21E NZS4203 compatible earthquake

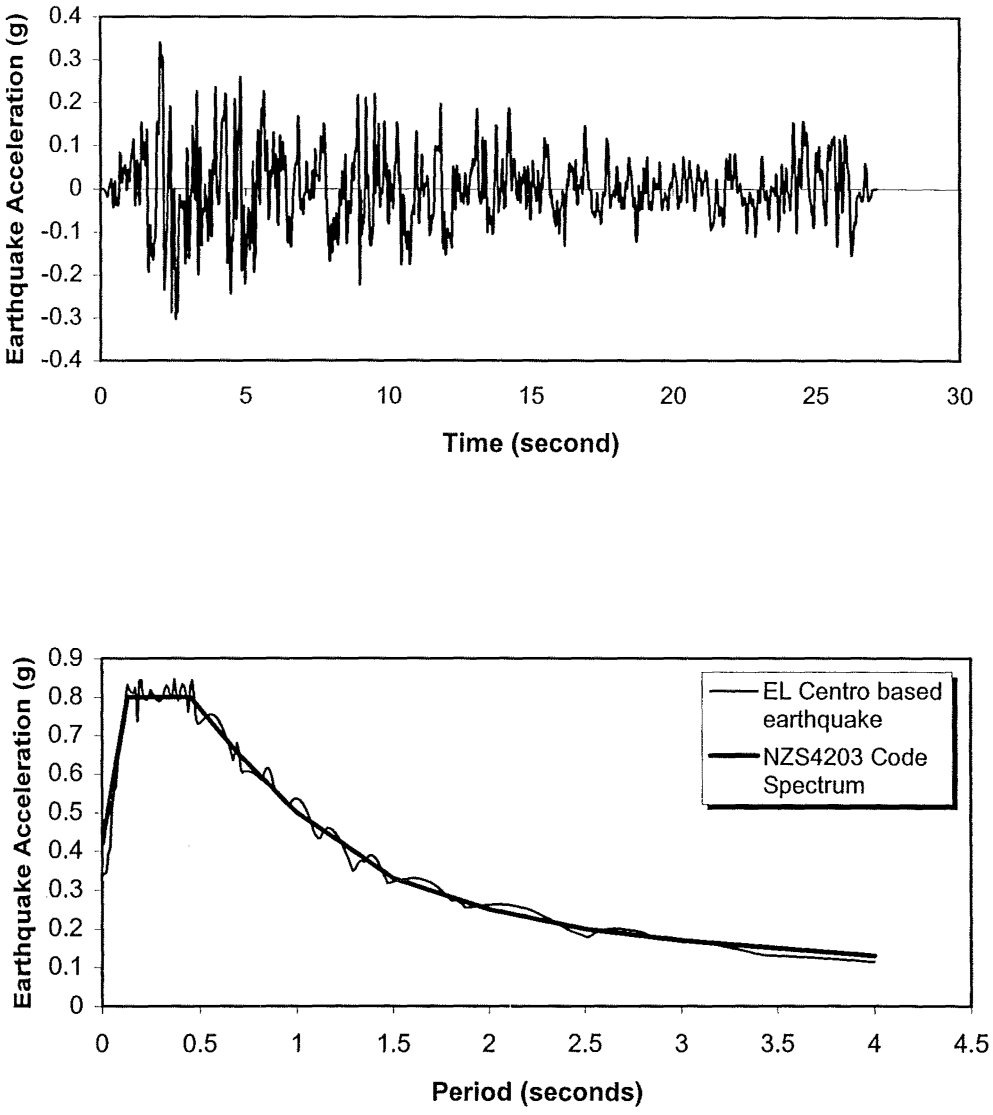


Figure 4.1 El Centro 1940 NZS4203 compatible earthquake time history and spectrum

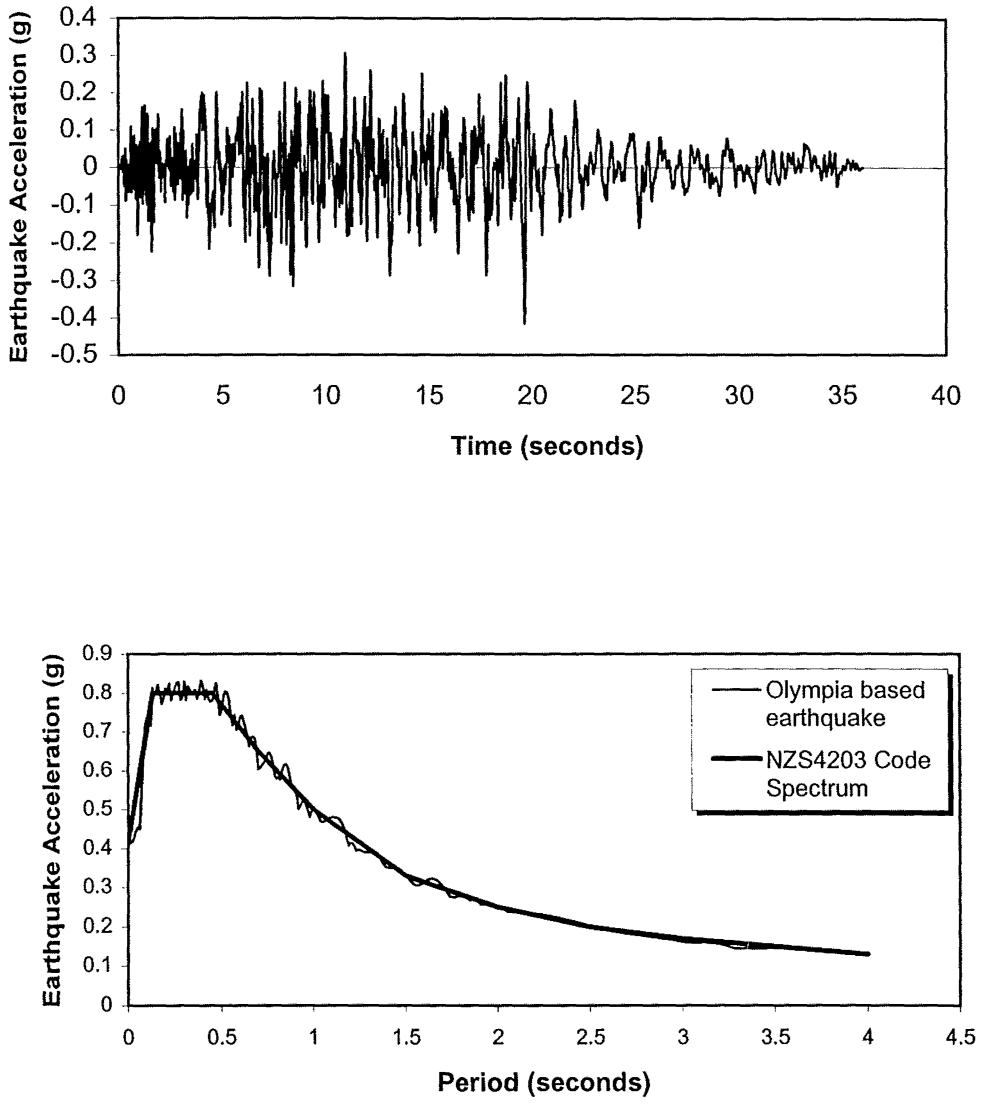


Figure 4.2 Olympia N86E NZS4203 compatible earthquake time history and spectrum

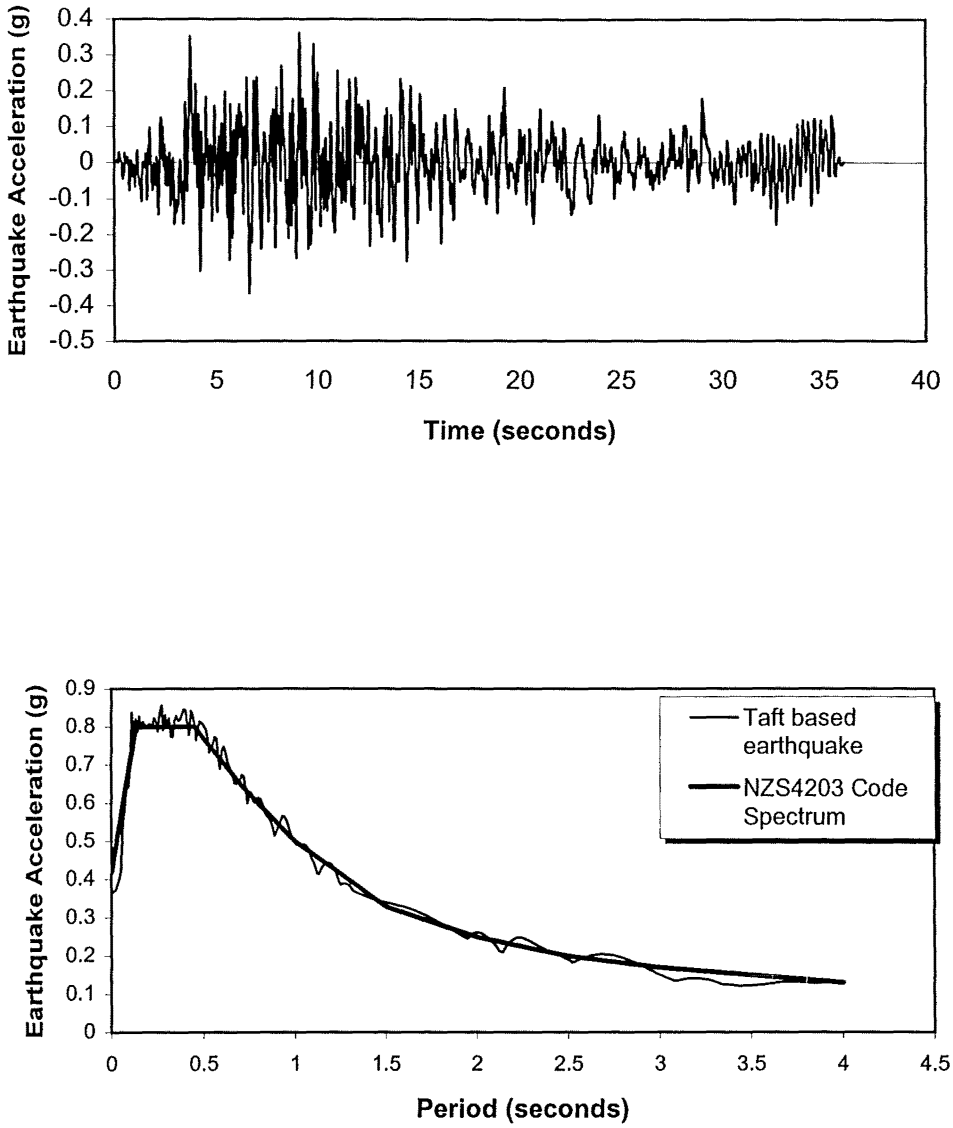


Figure 4.3 Taft N21E NZS4203 compatible earthquake time history and spectrum

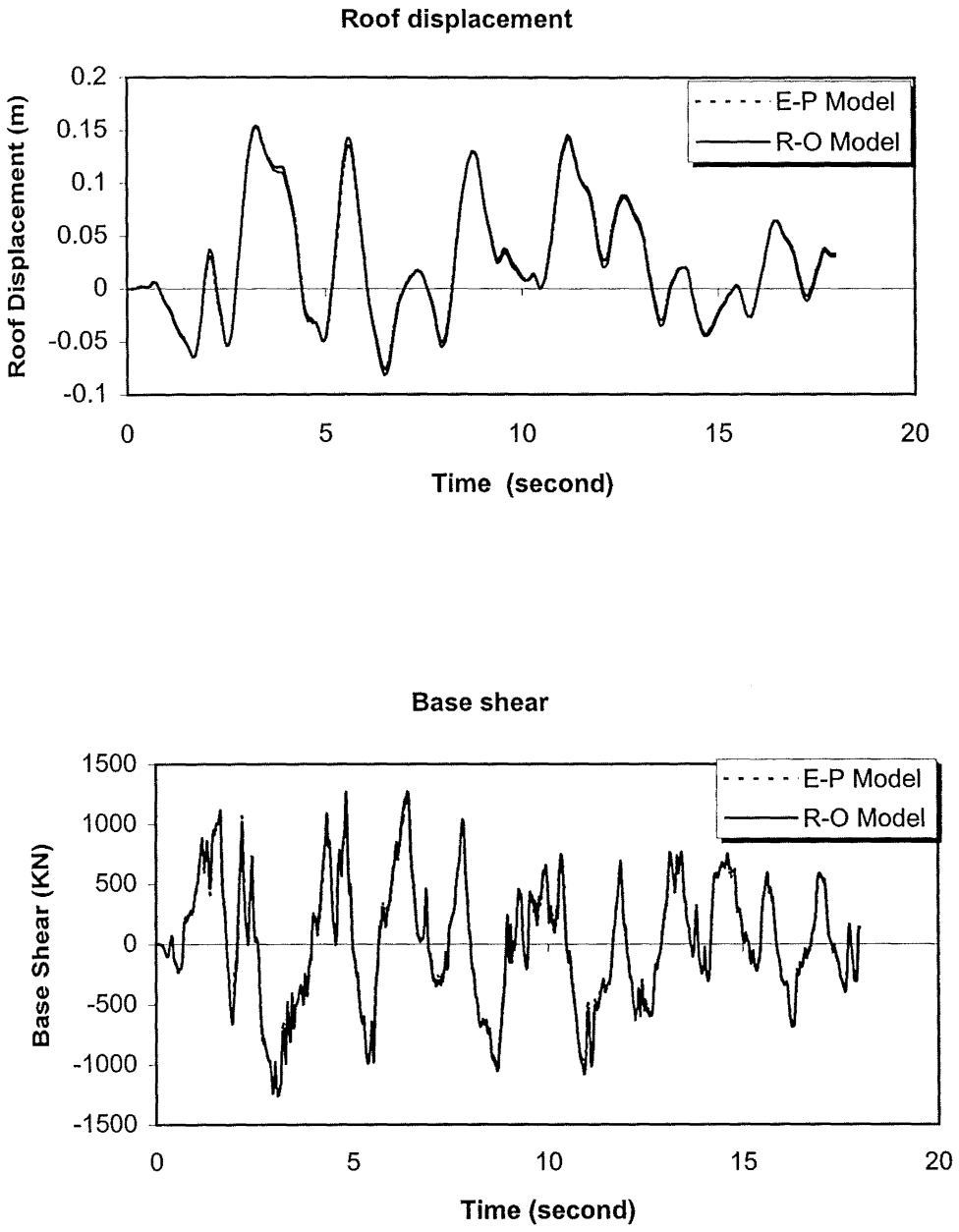


Figure 4.4 Comparison of some response time histories using two different models for the dampers under El Centro 1940 NZS4203 compatible earthquake

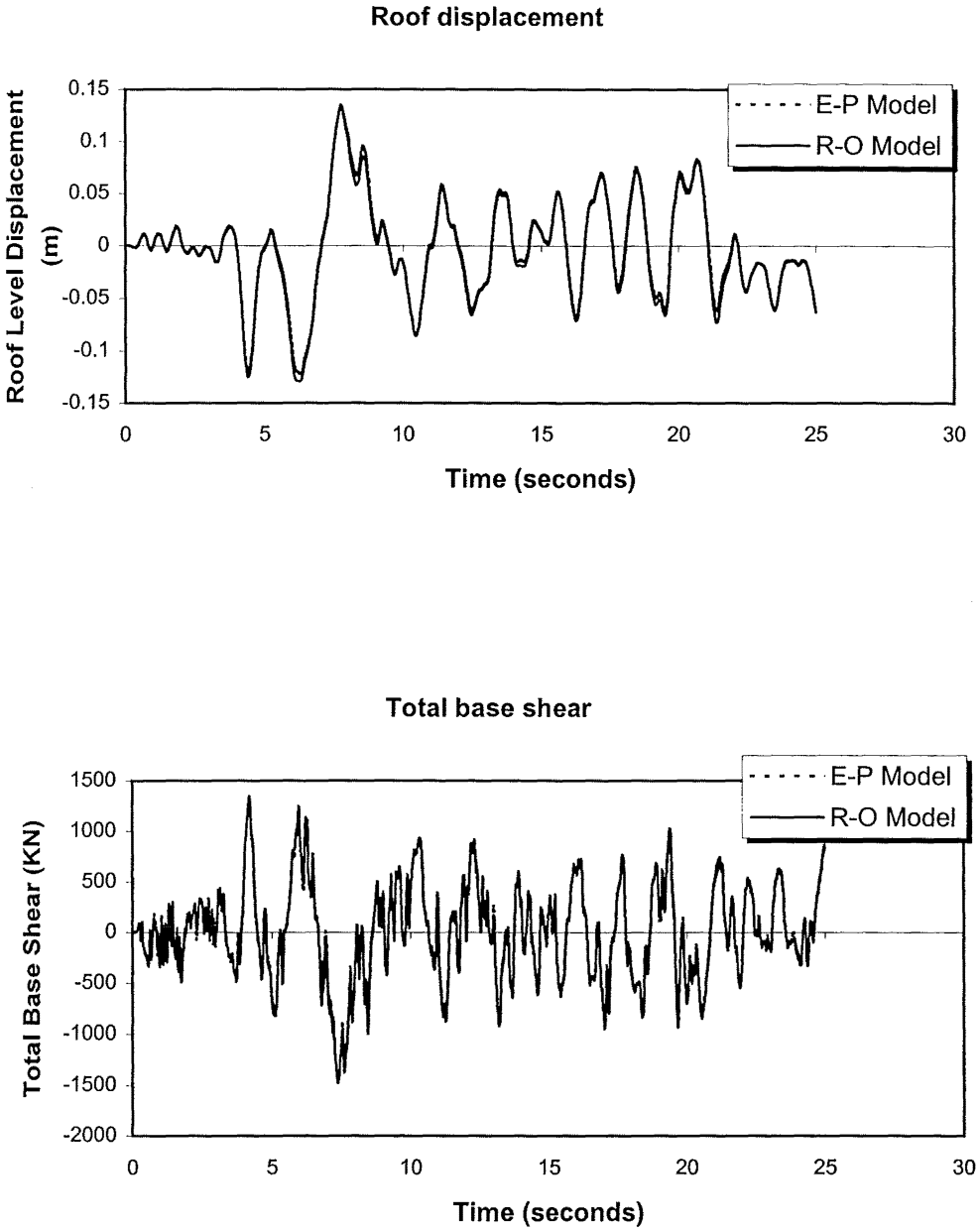


Figure 4.5 Comparison of some response time histories using two different models for the dampers under olympia N86E NZS4203 compatible earthquake

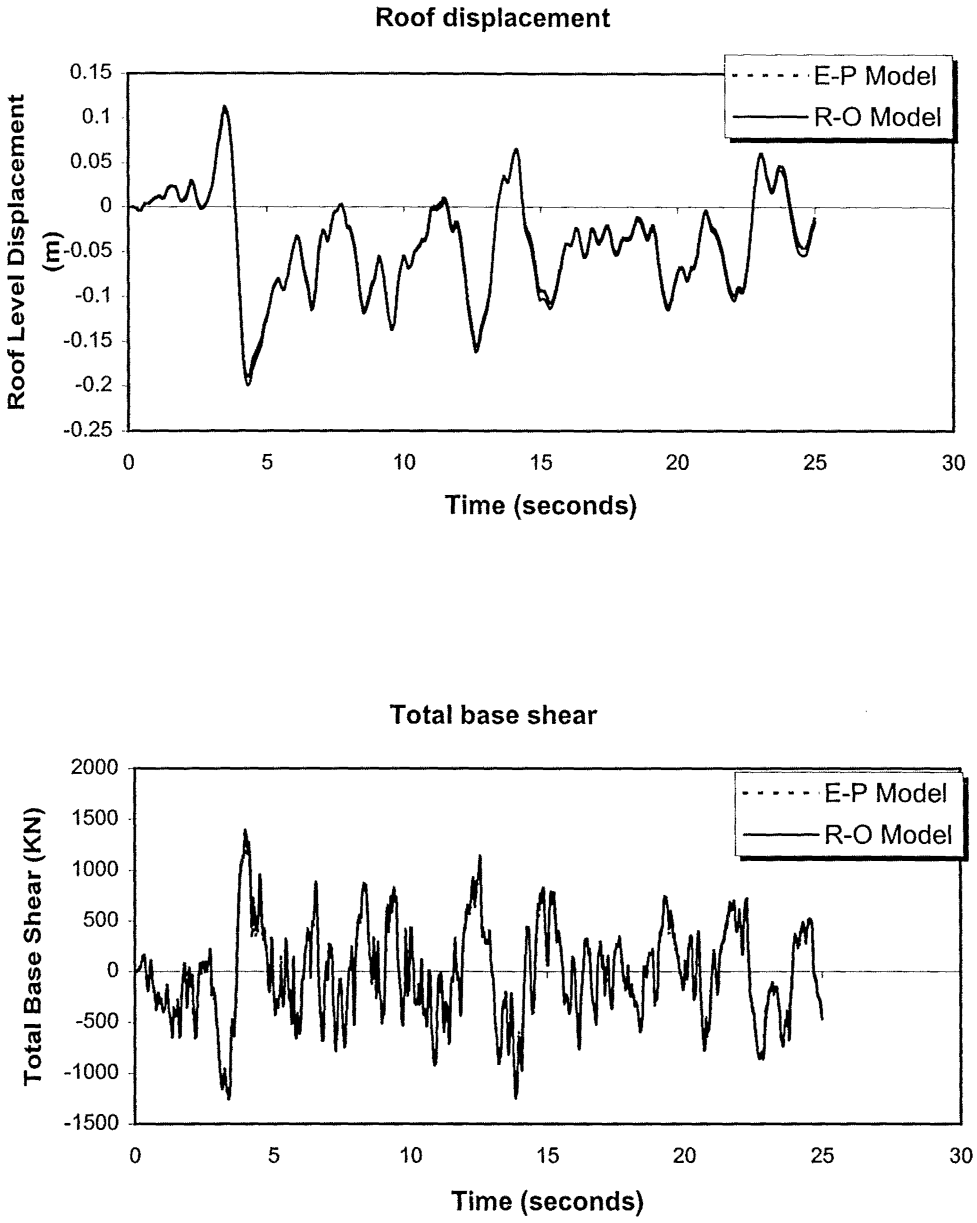


Figure 4.6 Comparison of some response time histories using two different models for the dampers under Taft N21E NZS4203 compatible earthquake

# CHAPTER 5

# PLACEMENT AND DISTRIBUTION OF THE SUPLEMENTAL DAMPERS IN THE STRUCTURE

## 5.1 PLACEMENT OF THE SUPPLEMENTAL DAMPERS IN THE STRUCTURE

It is first assumed that all the supplemental dampers in the structure are identical. Four types of placement of the dampers throughout the structure are discussed here. They are: only one damper at the 1st level; one damper every third level; one damper every second level; and one damper for every level (Fig.5.1). The number of dampers for these four types of distribution is 1, 4, 6, and 12 respectively. Two levels of yield strength of the dampers are adopted: 211KN and 422KN. The 211KN damper represents the one shown in Chapter 3 and the 422KN damper approximately represents two 211KN-yield-strength dampers for the relevant floor level.

Three NZS4203 code compatible time histories were used to conduct time history analyses of the structure with these different placements of the dampers. The results are shown in Table 5.1 to Table 5.6 and Fig.5.2 to Fig.5.4. The peak roof displacement and the peak interstorey drift are used as parameters for comparison. In these tables the results of all cases are compared with those of the original structure without dampers and the reductions due to the supplemental dampers are shown in brackets.

It can be seen that only one damper at the 1st level is not sufficient. Reduction of the response caused by the supplemental dampers is negligible. This means that additional damping caused by merely one damper is quite small in a multi-storey structure. While dampers are placed at every third level (4 dampers for the structure), the effect of the supplemental dampers becomes significant. While the number of dampers increases from 4 to 12, the response of the structure is reduced further. For the El Centro and Olympia N86E NZS4203 compatible earthquakes, this trend is more obvious. Response reduction due to the increase of the number of dampers is significant. For the TAFT N21E NZS4203 compatible earthquake this trend still holds but is not as significant as for the other two earthquakes.

Comparing the case in which dampers are placed at every second storey with a yield strength equal to 422KN with the one in which dampers are placed at every storey but with a yield strength equal to 211KN (half of the former case), the results are shown in Table 5.7—Table 5.9. It can be seen that the response of the latter case is smaller than the former case for all three earthquakes. It can also be observed that the differences of these two cases for all three different earthquakes are quite small. Hence, the placement of the supplemental dampers in which dampers are placed at every second storey can be effectively replaced by the case in which dampers are evenly placed at all storeys throughout the structure but with only half the yield strength.

Based on the above observation, it can be concluded that an uniform placement of the dampers throughout the structure is better than the case where dampers are just placed at some storeys. Hence, in this study the distribution in which dampers are placed at all storeys of the structure evenly was adopted.

## 5.2 DISTRIBUTION OF THE DAMPER YIELD STRENGTHS IN THE STRUCTURE

For a structure with the supplemental dampers which are placed at all storeys of the structure, a different distribution of the yield strength of the dampers over the height of the structure will lead to different structural responses. Is it necessary to have the same yield strength for all the dampers? What kind of distribution of the yield strength for the dampers in the structure should be adopted?

The intention here is to find out a satisfactory distribution of the damper strength rather than an optimal distribution (Lin et al., 1998a). Two parameters are widely used to measure the structural demand and response. They are the peak interstorey drift and the peak base shear. The peak interstorey drift is a good measure of the structural damage state and the non-structural damage experienced by the structure during the earthquake. The main purpose of incorporating the supplemental dampers into the structure is to reduce the displacement and deformation of structures. The peak base shear represents the demand on the foundations. It is not desirable that the peak base shear is greatly increased due to the supplemental dampers. Hence these two parameters are mainly used in the following comparisons.

For a given yield strength of the damper at the first storey of the structure, different distributions of strength levels of the dampers over the height of the structure can be chosen.

Four types of distributions of the yield strengths of the dampers are compared here. These four types of distribution of the yield strengths of the dampers correspond to four types of lateral load patterns that an earthquake might exert on a structure through its inertial forces. These four types of lateral load patterns are shown in Fig.5.5. The yield strengths of the dampers in the structure for these cases are proportional to the storey shear due to each type of lateral load pattern.

Case I: the distribution of the yield strengths of the dampers is proportional to the storey shear forces due to the first load pattern (only one lateral force acting at the top level). So the dampers over the height of the structure have the same yield strength. The distribution vector of the yield strengths of the dampers over the height of the structure is

[1,1,1,1,1,1,1,1,1,1,1,1,]

Case-II: the lateral load pattern is parabolic. The distribution vector of the yield strengths of the dampers over the height of the structure is (proportional to the storey shear due to this type of lateral load pattern)

[1,0.9985,0.9923,0.9785,0.9539,0.9154,0.86,0.7846,0.6862,0.5615,0.4077,0.2215]

Case-III: the lateral load pattern is an inverted-triangular distribution. The distribution vector of the yield strengths of the dampers over the height of the structure is (proportional to the storey shear due to this type of lateral load pattern)

[1,0.9872,0.9615,0.9231,0.8718,0.8077,0.7308,0.641,0.5385,0.4231,0.2949,0.1539]

Case-IV: the lateral load pattern is uniform. The distribution vector of the yield strengths of the dampers over the height of the structure is (proportional to the storey shear due to this type of lateral load distribution)

[1,0.9167,0.8333,0.75,0.6667,0.5833,0.5,0.4167,0.3333,0.25,0.1667,0.0833]

The common yield strength of the damper at the 1$^{st}$ level $F_{yd1}$ is taken to be 316.5KN (=211×1.5) and 422KN (=211×2). The peak interstorey drift and the peak base shear of these four cases under three different earthquakes are shown in Tables 5.10 to 5.15. All these four cases are compared with case-III and the diferences are shown in brackets.

For the El Centro 1940 NZS4203 compatible earthquake, case-III is the optimal case amongst these four cases (both $F_{yd1}$ = 316.5KN and 422KN, see Table 5.10 and Table 5.13). The peak interstorey drift of case-III is minimal. The peak base shear in case-III is only greater than that of case-IV by 4.95% yet the peak interstorey drift is smaller than that by 13.6% respectively. The reduction in the peak interstorey drift is the main purpose for utilising the supplemental dampers. Comparing case-I and case-III, it can be seen that the peak interstorey drift of case-I is greater than that of case-III by 15.925% and 22.39% for these two yield strengths of the damper at the 1$^{st}$ level. The peak base shear of case-I is also larger than that of case-III by 7.43-7.98%. Hence, It is not desirable to utilise the same yield strength of the dampers over the height of the structure.

For the Olympia N86E and Taft N21E NZS4203 compatible earthquakes, it can be seen again that case-III is better than case-I with respect to the peak interstorey drift and the peak base shear (Table 5.12, Table 5.14, Table 5.15) except the case in Table 5.11. But even in Table 5.11, the difference is quite small. The difference of cases-II, III and IV for these two earthquakes is quite small. Case-III is close to the optimal case. Again it can be concluded that it is not desirable to utilise the same yield strengths of the dampers over the height of the structure and case-III can also be regarded as the best strength distribution.

The distributions of maximum interstorey drifts in the storeys for case-I and case-III are shown in Fig.5.6, Fig.5.7 and Fig.5.8. It can be seen that for case-I the maximum interstorey drifts in the upper part of the structure are extremely small while in the lower part of the structure they are relatively larger. The distribution in case-III is more uniform than in case-I.

From the above comparison, it can be found that the response difference due to the different distributions of yield strengths of the dampers is not too great. However, from the point of view of the cost of the dampers it can be seen that it is not necessary to have the same damper strengths in all storeys.

Table 5.16 shows the comparison of the total yield strengths of the supplemental dampers for the four different distributions of the damper yield strengths. It can be seen that the total damper yield strengths in case-III are only 69.45% of case-I. Smaller dampers means lower cost. The cost in case-III is much less than case-I, yet the structural response in case-III is generally smaller than the one in case-I.

Fig.5.9 and Fig.5.10 show the damper force time history at the 1st, 6th, 10th, and the 12th levels of the structure with the supplemental dampers under the EL Centro 1940 NZS 4203 compatible earthquake for case-I and case-III respectively. It can be seen that in case-I the dampers at the 1st and 6th levels are into the yielding stage, but in many cycles the damper at the 10th level remains in its elastic stage and the damper at the 12th level never yields. In case-III dampers at different levels yield. This means that for case-I at the upper levels of the structure dampers do not yield simultaneously and some dampers do not yield. For case-III all devices yield simultaneously. This will lead to maximum energy dissipation.

From the above it can be deduced that the distribution of the yield strengths of the dampers along the height of the structure which are proportional to the storey shear due to the inverted triangular lateral load pattern is a satisfactory distribution. This distribution will be adopted for further analyses and design used in this study. There are some other advantages for adopting this distribution of damper strengths that can make analysis and design much easier. These will be discussed in later chapters.

## 5.3 INFLUENCE OF INITIAL STIFFNESS OF THE DAMPERS

The distribution of the strength levels of the dampers over the height of the structure is taken to be proportional to the storey shears due to the inverted-triangular lateral load pattern. The influence of different initial stiffness of the dampers is investigated here.

The ratio of the initial stiffness of the damping system to the initial stiffness of the original structure is $S_R$. It is assumed that the braces that connect the supplemental dampers to the structure are rigid. Hence, the initial stiffness of the damping system is equal to the initial stiffness of the dampers. The influence due to the flexibility of the braces will be discussed later.

It can be shown that:

$$K_d \cos^2 \theta = S_R K_{s1} \tag{5.1}$$

where $K_d$ = initial stiffness of the dampers

$K_{s1}$ = storey initial stiffness of the original structure

$\theta$ = angle of the brace with the damper relative to the horizontal

$S_R$ is taken to be 1, 3, 4, 5, 7, 10, and 15 respectively. The results are shown in Figs.5.11 — 5.13 for the three different code compatible earthquakes. The results for different stiffness ratios are compared with the case in which the stiffness ratio is taken to be 10 and are shown in Table 5.17 — Table 5.19. The peak roof displacement, peak interstorey drift and the total peak base shear are selected to represent the dynamic response of the structure.

From Figs.5.11 — 5.13 it can be observed that once the stiffness ratio $S_R$ reaches a certain value the dynamic response of the structure with the supplemental dampers varies very little with respect to different stiffness ratios. From Table 5.17 — Table 5.19 it can be seen that when the stiffness ratio is greater than 4, even up to 15 the difference in the dynamic response is very small. This shows that once the stiffness ratio exceeds 4, the variation of the initial stiffness of the dampers has very little influence on the dynamic response of the structure with the supplemental dampers. Similar trends for the influence of the initial stiffness of yielding steel dampers can be seen in Pong et al. (1994), Tsai et al. (1993) and Xia et al. (1992.)

## 5.4 INFLUENCE OF FLEXIBILITY OF BRACES

The supplemental dampers are connected to the structure by means of braces. In the foregoing analytical model for the structure with the supplemental dampers it was assumed that the braces used to connect the dampers to the structure were essentially rigid. The stiffness of the brace-damper assembly is represented by the stiffness of the damper. Actually the flexibility of the brace has an effect on the deformation and the effectiveness of the supplemental dampers. Hence the damper unit should be considered as a damper and a brace connected in series. If the brace is assumed to be rigid then the deformation of the damper would be the same as the deformation of the damper-brace assembly.

Since a damper and a brace are connected in series, the stiffness of a brace-damper assembly for the elastic range can be expressed as:

$$K_{bd} = \frac{K_b K_d}{K_b + K_d} = \frac{K_d}{1 + \frac{K_d}{K_b}} \tag{5.2}$$

where $K_{bd}$ = the stiffness of a brace-damper assemble in the elastic range,

$K_b$ = the stiffness of a brace

$K_d$ = the stiffness of a damper in the elastic range.

The force-deformation relationship for dampers is elasto-plastic while the force-deformation relationship for the brace is elastic. The force-deformation relationship for the brace-damper assemblies can also be represented by an elasto-plastic model. For a brace-damper assembly, the initial stiffness for the elasto-plastic model can be obtained from Eq(5.2). The yield force for a brace-damper assembly is equal to that of the damper itself.

From Eq(5.1) and (5.2) we can have:

$$\frac{K_d}{1+\frac{K_d}{K_b}}\cos^2\theta = S_R K_{s1} \tag{5.3}$$

From the study of the influence of the initial stiffness of the dampers mentioned above, it was known that to ensure the effectiveness of the dampers, the stiffness ratio $S_R$ must be greater than or equal to 4. From Eq(5.3) it can be obtained:

$$\frac{K_d}{K_{s1}}\frac{1}{1+\frac{K_d}{K_b}}\cos^2\theta \geq 4 \tag{5.4}$$

Thus

$$K_b \geq \frac{K_d}{\frac{K_d}{K_{s1}}\frac{\cos^2\theta}{4}-1} \tag{5.5}$$

If the requirement of eq(5.5) is met, the effectiveness of the dampers can be assured.

Hence, the stiffness of the dampers and the braces should meet the following requirements:

$$\begin{cases} K_d \geq \dfrac{4}{\cos^2\theta} K_{s1} \\ K_b \geq \dfrac{K_d}{\dfrac{K_d}{K_{s1}} \dfrac{\cos^2\theta}{4} - 1} \end{cases} \tag{5.6}$$

## 5.5 EFFECT OF THE SUPPLEMENTAL DAMPERS ON THE REDUCTION OF STRUCTURAL RESPONSES

The structural model introduced in Chapter 3 was used to conduct nonlinear time history analyses. The supplemental dampers were installed in all storeys as shown in Fig.3.5. The satisfactory distribution of the yield strengths of the dampers in the storeys is adopted (the yield strength of the damper at the 1st level $F_{yd1}$ = 422KN). The stiffness ratio is taken to be 10. The three NZS4203 code compatible time histories mentioned previously were used as the earthquake excitations. The comparisons of the distribution of maximum interstorey drifts in the storeys for the structure with the supplemental dampers as well as the structure without dampers are shown in Fig.5.14. The comparisons of the storey shear forces in the columns in the storeys of the structure with the supplemental dampers and the structure without dampers are shown in Fig.5.15. The maximum member ductilities for each storey are shown in Table 5.20 — Table 5.22. The roof displacement, roof acceleration, total base shear together with some of the interstorey drift response time histories are shown in Fig.5.16, Fig.5.17 and Fig.5.18.

Some preliminary conclusions can be made from these comparisons between the dynamic response of the structure with the supplemental dampers (with the satisfactory distribution of the yield strengths) and the structure without the dampers:

1. The supplemental dampers have a significant effect on the structural response under earthquake excitations.

2. Displacements, interstorey drifts and the accelerations of the structure are, in general, greatly reduced by the supplemental dampers.

3. The ductility demands on the main structure under the design earthquake is markedly reduced.

4. The total base shear of the structure with the supplemental dampers is increased slightly in comparison to that of the original structure without dampers. This is due to the additional forces associated with the dampers.

5. The storey shear forces in the columns in the storeys are reduced by the supplemental dampers. It can also be seen that the distribution of the storey shear forces is very close to that of the first mode shear distribution. The higher mode effect is greatly reduced for the structure having this distribution of dampers.

| | Peak Roof Displacement (cm) | |
|---|---|---|
| | $F_{yd}$ = 211KN | $F_{yd}$ = 422KN |
| Original structure without damper | 25.49 (0) | 25.49 (0) |
| One damper only | 24.91 (reduced by 2.28%) | 24.45 (reduced by 4.08%) |
| One damper Every third storey | 19.00 (reduced by 25.46%) | 17.08 (reduced by 32.99%) |
| One damper every second storey | 17.48 (reduced by 31.42%) | 15.79 (reduced by 38.05%) |
| One damper every storey | 15.26 (reduced by 40.13%) | 13.34 (reduced by 47.67%) |

Table 5.1 Comparison of the peak roof displacement for the structure with different number of dampers under El Centro 1940 NZS4203 compatible earthquake

| | Peak Interstorey Drift (cm) | |
|---|---|---|
| | $F_{yd}$ = 211KN | $F_{yd}$ = 422KN |
| Original structure without damper | 3.799 (0) | 3.799 (0) |
| One damper only | 3.784 (reduced by 0.395%) | 3.669 (reduced by 3.42%) |
| One damper Every third storey | 2.661 (reduced by 29.96%) | 2.432 (reduced by 35.98%) |
| One damper every second storey | 2.335 (reduced by 38.54%) | 2.149 (reduced by 43.43%) |
| One damper every storey | 1.996 (reduced by 47.46%) | 1.997 (reduced by 47.43%) |

Table 5.2 Comparison of the peak interstorey drift for the structure with different number of dampers under El Centro 1940 NZS4203 compatible earthquake

| | Peak Roof Displacement (cm) | |
|---|---|---|
| | $F_{yd}$ = 211KN | $F_{yd}$ = 422KN |
| Original structure without damper | 27.71 (0) | 27.71 (0) |
| One damper only | 27.38 (reduced by 1.19%) | 27.88 (increased by 0.61%) |
| One damper Every third storey | 22.12 (reduced by 20.17%) | 18.14 (reduced by 34.54%) |
| One damper every second storey | 18.96 (reduced by 31.58%) | 14.25 (reduced by 48.58%) |
| One damper every storey | 13.43 (reduced by 51.53%) | 10.63 (reduced by 61.64%) |

Table 5.3 Comparison of the peak roof displacement for the structure with different number of dampers under Olympia N86E NZS4203 compatible earthquake

| | Peak Interstorey Drift (cm) | |
|---|---|---|
| | $F_{yd}$ = 211KN | $F_{yd}$ = 422KN |
| Original structure without damper | 3.923 (0) | 3.923 (0) |
| One damper only | 3.935 (increased by 0.31%) | 4.015 (increased by 2.35%) |
| One damper Every third storey | 3.455 (reduced by 11.93%) | 2.959 (reduced by 24.57%) |
| One damper every second storey | 3.113 (reduced by 20.65%) | 2.338 (reduced by 40.4%) |
| One damper every storey | 2.176 (reduced by 44.53%) | 1.704 (reduced by 56.56%) |

Table 5.4 Comparison of the peak interstorey drift for the structure with different number of dampers under Olympia N86E NZS4203 compatible earthquake

| | Peak Roof Displacement (cm) | |
|---|---|---|
| | $F_{yd}$ = 211KN | $F_{yd}$ = 422KN |
| Original structure without damper | 27.34 (0) | 27.34 (0) |
| One damper only | 26.08 (reduced by 4.61%) | 27.09 (reduced by 0.91%) |
| One damper Every third storey | 20.47 (reduced by 25.13%) | 20.24 (reduced by 25.97%) |
| One damper every second storey | 19.92 (reduced by 27.14%) | 19.92 (reduced by 27.14%) |
| One damper every storey | 18.94 (reduced by 30.72%) | 17.62 (reduced by 35.55%) |

Table 5.5 Comparison of the peak roof displacement for the structure with different number of dampers under Taft N21E NZS4203 compatible earthquake

| | Peak Interstorey Drift (cm) | |
|---|---|---|
| | $F_{yd}$ = 211KN | $F_{yd}$ = 422KN |
| Original structure without damper | 3.901 (0) | 3.901 (0) |
| One damper only | 3.729 (reduced by 4.41%) | 3.801 (reduced by 2.56%) |
| One damper Every third storey | 2.708 (reduced by 30.58%) | 2.801 (reduced by 28.2%) |
| One damper every second storey | 2.640 (reduced by 32.33%) | 2.762 (reduced by 29.2%) |
| One damper every storey | 2.602 (reduced by 33.3%) | 2.701 (reduced by 30.76%) |

Table 5.6 Comparison of the peak interstorey drift for the structure with different number of dampers under Taft N21E NZS4203 compatible earthquake

| | Peak Roof Displacement (cm) | Peak Interstorey Drift (cm) |
|---|---|---|
| Dampers at every second storey (Fyd = 422KN) | 15.79 | 2.149 |
| Dampers at every storey (Fyd = 211KN) | 15.26 | 1.996 |
| Difference of these two cases | 3.36% | 7.12% |

Table 5.7 Comparison of the response for the structure with two particular placements of dampers under El Centro 1940 NZS4203 compatible earthquake

| | Peak Roof Displacement (cm) | Peak Interstorey Drift (cm) |
|---|---|---|
| Dampers at every second storey (Fyd = 422KN) | 14.25 | 2.338 |
| Dampers at every storey (Fyd = 211KN) | 13.43 | 2.176 |
| Difference of these two cases | 5.75% | 6.93% |

Table 5.8 Comparison of the response for the structure with two particular placements of dampers under Olympia N86E NZS4203 compatible earthquake

| | Peak Roof Displacement (cm) | Peak Interstorey Drift (cm) |
|---|---|---|
| Dampers at every second storey (Fyd = 422KN) | 19.92 | 2.762 |
| Dampers at every storey (Fyd = 211KN) | 18.94 | 2.602 |
| Difference of these two cases | 4.92% | 5.79% |

Table 5.9 Comparison of the response for the structure with two particular placements of dampers under Taft N21E NZS4203 compatible earthquake

| | Peak interstorey drift (cm) | | peak base shear (KN) | |
|---|---|---|---|---|
| Case-I | 2.003 | (15.92%) | 1379.3 | (7.43%) |
| Case-II | 1.807 | (4.57%) | 1320.1 | (2.82%) |
| Case-III | 1.728 | (0) | 1283.9 | (0) |
| Case-IV | 1.963 | (13.6%) | 1220.4 | (-4.95%) |

Table 5.10 Comparison of the response for the structure with four different distributions of the yield strength of the dampers under El Centro 1940 NZS4203 compatible earthquake ($F_{yd1}$=316.5KN)

| | Peak interstorey drift (cm) | | peak base shear (KN) | |
|---|---|---|---|---|
| Case-I | 1.712 | (-5.36%) | 1447.2 | (-0.44%) |
| Case-II | 1.706 | (-5.69%) | 1445.7 | (-0.54%) |
| Case-III | 1.809 | (0) | 1453.6 | (0) |
| Case-IV | 2.053 | (13.32%) | 1451.0 | (-0.18%) |

Table 5.11 Comparison of the response for the structure with four different distributions of the yield strength of the dampers under Olympia N86E NZS4203 compatible earthquake ($F_{yd1}$=316.5KN)

| | Peak interstorey drift (cm) | | peak base shear (KN) | |
|---|---|---|---|---|
| Case-I | 2.666 | (10.62%) | 1482.2 | (6.13%) |
| Case-II | 2.494 | (3.49%) | 1445.8 | (3.52%) |
| Case-III | 2.410 | (0) | 1396.6 | (0) |
| Case-IV | 2.370 | (-1.66%) | 1330.0 | (-4.77%) |

Table 5.12 Comparison of the response for the structure with four different distributions of the yield strength of the dampers under Taft N21E NZS4203 compatible earthquake ($F_{yd1}$=316.5KN)

| | Peak interstorey drift (cm) | | peak base shear (KN) | |
|---|---|---|---|---|
| Case-I | 1.984 | (22.39%) | 1502.7 | (7.98%) |
| Case-II | 1.760 | (8.58%) | 1442.0 | (3.62%) |
| Case-III | 1.621 | (0) | 1391.6 | (0) |
| Case-IV | 1.842 | (13.63%) | 1307.2 | (-6.07%) |

Table 5.13 Comparison of the response for the structure with four different distributions of the yield strength of the dampers under El Centro 1940 NZS4203 compatible earthquake ($F_{yd1}$=422KN)

| | Peak interstorey drift (cm) | | peak base shear (KN) | |
|---|---|---|---|---|
| Case-I | 1.705 | (2.9%) | 1548.6 | (2.99%) |
| Case-II | 1.716 | (3.56%) | 1530.3 | (1.77%) |
| Case-III | 1.657 | (0) | 1503.7 | (0) |
| Case-IV | 1.658 | (0.06%) | 1459.6 | (-2.93%) |

Table 5.14 Comparison of the response for the structure with four different distributions of the yield strength of the dampers under Olympia N86E NZS4203 compatible earthquake ($F_{yd1}$=422KN)

| | Peak interstorey drift (cm) | | peak base shear (KN) | |
|---|---|---|---|---|
| Case-I | 2.693 | (11.84%) | 1641.4 | (7.32%) |
| Case-II | 2.484 | (3.16%) | 1564.8 | (2.32%) |
| Case-III | 2.408 | (0) | 1529.4 | (0) |
| Case-IV | 2.348 | (-2.49%) | 1418.3 | (-7.26%) |

Table 5.15 Comparison of the response for the structure with four different distributions of the yield strength of the dampers under Taft N21E NZS4203 compatible earthquake ($F_{yd1}$=422KN)

| | Total yield strengths of the supplemental dampers (KN) | |
|---|---|---|
| | $F_{yd1}$=316.5KN | $F_{yd1}$=422KN |
| Case-I | 3798 | 5064 |
| Case-II | 2962.47 (78% of Case-I) | 3949.96 (78% of Case-I) |
| Case-III | 2637.55 (69.45% of Case-I) | 3516.74 (69.45% of Case-I) |
| Case-IV | 2057.25 (54.17% of Case-I) | 2743 (54.17% of Case-I) |

Table 5.16 Comparison of the total yield strengths of the supplemental dampers for the four different distributions of the yield strength of the dampers

| Stiffness Factor ($S_R$) | Peak Roof Displacement (cm) | Peak Interstorey Drift (cm) | Peak Base Shear (KN) |
|---|---|---|---|
| 1 | 16.78 (14.23%) | 2.251 (38.87%) | 1398.2 (0.47%) |
| 3 | 15.37 (4.63%) | 1.700 (4.87%) | 1368.4 (-1.67%) |
| 4 | 15.08 (2.66%) | 1.653 (1.97%) | 1377.8 (-0.99%) |
| 5 | 14.95 (1.77%) | 1.629 (0.49%) | 1382.0 (-0.69%) |
| 7 | 14.81 (0.82%) | 1.621 (0) | 1386.7 (-0.35%) |
| 10 | 14.69 (0) | 1.621 (0) | 1391.6 (0) |
| 15 | 14.51 (-1.23%) | 1.625 (0.25%) | 1395.4 (0.27%) |

Table 5.17 Comparison of the response of the structure with different initial stiffness of the supplemental dampers under El Centro 1940 NZS4203 compatible earthquake

| Stiffness Factor ($S_R$) | Peak Roof Displacement (cm) | Peak Interstorey Drift (cm) | Peak Base Shear (KN) |
|---|---|---|---|
| 1 | 13.78 (20.88%) | 1.810 (9.23%) | 1495.8 (-0.53%) |
| 3 | 12.87 (12.89%) | 1.797 (8.45%) | 1501.3 (-0.16%) |
| 4 | 12.41 (8.86%) | 1.765 (6.52%) | 1512.8 (0.61%) |
| 5 | 12.05 (5.70%) | 1.733 (4.59%) | 1514.8 (0.74%) |
| 7 | 11.65 (2.19%) | 1.689 (1.93%) | 1507.5 (0.25%) |
| 10 | 11.40 (0) | 1.657 (0) | 1503.7 (0) |
| 15 | 11.13 (-2.37%) | 1.600 (-3.44%) | 1502.0 (-0.11%) |

Table 5.18 Comparison of the response of the structure with different initial stiffness of the Supplemental dampers under Olympia N86E NZS4203 compatible earthquake

| Stiffness Factor ($S_R$) | Peak Roof Displacement (cm) | Peak Interstorey Drift (cm) | Peak Base Shear (KN) |
|---|---|---|---|
| 1 | 20.65 (10.61%) | 2.884 (19.77%) | 1541.0 (0.76%) |
| 3 | 19.44 (4.12%) | 2.557 (6.19%) | 1457.3 (-4.71%) |
| 4 | 19.38 (3.80%) | 2.536 (5.32%) | 1485.0 (-2.90%) |
| 5 | 19.26 (3.16%) | 2.522 (4.73%) | 1495.7 (-2.20%) |
| 7 | 18.98 (1.66%) | 2.472 (2.66%) | 1514.8(-0.96%) |
| 10 | 18.67 (0) | 2.408 (0) | 1529.4 (0) |
| 15 | 18.31 (-1.93%) | 2.359 (-2.03%) | 1540.4 (0.72%) |

Table 5.19 Comparison of the response of the structure with different initial stiffness of the Supplemental dampers under Taft N21E NZS4203 compatible earthquake

| | Maximum member ductility demand at the storeys | |
|---|---|---|
| Storey level | Original structure without damper | Structure with the supplemental dampers |
| 1 | 3.599 | 2.150 |
| 2 | 3.837 | 2.281 |
| 3 | 4.377 | 2.302 |
| 4 | 5.245 | 2.214 |
| 5 | 4.786 | 2.165 |
| 6 | 6.680* | 2.425 |
| 7 | 6.224 | 2.736 |
| 8 | 6.346 | 2.799* |
| 9 | 5.025 | 2.119 |
| 10 | 4.335 | 1.679 |
| 11 | 3.90 | 1.192 |
| 12 | 2.301 | < 1 |

Table 5.20 Comparison of the member ductility demands in the storeys for the structure without dampers and with dampers under the El Centro 1940 NZS4203 compatible earthquake (* indicates the maximum value for all members)

| | Maximum member ductility demand at the storeys | |
|---|---|---|
| Storey level | Original structure without damper | Structure with the supplemental dampers |
| 1 | 4.912 | 2.750* |
| 2 | 5.992 | 2.532 |
| 3 | 5.856 | 2.417 |
| 4 | 7.480 | 1.962 |
| 5 | 6.482 | 1.633 |
| 6 | 6.076 | 1.664 |
| 7 | 7.420 | 1.802 |
| 8 | 8.762* | 1.967 |
| 9 | 6.911 | 1.698 |
| 10 | 5.328 | 1.325 |
| 11 | 3.360 | 1.089 |
| 12 | 1.861 | < 1 |

Table 5.21 Comparison of the member ductility demands in the storeys for the structure without dampers and with dampers under the Olympia N86E NZS4203 compatible earthquake (* indicates the maximum value for all members)

| | Maximum member ductility demand at the storeys | |
|---|---|---|
| Storey level | Original structure without damper | Structure with the supplemental dampers |
| 1 | 3.365 | 2.952 |
| 2 | 4.102 | 3.364 |
| 3 | 5.148 | 3.439 |
| 4 | 7.196 | 3.621* |
| 5 | 5.892 | 2.795 |
| 6 | 6.203 | 2.974 |
| 7 | 7.205* | 3.284 |
| 8 | 6.838 | 3.388 |
| 9 | 5.909 | 2.552 |
| 10 | 5.128 | 1.828 |
| 11 | 3.764 | 1.193 |
| 12 | 1.852 | < 1 |

Table 5.22 Comparison of the member ductility demands in the storeys for the structure without dampers and with dampers under the Taft N21E NZS4203 compatible earthquake (* indicates the maximum value for all members)

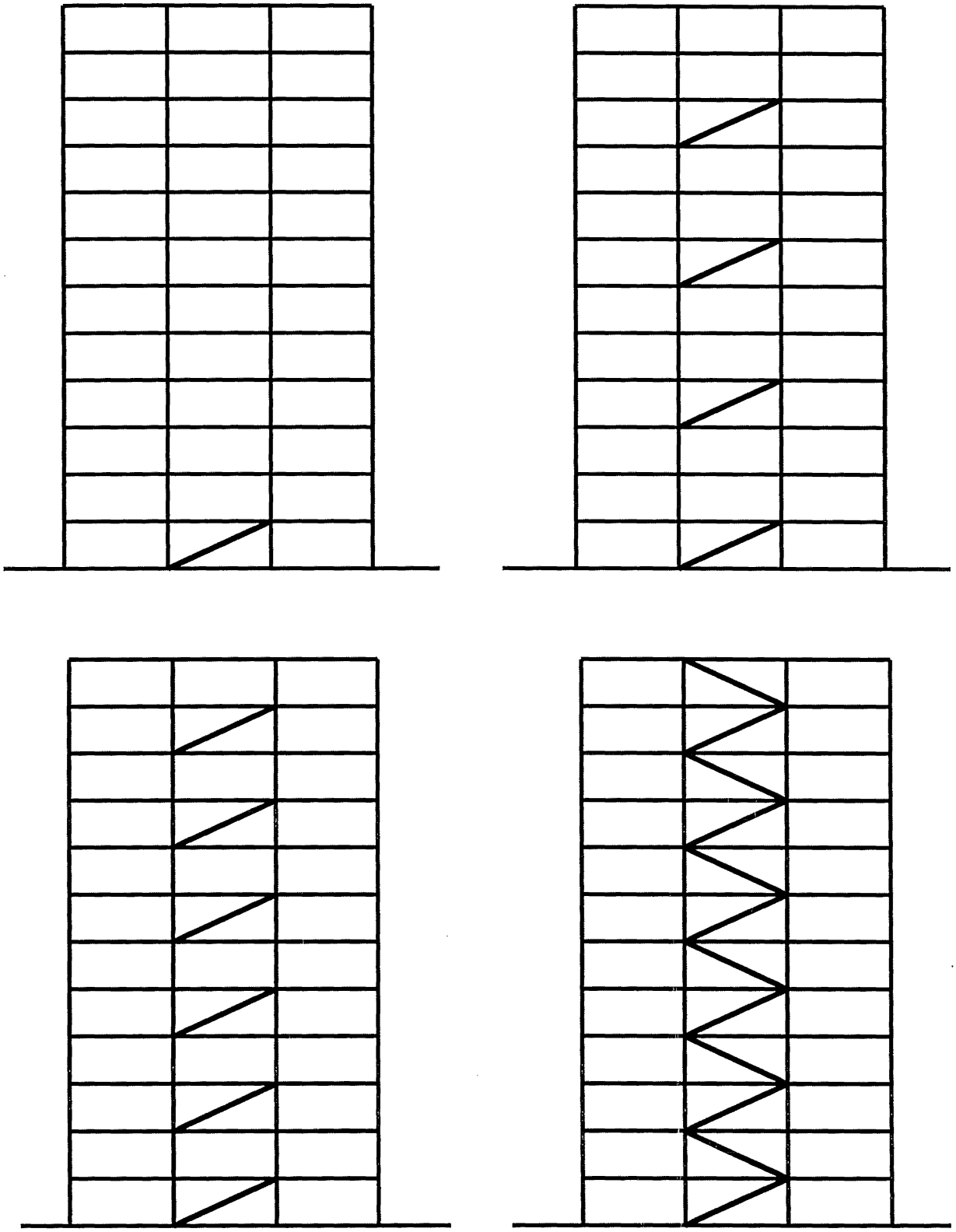

Figure 5.1 Four types of the placements of the supplemental dampers in the structure

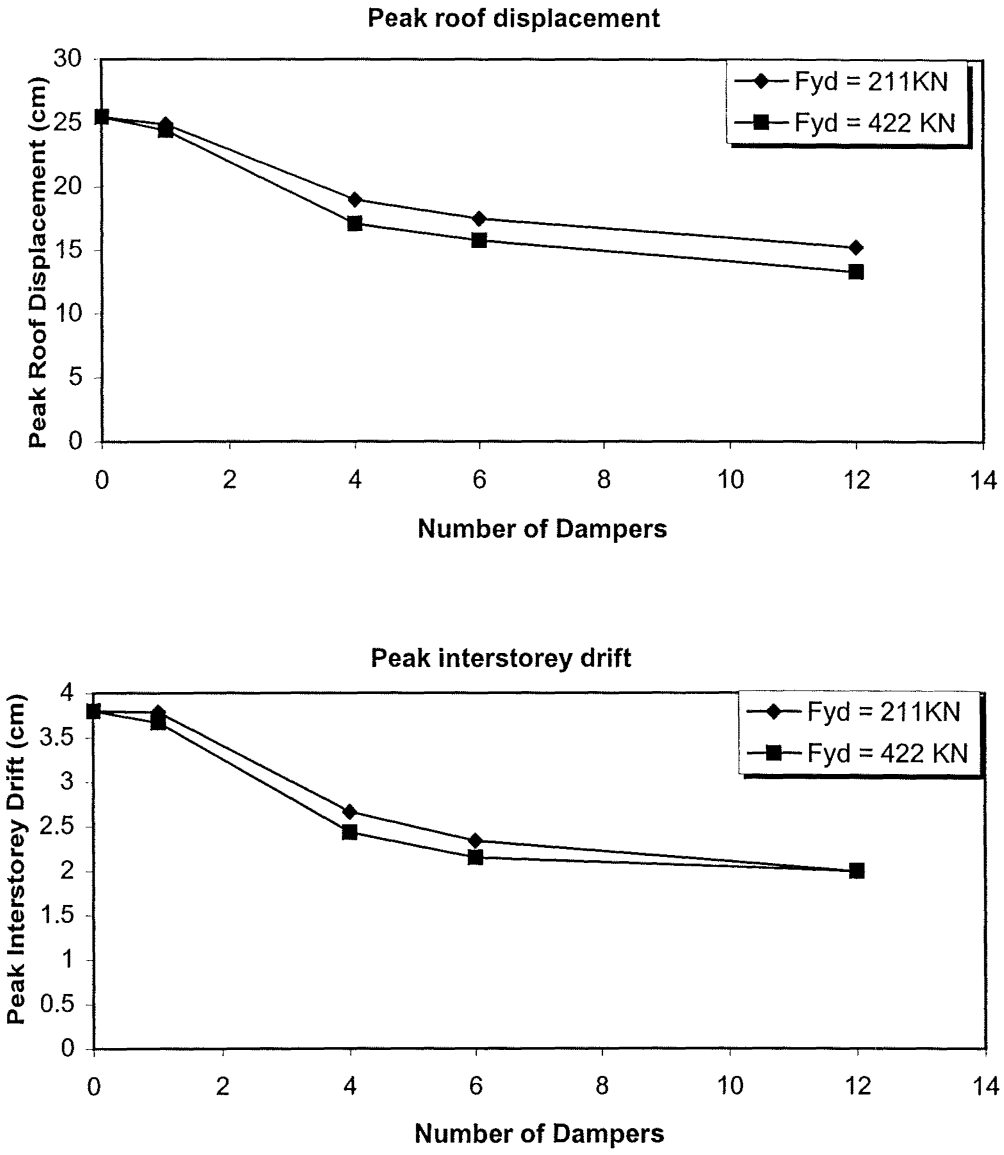


Figure 5.2 The peak roof displacement and interstorey drift response of the structure with different placements of the dampers under the El Centro 1940 NZS4203 compatible earthquake

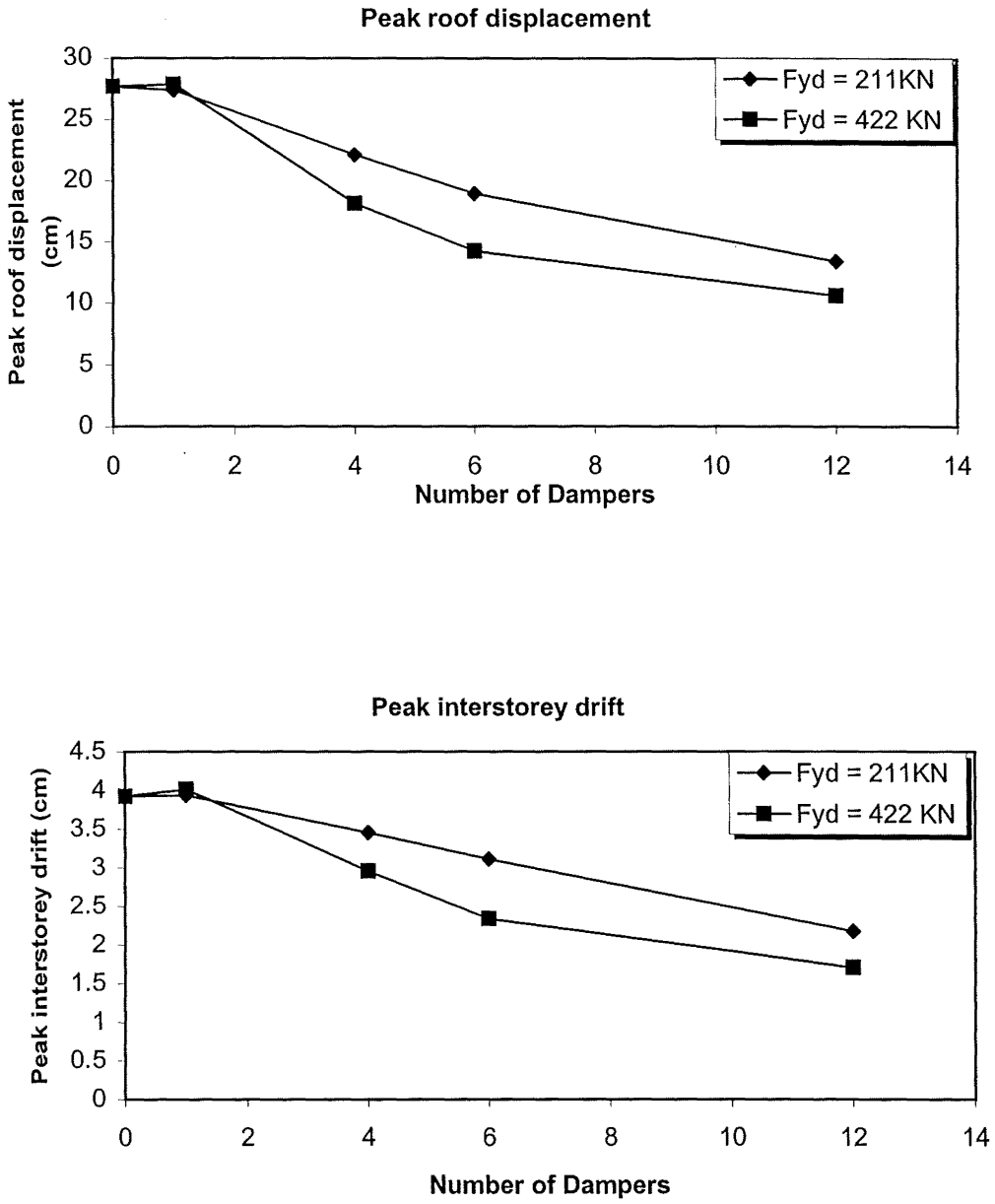


Figure 5.3 The peak roof displacement and interstorey drift response of the structure with different placements of the dampers under the Olympia N86E NZS4203 compatible earthquake

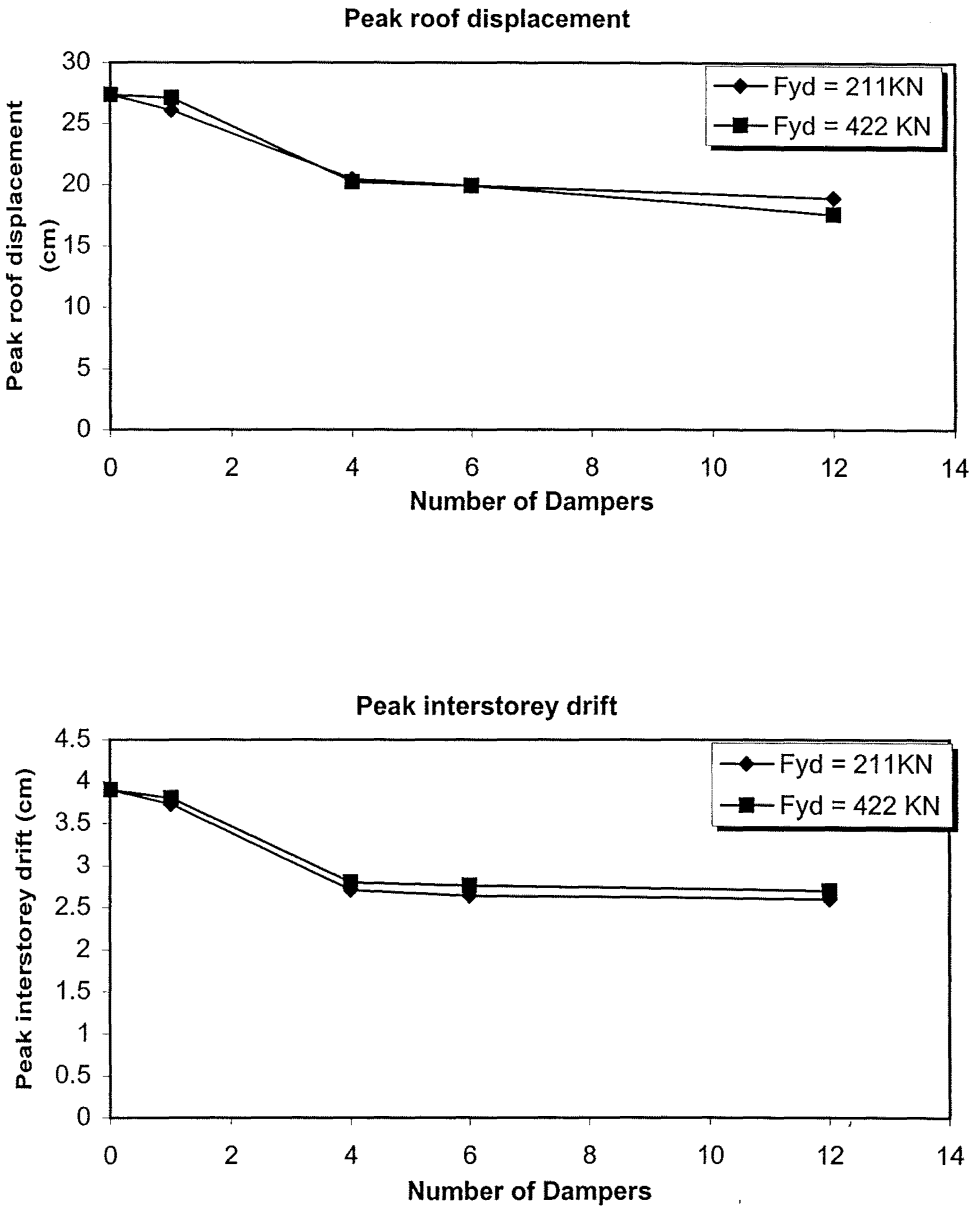


Figure 5.4 The peak roof displacement and interstorey drift response of the structure with different placements of the dampers under the Taft N21E NZS4203 compatible earthquake

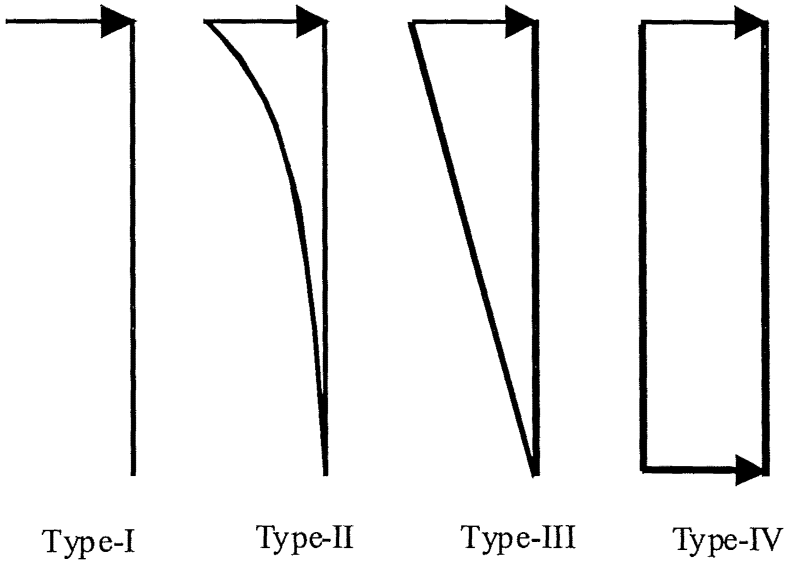


Figure 5.5 Four types of lateral load patterns

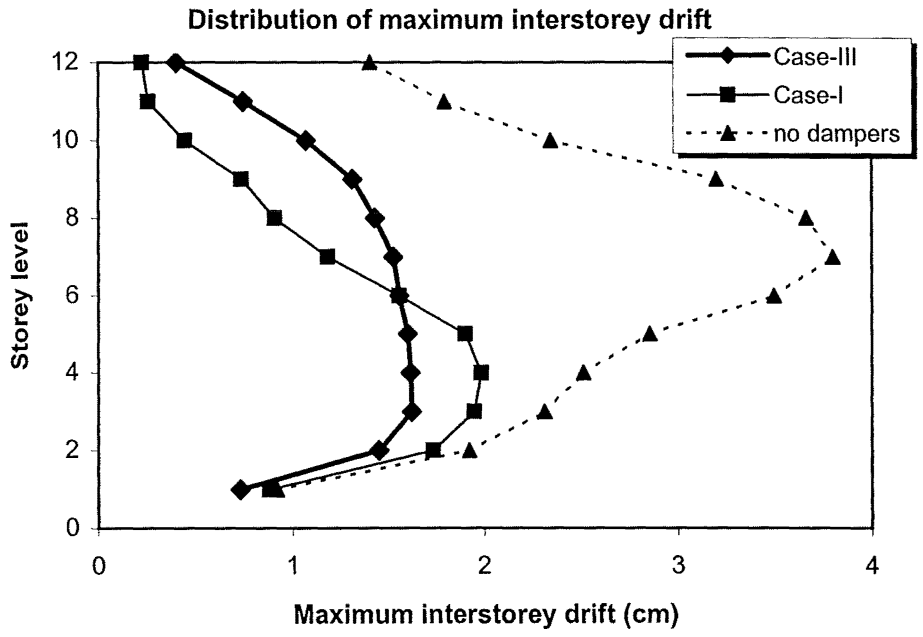


Figure 5.6 Comparison of the distribution of maximum interstorey drifts in the storeys for case-I and case-III under the El Centro 1940 NZS4203 compatible earthquake

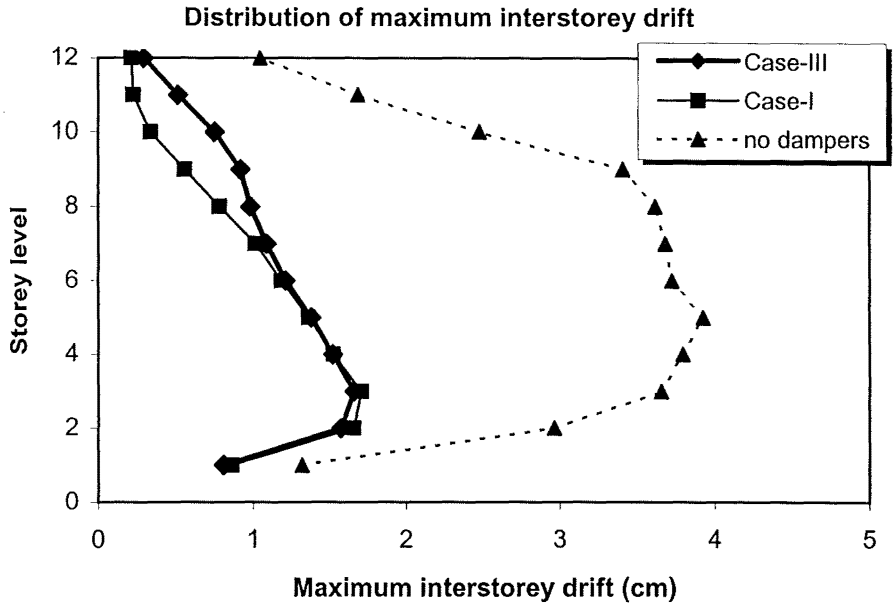


Figure 5.7 Comparison of the distribution of maximum interstorey drifts in the storeys for case-I and case-III under the Olympia N86E NZS4203 compatible earthquake

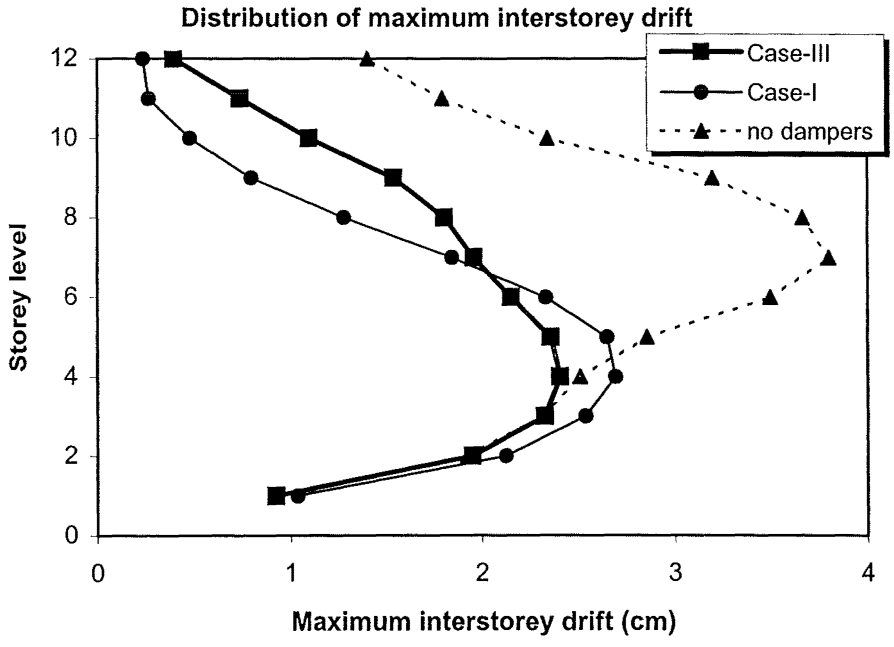


Figure 5.8 Comparison of the distribution of maximum interstorey drifts in the storeys for case-I and case-III under the Taft N21E NZS4203 compatible earthquake

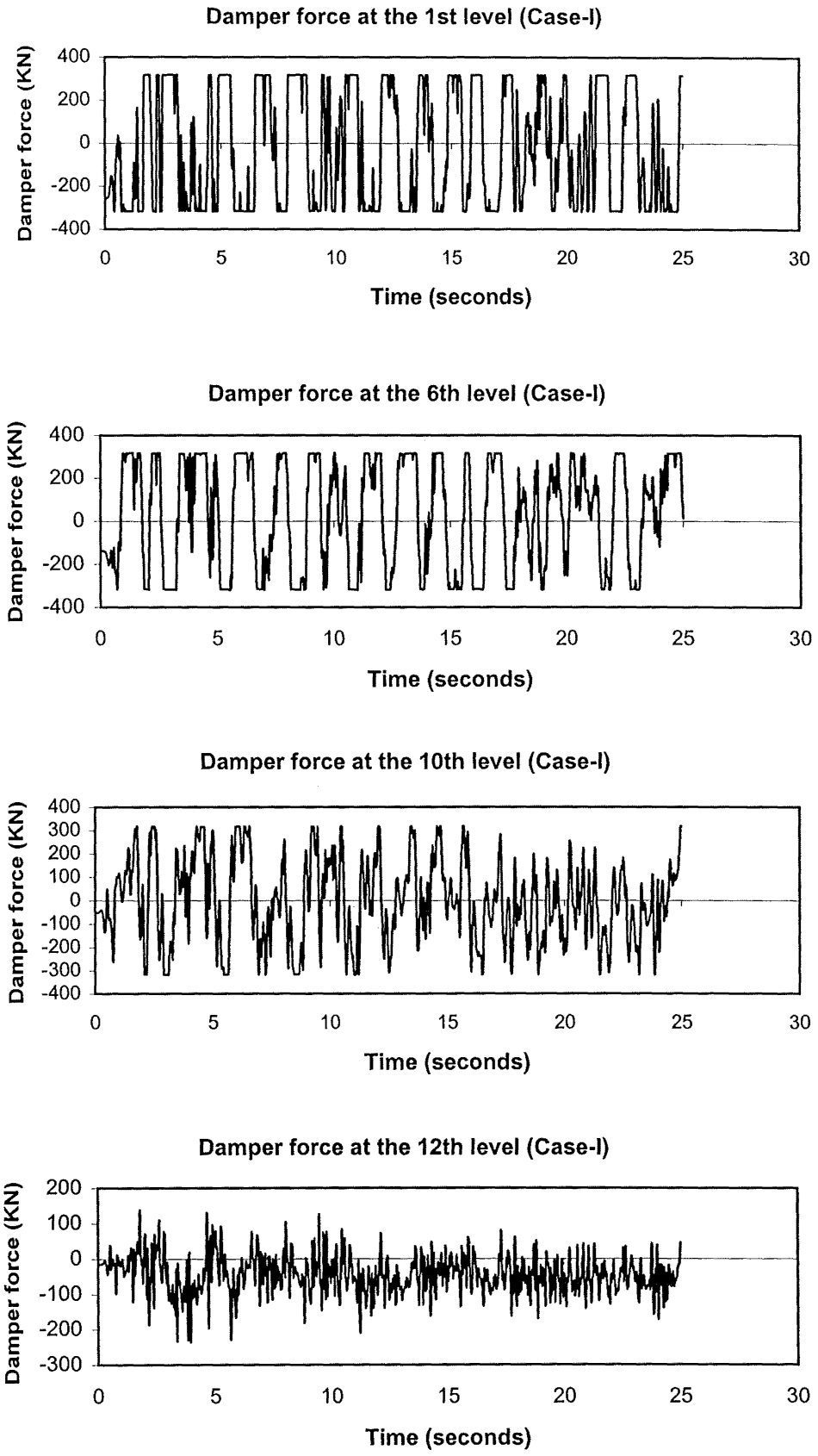


Figure 5.9 Damper force time history of the dampers at some levels of the structure for case-I under the El Centro 1940 NZS4203 compatible earthquake

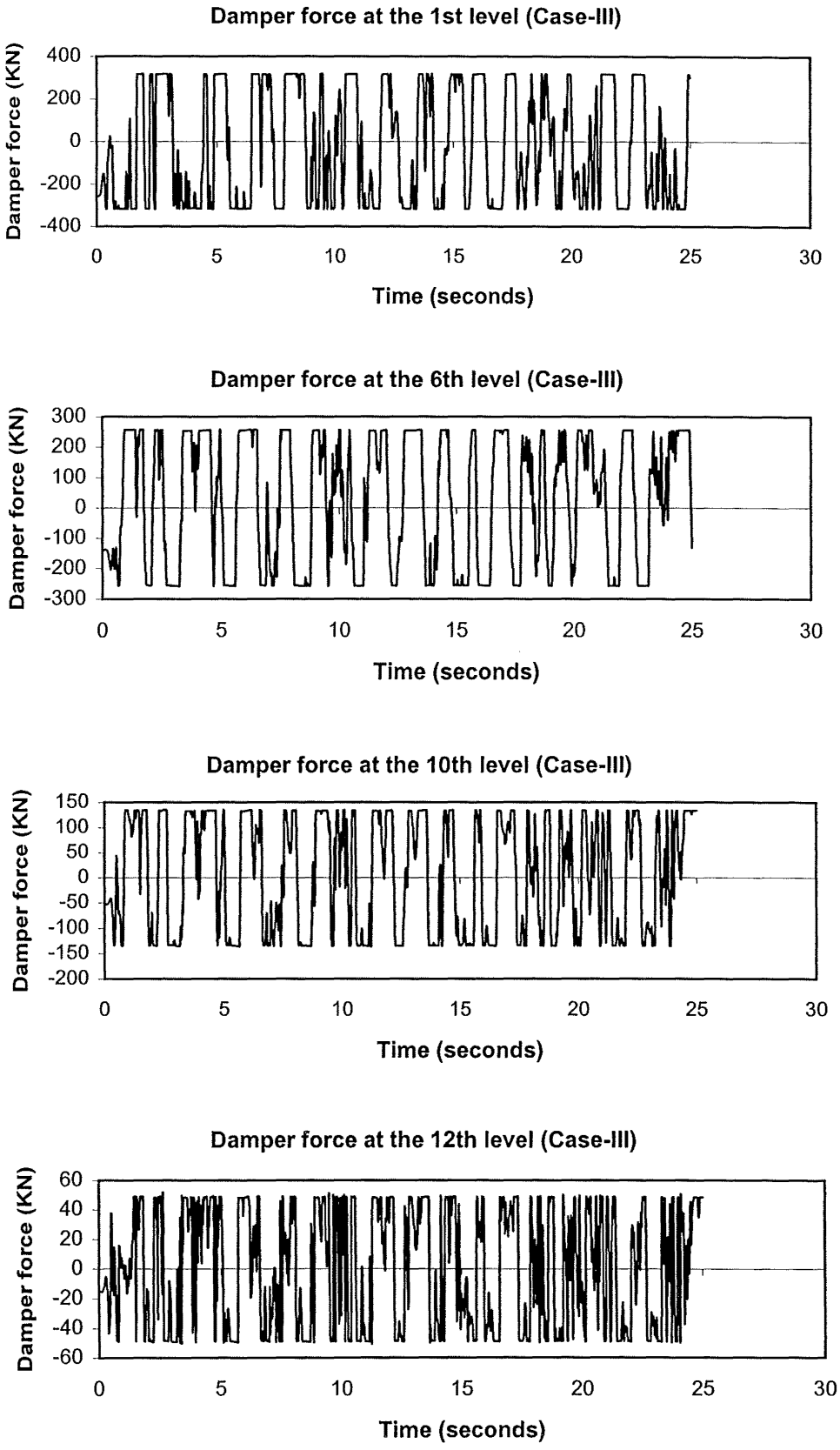


Figure 5.10 Time history of the damper forces at some levels of the structure for case-III under the El Centro 1940 NZS4203 compatible earthquake

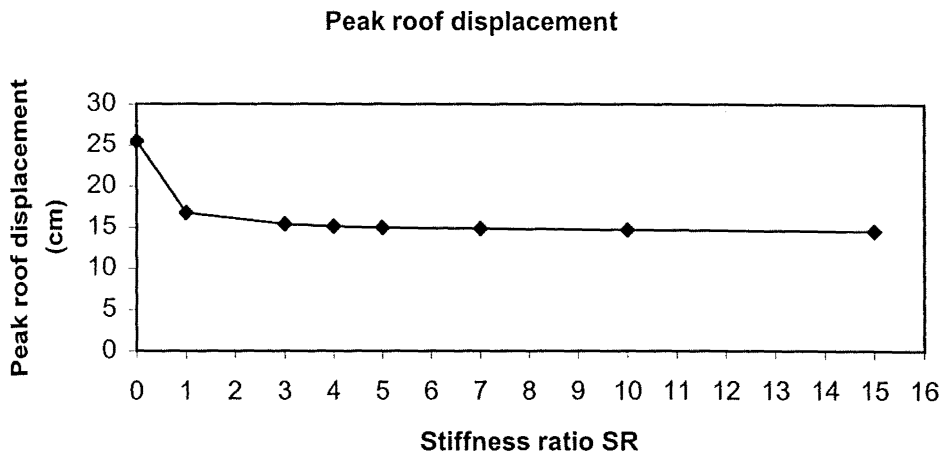


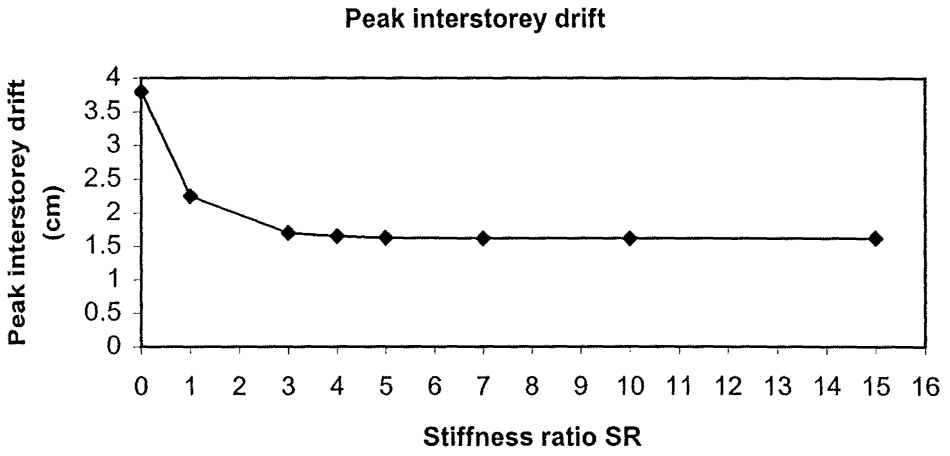


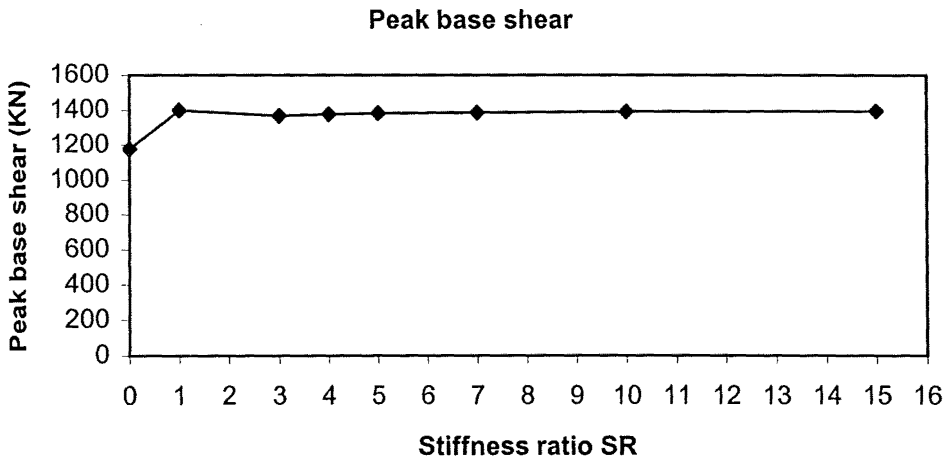


Figure 5.11 Variation of the response of the structure with respect to stiffness ratio SR under the El Centro 1940 NZS4203 compatible earthquake

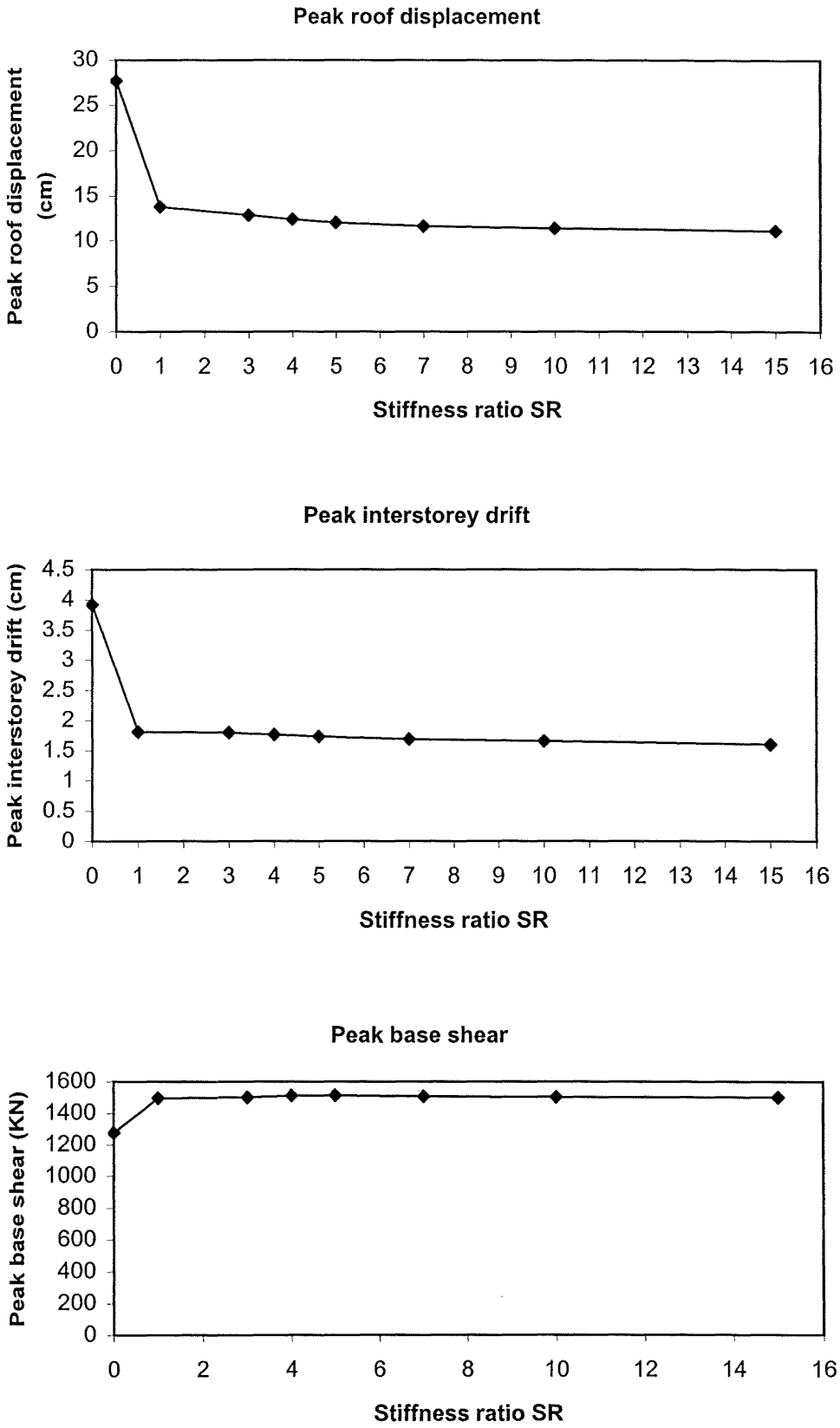


Figure 5.12 Variation of the response of the structure with respect to stiffness ratio SR under the Olympia N86E NZS4203 compatible earthquake

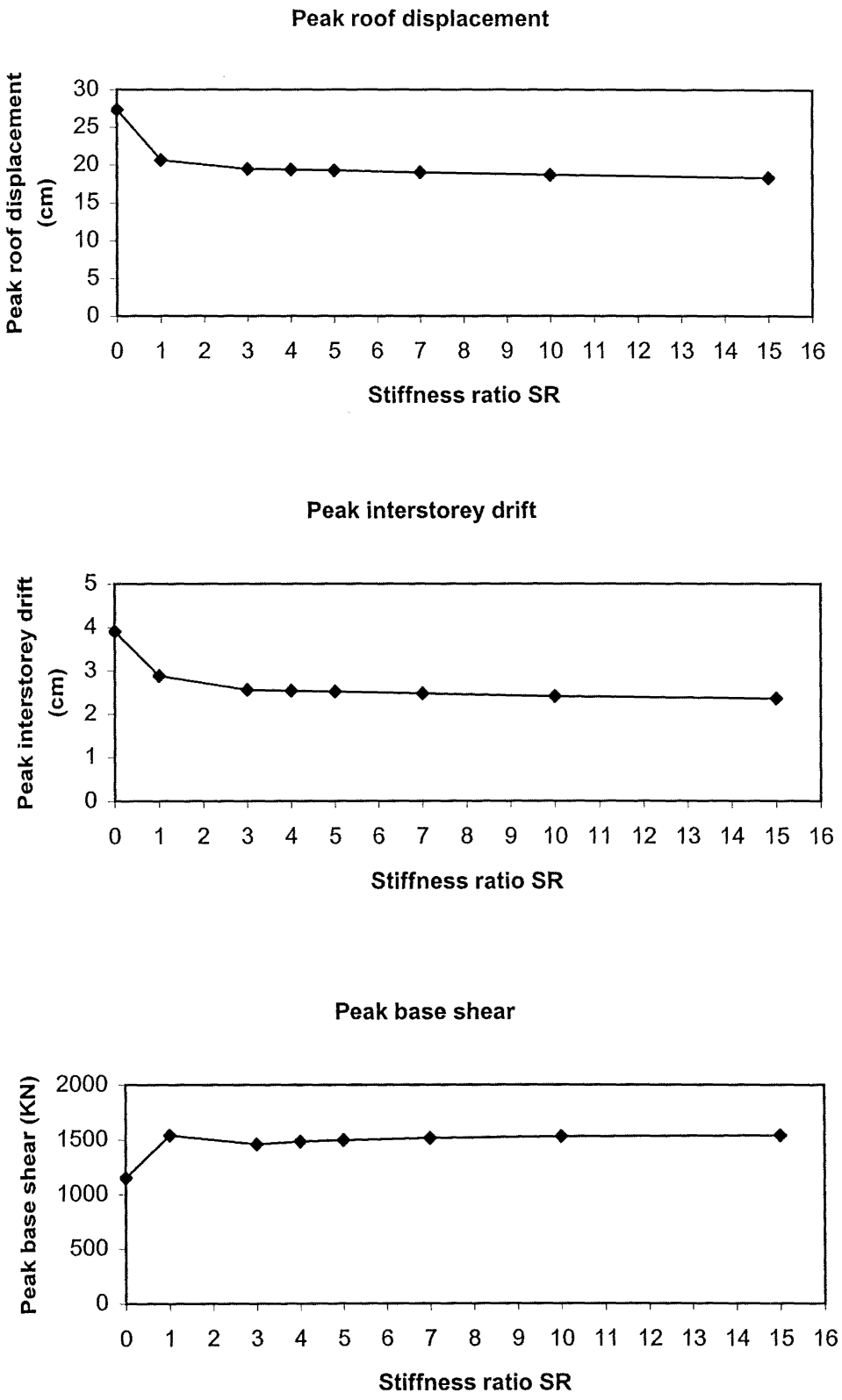


Figure 5.13 Variation of the response of the structure with respect to stiffness ratio SR under the Taft N21E NZS4203 compatible earthquake

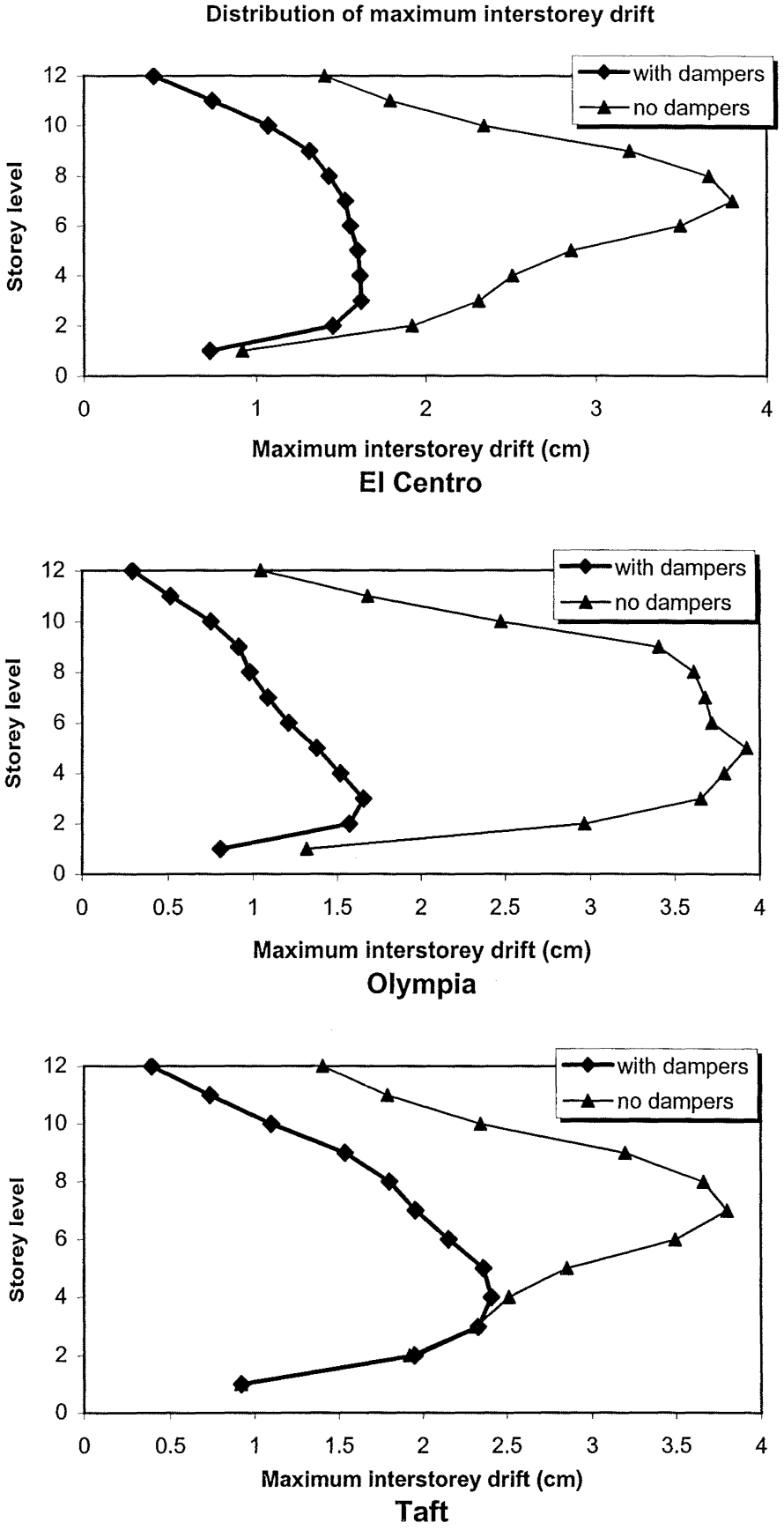


Figure 5.14 Comparison of the distribution of maximum interstorey drifts in the storeys for the structure with the dampers and without dampers under the three NZS4203 compatible earthquakes

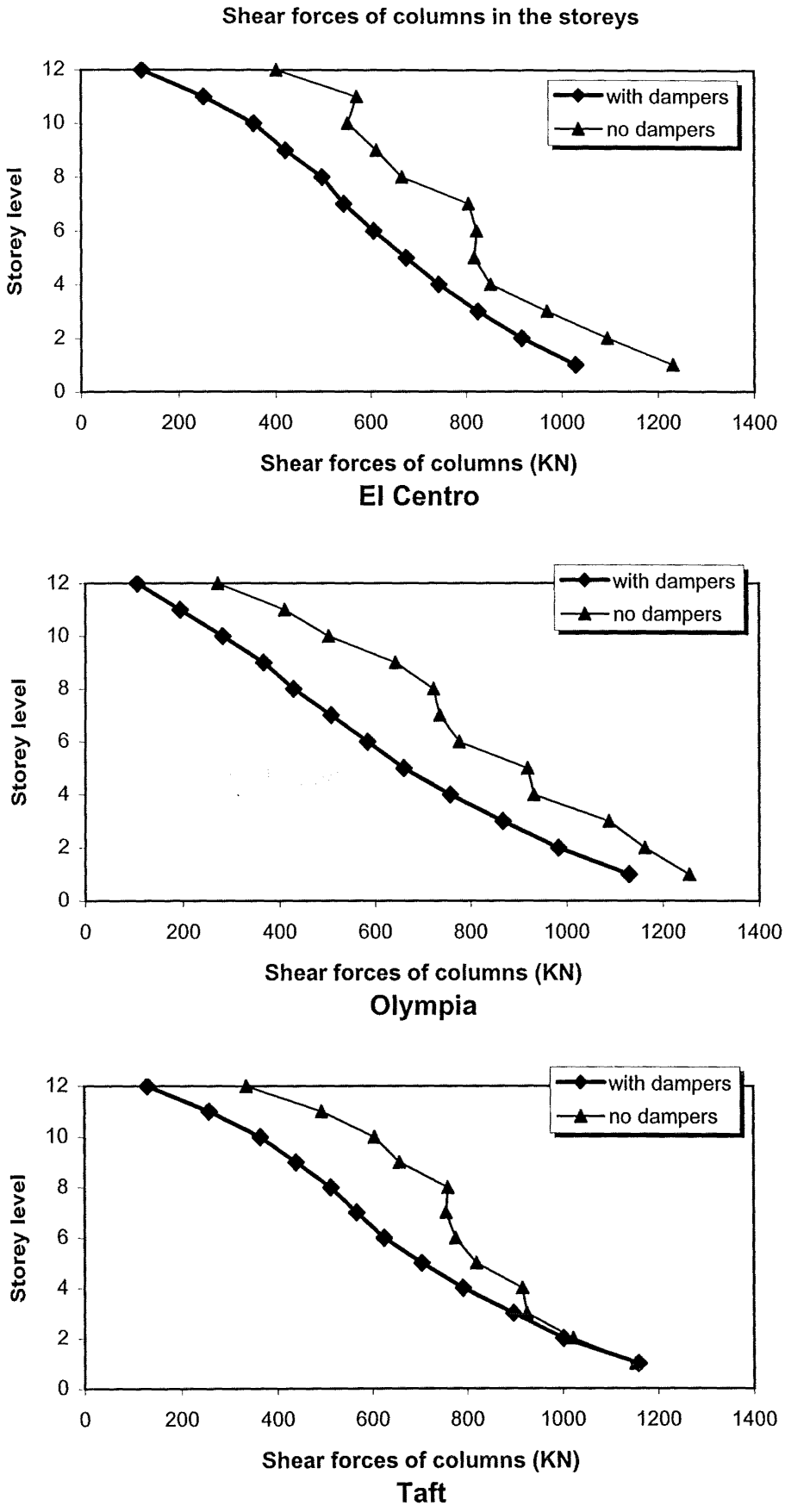


Figure 5.15 Comparison of the distribution of shear forces of columns in the storeys for the structure with the dampers and without dampers under the three NZS4203 compatible earthquakes

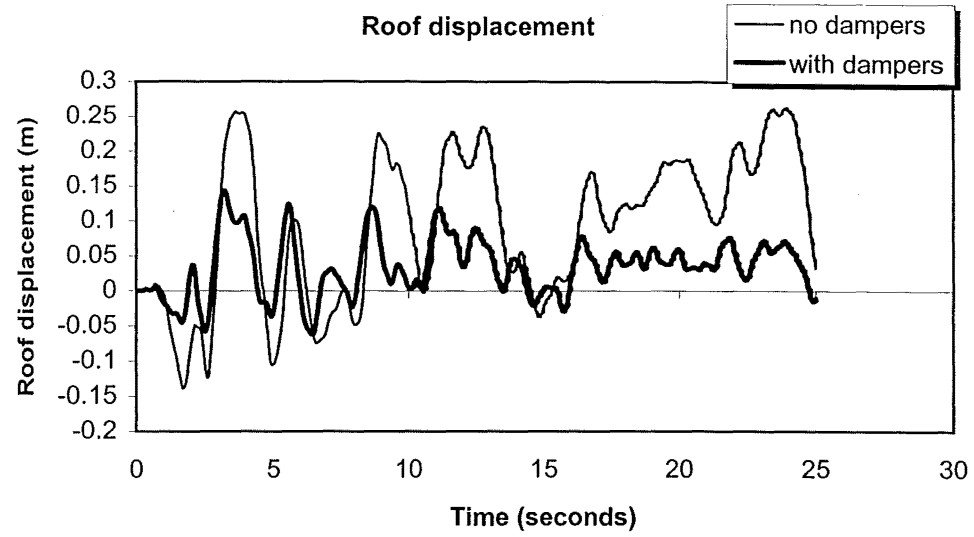


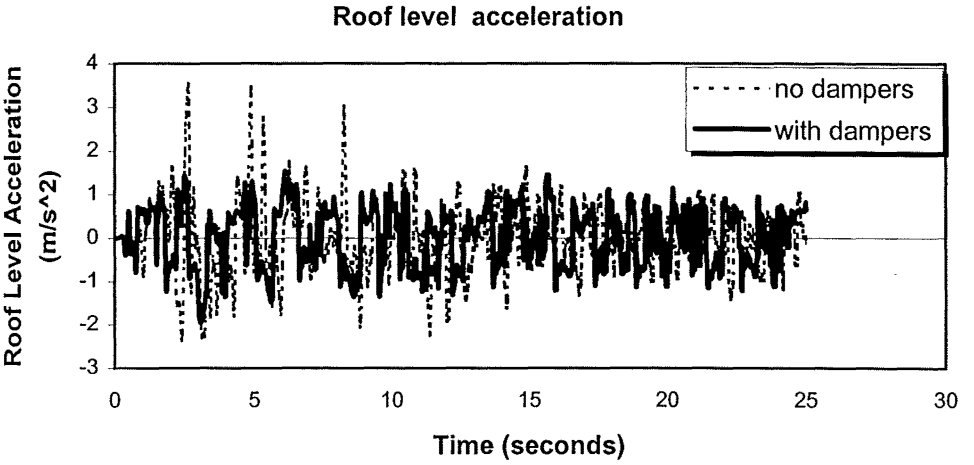


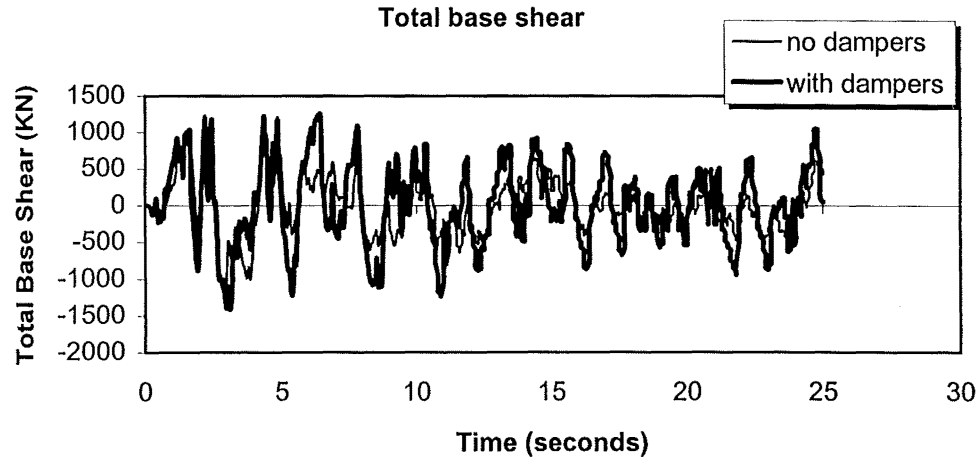


Figure 5.16 Comparison of responses of the structure with dampers and without dampers under the El Centro 1940 NZS4203 compatible earthquake

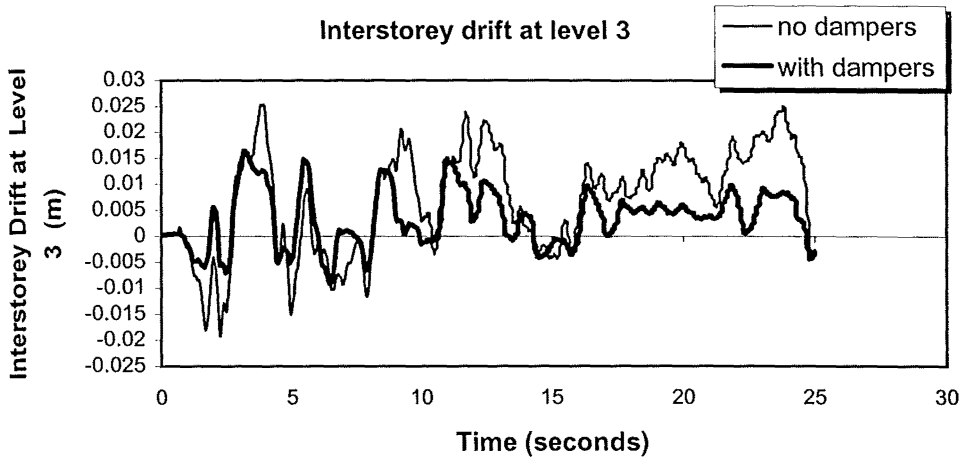


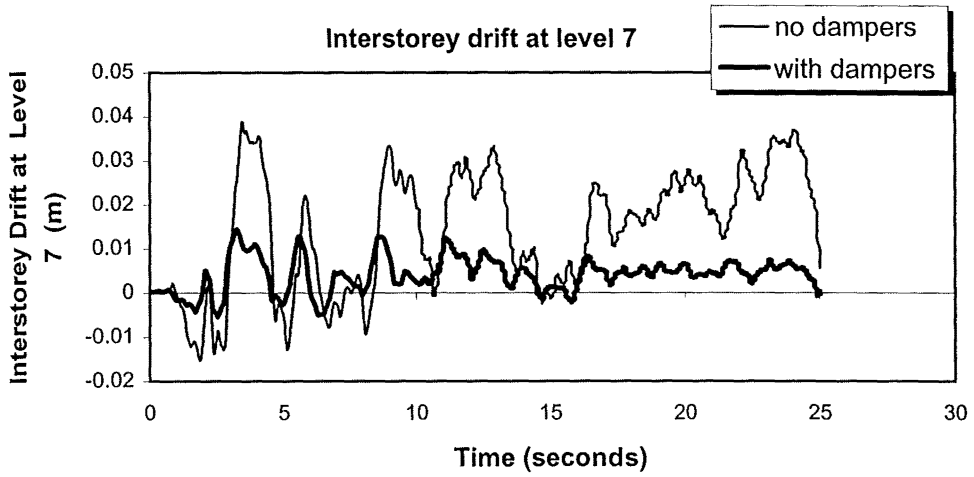


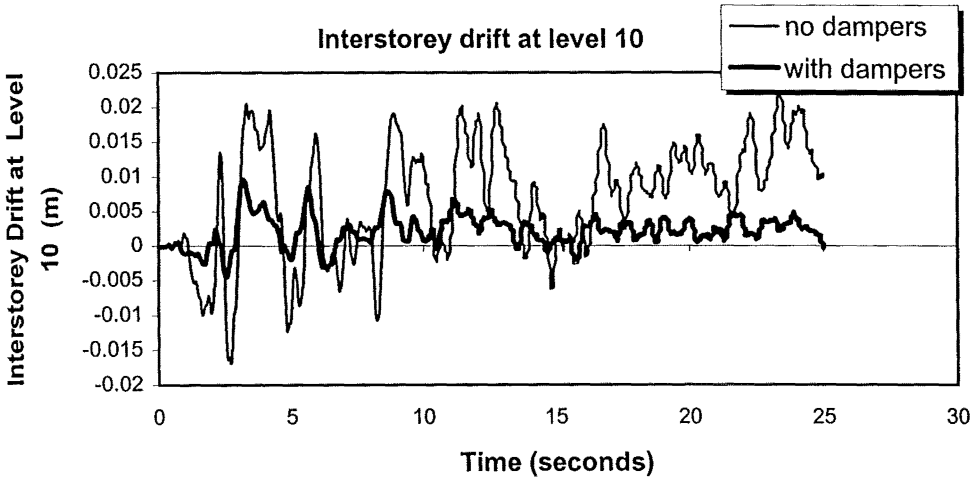


Figure 5.16 (contd) Comparison of responses of the structure with dampers and without dampers under the El Centro 1940 NZS4203 compatible earthquake

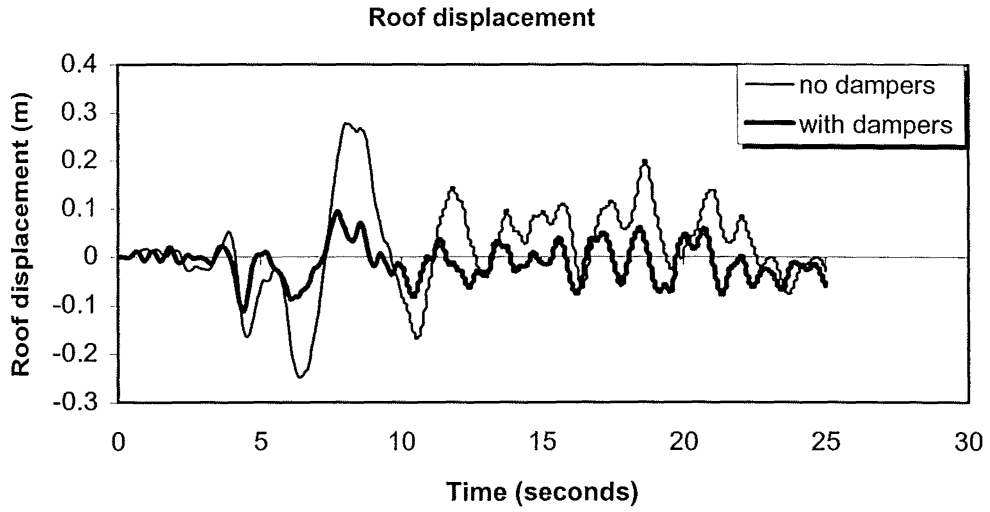


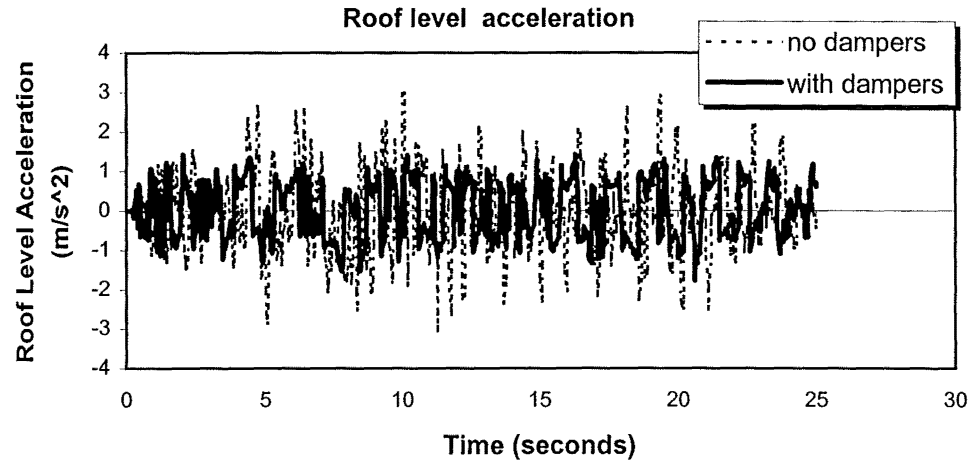


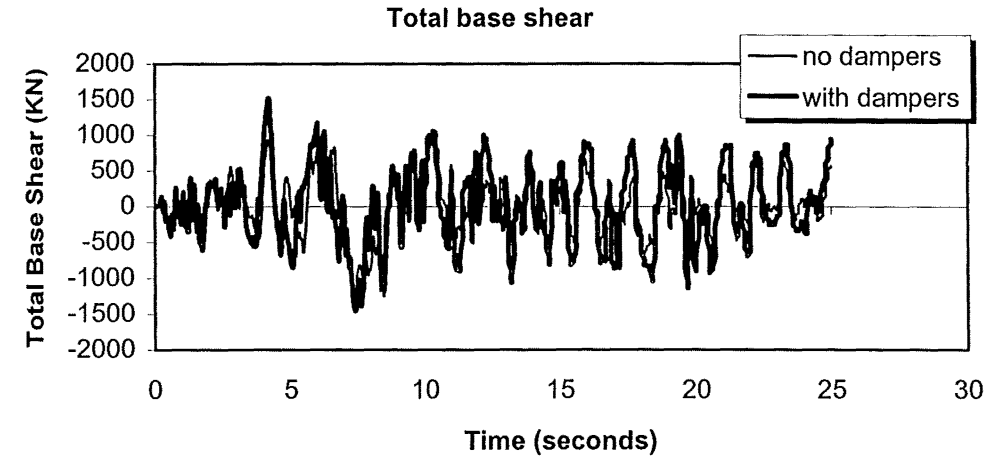


Figure 5.17 Comparison of responses of the structure with dampers and without dampers under the Olympia N86E NZS4203 compatible earthquake

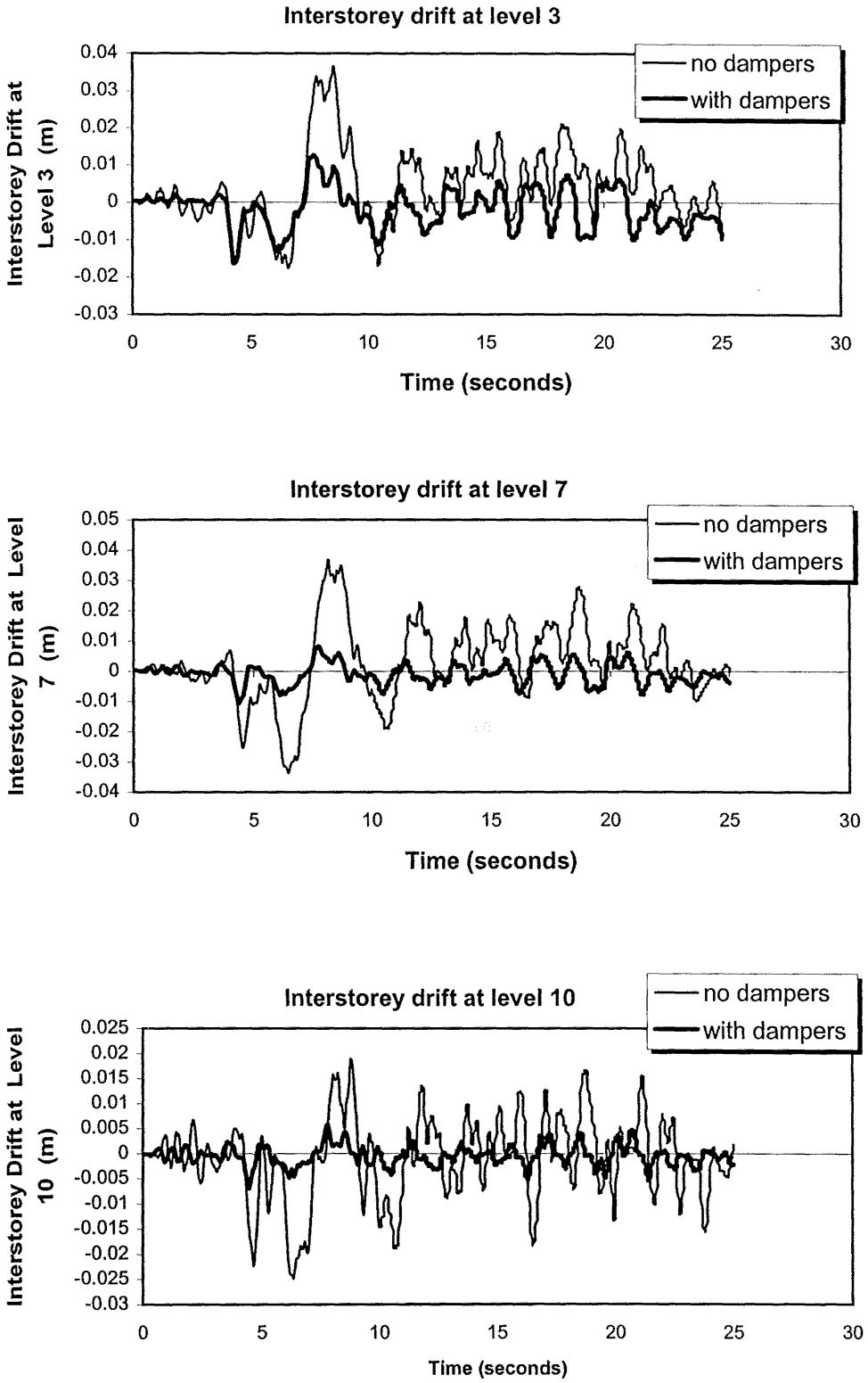


Figure 5.17 (contd) Comparison of responses of the structure with dampers and without dampers under the Olympia N86E NZS4203 compatible earthquake

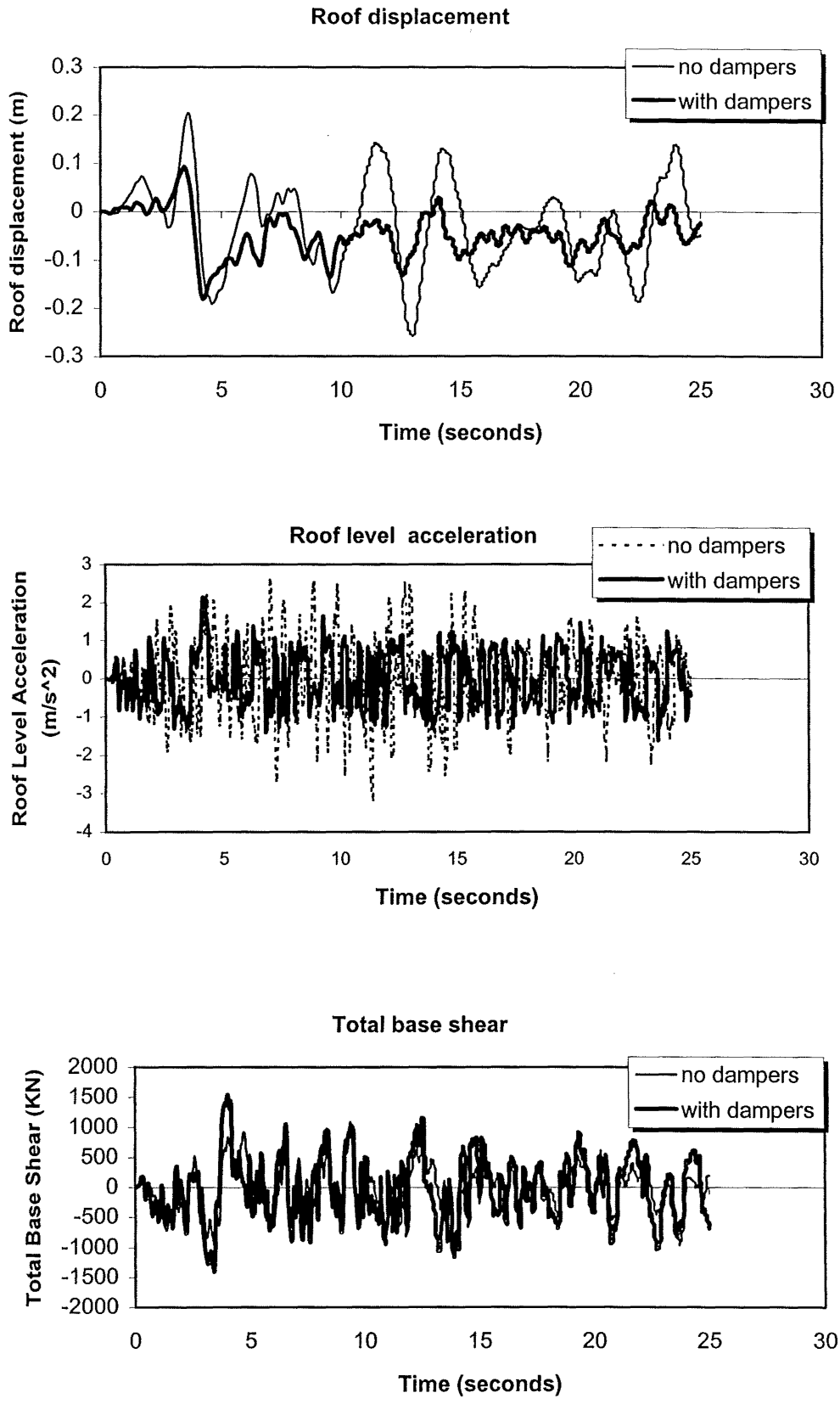


Figure 5.18 Comparison of responses of the structure with dampers and without dampers under the Taft N21E NZS4203 compatible earthquake

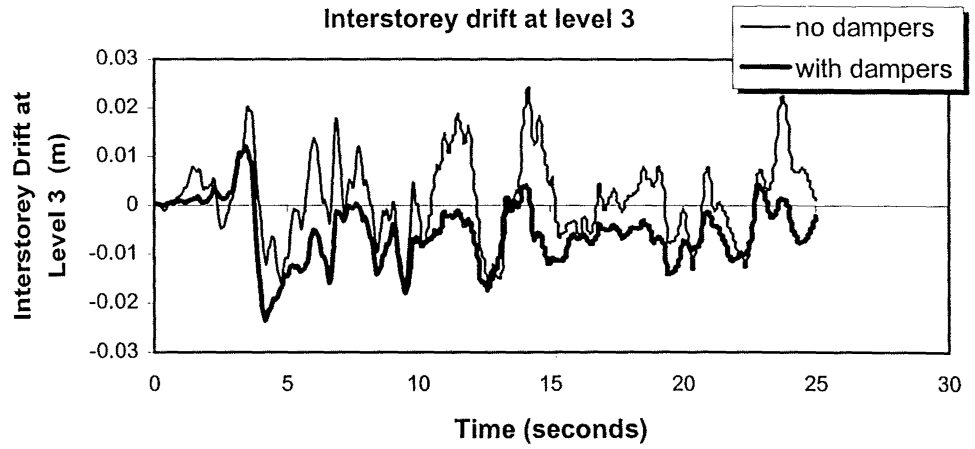


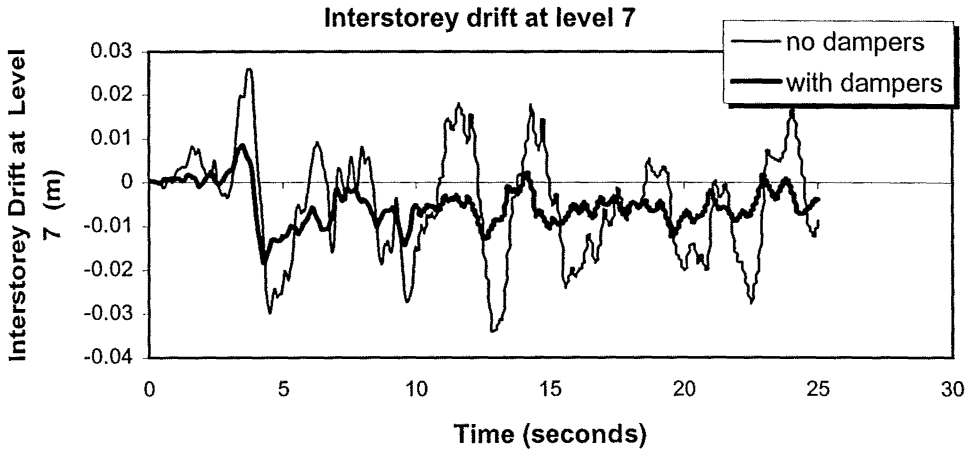


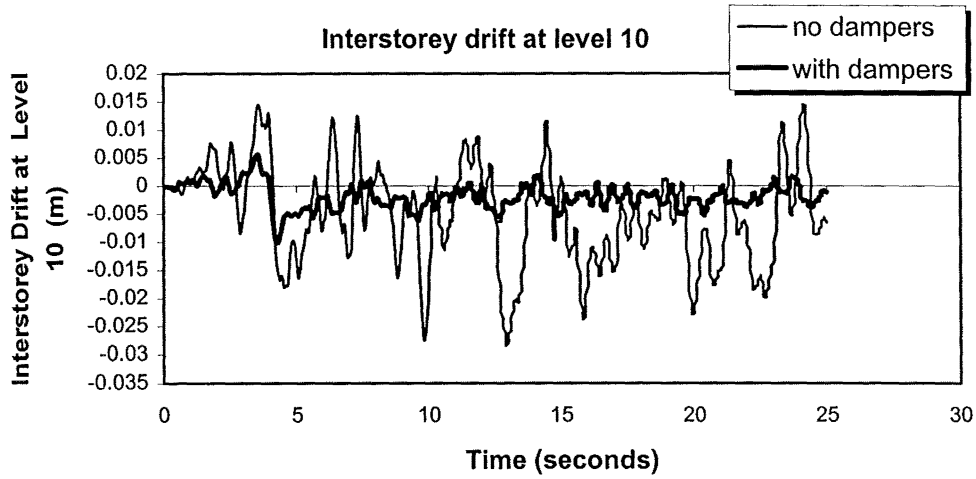


Figure 5.18 (contd) Comparison of responses of the structure with dampers and without dampers under the Taft N21E NZS4203 compatible earthquake

# CHAPTER 6

# PUSHOVER ANALYSIS OF THE STRUCTURE WITH THE SUPPLEMENTAL DAMPERS AND THE EQUIVALENT SDOF SYSTEM

The results of the previous chapter were based on nonlinear dynamic time history analyses of a MDOF structure. The nonlinear dynamic time history analysis of a MDOF structure is not practical for everyday design use. Such an analysis requires additional data (time histories of several ground motions and the information on the hysteretic behaviour of the structural members). Hence, the results are not necessarily reliable due to uncertainties in this input data. In this study, efforts have been made to establish a simplified nonlinear static analytical and design method for a structure with supplemental dampers.

For carrying out the simplified nonlinear static analysis of a structure with supplemental dampers, pushover analyses and an equivalent SDOF system of the structure with dampers are necessary.

## 6.1 PUSHOVER ANALYSIS OF THE STRUCTURE WITH SUPPLEMENTAL DAMPERS

### 6.1.1 Base Shear-Roof Displacement Relationship for the Structure

An inverted triangular lateral load pattern was adopted to conduct the pushover analyses of both the original structure without dampers and the structure with the supplemental dampers. For the structure with the supplemental dampers, the distribution of the yield strengths of the dampers over the height of the structure is taken to be proportional to the storey shear due to the inverted triangular lateral load pattern. The base shear-roof displacement relationship is used to reflect the overall capacity of the structure. The change of the stiffness of the structure with respect to the roof displacement can be clearly seen from the base shear-roof displacement curve.

The base shear-roof displacement curve of the original structure without damper is shown in Fig.6.1 (solid line). This curve can be suitably approximated by a bi-linear relationship (see dashed line in Fig.6.1).

Two magnitudes of the yield strength of the damper at the 1st floor level are considered here ($F_{yd1}$=211KN and $F_{yd1}$=422KN). The base shear-roof displacement curves of the structure with the dampers are shown in Fig.6.2 and Fig.6.3 respectively (base shear here includes shear forces in the columns and the horizontal force due to the damper at the 1st storey level). For comparison, the base shear – roof displacement curve for the original structure without dampers are also shown in these figures. It can be seen that during the first stage when the supplemental dampers are in their elastic stage the tangent stiffness of the structure is greatly increased. Once the dampers yield, the tangent stiffness of the structure with the dampers is almost the same as that of the original structure. This shows that all the dampers yield simultaneously.

The base shear-roof displacement relationship for the structure with dampers can be approximately represented by a tri-linear curve (see also Fig.6.8). From Fig.6.2 it can be observed that once the dampers yield the curve for the structure with the dampers is almost parallel to the curve for the original structure without dampers. This tri-linear curve can be regarded as consisting of two curves: one is the bilinear curve that represents the base shear-roof displacement relationship of the original structure without dampers, the other is the elasto-plastic curve that represents the total base shear-roof displacement relationship of the damping system (see Fig.6.8). Hence, the structure with the supplemental dampers can be considered as a dual system — the original structure without dampers and the supplemental damping system.

Once the base shear–roof displacement relationship of the structure is known, the initial stiffness, yield displacement, yield base shear, and the ductility of the structure for the displacement that the structure might experience in a earthquake can be obtained. These are very important data for carrying out a simplified nonlinear static analysis.

### 6.1.2 Deflected Shape of the Structure

A further important piece of information that can be obtained from the pushover analysis is the deflected shape (or displacement profile) of the structure. If the response of the structure is dominated by the first mode, this deflected shape can represent a realistic displacement profile of the structure at a target displacement during an earthquake. The normalised deflected shape vectors of the structure with the supplemental dampers and the original structure

without the supplemental dampers at different ductilities are shown in Tables 6.1, 6.2 and Fig.6.4. The ductilities here refer to the structure ductility and are equal to the ratio of the target displacement to the yield displacement of the original structure. The ductility of the structure is taken to be 1, 2, and 3 respectively for comparison. In practice, for the structure with the supplemental dampers, the ductility of the structure is usually less than 2.

As the distribution of the yield strengths of the supplemental dampers over the height of the structure is taken to be proportional to the storey shear due to the inverted triangular lateral load pattern. It can be seen that for this type of distribution of the yield strengths of the dampers, the deflected shape of the structure with the dampers is very close to that of the original structure without dampers. Hence, the deflected shape of the structure with the supplemental dampers can be accurately estimated by that of the original structure at the same target displacement (ductility).

The deflected shape of a structure with supplemental dampers where the yield strengths are constant over the height of the structure can also be obtained from a pushover analysis. This deflected shape is also compared with that of the original structure without dampers. The results are shown in Table 6.3 and Fig.6.5 for yield strength of 422KN for different ductilities. It can be seen that the differences in the deflected shapes of the structure with the supplemental dampers and the original structure become much larger for this distribution of the damper yield strengths. This is one reason why the distribution of the damper yield strengths being proportional to the storey shear due to the inverted triangular lateral load pattern is to be preferred.

### 6.1.3 Lateral Load Pattern

The lateral load patterns are intended to represent and to provide bounds for the distribution of inertia forces in a design earthquake. It is clear that the distribution of inertia forces will vary with the severity of the earthquake and with time during an earthquake. If an invariant load pattern is used, the basic assumptions are that the distribution of inertia forces will be constant during the earthquake and that the displacement shape (profile) obtained from this invariant load pattern will be close to the one expected in the design earthquake.

A refined pushover analysis has been proposed recently (Satyarno et al., 1998) at the University of Canterbury. By using the modified Rayleigh vibration shape, a realistic pattern

of the lateral load can be determined. Using this method, the change of the lateral load pattern as more and more plastic hinges are formed, can be included.

Pushover analyses using an invariant inverted triangular lateral load pattern and the adaptive load pattern of the structure with the supplemental dampers were conducted. The base shear-roof displacement curves from both pushover analyses are shown in Fig.6.6. It can be seen that these two curves are quite close to each other. The deflected shapes at different ductilities from both pushover analyses are also compared in Fig.6.7. It can also be observed that the deflected shapes are very close to each other. Hence, for this type of the distribution of the damper yield strengths, the inverted triangular lateral load pattern can give a good approximation for the pushover analysis of the structure (Lin et al., 1998a).

## 6.2 EQUIVALENT SDOF SYSTEM FOR A MDOF STRUCTURE

### 6.2.1 Introduction

The analytical simplicity of equivalent single degree of freedom (SDOF) systems and the availability of well established methods to perform the analysis have made SDOF systems very useful tools for estimating the characteristics of the dynamic response of MDOF structures. Although not completely accurate, the analysis of SDOF systems can possibly represent the overall behaviour of MDOF structures provided their response is dominated by the first mode. The simplified nonlinear static analysis is based on the assumption that the response of the structure can be related to the response of a SDOF system. The formulation of the equivalent SDOF system is based on the assumption that the displacement shape (profile) of the MDOF structure can be represented by a shape vector $\{\Phi\}$ that remains relatively constant throughout the time history of the response, regardless of the level of deformation.

The underlying assumption in obtaining the equivalent SDOF system is that the structure vibrates in its fundamental mode. The higher mode effects are ignored during this transformation. The equivalent SDOF models attempt to model both the displacement and the resistance of MDOF structures. Consequently, some assumptions have been necessary to define the equivalent resistance function. These assumptions usually require inconsistencies in the mathematical derivation of the equivalent SDOF models (Qi et al., 1991).

The force-displacement characteristic of the equivalent SDOF system is critical in determining its dynamic structural behaviour. It is known that the pushover analysis of the MDOF structure will usually produce a base shear-roof displacement relationship that can represent the global force-displacement relationship of the whole structure. The force-displacement relationship of the equivalent SDOF system can be determined from the base shear-roof displacement relationship of the MDOF structure obtained from a pushover analysis.

Several variants have been proposed for the transformation of a MDOF structure to an equivalent SDOF system. Saiidi et al. (1981) developed a simple "low-cost" equivalent SDOF model (which was called Q-model) for the calculation of displacement histories for multistorey reinforced concrete structures subjected to strong ground motions. The nonlinear characteristics of the frame are reflected in the properties assigned to the rotational spring in the SDOF system. The nonlinear behaviour of the spring was approximated by a bilinear relationship. A pushover analysis was used to obtain the nonlinear spring properties. The load distribution of lateral forces for carrying out the pushover analysis was taken to be an inverted triangular one because it was simple, and it gave acceptable results. The relationship of Q-model to the MDOF structure is shown in Fig.6.9.

Qi et al. (1991), Fajfar et al. (1987, 1988, 1996) have also developed an equivalent SDOF model.

The following derivation of the equivalent SDOF system is based on the procedure proposed by Qi et al. and Fajfar et al..

### 6.2.2 Derivation of Equivalent SDOF System

It is known that elastic MDOF structures are readily transformed to an equivalent SDOF systems using the orthogonal mode shapes of free vibration. However, if inelastic response occurs, a more general approach is needed to carry out the transformation.

The equation of motion for an idealised SDOF system under earthquake ground excitations can be written as

$$m\ddot{u}(t)+c\dot{u}(t)+r(t)=-m\ddot{u}_g(t) \tag{6.1}$$

where *u(t)* is the relative displacement of the mass *m* with respect to the ground, *r(t)* is the nonlinear restoring force of the system, *m* and *c* are the mass and damping coefficients of the system, $\ddot{u}_g(t)$ is the ground acceleration.

Dividing both sides of equation (6.1) by *m* gives

$$\ddot{u}(t)+2\xi\omega\dot{u}(t)+\frac{r(t)}{m}=-\ddot{u}_g(t) \tag{6.2}$$

For multi-storey frames:

$$[M]\{\ddot{u}(t)\}+[C]\{\dot{u}(t)\}+\{R(t)\}=-M\{r\}\ddot{u}_g(t) \tag{6.3}$$

where [*M*] is a diagonal mass matrix having masses $m_i$ equal to the lumped mass at the *ith* story level, [*C*] is a damping matrix, $\{R(t)\}$ is the resistance vector, $\{u(t)\}$ is the displacement vector.

To transform a MDOF structure to an equivalent SDOF system, a constant deflected shape $\{\phi\}$ is assumed. This shape vector can be obtained from a pushover analysis. The shape vector is normalised with respect to the roof displacement.

$$\{u(t)\}=\{\phi\}x(t) \tag{6.4}$$

Where *x(t)* represents the magnitude of the displacement at the roof level.

Substituting Eq(6.4) into Eq(6.3), we get

$$[M]\{\phi\}\ddot{x}(t)+[C]\{\phi\}\dot{x}(t)+\{R(t)\}=-[M]\{r\}\ddot{u}_g(t) \tag{6.5}$$

Pre-multiplying Eq(6.5) by $\{\phi\}^T$ gives

$$M^*\ddot{x}(t)+C^*\dot{x}(t)+R^*(t)=-L^*\ddot{u}_g(t) \tag{6.6}$$

where $\begin{cases} M^* &= \{\phi\}^T [M] \{\phi\} \\ C^* &= \{\phi\}^T [C] \{\phi\} \\ R^*(t) &= \{\phi\}^T \{R(t)\} \\ L^* &= \{\phi\}^T [M] \{r\} \end{cases}$

Dividing both sides of Eq(6.6) by $M^*$ and noting that $\frac{C^*}{M^*} = 2\xi\omega^*$ , where $\xi$ is the fraction of critical damping

$$\ddot{x}(t) + 2\xi\omega^* \dot{x}(t) + \frac{R^*(t)}{M^*} = -\frac{L^*}{M^*} \ddot{u}_g(t) \tag{6.7}$$

Let

$$x(t) = \frac{L^*}{M^*} x^*(t) \tag{6.8}$$

Substituting Eq(6.8) into Eq(6.7)

$$\frac{L^*}{M^*} \ddot{x}^*(t) + 2\xi\omega^* \frac{L^*}{M^*} \dot{x}^*(t) + \frac{R^*(t)}{M^*} = -\frac{L^*}{M^*} \ddot{u}_g(t)$$

Then we have

$$\ddot{x}^*(t) + 2\xi\omega^* \dot{x}^*(t) + \frac{R^*(t)}{L^*} = -\ddot{u}_g(t) \tag{6.9}$$

This is the equation of motion for an equivalent SDOF system under earthquake ground excitations.

Comparing Eq(6.2) with Eq(6.9) and letting $\omega = \omega^*$ leads to

$$\frac{r(t)}{m} = \frac{R^*(t)}{L^*} \tag{6.10}$$

From the relationship of Eq(6.8) we know that the global displacement ductility ratio of the structure and the displacement ductility ratio of the SDOF system are equal,

$$\frac{x(t)}{x_y} = \frac{x^*(t)}{x_y^*} \tag{6.11}$$

where $x_y$ is the yield displacement at the roof level of the MDOF structure, $x_y^*$ is the yield displacement of the equivalent SDOF system.

The characteristics of the equivalent SDOF system can therefore be determined as:

$$\begin{aligned} m &= L^* = \{\phi\}^T [M] \{1\} \\ r(t) &= R^*(t) = \{\phi\}^T \{R(t)\} \\ r_y &= R_y^* = \{\phi\}^T \{R_y(t)\} \end{aligned} \tag{6.12}$$

where $r_y$ is the yield force of the equivalent SDOF system and $\{R_y(t)\}$ is the storey resistance vector at the yield of the MDOF structure.

It must be noticed that the definition of the resistance of the equivalent SDOF system is not equal to the base shear of the MDOF structure. *R*(t)* is the dot product of the deflected shape vector and the applied load vector.

The distribution of the lateral loads for carrying out the pushover analysis is $\{\psi\}$ (also called the load pattern). $\{\psi\}$ is normalized by setting $\psi_n = 1.0$ ( at the roof level of the structure).

If the assumed deflected shape $\{\phi\}$ is taken to be the same as that resulting from the static application of the dynamic loads, the distribution of the lateral resistance is equal to the distribution of the lateral loads.

$$R(t) = \{\psi\} p$$

where $p$ is the load factor.

This means that:

$$Q = p\sum_{1}^{n}\psi_i$$

where $Q$ – base shear of the MDOF structure.

So $p = \frac{Q}{\sum\psi_i}$, then

$$\{R(t)\} = \frac{\{\psi\}}{\sum\psi_i}Q \tag{6.13}$$

Substituting Eq(6.13) into Eq(6.12):

$$R^* = \frac{\{\phi\}^T\{\psi\}}{\sum\psi_i}Q = \frac{\sum\phi_i\psi_i}{\sum\psi_i}Q \tag{6.14}$$

Through the pushover analysis, a base shear – roof displacement relationship for a MDOF structure ($Q$-$x$ relationship in Fig.6.10) can be obtained. By means of Eq(6.8) and Eq(6.14), the force – displacement characteristics of its equivalent SDOF system ( $R^*$-$x^*$ relationship in Fig.6.10) can be determined.

### 6.2.3 Influence of the Deflected Shape

From the procedure of transforming a MDOF structure to its equivalent SDOF system shown above, it can be observed that one of the important assumptions is that the deflected shape vector remains constant. The influence of choosing different deflected shape vectors at different target displacements on the characteristics of the equivalent SDOF system is investigated here.

From the procedure mentioned above it is known that the critical factors that convert a MDOF structure to its equivalent SDOF system are:

$$\frac{M^*}{L^*},\ \frac{\sum\phi_i\psi_i}{\sum\psi_i}\ ,\ \text{where } L^* = \sum_{i=1}^{N} m_i\phi_i\ , M^* = \sum_{i=1}^{N} m_i\phi_i^{\,2}$$

For an inverted triangular distribution of the lateral force $\psi_i = \frac{i}{N}$, where $i$ is the storey number and $N$ is the total number of storeys.

The influence of the deflected shape vector at different ductilities on these two factors is investigated as follows:

For the 12-storey frame structure the mass vector is

$$[M]^T = \{124.67,124.67,124.67,124.67,121.23,121.23,121.23,121.23,117.98,117.98,117.98,109.04\}$$

The deflected shape vector at different ductilities ($\mu$ = 1, 2, 3) is shown in Table 6.1 and 6.2. The deflected shape vector at a ductility of 1.5 is:
{0.0396, 0.1195, 0.2133, 0.3147, 0.4252, 0.5379, 0.6478, 0.7508, 0.8461, 0.9224, 0.9728, 1}

The values of the two factors $\frac{M^*}{L^*}$, $\frac{\sum \phi_i \psi_i}{\sum \psi_i}$ for different target displacement (ductility $\mu$ = 1, 1.5, 2, 3) are shown in Table 6.4.

Comparing these cases for different ductilities, it can be seen that for ductilities greater than 1.5, the variances of $\frac{M^*}{L^*}$, $\frac{\sum \phi_i \psi_i}{\sum \psi_i}$ are very small (3.56% and 2.76% respectively). This means that for a structure at large displacements, a constant deflected shape vector gives a good approximation. This also agrees with the results from Fajfar et al. (1987, 1988) and Moehle (1984).

For a structure with supplemental dampers, the ductility of the structure is expected to fall into the range of 1~2. The variation of $\frac{M^*}{L^*}$, $\frac{\sum \phi_i \psi_i}{\sum \psi_i}$ for ductilities $\mu$ =1~2 are also small (3.3% and 3.4% respectively). Hence, the assumption of a constant deflected shape is sufficiently accurate.

Another factor $[\phi_i - \phi_{i-1}]_{\max}$ that can be used to determine the peak interstorey drift is also investigated here for different ductilities. It can be seen that the difference of $[\phi_i - \phi_{i-1}]_{\max}$ is relatively large in comparison to the above two factors. This factor does not reflect the

influence of deflected shape on the transformation of a MDOF structure to its equivalent SDOF system but is useful for estimating interstorey drifts of the MDOF structure.

One question to be answered is what is the best choice of the deflected shape $\{\phi\}$. It has been proposed by several investigators that the best choice is the normalised deflected shape at the target displacement level (ATC 33.03). Since this displacement is not known prior to the analysis, an iteration process will have to be performed.

### 6.2.4 Time History Analysis of Equivalent SDOF System

As mentioned above, the force-displacement characteristics of the equivalent SDOF system can be obtained from a MDOF structure. A time history analysis of the equivalent SDOF system can be performed. The peak displacement and force of the SDOF system can be obtained. Through Eq(6.8) and Eq(6.14) the peak roof displacement and the peak base shear of the MDOF structure can be estimated as follows:

$$\begin{aligned} x_t &= \frac{L^*}{M^*} x_t^* \\ Q_t &= \frac{\sum \psi_i}{\sum \phi_i \psi_i} R_t^* \end{aligned} \tag{6.15}$$

where $x_t$*, $R_t$* is the peak displacement and peak force of the equivalent SDOF system respectively, $x_t$, $Q_t$ is the peak roof displacement and the peak base shear of the MDOF structure respectively.

From the assumed constant deflected shape, the peak interstorey drift can also be estimated.

From Eq(6.4), the peak interstorey drift can be calculated as:

$$ID_{\max} = [\phi_i - \phi_{i-1}]_{\max} x_t \tag{6.16}$$

where $\phi_i$ is the ith term of the normalised deflected shape $\{\phi\}$ at the target displacement.

The peak interstorey drift index can be estimated as:

$$IDI_{\max} = \left[\frac{\phi_i - \phi_{i-1}}{h_i}\right]_{\max} x_t \tag{6.17}$$

where $h_i$ is the storey height at the $i$th level.

### 6.2.4.1 Original Structure Without Dampers

As mentioned above, the base shear-roof displacement relationship of the original MDOF structure without dampers can be approximated by a bilinear curve. The force-displacement characteristics of the equivalent SDOF system for the original structure can then be obtained through Eq(6.8) and Eq(6.14).

The force-displacement characteristics of the original MDOF structure are:
Yield base shear $F_{y0}$ = 780KN, roof displacement at yield $\Delta_{y0}$ = 11.0cm, the ratio of the stiffness after yield to the initial elastic stiffness of the original structure $r_0$ = 5%.

The deflected shape at the target roof displacement of 25.5cm is taken to be the constant shape for transforming the original MDOF structure to its equivalent SDOF system. The deflected shape vector is
{0.03092, 0.1019, 0.1976, 0.3105, 0.4364, 0.5656, 0.6882, 0.7959, 0.8828, 0.9436, 0.9810, 1}

Therefore

$\frac{M^*}{L^*}$ =0.7717, and $\frac{\sum \phi_i \psi_i}{\sum \psi_i} = 0.7564.$

The hysteresis rule for this equivalent SDOF system is the bilinear hysteresis rule. Therefore, the force-displacement characteristics of the equivalent SDOF system are:

$$F_{y0}^* = \frac{\sum \phi_i \psi_i}{\sum \psi_i} F_{y0} = 0.7564 \times 780 = 589.992KN$$

$$\Delta_{y0}^* = \frac{M^*}{L^*} \Delta_{y0} = 0.7717 \times 11.0 = 8.489cm$$

The ratio of after yield stiffness to the initial elastic stiffness $r_0^* = 5\%$

The three NZS4203 code compatible earthquakes are used to conduct nonlinear time history analyses of the original MDOF structure without dampers and its equivalent SDOF system. The results are compared in Table 6.5, 6.6, 6.7 and Fig.6.12, 6.13, 6.14. It can be seen that the peak roof displacements are quite similar for both the MDOF structure and the equivalent SDOF system. Especially for the El Centro NZS4203 code compatible earthquake and the Olympia N86E NZS4203 code compatible earthquake, the differences in the peak roof displacements for MDOF structure and the SDOF system are 3.6% and 4.48% respectively. For the Taft N21E NZS4203 compatible earthquake, the difference in the peak roof displacement is 11.99%.

The differences of the peak base shear between the MDOF structure and its equivalent SDOF system are larger than those of the peak roof displacement, from 26.26 to 34%. This is due to the higher mode effect.

It can be concluded that displacement of a MDOF structure can be estimated by its equivalent SDOF system as a reasonably good approximation. The displacement response is dominated by the first mode for a MDOF frame structure with a regular distribution of mass and stiffness. The base shear response is more affected by higher modes. This conclusion agrees with the results from several investigators (Fajfar et al., 1987, 1988).

#### 6.2.4.2 Structure With Supplemental Dampers

The distribution of the yield strengths of the supplemental dampers over the height of the structure is taken to be proportional to the storey shear due to the inverted triangular lateral load pattern. The supplemental dampers are placed at all storeys. From chapter 5 it is known that for this type of distribution of the dampers, all the dampers will enter their yield stage simultaneously. Also the structure with the supplemental dampers can be considered as a dual system - the original structure without dampers and the supplemental damping system (Lin et al., 1998).

As mentioned above, the force-displacement characteristics of the original structure without dampers can be represented by its base shear – roof displacement relationship obtained from a pushover analysis.

The force-displacement characteristics of the supplemental damping system can also be represented by its base shear-roof displacement relationship. This base shear-roof displacement relationship is an elasto-plastic relationship. Obviously, the yield force of this elasto-plastic relationship for MDOF structure and its value for the equivalent SDOF system can be expressed as follows:

$$F_{yd} = F_{yd1}\cos\theta$$
$$F_{yd}^{*} = \frac{\sum \phi_i \psi_i}{\sum \psi_i} F_{yd} \tag{6.18}$$

where $F_{yd}$ = yield force of the supplemental damping system for the MDOF structure,

$F_{yd1}$= yield force of the supplemental damper at the 1st floor level,

$F_{yd}^{*}$ = yield force of the supplemental damping system for the SDOF system,

$\theta$ = the slope of the braces supporting dampers with respect to horizontal level.

For this case $F_{yd1}$ = 211KN, $\cos\theta$= 0.91, hence, $F_{yd}$ = 211×0.91=192.01KN.

Since the original structure and the supplemental damping system of this dual system have the same displacement, the deflected shape of the supplemental damping system is also the same as that of the original structure. The deformation of the damper at the 1st floor level $\delta_1$ can be calculated as:

$$\delta_1 = \Delta_d \phi_1 \cos\theta \tag{6.19}$$

where $\delta_1$ = the deformation of the damper at the 1st floor level,

$\Delta_d$= the displacement of the supplemental damping system at roof level,

$\phi_1$ = the value of the normalised deflected shape vector at the 1st floor level.

Hence, the yield displacement of the elasto-plastic relationship for the supplemental damping system can be obtained as:

$$\Delta_{yd} = \frac{\delta_{y1}}{\phi_1 \cos\theta} \tag{6.20}$$

where $\Delta_{yd}$ = yield displacement of the supplemental damping system,

$\delta_{y1}$ = yield deformation of the damper at the 1st floor level.

It has been shown that the variation of the initial elastic stiffness of the dampers has very little effect on the dynamic response of the structure with the dampers once the value of the initial elastic stiffness of the dampers reach a certain level. Hence, the yield displacement of the supplemental damping system can be estimated through Eq(6.20) in which $\phi_1$ is taken from the constant deflected shape without great error.

For transformation of the MDOF structure with supplemental dampers to its equivalent SDOF system, the dual system can be considered as a single degree of freedom mass connected to the ground by two springs — one representing the original structure and the other representing the supplemental damping system (see Fig.6.11).

The force-displacement characteristics of the spring for the original structure can be calculated as follows:

The deflected shape at the target roof displacement (in this case, about 18cm) is taken to be the constant shape for transforming the original MDOF structure to its equivalent SDOF system. The deflected shape vector is

{0.03394, 0.1071, 0.2007, 0.3087, 0.4287, 0.5517, 0.6690, 0.7740, 0.8642, 0.9329, 0.9771, 1}

$$\frac{M^*}{L^*}=0.7606,\ \frac{\sum\phi_i\psi_i}{\sum\psi_i}=0.7470.$$

The hysteresis rule for this spring is bilinear. The base shear-roof displacement curve of the original structure is already known. Hence, the force-displacement characteristics of the spring representing the original structure can be calculated as follows:

$$F_{y0}^*=\frac{\sum\phi_i\psi_i}{\sum\psi_i}F_{y0}=0.7470\times 780=582.66KN$$

$$\Delta_{y0}^*=\frac{M^*}{L^*}\Delta_{y0}=0.7606\times 11.0=8.367cm$$

The ratio of after yield stiffness to the initial elastic stiffness $r_0^*=5\%$

The force-displacement characteristics of the spring representing the supplemental damping system can also be calculated as below. The hysteresis rule for this spring is an elasto-plastic model.

$\delta_{y1} = 0.09\times10^{-3}$m, $\phi_1 = 0.03394$

$$\Delta_{yd} = \frac{\delta_{y1}}{\phi_1 \cos\theta} = \frac{0.09\times10^{-3}}{0.03394\times0.91} = 2.914\times10^{-3}\text{m}$$

$$F^*_{yd} = \frac{\sum\phi_i\psi_i}{\sum\psi_i}F_{yd} = 0.7470\times192.01 = 143.43\text{KN}$$

$$\Delta^*_{yd} = \frac{M^*}{L^*}\Delta_{yd} = 0.7606\times2.914\times10^{-3} = 2.216\times10^{-3}\text{m}$$

where

$\Delta^*_{yd}$ = the yield displacement of the spring representing the supplemental damping system,

$F^*_{yd}$ = the yield force of the spring representing the supplemental damping system.

The three NZS4203 code compatible earthquakes are used to conduct nonlinear time history analyses of the MDOF structure with supplemental dampers and its equivalent SDOF system. The results are compared in Tables 6.8, 6.9, 6.10 and Figs.6.15, 6.16, 6.17.

It can be seen that the differences of the peak roof displacements between the MDOF structure and its equivalent SDOF system are very small for these three earthquakes (only 1.65~2.88%). These differences are smaller than those for the original structure without dampers.

The differences of the peak base shear between the MDOF structure and its equivalent SDOF system are larger than those for the peak roof displacement. They are from 20~30%. This is again due to the higher mode effect.

The main purpose of incorporating the supplemental dampers into a structure is to control the displacement and deformation of the structure. The main concern here is the displacement response. Hence the response of the structure with the supplemental dampers can be accurately estimated by its equivalent SDOF system.

Comparing Figs.6.12, 6.13, 6.14 with Figs.6.15, 6.16, 6.17 respectively, it can be observed that in Figs.6.15, 6.16, 6.17 the responses for the MDOF structure with dampers and the SDOF system have very similar shape. This is especially so in Fig.6.15, where the two responses are almost the same. In Fig.6.16, 6.17 some variation occurs. This is due to the characteristics of the bilinear hysteresis loop. This means that the displacement time history for the MDOF structure is very similar to that of the SDOF system. It can be concluded that the distribution of the damper yield strengths adopted here makes the structure respond predominantly in the first mode shape. This also shows that the structure with supplemental dampers with this distribution of yield strengths can be considered as a dual system — the original system and the damping system. These two systems can be further represented simply using the bilinear model and the elasto-plastic model respectively.

| Ductility | $\mu = 1$ | | $\mu = 2$ | | $\mu = 3$ | |
|---|---|---|---|---|---|---|
| Story Level | Original structure (no damper) | structure with dampers | Original structure (no damper) | structure with dampers | Original structure (no damper) | structure with dampers |
| 1 | 0.04037 | 0.04411 | 0.03394 | 0.0352 | 0.03018 | 0.03247 |
| 2 | 0.1180 | 0.1291 | 0.1071 | 0.1118 | 0.1008 | 0.1082 |
| 3 | 0.2053 | 0.2237 | 0.2007 | 0.210 | 0.1971 | 0.210 |
| 4 | 0.2952 | 0.3197 | 0.3087 | 0.3222 | 0.3111 | 0.3282 |
| 5 | 0.3931 | 0.4222 | 0.4287 | 0.4453 | 0.4382 | 0.4573 |
| 6 | 0.4993 | 0.5291 | 0.5517 | 0.5702 | 0.5687 | 0.5876 |
| 7 | 0.6106 | 0.6359 | 0.6690 | 0.6881 | 0.6925 | 0.7096 |
| 8 | 0.7219 | 0.7387 | 0.7740 | 0.7924 | 0.8013 | 0.8155 |
| 9 | 0.8286 | 0.8366 | 0.8642 | 0.8787 | 0.8881 | 0.8985 |
| 10 | 0.9141 | 0.9161 | 0.9329 | 0.9406 | 0.9471 | 0.9530 |
| 11 | 0.9697 | 0.9696 | 0.9771 | 0.9793 | 0.9824 | 0.9842 |
| 12 | 1 | 1 | 1 | 1 | 1 | 1 |

Table 6.1 Comparison of deflected shape vector of the structure without and with supplemental dampers at different ductility values ($F_{yd1}$ = 211KN)

| Ductility | $\mu = 1$ | | $\mu = 2$ | | $\mu = 3$ | |
|---|---|---|---|---|---|---|
| Story Level | Original structure (no damper) | structure with dampers | Original structure (no damper) | structure with dampers | Original structure (no damper) | structure with dampers |
| 1 | 0.04037 | 0.04404 | 0.03394 | 0.03492 | 0.03018 | 0.03178 |
| 2 | 0.1180 | 0.1287 | 0.1071 | 0.1103 | 0.1008 | 0.1057 |
| 3 | 0.2053 | 0.2229 | 0.2007 | 0.2069 | 0.1971 | 0.2056 |
| 4 | 0.2952 | 0.3187 | 0.3087 | 0.3178 | 0.3111 | 0.3226 |
| 5 | 0.3931 | 0.4211 | 0.4287 | 0.4404 | 0.4382 | 0.4516 |
| 6 | 0.4993 | 0.5279 | 0.5517 | 0.5655 | 0.5687 | 0.5827 |
| 7 | 0.6106 | 0.6347 | 0.6690 | 0.6842 | 0.6925 | 0.7058 |
| 8 | 0.7219 | 0.7374 | 0.7740 | 0.7898 | 0.8013 | 0.8129 |
| 9 | 0.8286 | 0.8354 | 0.8642 | 0.8775 | 0.8881 | 0.8972 |
| 10 | 0.9141 | 0.9150 | 0.9329 | 0.9402 | 0.9471 | 0.9525 |
| 11 | 0.9697 | 0.9691 | 0.9771 | 0.9792 | 0.9824 | 0.9841 |
| 12 | 1 | 1 | 1 | 1 | 1 | 1 |

Table 6.2 Comparison of deflected shape vector of the structure without and with supplemental dampers at different ductility values ($F_{yd1}$ = 422KN)

| Ductility | μ = 1 | | μ = 2 | |
|---|---|---|---|---|
| Story Level | Original structure (no damper) | structure with dampers | Original structure (no damper) | structure with dampers |
| 1 | 0.04037 | 0.05468 | 0.03394 | 0.04422 |
| 2 | 0.1180 | 0.1612 | 0.1071 | 0.1429 |
| 3 | 0.2053 | 0.2805 | 0.2007 | 0.2690 |
| 4 | 0.2952 | 0.4017 | 0.3087 | 0.4080 |
| 5 | 0.3931 | 0.5250 | 0.4287 | 0.5499 |
| 6 | 0.4993 | 0.6418 | 0.5517 | 0.6799 |
| 7 | 0.6106 | 0.7460 | 0.6690 | 0.7886 |
| 8 | 0.7219 | 0.8338 | 0.7740 | 0.8723 |
| 9 | 0.8286 | 0.9039 | 0.8642 | 0.9321 |
| 10 | 0.9141 | 0.9494 | 0.9329 | 0.9677 |
| 11 | 0.9697 | 0.9764 | 0.9771 | 0.9868 |
| 12 | 1 | 1 | 1 | 1 |

Table 6.3 Comparison of deflected shape vector of the structure without and with supplemental dampers at different ductility values (with constant damper yield strengths $F_{ydi}$ = 422KN, i = 1, …, N)

| Ductility (μ) | $\frac{M^*}{L^*}$ | $\frac{\sum \phi_i \psi_i}{\sum \psi_i}$ | $[\phi_i - \phi_{i-1}]_{max}$ |
|---|---|---|---|
| 1 | 0.7363 | 0.7224 | 0.1113 |
| 1.5 | 0.7480 | 0.7386 | 0.1127 |
| 2 | 0.7606 | 0.7470 | 0.123 |
| 3 | 0.7746 | 0.7590 | 0.1238 |

Table 6.4 Influence of deflected shape on the transformation of the MDOF structure to its equivalent SDOF system

| | Peak roof displacement (cm) | Peak base shear (KN) |
|---|---|---|
| MDOF structure | 25.487 | 1178.8 |
| SDOF system | 24.569 | 828.08 |
| Difference | 3.60% | 29.75% |

Table 6.5 Comparison of dynamic response of the original MDOF structure without dampers and its equivalent SDOF system under the El Centro NZS4203 code compatible earthquake

| | Peak roof displacement (cm) | Peak base shear (KN) |
|---|---|---|
| MDOF structure | 27.71 | 1278.2 |
| SDOF system | 28.95 | 843.46 |
| Difference | 4.48% | 34.0% |

Table 6.6 Comparison of dynamic response of the original MDOF structure without dampers and its equivalent SDOF system under the Olympia N86E NZS4203 code compatible earthquake

| | Peak roof displacement (cm) | Peak base shear (KN) |
|---|---|---|
| MDOF structure | 27.34 | 1152.1 |
| SDOF system | 30.618 | 849.55 |
| Difference | 11.99% | 26.26% |

Table 6.7 Comparison of dynamic response of the original MDOF structure without dampers and its equivalent SDOF system under the Taft N21E NZS4203 code compatible earthquake

| | Peak roof displacement (cm) | Peak base shear (KN) |
|---|---|---|
| MDOF structure | 17.74 | 1262.7 |
| SDOF system | 18.25 | 997.71 |
| Difference | 2.88% | 21% |

Table 6.8 Comparison of dynamic response of the MDOF structure with dampers and its equivalent SDOF system under the El Centro NZS4203 compatible earthquake

| | Peak roof displacement (cm) | Peak base shear (KN) |
|---|---|---|
| MDOF structure | 16.99 | 1432.2 |
| SDOF system | 16.71 | 992.25 |
| Difference | 1.65% | 30.72% |

Table 6.9 Comparison of dynamic response of the MDOF structure with dampers and its equivalent SDOF system under the Olympia N86E NZS4203 compatible earthquake

| | Peak roof displacement (cm) | Peak base shear (KN) |
|---|---|---|
| MDOF structure | 21.20 | 1272.7 |
| SDOF system | 20.64 | 1006.2 |
| Difference | 2.64% | 20.94% |

Table 6.10 Comparison of dynamic response of the MDOF structure with dampers and its equivalent SDOF system under the Taft N21E NZS4203 compatible earthquake

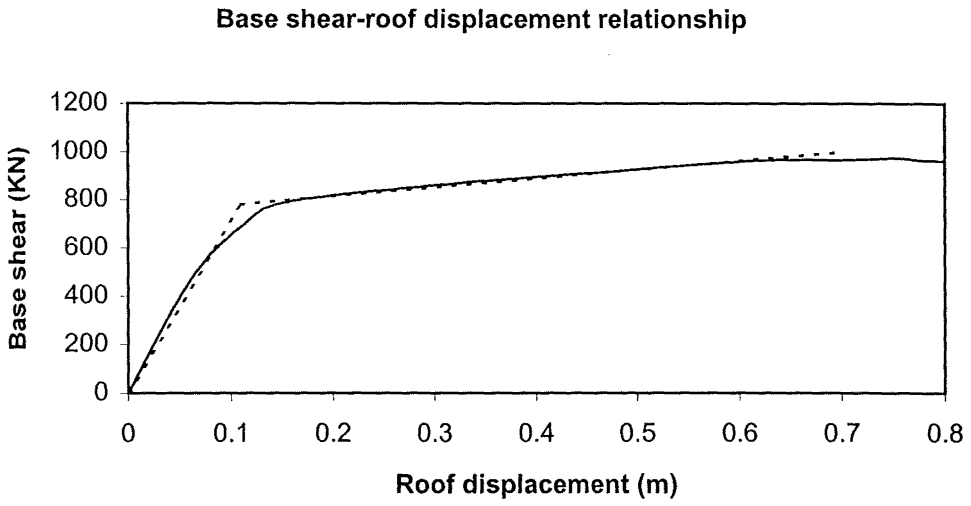


Figure 6.1 Base shear-roof displacement relationship of the structure without damper

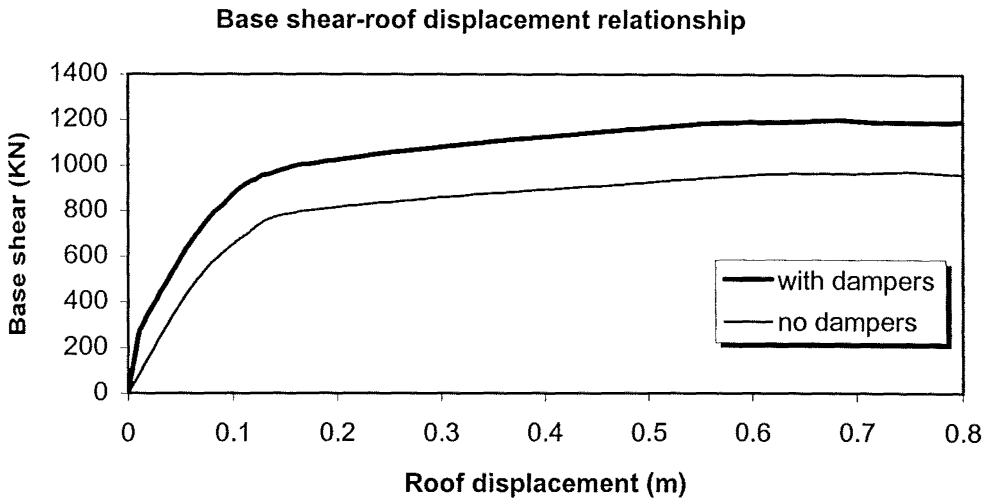


Figure 6.2 Base shear-roof displacement relationship of the structure without and with the supplemental dampers (Fyd1=211KN)

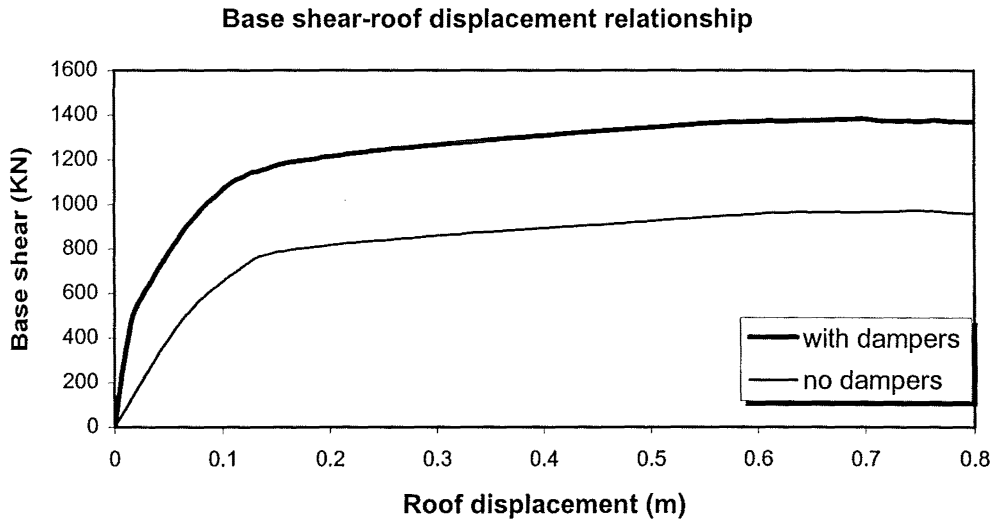


Figure 6.3 Base shear-roof displacement relationship of the structure without and with the supplemental dampers (Fyd1=422KN)

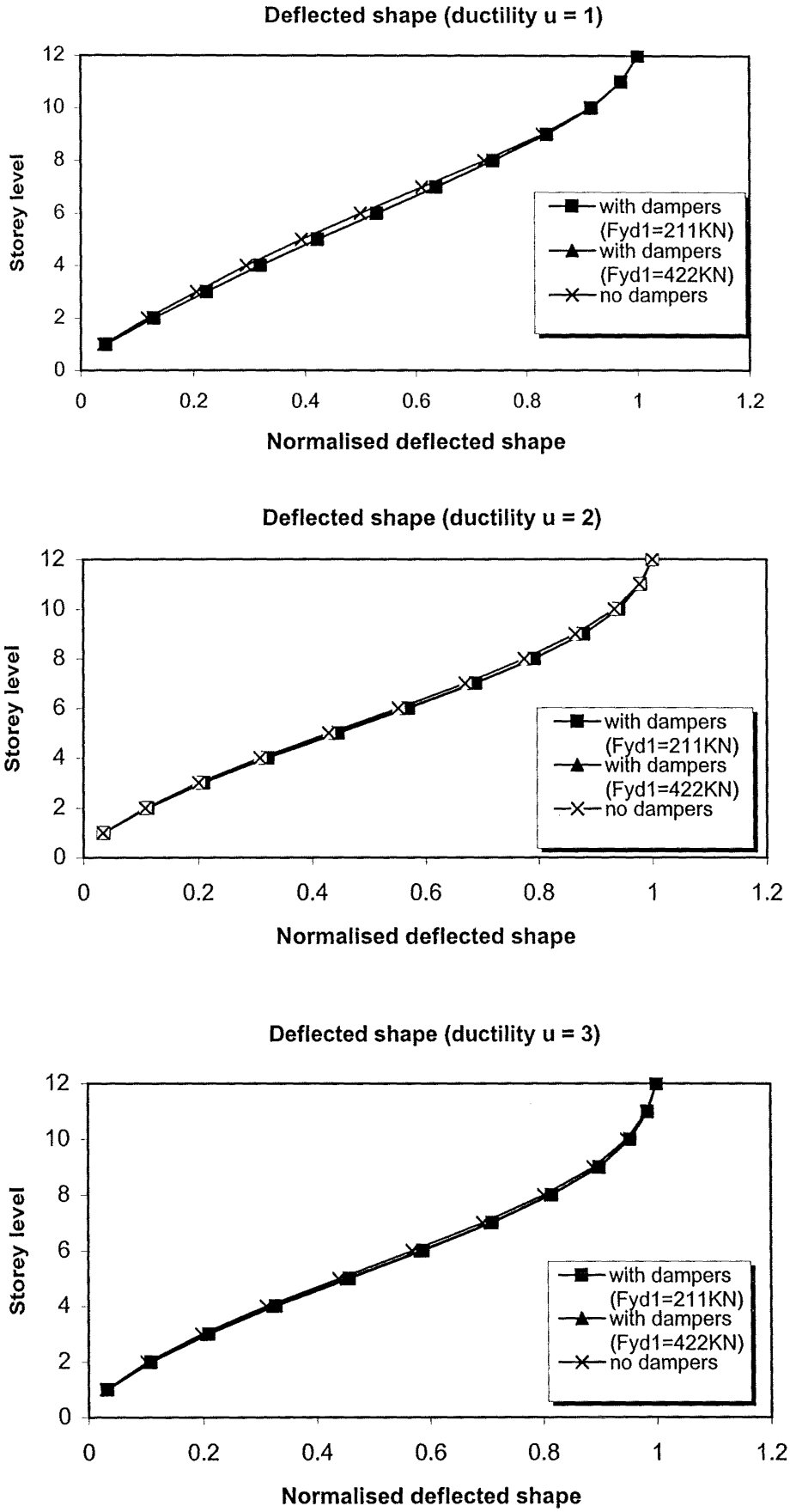


Figure 6.4 Comparison of the deflected shapes of the structure without dampers and the structure with the dampers for different ductilities

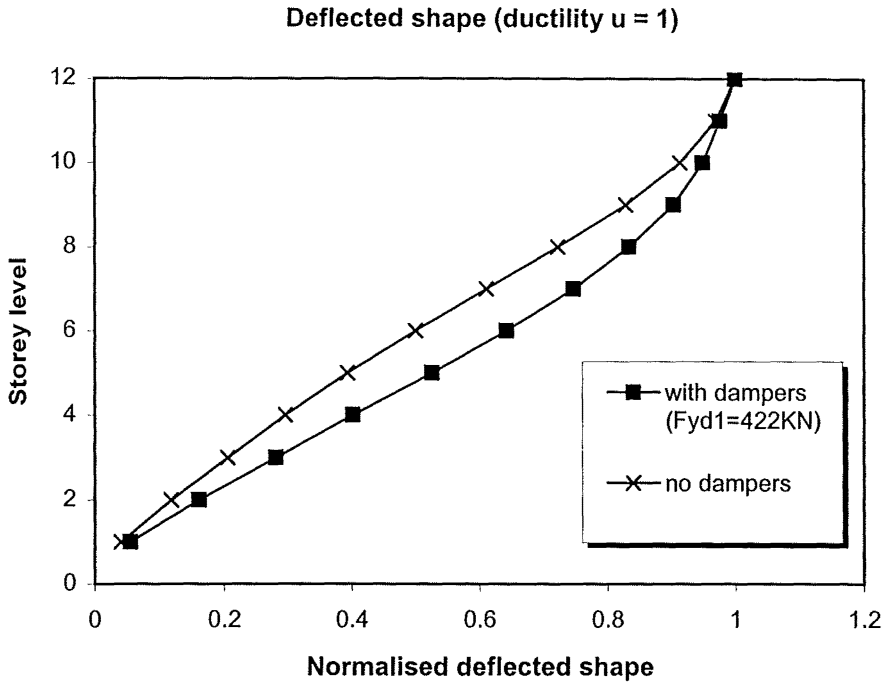


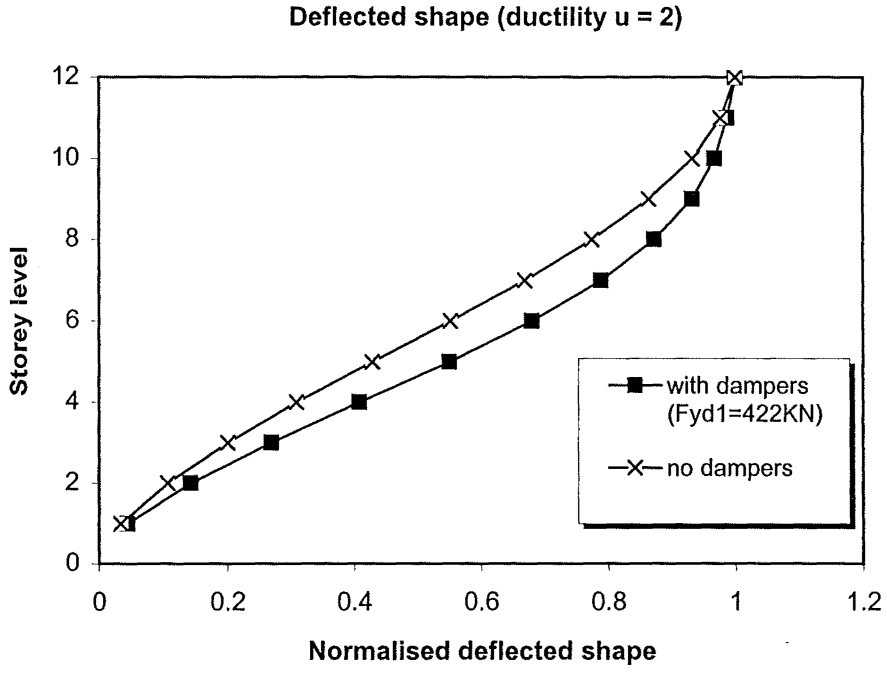


Figure 6.5 Comparison of deflected shapes of the structure without dampers and the structure with the dampers which have the same yield strength at all levels (422KN) for different ductilities

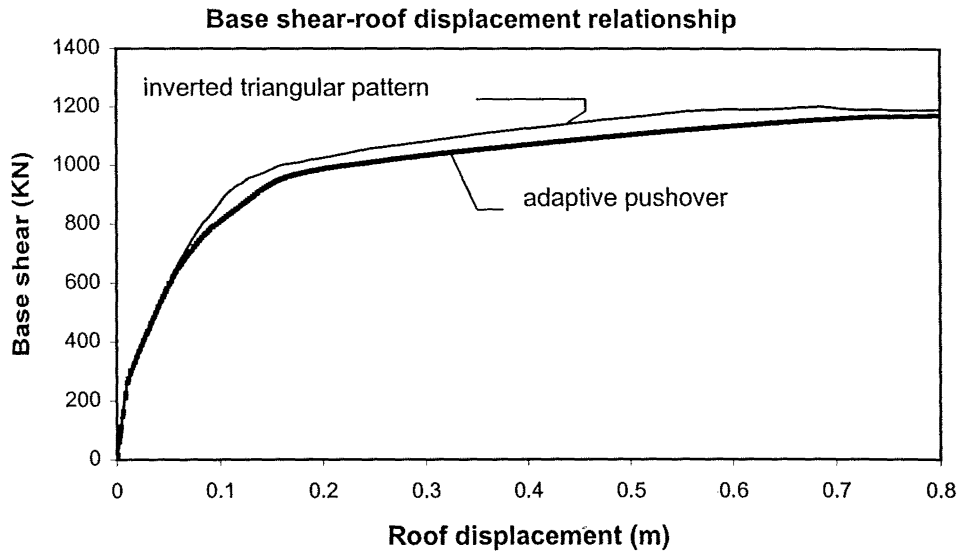


Figure 6.6 Comparison of the base shear-roof displacement curve of the structure with the dampers obtained from an inverted triangular load pattern and the adaptive pushover analysis

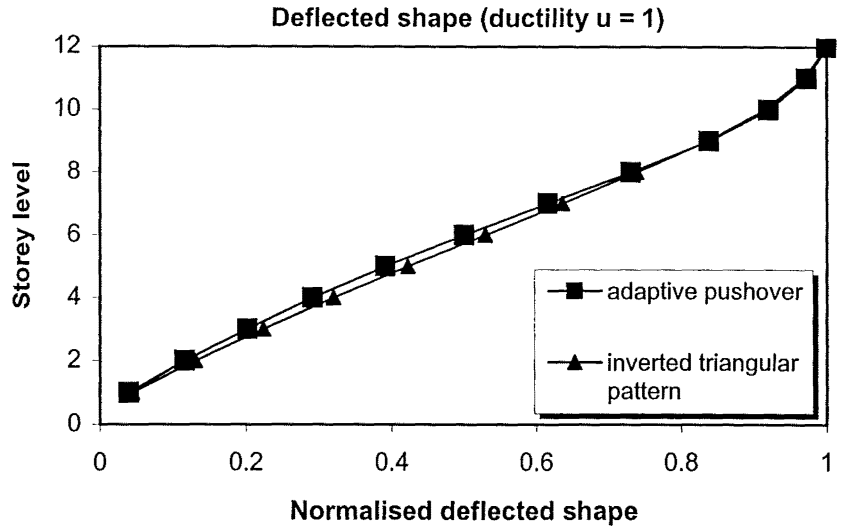


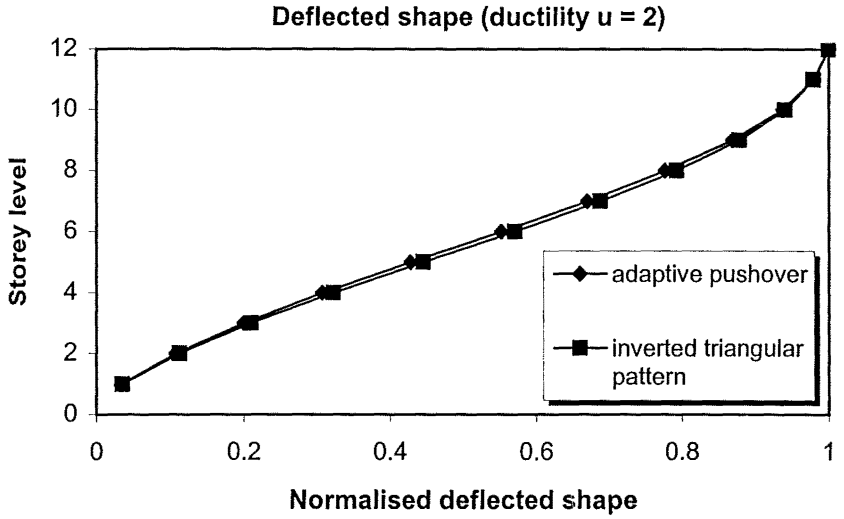


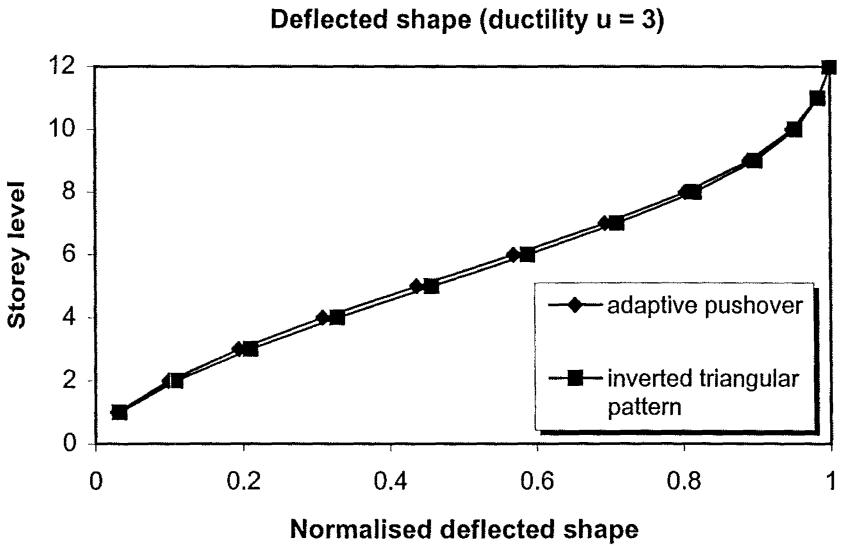


Figure 6.7 Comparison of the deflected shape of the structure with the dampers obtained from an inverted triangular load pattern and the adaptive pushover analysis

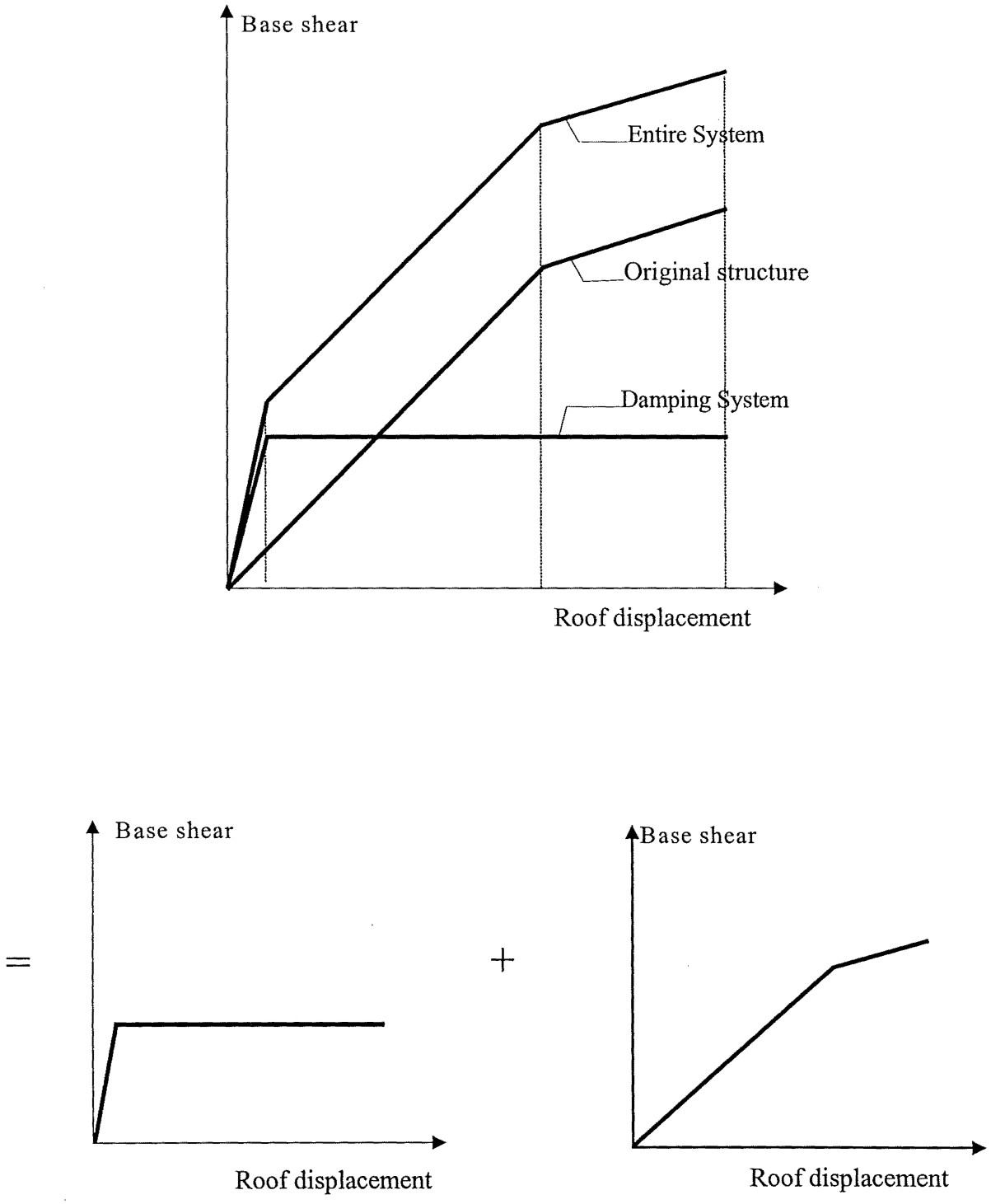


Figure 6.8 Base shear-roof displacement relationship of the structure with the dampers

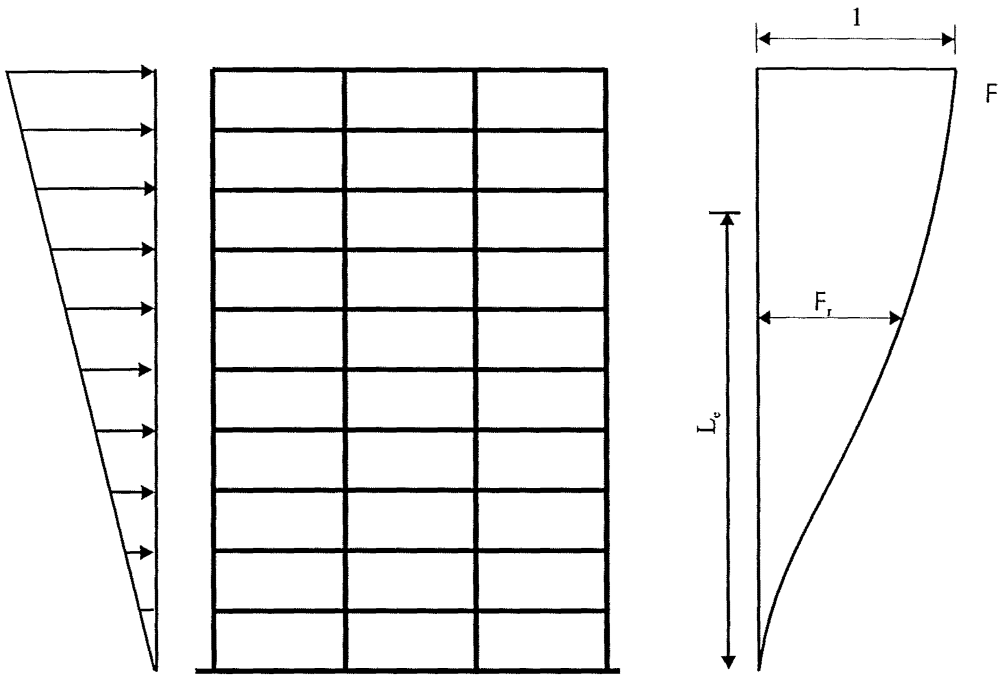


( a ) Static Lateral Loads

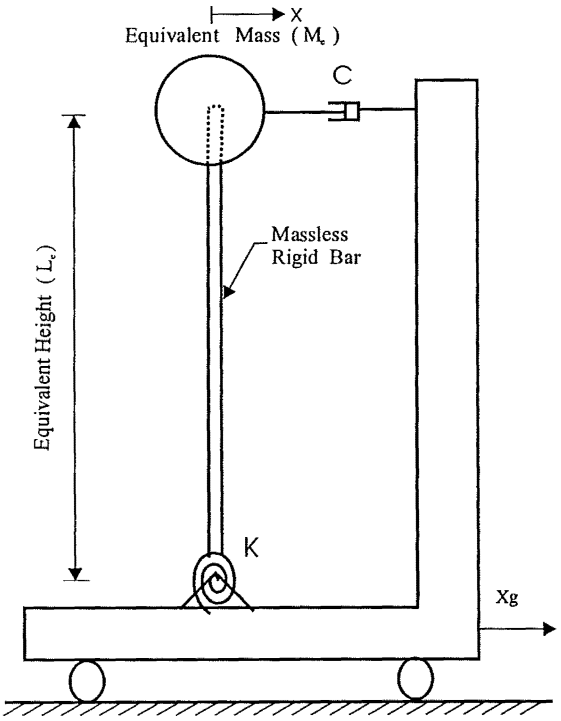


( b ) Q-Model

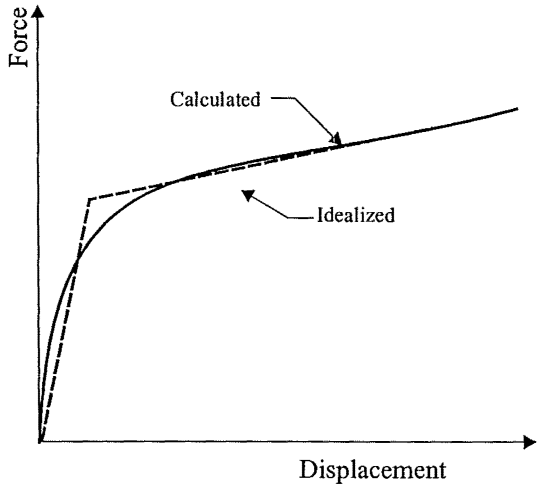


( c ) Force-Displacement Relationship

Figure 6.9 Relationship of Q-Model to a Multistorey Structure
(from Saiidi et al., 1981)

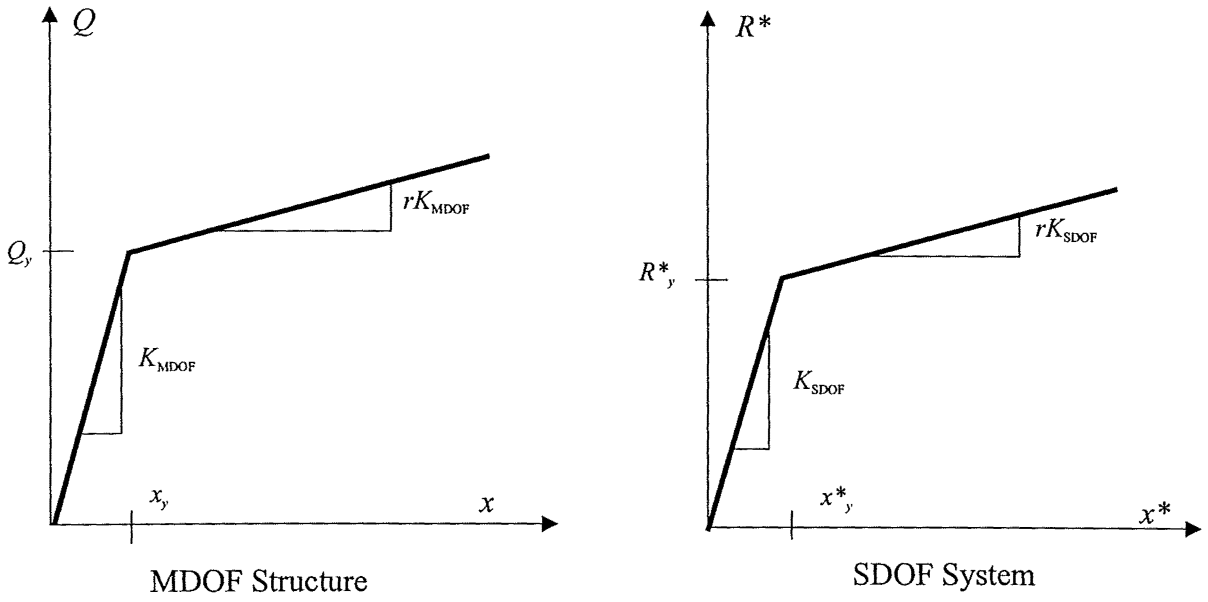


Figure 6.10. Force-displacement characteristics of MDOF structure and equivalent SDOF system

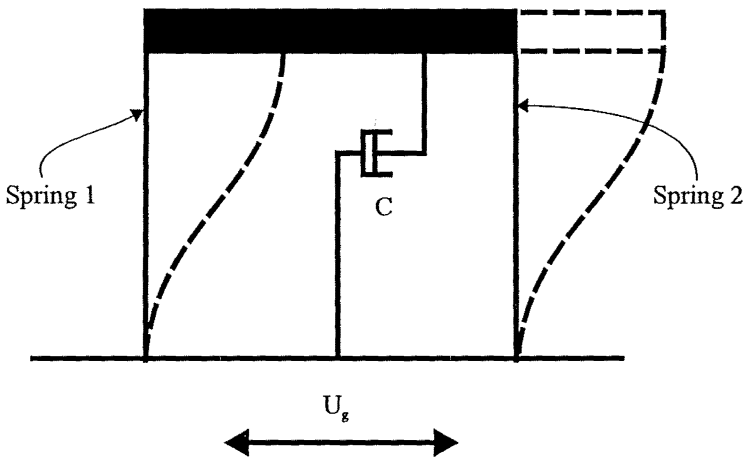


Spring 1 = Represent the original structure

Spring 2 = Represent the supplemental damping system

Figure 6.11 The equivalent SDOF system for a structure with supplemental dampers

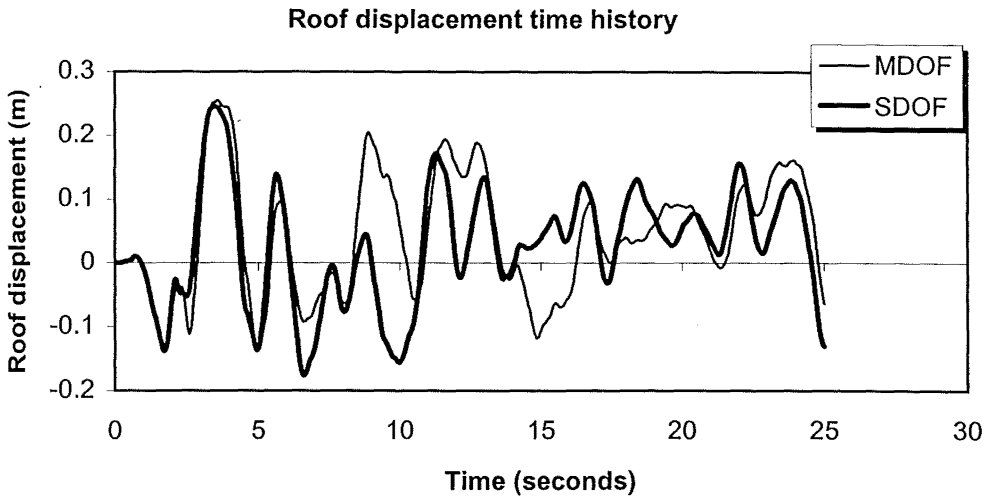


Figure 6.12 Roof displacement time histories of both the original MDOF structure without dampers and its equivalent SDOF system under the El Centro NZS4203 compatible earthquake

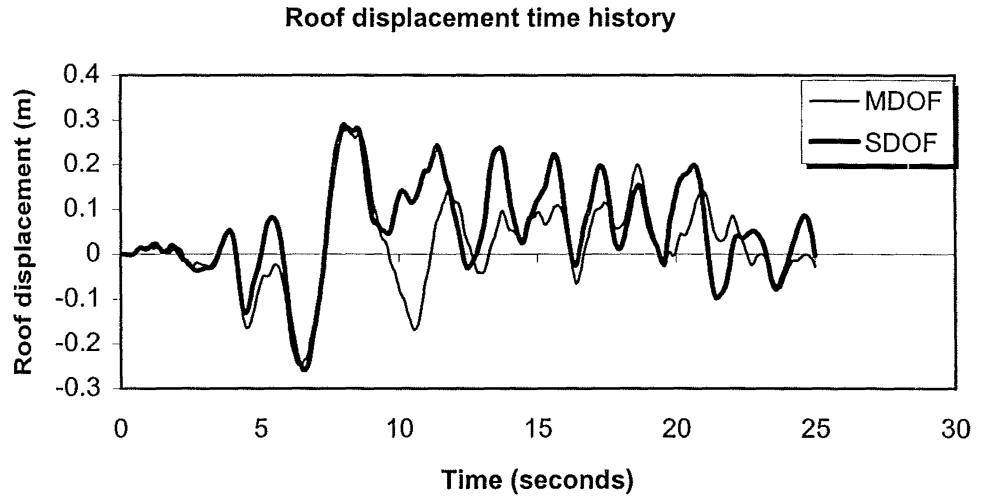


Figure 6.13 Roof displacement time histories of both the original MDOF structure without dampers and its equivalent SDOF systen under the Olympia N86E NZS4203 compatible earthquake

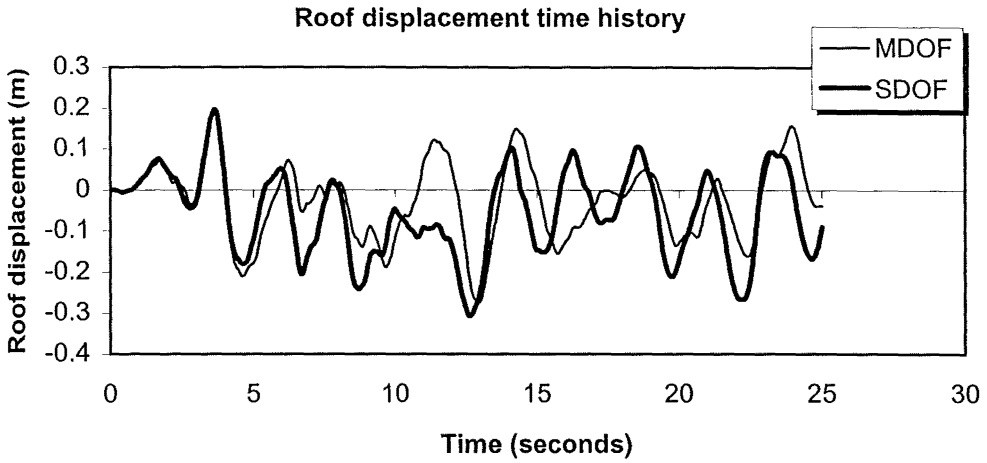


Figure 6.14 Roof displacement time histories of both the original MDOF structure without dampers and its equivalent SDOF system under Taft N21E NZS4203 compatible earthquake

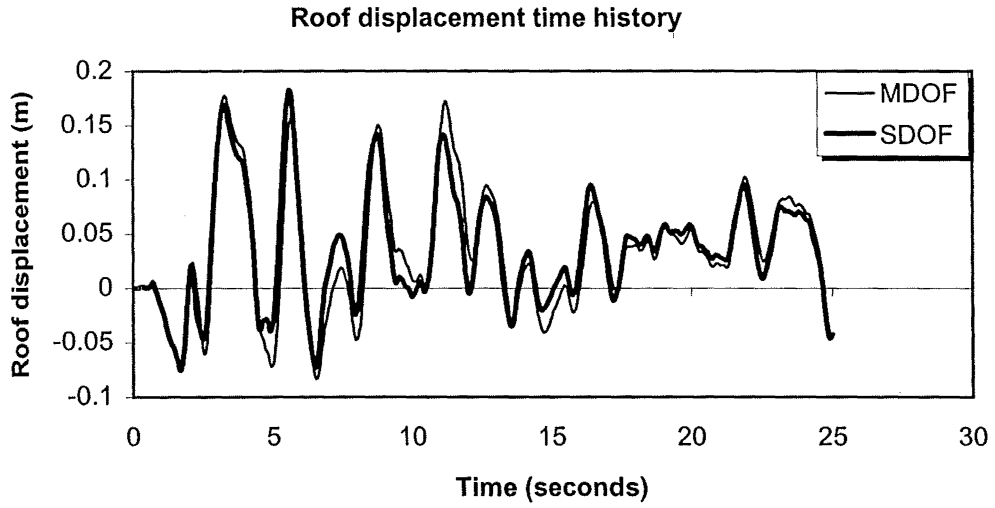


Figure 6.15 Roof displacement time histories of both the MDOF structure with the dampers and its equivalent SDOF system under the El Centro NZS4203 compatible earthquake

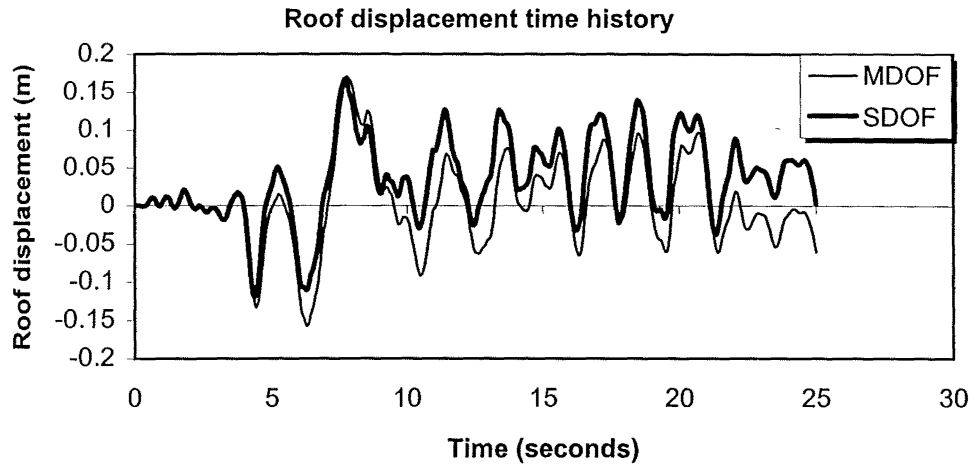


Figure 6.16 Roof displacement time histories of both the MDOF structure with the dampers and its equivalent SDOF system under the Olympia N86E NZS4203 compatible earthquake

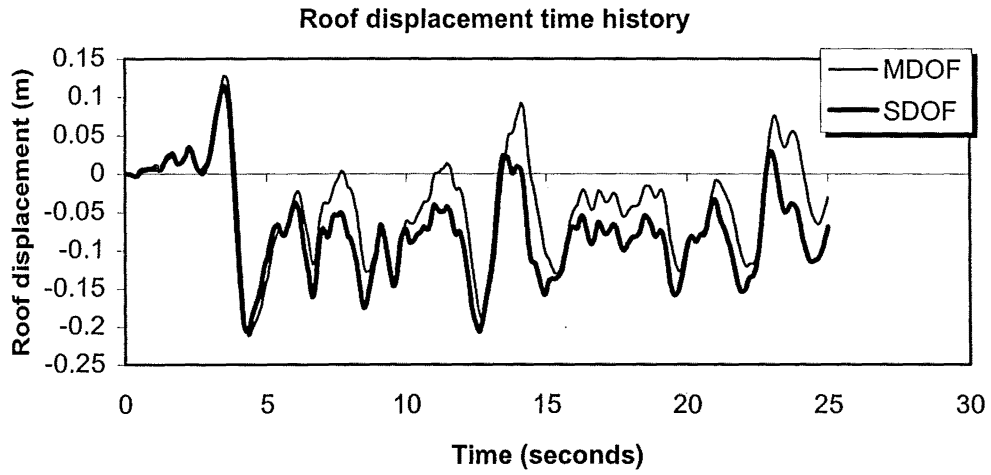


Figure 6.17 Roof displacement time histories of both the MDOF structure with the dampers and its equivalent SDOF system under the Taft N21E NZS4203 compatible earthquake

# CHAPTER 7

# EQUIVALENT VISCOUS DAMPING RATIO

## 7.1 INTRODUCTION

Damping is basically a dissipation of energy that occurs in vibration systems. The sources of damping for structures with supplemental dampers include damping in the original structure and added damping due to the supplemental dampers. In chapter 3 it has been shown how the effect of the supplemental dampers can be taken in to account in a MDOF structure for time history analyses under earthquake excitations. In the analyses, the effect of the dampers is included in an implicit way. For the purpose of a simplified analysis and design, often a SDOF system with a damping effect, which is expressed in an explicit and direct way, is adopted.

This chapter discusses how to estimate the damping values for MDOF structures with supplemental dampers and express the effect of the supplemental dampers in an explicit way.

### 7.1.1 Representation of Damping

Damping can be represented in three different ways (Brebbia et al., 1985):
(1) Viscous damping
(2) Coulomb damping
(3) Hysteretic damping

These are ways of representing damping only and do not imply any particular mechanism for damping.

(1) Viscous damping

Viscous damping is defined such that the damping force is proportional to a velocity (Fig.7.1).

$$F_d = -c\dot{u}$$

where $c$ = the constant of viscosity

$\dot{u}$ = velocity of mass

$F_d$ = damping force.

In general it can be shown that the energy dissipated per cycle when the system is steadily excited by an imposed forcing function of frequency ω with displacement amplitude $A$, is given by

$$\Delta U = \pi c \omega A^2$$

Hence the energy loss increases as the square of the amplitude and is proportional to the exciting frequency and the dashpot constant.

(2) Coulomb damping

Coulomb damping (or frictional damping) can be regarded as existing when the damping force is a constant (depending only on the normal reaction) and opposes the motion of the mass. The damping force can be written as:

$$F_d = -\varsigma(\text{sign}\,\dot{u}) = -\varsigma\frac{\dot{u}}{|\dot{u}|}$$

where $\zeta$ = a constant.

The frequency of the damped motion is not altered by the presence of Coulomb damping. Since the force is constant, the energy dissipated per cycle is proportional to the amplitude, $A$. $\Delta U$ is given by

$$\Delta U = 4\zeta A$$

(3) Hysteretic damping

Hysteretic damping is sometimes termed structural damping. There are three possible mathematical models of hysteretic damping (Reid, 1956, Bishop, 1955). The equations of motion including hysteretic damping with respect to these three models are shown as follows:

(a) $m\ddot{u} + c\left|\frac{u}{\dot{u}}\right|\dot{u} + ku = f(t)$

(b) $m\ddot{u} + k(1 + i\eta)u = f(t)$

(c) $m\ddot{u} + \frac{h}{\omega}\dot{u} + ku = f(t)$

where $h$ = a constant

$\eta$ = the loss factor ( $k\eta = h$ )

$\omega$ = the excitation frequency.

In a steady state response, these three models for hysteretic damping give the same results for the dissipated energy per cycle (Brebbia et al., 1985):

$$\Delta U = \pi h A^2$$

where $A$ = the amplitude of motion.

It can be seen that the dissipated energy is independent of the frequency of the exciting force. This is one major advantage for this damping representation. It represents a characteristic often observed in real structures.

The viscous damping representation is found to cause the response for higher models of real structures to be underestimated. This can be partly compensated by replacing $c\dot{u}$ with $\frac{h}{\omega}\dot{u}$ in the equation of motion.

However, the problem with this definition of the hysteretic damping is that it can be shown to flout the fundamental rule of causality, i.e. hysteretic damping implies that the present state of

system depends not only on all its past states but also on all future states (Brebbia et al., 1985).

These three representations mentioned above are basic representations of damping models. These models can also be extended by including additional terms in the equation of motion. For example, they could be: general Maxwell model (Brebbia et al., 1985) and Biot's linear hysteretic damping model (Caughey, 1962).

### 7.1.2 Equivalent Viscous Damping

In application, the viscous damping model is often used because of its mathematical simplicity. A linear structure with viscous damping is a linear system. The other damping models may introduce nonlinearity.

Jacobsen proposed a description of the steady-state response of a nonlinearly damped oscillator by means of an equivalent viscous damping coefficient. This is an idea of replacing a nonlinear system by an "equivalent" linear system whose behaviour will be an approximation to that of the nonlinear system. This makes it possible for certain limited problems to extend the well-known results of linear analysis to such nonlinear problems. By a comparison of the various criteria of equivalence with the exact solutions for specific problems, and with experimental results, Jacobsen concluded that the most useful criterion is that of the equivalence of energy dissipated per cycle (Jacobsen, 1930).

Jacobsen (1930, 1960) defined the equivalent damping coefficient ratio $\nu_{eq}$ as:

$$\nu_{eq} \approx \frac{1}{2\pi} \frac{\text{hysteretic Work Area}}{\text{Work Area under Skeleton relationship}} \equiv \frac{1}{2\pi} \frac{\Delta W}{W}$$

Jacobsen (1960) mentioned that for small damping values and for almost linear systems the equivalent viscous damping is likely to be justifiable.

Hudson (1965) considered the bi-linear model for hysteretic systems that are strongly nonlinear. He used the model to justify the use of equivalent viscous damping for the response spectrum approach for earthquake engineering. The accuracy of the representation was illustrated by comparison with digital solutions for bilinear and curved hysteresis loops.

Jennings (1968) examined in detail some of the different ways in which equivalent viscous damping can be defined for the steady-state response of yielding structures to sinusoidal excitation. There are six methods for defining the equivalent viscous damping for yielding structures:

(1) Resonant amplitude matching — the frequency shift shown by the response of the yielding structure is not considered. The associated linear oscillator is specified to have the same mass as the yielding structure and the natural period of the linear oscillator is chosen equal to that for small oscillations of the yielding structure.

(2) Dynamic Stiffness — to model the frequency shift as well as the amplitude nonlinearities of the steady-state response of a yielding oscillator. The associated linear structure has the same mass as the yielding oscillator and the spring constant of the linear oscillator is chosen to that the resonant frequencies of the two structures are identical. The resonant amplitudes are matched and the energies dissipated per cycle by the two structures are made to be the same.

(3) Dynamic Mass — to keep the spring constant of the linear structure at the initial level, and simply to change the mass of the linear structure to model the frequency shift shown by the yielding structure. An associated linear oscillator could be defined as follows: the stiffness of the associated linear structure would equal the initial stiffness of the yielding structure and the mass of the linear structure would be varied to match the resonant frequencies of the two structures. The resonant amplitudes and energies dissipated per cycle would also be set to be equal.

(4) Constant Critical damping — to define the associated linear oscillator in such a way that the critical damping coefficient remains constant while retaining the natural frequency shift modeling the behaviour of the yielding oscillator. The resonant amplitudes and the energies dissipated per cycle are matched as before.

(5) Geometric Stiffness — the stiffness of the associated linear structure is fixed by the geometry of the hysteresis loop. The resonant amplitudes of the yielding and the associated linear structure and the energies dissipated at resonance are then equated. The masses of the two structures are equal.

(6) Geometrical Energy Method — an associated linear structure is not used, rather the geometry of the skeleton curve and the hysteresis loop define the equivalent viscous damping according to the following formula:

$$\eta(A) = (1/2\pi) \text{ (friction work area / work area under skeleton curve)}$$

Rea et al. (1969) conducted dynamic tests on a model steel structure. He chose the Ramberg-Osgood model to represent the hysteresis loops. He gave four definitions of damping capacity $\zeta$ because there were four ways that $W$ (energy stored in the steady-state vibration) may be defined. He provided a description of the damping capacity of the model structure as a function of amplitude up to the maximum ductility factor obtained (Fig.7.2). The definition of damping capacity $\zeta_1$ has been used by Hudson (1965), the definition $\zeta_2$ by Rosenblueth, and definition $\zeta_3$ by Jacobsen (1960) and Hudson (1965). These definitions of damping capacity have been discussed by Jennings (1968): the definition of damping capacity $\zeta_1$ corresponds to (1) — resonant amplitude matching, the definition $\zeta_2$ corresponds to (5) — geometric stiffness, the definition $\zeta_3$ corresponds to (6) — geometrical energy method.

Iwan et al. (1979) assessed the accuracy of the various available approximate methods for defining equivalent linear systems for simple nonlinear structures subjected to earthquake excitations and suggested improved methods as appropriate. In their study, a broad class of approximate methods was considered ranging from those based on harmonic response behaviour to those based on stationary random response behaviour. The basis of their study is that the proper equivalent viscous damping ratio and the effective period should be adopted to represent the nonlinear behaviour of structures.

For the structure with supplemental dampers, it is expected that the main structure will remain almost in its elastic stage or only have small inelastic deformations. It is reasonable to use the equivalent viscous damping ratio to evaluate the damping effect through comparison between the dissipated energy and the system maximum strain energy. For a SDOF system, the widely accepted relationship between energy dissipation per cycle $E_d$, equivalent viscous damping $\xi$ and maximum elastic strain energy $E_s$ has been proposed by Clough et al. (1975) as:

$$\xi = \frac{E_d}{4\pi E_s} \tag{7.1}$$

Turkington et al (1987) in their study showed that the inelastic behaviour of the most typical bridges supported on lead-rubber bearings can be reasonably represented by an elastic SDOF structure model with an "effective period" and "effective damping". It was found that the period shift from the initial elastic period to the effective period and the increased damping due to the hysteretic behaviour of the dissipator can be estimated from the periods calculated for the initial and post elastic bearing stiffness and the lead dissipator yield strength. Hence, the response can be predicted directly from elastic response spectra rather than from inelastic response spectra.

Although the conclusion from Turkington et al. is for bridges supported on lead-rubber bearings, the basic concept in this result is to adopt "effective damping" and "effective period" to represent the effect of lead-rubber bearings. This concept could also be applied to building structures with supplemental lead dampers to use the "equivalent viscous damping" and the "effective period" of the structure to consider the effect of the dampers. Due to the complexity of a MDOF structure, the higher damping effect on the response spectra and the inelastic deformations of the main structure, some modifications are necessary to carry out a simplified analysis of structures with supplemental dampers under design earthquakes. This will be discussed in detail in chapter 8. In this chapter, the estimate of the equivalent viscous damping due to the supplemental dampers and inelastic deformations of the structure and the effective period of the structure with dampers will be investigated.

## 7.2 EQUIVALENT VISCOUS DAMPING RATIO DUE TO THE SUPPLEMENTAL DAMPERS

It is assumed that the original structure has a regular mass and stiffness distribution, and that the distribution of the yield strengths of the supplemental dampers over the height of the structure is proportional to the storey shear force due to the inverted triangular lateral load pattern. From Chapter 6 we can see that for this type of structure with supplemental dampers, the dynamic response is dominated by the first mode. An equivalent SDOF system can be a very useful tool for conducting the analysis and design of such a structure with supplemental dampers.

In Chapter 6 the equivalent SDOF system was analysed using time history analyses. A more effective and simpler method is the simplified nonlinear static method. For this simplified static method, the effect of the supplemental dampers can be considered by means of the equivalent viscous damping ratio due to the dampers and the effective period of the structure (Lin et al., 1998b). Hence the equivalent viscous damping due to the supplemental dampers and the effective period of the structure will be investigated in this chapter.

### 7.2.1 SDOF System

The SDOF system includes both the original structural frame system and the supplemental damping system. The two systems act in parallel and can be described as a dual system (see Fig.7.3).

Scholl (1993a) proposed a design criteria for a yielding and friction energy dissipator for an elastic SDOF structure. The criteria were based on the energy dissipated by the devices, the strain energy in the damped-structure system and the supplemental equivalent viscous damping desired for a structure. In these design criteria the equivalent viscous damping ratio and the effective stiffness of the structure due to the dampers were considered. Similar procedures for calculating the equivalent viscous damping ratio and the effective stiffness of the structure due to the supplemental dampers for a SDOF system are adopted here. A different definition of the strain energy of the supplemental damping system is used, and the inelastic effect of the original structure is also considered.

#### 7.2.1.1 Equivalent Viscous Damping Ratio

The initial elastic stiffness of the original structure (for the SDOF system) is $K_s$. The yield force of the original structure is $P_y$. The yield displacement of the original structure is $\Delta_{y0}$. $P$ is the elastic force in the original structure at a given response displacement $\Delta$ if the structure remained elastic. $rK_s$ is the post yielding stiffness of the original structure. The elasto-plastic hysteresis model is adopted to represent the force-deformation behaviour of the supplemental damping system. The initial elastic stiffness of the supplemental damping system is $S_RK_s$, and the yielding force of the supplemental damping system is designated as $F_RP$. See Fig.7.3

From Fig.7.3, we have following relationship:

$$\begin{aligned} \mu &= \frac{\Delta}{\Delta_{y0}} \\ P_y &= \frac{P}{\mu} \\ F_{yd} &= F_R P \\ \Delta_{yd} &= \frac{F_{yd}}{K_d} = \frac{F_R P}{S_R K_s} = \frac{F_R}{S_R}\Delta \end{aligned} \tag{7.2}$$

where $\mu$ = ductility of the original structure with respect to the yield displacement of the original structure,

$F_{yd}$ = yield strength of the supplemental damper,

$S_R$ = the stiffness factor, that is the ratio of the initial stiffness of the supplemental damping system to the initial stiffness of the original structure,

$F_R$ = the force factor, that is the ratio of the yield strength of the supplemental dampers to the elastic force P of the original structure at a target displacement,

$\Delta_{yd}$ = the yield deformation of the supplemental dampers.

Then the hysteretic energy dissipated in a loading cycle is:

$$\begin{aligned} E_d &= 4F_{yd}(\Delta - \Delta_{yd}) \\ &= 4F_R P\left(\Delta - \frac{F_R}{S_R}\Delta\right) \\ &= 4F_R P\left(1 - \frac{F_R}{S_R}\right)\Delta \end{aligned} \tag{7.3}$$

The maximum elastic strain energy of the dual system is:

$$\begin{aligned} E_s &= E_{s1} + E_{s2} \\ &= \frac{1}{2}F_R P\Delta + \frac{1}{2}\left[P_y + rK_s(\Delta - \Delta_{y0})\right]\Delta \\ &= \frac{1}{2}F_R P\Delta + \frac{1}{2}\left[\frac{P}{\mu} + r\frac{P}{\Delta}\left(1 - \frac{1}{\mu}\right)\Delta\right]\Delta \\ &= \frac{1}{2}F_R P\Delta + \frac{1}{2}\left[\frac{1}{\mu} + r\left(1 - \frac{1}{\mu}\right)\right]P\Delta \\ &= \frac{1}{2}\left[F_R + \frac{1}{\mu} + r\left(1 - \frac{1}{\mu}\right)\right]P\Delta \end{aligned} \tag{7.4}$$

where $E_{s1}$ and $E_{s2}$ are the maximum elastic strain energy of the supplemental damping system and the original structure respectively.

From Eq(7.1), (7.3) and (7.4), the equivalent viscous damping due to the damping system is:

$$\xi_d = \frac{E_d}{4\pi E_s} = \frac{2}{\pi} \frac{F_R\left(1-\frac{F_R}{S_R}\right)}{F_R + \frac{1}{\mu} + r\left(1-\frac{1}{\mu}\right)} \tag{7.5}$$

### 7.2.1.2 Effective Period of the SDOF System

The original structural system and the supplemental damping system are in parallel. Hence, the effective stiffness of the structure with the supplemental dampers can be obtained by adding the stiffness of both the original structural system and the supplemental damping system directly.

$$\begin{aligned} K_{eff} &= K_{\text{sec},d} + K_{\text{sec},s} \\ &= \frac{F_R P}{\Delta} + \frac{P_y + rK_s\left(\Delta - \Delta_{y0}\right)}{\Delta} \\ &= \frac{F_R P}{\Delta} + \frac{\frac{P}{\mu} + rK_s\Delta\left(1-\frac{1}{\mu}\right)}{\Delta} \\ &= \frac{P}{\Delta}\left[F_R + \frac{1}{\mu} + r\left(1-\frac{1}{\mu}\right)\right] \\ &= \frac{\mu F_R + 1 + r(\mu - 1)}{\mu} K_s \end{aligned} \tag{7.6}$$

where $K_{eff}$ = effective stiffness of the structure with supplemental dampers at a ductility of $\mu$, $K_{sec,d}$ and $K_{sec,s}$ = the secant stiffness of supplemental damping system and the secant stiffness of the original structure at a ductility of $\mu$ respectively.

The effective period of the structure with the supplemental dampers at a ductility of $\mu$ can be calculated as:

$$T_{eff} = 2\pi\sqrt{\frac{M}{K_{eff}}}$$
$$= 2\pi\sqrt{\frac{M}{K_s}}\sqrt{\frac{\mu}{\mu F_R + 1 + r(\mu - 1)}}$$
$$= T_0\sqrt{\frac{\mu}{\mu F_R + 1 + r(\mu - 1)}} \qquad (7.7)$$

where $T_{eff}$ = the effective period of the structure with supplemental dampers at a ductility of $\mu$,

$T_0 = 2\pi\sqrt{\frac{M}{K_s}}$ = The initial period of the original structure without dampers.

For ductilities of 1 and 2, the relationship between $F_R$, $S_R$ and the equivalent viscous damping ratio $\xi_d$ is shown in Figs.7.4, 7.5. For the practical range of $F_R < 0.4$, it can be seen that $S_R$ has very little influence on the $\xi$ once $S_R > 4$.

### 7.2.2 MDOF Structure

As mentioned before, a regular MDOF structure with supplemental dampers that have a satisfactory distribution of the yield strengths can be adequately approximated by its equivalent SDOF system as far as the displacement response is concerned. This has been shown by nonlinear time history analyses. This needs to be verified for nonlinear static analyses. It has been shown that the effect of the supplemental dampers can be represented by the equivalent viscous damping ratio and the effective stiffness of the structure with the dampers (Lin et al., 1998b). The equivalent viscous damping ratio due to the supplemental dampers and the effective period of the structure with the dampers for a MDOF structure was investigated as follows.

#### 7.2.2.1 Equivalent Viscous Damping Ratio

The modal strain energy method has been adopted to estimate the equivalent viscous damping ratio provided by the viscoelastic dampers (Zhang et al., 1989, Johnson et al., 1982). In this method, the formula of Eq(7.1) is generalised to a MDOF structure by considering $\xi$ as a modal damping ratio, and $E_d$ and $E_s$ as dissipated energy and maximum strain energy for each vibrational mode.

The equivalent viscous damping ratio for the ith mode can be estimated according to this formula:

$$\xi_i = \frac{E_d^{\ i}}{4\pi E_s^{\ i}} \tag{7.8}$$

where $E_d^{\ i}$ = the energy dissipated by the supplemental dampers per cycle for the $i$th vibration mode,

$E_s^{\ i}$ = the strain energy of the structure with the supplemental dampers for the $i$th vibration mode

$\xi_i$ = the equivalent viscous damping ratio for the $i$th vibration mode.

In carrying out the nonlinear static analysis, only the first mode effect is considered and higher mode effects are ignored. Hence, Eq(7.8) only applies to the first mode in this study.

The strain energy of the structure with the supplemental dampers can be expressed as:

$$E_s = \frac{1}{2}\{u\}^T [K_{eff}]\{u\} \tag{7.9}$$

where $\{u\}$ = a displacement vector of the structure at the target displacement,

$[K_{eff}]$ = effective secant stiffness matrix of the structure at the target displacement.

The displacement vector can be represented by the deflected shape vector at the target roof displacement.

$$\{u\} = \{\phi\} x_t \tag{7.10}$$

where $x_t$ = displacement amplitude at the roof level of the structure.

It has been shown that the constant deflected shape used for transforming the MDOF structure to its equivalent SDOF system represents the displacement with fairly good accuracy. Hence, the constant deflected shape at the target displacement can be used to represent $\{\phi\}$ in Eq(7.10)

From the equilibrium equation it is known that

$$\{F\} = [K_{eff}]\{\phi\}x_t \tag{7.11}$$

where $\{F\}$ = the lateral force vector

From Eq(7.9), (7.10), (7.11) the strain energy is given by

$$E_s = \frac{1}{2}\{\phi\}^T\{F\}x_t \tag{7.12}$$

It is assumed that the distribution of the applied lateral forces is an inverted triangular one. Then

$$\frac{F_i}{Q} = \frac{i}{\sum_{i=1}^{N} i} = \frac{i}{\frac{N(N+1)}{2}}$$

where $Q$ = base shear of the structure at the target displacement,

$N$ = the total number of storeys of the structure.

Hence, for this inverted triangular distribution the $i$th term of the lateral force vector $\{F\}$is:

$$F_i = i\frac{2}{N(N+1)}Q \tag{7.13}$$

From Eq(7.12) and (7.13), we have:

$$\begin{aligned} E_s &= \frac{1}{2}\left(\sum_{i=1}^{N} F_i\phi_i\right)x_t \\ &= \frac{x_t Q}{N(N+1)}\sum_{i=1}^{N} i\phi_i \end{aligned} \tag{7.14}$$

As all the supplemental dampers have an elasto-plastic force-displacement relationship, then:

$$\begin{aligned} E_{di} &= 4F_{ydi}\left(\Delta_{di} - \Delta_{ydi}\right) \\ \Delta_{di} &= \left(\phi_i - \phi_{i-1}\right)x_t \cos\theta \end{aligned} \tag{7.15}$$

where $E_{di}$ = energy dissipated per cycle by the dampers at the $i$th storey,

$\Delta_{di}$ = damper deformation at the $i$th storey at the target displacement,

$\Delta_{ydi}$ = yield deformation of the damper at the $i$th storey,

$F_{ydi}$ = yield strength of the damper at the $i$th storey,

$\phi_i$ = the $i$th term of the normalised constant deflected shape at the target displacement,

$\theta$ = Slope of the braces supporting the dampers with respect to the horizontal floor.

For practical lead dampers, $\Delta_{ydi}$ is very small compared to $\Delta_{di}$ ($\frac{\Delta_{ydi}}{\Delta_{di}} < 1\%$). Eq(7.15) becomes:

$$\begin{aligned} E_{di} &\approx 4F_{ydi}\Delta_{di} \\ &= 4F_{ydi}\left(\phi_i - \phi_{i-1}\right)x_t \cos\theta \end{aligned} \tag{7.16}$$

From the assumption that the distribution of the yield strengths of the dampers in every storey along the height of the structure is proportional to the storey shear force developed due to an inverted triangular lateral load pattern, Eq(7.13) leads to:

$$\begin{aligned} \frac{F_{ydi}}{F_{yd1}} &= \frac{\sum_{j=i}^{N} F_j}{\sum_{j=1}^{N} F_j} \\ &= \frac{\frac{2}{N(N+1)}Q\sum_{j=i}^{N} j}{Q} \\ &= \frac{2}{N(N+1)}\sum_{j=i}^{N} j \end{aligned} \tag{7.17}$$

where $F_{ydi}$ = the yield strength of the damper at level $i$,

$F_{yd1}$ = the yield strength of the damper at the 1st floor level.

Defining

$$F_R = \frac{F_{yd1}\cos\theta}{F_0} \tag{7.18}$$

where $F_R$ = the force factor for the MDOF structure

$F_0$ = elastic base shear of the original structure without dampers if the original structure remained elastic

The total base shear of the structure at the target displacement is:

$$\begin{aligned} Q &= F_{yd1}\cos\theta + F_{y0} + (x_t - x_{t,y})rK_{s0} \\ &= F_R F_0 + \frac{F_0}{\mu} + r\left(1-\frac{1}{\mu}\right)F_0 \\ &= F_0\left[F_R + \frac{1}{\mu} + r\left(1-\frac{1}{\mu}\right)\right] \end{aligned} \tag{7.19}$$

where, $F_{y0}$ = yield base shear of the original structure.

Substituting Eq(7.14), (7.16), (7.17), (7.18), (7.19) into Eq(7.8) gives:

$$\begin{aligned} \xi_d &= \frac{\sum_{i=1}^{N} E_{di}}{4\pi E_s} \\ &= \frac{\sum_{i=1}^{N} 4F_{ydi}(\phi_i - \phi_{i-1})x_t\cos\theta}{4\pi\frac{x_t Q}{N(N+1)}\sum_{i=1}^{N} i\phi_i} = \frac{\sum_{i=1}^{N} F_{ydi}(\phi_i - \phi_{i-1})\cos\theta}{\pi\frac{Q}{N(N+1)}\sum_{i=1}^{N} i\phi_i} \\ &= \frac{\sum_{i=1}^{N}\left[\frac{2F_{yd1}}{N(N+1)}\left(\sum_{j=i}^{N} j\right)(\phi_i - \phi_{i-1})\cos\theta\right]}{\pi\frac{Q}{N(N+1)}\sum_{i=1}^{N} i\phi_i} = \frac{2F_R F_0\sum_{i=1}^{N}\left[\left(\sum_{j=i}^{N} j\right)(\phi_i - \phi_{i-1})\right]}{\pi F_0\left[F_R + \frac{1}{\mu} + r\left(1-\frac{1}{\mu}\right)\right]\sum_{i=1}^{N} i\phi_i} \\ &= \frac{2F_R\sum_{i=1}^{N}\left[\left(\sum_{j=i}^{N} j\right)(\phi_i - \phi_{i-1})\right]}{\pi\left[F_R + \frac{1}{\mu} + r\left(1-\frac{1}{\mu}\right)\right]\sum_{i=1}^{N} i\phi_i} \end{aligned} \tag{7.20}$$

where $\mu = \dfrac{x_t}{x_{t,y}}$ is the ductility of the structure at the target displacement,

$x_{t,y}$ = the yield roof displacement of the original structure without dampers,

$\xi_d$ = the equivalent viscous damping ratio of the structure due to the supplemental dampers.

It can be seen that:

$$\begin{aligned}
&\sum_{i=1}^{N}\left[\left(\sum_{j=i}^{N} j\right)(\phi_i - \phi_{i-1})\right] \\
&= \left(\sum_{j=1}^{N} j\right)(\phi_1 - \phi_0) + \left(\sum_{j=2}^{N} j\right)(\phi_2 - \phi_1) + \left(\sum_{j=3}^{N} j\right)(\phi_3 - \phi_2) + \cdots + \left(\sum_{j=N}^{N} j\right)(\phi_N - \phi_{N-1}) \\
&= \phi_1 + 2\phi_2 + 3\phi_3 + \cdots + N\phi_N \\
&= \sum_{i=1}^{N} i\phi_i
\end{aligned} \tag{7.21}$$

Substituting Eq(7.21) into Eq(7.20) gives:

$$\xi = \frac{2}{\pi}\frac{F_R}{\left[F_R + \dfrac{1}{\mu} + r\left(1 - \dfrac{1}{\mu}\right)\right]} \tag{7.22}$$

Rearranging Eq(7.22) gives:

$$F_R = \frac{\pi\xi[1 + r(\mu - 1)]}{(2 - \pi\xi)\mu} \tag{7.22a}$$

The force factor $F_R$ in Eq(7.22) can be expressed as:

$$\begin{aligned}
F_R &= \frac{F_{yd1}\cos\theta}{F_0} \\
&= \frac{\dfrac{\sum \phi_i \psi_i}{\sum \psi_i}}{\dfrac{\sum \phi_i \psi_i}{\sum \psi_i}} \frac{F_{yd1}\cos\theta}{F_0} = \frac{F_{yd}}{P}
\end{aligned} \tag{7.23}$$

where $\psi_i = \frac{i}{N}$ is the $i$th term of the normalised lateral load pattern vector for an inverted triangular distribution lateral load pattern,

$F_{yd}$ = yield strength of the damping system for the equivalent SDOF system,

$P$ = elastic force of the original structural system for the equivalent SDOF system.

Comparing Eqs(7.22), (7.23) with Eq(7.5), it can be found that $F_R$ in Eq(7.22) for a MDOF structure is equivalent to $F_R$ in Eq(7.5) for the SDOF system. The only difference between Eq(7.22) and Eq(7.5) is the term $\left(1-\frac{F_R}{S_R}\frac{1}{\mu}\right)$. This is because of the omission of the term $\Delta_{yi}$ in Eq(7.15) when deriving Eq(7.22). This difference is very small for lead dampers. Hence, it can be concluded that the modal strain energy method of the MDOF structure and the equivalent SDOF system give almost the same estimate of the equivalent viscous damping ratio due to the supplemental dampers.

#### 7.2.2.2 Effective Period of the MDOF Structure

The first mode effective period of the MDOF structure with the supplemental dampers at the target displacement can be calculated from the Rayleigh method (as defined in NZS4203, 1992):

$$T_{eff} = 2\pi\sqrt{\frac{\sum\left(W_i u_i^2\right)}{g\sum\left(F_i u_i\right)}} \tag{7.24}$$

where $u_i = \phi_i x_t$ is the lateral displacement of the structure at level i (obtained from Eq(7.10)),

$W_i = m_i g$ = seismic weight at level $i$,

$F_i$ = lateral load applied at level $i$.

Hence, Eq(7.24) can also be expressed as:

$$T_{eff} = 2\pi \sqrt{\frac{\sum_{i=1}^{N} m_i \phi_i^{\,2}}{\sum_{i=1}^{N} F_i \phi_i}\, x_t} \tag{7.25}$$

For an inverted triangular distribution of the lateral force, substituting Eq(7.13) and (7.19) into Eq(7.25) gives:

$$\begin{aligned}
T_{eff} &= 2\pi \sqrt{\frac{\sum_{i=1}^{N} m_i \phi_i^{\,2}}{\left(\sum_{i=1}^{N} i\phi_i\right)\frac{2}{N(N+1)} Q}\, x_t} \\
&= 2\pi \sqrt{\frac{\sum_{i=1}^{N} m_i \phi_i^{\,2}}{\left(\sum_{i=1}^{N} i\phi_i\right)\frac{2}{N(N+1)}\left[F_R + \frac{1}{\mu} + r\left(1-\frac{1}{\mu}\right)\right] F_0}\, x_t} \\
&= 2\pi \sqrt{\frac{\mu}{\mu F_R + 1 + r(\mu - 1)}} \sqrt{\frac{\sum_{i=1}^{N} m_i \phi_i^{\,2}}{\left(\sum_{i=1}^{N} i\phi_i\right)\frac{2}{N(N+1)}}\, \frac{x_t}{F_0}} \\
&= 2\pi \sqrt{\frac{\mu}{\mu F_R + 1 + r(\mu - 1)}} \sqrt{\frac{\sum_{i=1}^{N} m_i \phi_i \quad \sum_{i=1}^{N} m_i \phi_i^{\,2}}{\left(\sum_{i=1}^{N} i\phi_i\right)\frac{2}{N(N+1)} F_0 \quad \sum_{i=1}^{N} m_i \phi_i}\, x_t}
\end{aligned} \tag{7.26}$$

For an inverted triangular distribution of lateral force, the normalised lateral force distribution vector is :

$$\psi_i = \frac{i}{N} \tag{7.27}$$

where $\psi_i$ is the $i$th term of the normalised distribution vector $\{\psi\}$.

From Eq(6.14) and Eq(7.27) we have

$$R^* = \frac{\sum \phi_i \psi_i}{\sum \psi_i} F_0 = \frac{\sum_{i=1}^{N} \phi_i \frac{i}{N}}{\sum_{i=1}^{N} \frac{i}{N}} F_0 = \frac{\sum_{i=1}^{N} i\phi_i}{\frac{N(N+1)}{2}} F_0 = \left( \sum_{i=1}^{N} i\phi_i \right) \frac{2}{N(N+1)} F_0 \qquad (7.28)$$

where $R^*$ = elastic base force of the equivalent SDOF system for the original structure without dampers at the target displacement.

From Eq(6.8), $x^*$ is given by:

$$x^* = \frac{\sum_{i=1}^{N} m_i \phi_i^{\,2}}{\sum_{i=1}^{N} m_i \phi_i} x_t \qquad (7.29)$$

where $x^*$ = displacement of the equivalent SDOF system at the target displacement.

Substituting Eq(7.28) and (7.29) into Eq(7.26):

$$T_{eff} = 2\pi \sqrt{\frac{\mu}{\mu F_R + 1 + r(\mu - 1)}} \sqrt{\frac{\sum_{i=1}^{N} m_i \phi_i}{R^*}} x^* \qquad (7.30)$$

where $\sum_{i=1}^{N} m_i \phi_i = M^*$ is the mass of the equivalent SDOF system.

Further, as above

$$2\pi \sqrt{\frac{\sum_{i=1}^{N} m_i \phi_i}{R^*}} x^* = 2\pi \sqrt{\frac{M^*}{K_S}} = T_0 \qquad (7.31)$$

where $T_0$ = the initial period of the equivalent SDOF system of the original structure without dampers.

Eq(7.30) can be rewritten as:

$$T_{eff} = T_0 \sqrt{\frac{\mu}{\mu F_R + 1 + r(\mu - 1)}} \tag{7.32}$$

It is known that the MDOF structure and its equivalent SDOF system have the same ductility and $r$ is also the same for both systems. $F_R$ in Eq(7.32) for the MDOF structure is equivalent to $F_R$ in Eq(7.7) for the SDOF system. Comparing Eq(7.7) and Eq(7.32), the MDOF structure and its equivalent SDOF system have the same effective period at the target displacement .

By comparison of the MDOF structure and its equivalent SDOF system, it has been found that both systems have the same effective period and the equivalent viscous damping ratio due to the supplemental dampers at the target displacement. Hence, it can be concluded that for a regular MDOF structure supplemental dampers, the effect of the dampers can be effectively estimated by its equivalent SDOF system for the distribution of damper strengths mentioned above.

## 7.3 GENERALISED DERIVATION OF A MDOF STRUCTURE

For a structure whose lateral load pattern is greatly different from the inverted triangular shape, the distribution of the yield strengths of the supplemental dampers used above may not be the best solution. In this case, the best distribution of the yield strengths of the supplemental dampers over the height of the structure could be proportional to the storey shear force due to a lateral load distribution $\{P\} = [M]\{\phi\}$. This can be verified using a procedure similar to that shown in the earlier part of this chapter.

In the general case, Fajfar et al. (1996) suggested that for the pushover analysis the lateral load distribution $\{P\} = [M]\{\phi\}$ should be used. $\{\phi\}$ is a constant deflected shape that can be obtained at the target displacement.

### 7.3.1 Equivalent Viscous Damping Ratio

For the distribution of the yield strengths of the dampers proportional to the storey shear force due to a lateral load distribution $\{P\} = [M]\{\phi\}$, the $i$th term of the lateral force vector $\{F\}$at level $i$ is:

$$\frac{F_i}{Q} = \frac{m_i \phi_i}{\sum_{i=1}^{N} m_i \phi_i} \tag{7.33}$$

where $F_i$ = the lateral force at level $i$,

$Q$ = base shear of the structure at the target displacement,

$N$ = the total number of storeys of the structure.

From Eqs(7.12) and (7.33), the maximum strain energy of the structure with the supplemental dampers is:

$$\begin{aligned} E_s &= \frac{1}{2}\left(\sum_{i=1}^{N} F_i \phi_i\right) x_t \\ &= \frac{1}{2} \frac{\sum_{i=1}^{N} m_i \phi_i^2}{\sum_{i=1}^{N} m_i \phi_i} x_t Q \end{aligned} \tag{7.34}$$

From Eq(7.33), the yield strengths of the dampers at the storey levels can be written as:

$$\frac{F_{ydi}}{F_{yd1}} = \frac{\sum_{j=i}^{N} F_j}{\sum_{j=1}^{N} F_j} = \frac{Q \frac{\sum_{j=i}^{N} m_j \phi_j}{\sum_{j=1}^{N} m_j \phi_j}}{Q \frac{\sum_{j=1}^{N} m_j \phi_j}{\sum_{j=1}^{N} m_j \phi_j}} = \frac{\sum_{j=i}^{N} m_j \phi_j}{\sum_{j=1}^{N} m_j \phi_j} \tag{7.35}$$

where $F_{ydi}$ = the yield strength of the damper at level $i$,

$F_{yd1}$ = the yield strength of the damper at the 1st level.

Eq(7.16), (7.18), (7.19) are still valid.

Substituting Eq(7.34), (7.16), (7.35), (7.18), (7.19) into Eq(7.8)

$$\xi_d = \frac{\sum_{i=1}^{N} E_{di}}{4\pi E_s} = \frac{\sum_{i=1}^{N} 4F_{ydi}(\phi_i - \phi_{i-1})x_t \cos\theta}{4\pi \frac{1}{2}\frac{\sum_{i=1}^{N} m_i\phi_i^2}{\sum_{i=1}^{N} m_i\phi_i} x_t Q} = \frac{2}{\pi}\frac{\sum_{i=1}^{N} F_{ydi}(\phi_i - \phi_{i-1})\cos\theta}{\frac{\sum_{i=1}^{N} m_i\phi_i^2}{\sum_{i=1}^{N} m_i\phi_i} Q}$$

$$= \frac{2}{\pi}\frac{\sum_{i=1}^{N}\left[F_{yd1}\frac{\sum_{j=i}^{N} m_j\phi_j}{\sum_{j=1}^{N} m_j\phi_j}(\phi_i - \phi_{i-1})\cos\theta\right]}{\frac{\sum_{i=1}^{N} m_i\phi_i^2}{\sum_{i=1}^{N} m_i\phi_i} Q} = \frac{2}{\pi}\frac{F_R F_0 \sum_{i=1}^{N}\left[\left(\sum_{j=i}^{N} m_j\phi_j\right)(\phi_i - \phi_{i-1})\right]}{F_0\left[F_R + \frac{1}{\mu} + r\left(1 - \frac{1}{\mu}\right)\right]\sum_{i=1}^{N} m_i\phi_i^2}$$

$$= \frac{2}{\pi}\frac{F_R \sum_{i=1}^{N}\left[\left(\sum_{j=i}^{N} m_j\phi_j\right)(\phi_i - \phi_{i-1})\right]}{\left[F_R + \frac{1}{\mu} + r\left(1 - \frac{1}{\mu}\right)\right]\sum_{i=1}^{N} m_i\phi_i^2} \tag{7.36}$$

It can be seen that:

$$\begin{aligned}
&\sum_{i=1}^{N}\left[\left(\sum_{j=i}^{N} m_j\phi_j\right)(\phi_i - \phi_{i-1})\right] \\
&= (m_1\phi_1 + m_2\phi_2 + \cdots + m_N\phi_N)\phi_1 + (m_2\phi_2 + \cdots + m_N\phi_N)(\phi_2 - \phi_1) + \cdots + m_N\phi_N(\phi_N - \phi_{N-1}) \\
&= m_1\phi_1^2 + m_2\phi_2^2 + \cdots + m_N\phi_N^2 \\
&= \sum_{i=1}^{N} m_i\phi_i^2
\end{aligned} \tag{7.37}$$

Substituting Eq(7.37) into Eq(7.36) gives:

$$\begin{aligned}
\xi_d &= \frac{2}{\pi}\frac{F_R \sum_{i=1}^{N} m_i\phi_i^2}{\left[F_R + \frac{1}{\mu} + r\left(1 - \frac{1}{\mu}\right)\right]\sum_{i=1}^{N} m_i\phi_i^2} \\
&= \frac{2}{\pi}\frac{F_R}{\left[F_R + \frac{1}{\mu} + r\left(1 - \frac{1}{\mu}\right)\right]}
\end{aligned} \tag{7.38}$$

Eq(7.38) is the same as Eq(7.22). Comparing Eqs(7.22), (7.23) with Eq(7.5) , it can be seen that $F_R$ in Eq(7.38) is equivalent to $F_R$ in Eq(7.5). The only difference between Eq(7.38) and Eq(7.5) is the term $\left(1-\frac{F_R}{S_R}\frac{1}{\mu}\right)$. This is because of the neglect of the term $\Delta_{yi}$ in Eq(7.15). This difference is very small for lead dampers. Hence, it can be deduced that in the general case the modal strain energy method of the MDOF structure and the equivalent SDOF system also give the same equivalent viscous damping ratio due to the supplemental dampers.

### 7.3.2 Effective Period of the MDOF Structure

From Eq(7.33), Eq(7.25) becomes:

$$T_{eff} = 2\pi\sqrt{\frac{\sum_{i=1}^{N} m_i\phi_i^2}{\sum_{i=1}^{N} F_i\phi_i}x_t} = 2\pi\sqrt{\frac{\sum_{i=1}^{N} m_i\phi_i^2}{\frac{\sum_{i=1}^{N} m_i\phi_i^2}{\sum_{i=1}^{N} m_i\phi_i}Q}x_t} = 2\pi\sqrt{\frac{\sum_{i=1}^{N} m_i\phi_i}{Q}x_t} \tag{7.39}$$

Substituting Eq(7.19) into Eq(7.39) gives:

$$\begin{aligned} T_{eff} &= 2\pi\sqrt{\frac{\sum_{i=1}^{N} m_i\phi_i}{F_0\left[F_R+\frac{1}{\mu}+r\left(1-\frac{1}{\mu}\right)\right]}x_t} \\ &= 2\pi\sqrt{\frac{\sum_{i=1}^{N} m_i\phi_i}{\frac{\sum_{i=1}^{N} m_i\phi_i^2}{\sum_{i=1}^{N} m_i\phi_i}F_0\left[F_R+\frac{1}{\mu}+r\left(1-\frac{1}{\mu}\right)\right]}\frac{1}{\sum_{i=1}^{N} m_i\phi_i}\sum_{i=1}^{N} m_i\phi_i^2 x_t} \end{aligned} \tag{7.40}$$

For the lateral load distribution of $\{P\} = [M]\{\phi\}$, we have:

$$\psi_i = \frac{m_i\phi_i}{\sum_{i=1}^{N} m_i\phi_i}$$

Hence, Eq(6.14) becomes:

$$R^* = \frac{\sum \phi_i \psi_i}{\sum \psi_i} F_0 = \frac{\dfrac{\sum_{i=1}^{N} m_i\phi_i^2}{\sum_{i=1}^{N} m_i\phi_i}}{\dfrac{\sum_{i=1}^{N} m_i\phi_i}{\sum_{i=1}^{N} m_i\phi_i}} F_0 = \frac{\sum_{i=1}^{N} m_i\phi_i^2}{\sum_{i=1}^{N} m_i\phi_i} F_0 \tag{7.41}$$

where $F_0$ = elastic base shear of the original structure without dampers if the original structure remained elastic,

$R^*$ = elastic base shear force of the equivalent SDOF system for the original structure without dampers at the target displacement.

From Eq(6.8) we have:

$$x^* = \frac{\sum_{i=1}^{N} m_i\phi_i^2}{\sum_{i=1}^{N} m_i\phi_i} x_t \tag{7.42}$$

where $x^*$ = displacement of the equivalent SDOF system.

Substituting Eq(7.41) and (7.42) into Eq(7.40) gives:

$$\begin{aligned} T_{eff} &= 2\pi \sqrt{\frac{\mu}{\mu F_R + 1 + r(\mu - 1)}} \sqrt{\frac{\sum_{i=1}^{N} m_i\phi_i}{R^*} x^*} \\ &= 2\pi \sqrt{\frac{\mu}{\mu F_R + 1 + r(\mu - 1)}} \sqrt{\frac{M^*}{R^*} x^*} \\ &= 2\pi \sqrt{\frac{M^*}{K_s}} \sqrt{\frac{\mu}{\mu F_R + 1 + r(\mu - 1)}} = T_0 \sqrt{\frac{\mu}{\mu F_R + 1 + r(\mu - 1)}} \end{aligned} \tag{7.43}$$

Eq(7.43) is exactly the same as Eq(7.32). $F_R$ in Eq(7.43) is equivalent to $F_R$ in Eq(7.7). Comparing Eq(7.7) and Eq(7.32), again it can be seen that the MDOF structure and its equivalent SDOF system have the same effective period at the target displacement.

It can be concluded that in the general case, in which the lateral load distribution $\{P\} = [M]\{\phi\}$ is used, the effect of the supplemental dampers on a MDOF structure can be estimated by its equivalent SDOF system provided that its dynamic response is dominated by the first mode. The lateral load pattern used to perform the pushover analysis and for converting the MDOF structure to the SDOF system is $\{P\} = [M]\{\phi\}$.

The 12-storey frame structure model used in the previous chapters is again used with the supplemental dampers at every storey but the distribution of the yield strengths of the supplemental dampers over the height of the structure is taken to be proportional to the storey shear force due to a vertical distribution of lateral load distribution $\{P\} = [M]\{\phi\}$.

The deflected shape vector of the structure with the dampers at a ductility of 1.5 is:
{0.0396, 0.1195, 0.2133, 0.3147, 0.4252, 0.5379, 0.6478, 0.7508, 0.8461, 0.9224, 0.9728, 1}.
Thus the distribution of the lateral load vector of $\{P\} = [M]\{\phi\}$ (normalised) is:
{0.04528, 0.1366, 0.2439, 0.3598, 0.4727, 0.598, 0.7202, 0.8347, 0.9155, 0.998, 1.0526, 1}.

The distribution vector (normalised) of the yield strengths of the supplemental dampers over the height of the structure is (proportional to the storey shear force due to a vertical distribution of lateral load $\{P\} = [M]\{\phi\}$):
{1, 0.9939, 0.9753, 0.9423, 0.8935, 0.8294, 0.7484, 0.6508, 0.5376, 0.4135, 0.2782, 0.1356}

The yield strength of the damper at the 1st floor level is taken to be 422KN. The three NZS4203 compatible earthquakes were used to conduct nonlinear time history analyses. The dynamic response was compared with the case in which the distribution of the yield strengths of the dampers was taken to be proportional to the storey shear due to the inverted triangular lateral load pattern (with the same yield strength of the damper at the 1st floor level). This comparison is shown in Tables 7.1, 7.2, and 7.3.

It can be seen from Tables 7.1, 7.2, 7.3 that the dynamic responses of the two cases are almost the same. This shows that for this structural model the distribution of the yield strengths of the supplemental dampers that is taken to be proportional to the storey shear due to the inverted triangular lateral load pattern is satisfactory. For regular framed structures this distribution of the supplemental dampers can be used because of simplicity. For irregular structures, or for structures where the displacement shape is greatly different from the inverted triangular one, yield strengths of the supplemental dampers that is proportional to the storey shear force due to a lateral load $\{P\} = [M]\{\phi\}$ may be a better choice.

For the purpose of this study the distribution of damper yield strengths that is proportional to the storey shear due to the inverted triangular lateral load pattern is adopted for the following seismic analyses and design.

## 7.4 ESTIMATE OF THE EQUIVALENT VISCOUS DAMPING DUE TO THE INELASTIC DEFORMATION OF THE STRUCTURE

It has been shown that the effect of the supplemental dampers can be represented by the equivalent viscous damping ratio and the effective period of the structure. For a nonlinear static analysis, there are two ways to consider the effect of the inelastic deformation of the original structure. One is to adopt an inelastic design spectra. Different values of ductility are included in these spectra. Another way is to use the equivalent viscous damping ratio due to the inelastic deformation of the original structure and its influence on the effective stiffness of the structure. The influence on the effective stiffness of the structure due to the inelastic deformation of the original structure has already been considered in the procedure of calculating the effective period of the structure as shown above. There are several methods for estimating the equivalent viscous damping due to the inelastic displacement of the original structure.

1. Method proposed by Li et al. (1995)

The hysteretic energy dissipation per cycle is

$$E_{dc} = 4\eta F_y \left(u_{\max} - u_y\right) \tag{7.44}$$

where $\eta$ is the ratio of the area enclosed in the hysteresis loop versus the area of the parallelogram $\left[4F_y\left(u_{\max}-u_y\right)\right]$. This factor is influenced by bond slip or "pinching" in reinforced concrete elements ($\eta$ = 0.4 - 0.5).

The equivalent damping can be approximated by:

$$\Delta\xi_0 = \frac{4\eta\left(\mu_{\max}-2\right)}{\pi\mu_{\max}\left[2+r\left(\mu_{\max}-2\right)\right]} \tag{7.45}$$

where $\mu = \frac{u_{\max}}{u_y}$,

$r$ = ratio of post yield stiffness to the initial stiffness,

$\Delta\xi_0$ = equivalent viscous damping due to the inelastic deformation of the structure.

This method produces an acceptable agreement for the maximum deformation ductilities larger than 2. For small values of ductility, the damping increase is negligible and need not be considered.

2. Method proposed by Shibata et al., 1976 (also see Moehle, 1984)

This method is based on the substitute-structure method. In the substitute-structure method the effective stiffness of the yielding structure is taken to be the secant stiffness for cyclic oscillations. The increase of the equivalent viscous damping due to the inelastic deformation of the structure can be approximated by:

$$\Delta\xi_0 = \frac{1-\frac{1}{\sqrt{\mu}}}{5} \tag{7.46}$$

where $\mu$ = ductility of the structure.

3. Method proposed by Iwan (1980)

In this method for structures whose periods are in the range of 0.4 - 4.0 seconds, the peak response of a fairly wide range of hysteretic structures can be obtained approximately from the linear response spectrum by using an effective period shift and increased damping. A

simple empirical formula for the effective period shift and increased damping of a class of hysteretic systems has been presented as follows:

$$\frac{T_{eff}}{T_0} = 1 + 0.121(\mu - 1)^{0.939}$$
$$\Delta\xi_0 = 0.0587(\mu - 1)^{0.371} \tag{7.47}$$

Table 7.4 gives the result from these three methods. Method 2 (shown in Eq(7.46)) is adopted in this study to estimate the equivalent viscous damping ratio due to inelastic deformation of the original structure because of its simplicity and the idea behind the substitute-structure method better fitting the method used in this study.

| | Peak roof displacement (cm) | Peak interstorey drift (cm) | Peak base shear (KN) |
|---|---|---|---|
| {P} = [M]{ϕ} lateral load pattern | 14.65 | 1.615 | 1391.4 |
| Inverted triangular Lateral load pattern | 14.69 | 1.621 | 1391.6 |
| Difference | 0.27% | 0.37% | 0.01% |

Tables 7.1 Comparison of the dynamic response of the structure with the two different distributions of damper yield strengths under the El Centro 1940 NZS4203 compatible earthquake

| | Peak roof displacement (cm) | Peak interstorey drift (cm) | Peak base shear (KN) |
|---|---|---|---|
| $\{P\} = [M]\{\phi\}$ lateral load pattern | 11.398 | 1.663 | 1509.7 |
| Inverted triangular Lateral load pattern | 11.399 | 1.657 | 1503.7 |
| Difference | 0.01% | 0.36% | 0.4% |

Tables 7.2 Comparison of the dynamic response of the structure with the two different distributions of damper yield strengths under the Olympia N86E NZS4203 compatible earthquake

| | Peak roof displacement (cm) | Peak interstorey drift (cm) | Peak base shear (KN) |
|---|---|---|---|
| $\{P\} = [M]\{\phi\}$ lateral load pattern | 18.68 | 2.396 | 1528.8 |
| Inverted triangular Lateral load pattern | 18.67 | 2.408 | 1529.4 |
| Difference | 0.05% | 0.49% | 0.04% |

Tables 7.3 Comparison of the dynamic response of the structure with the two different distributions of damper yield strengths under the Taft N21E NZS4203 compatible earthquake

| $\mu_{max}$ | 1.5 | 1.8 | 2.0 | 2.2 | 2.4 | 2.6 | 3.0 |
|---|---|---|---|---|---|---|---|
| Method 1 ($\alpha$=0.05,$\eta$ = 0.4 ) | 0 | 0 | 0 | 2.3% | 4.2% | 5.79% | 7.91% |
| Method 2 | 3.67% | 5.09% | 5.86% | 6.52% | 7.09% | 7.60% | 8.45% |
| Method 3 | 4.54% | 5.40% | 5.87% | 6.28% | 6.65% | 6.99% | 7.59% |

Table 7.4 Equivalent viscous damping ratio due to the inelastic deformation of structures

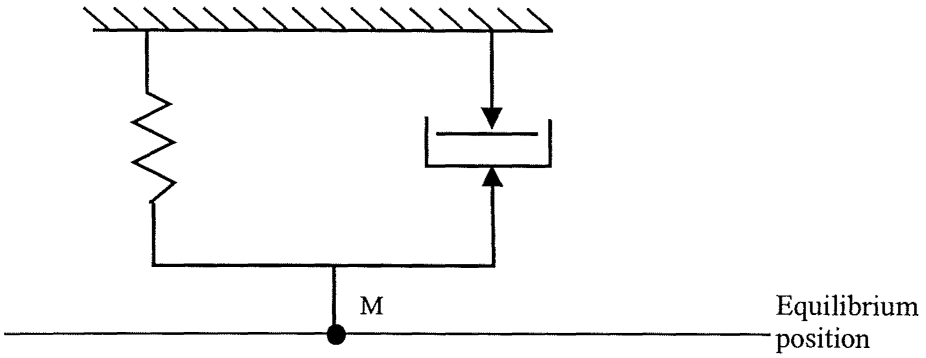


(1) Viscous damping

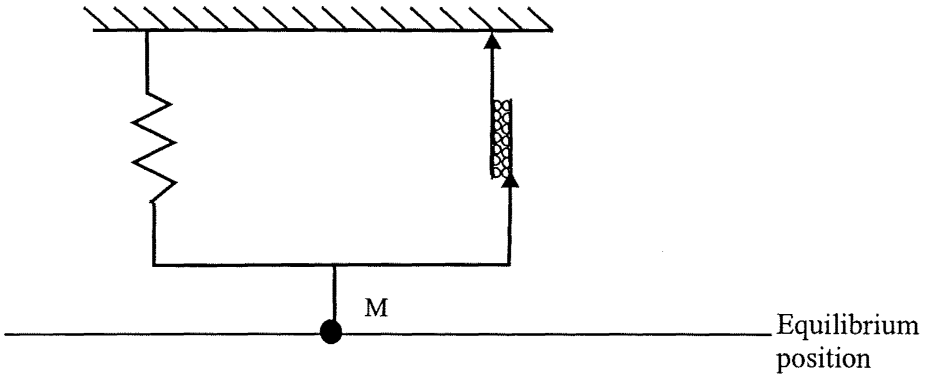


(2) Coulomb damping

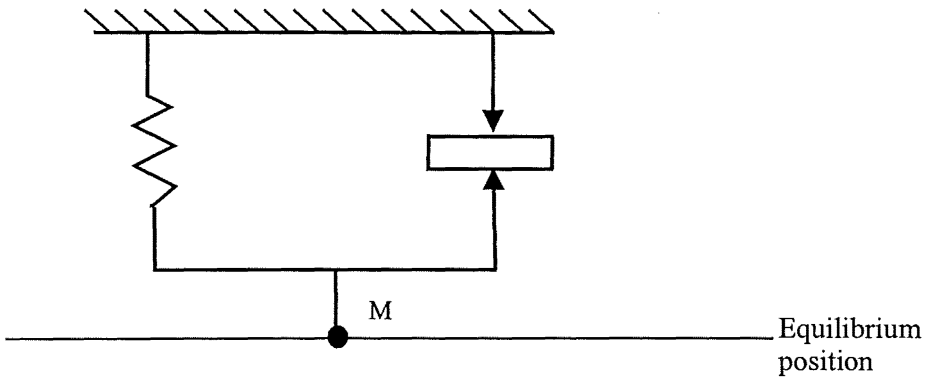


(3) Hysteretic damping

Figure 7.1 Representation of damping (from Brebbia, 1985)

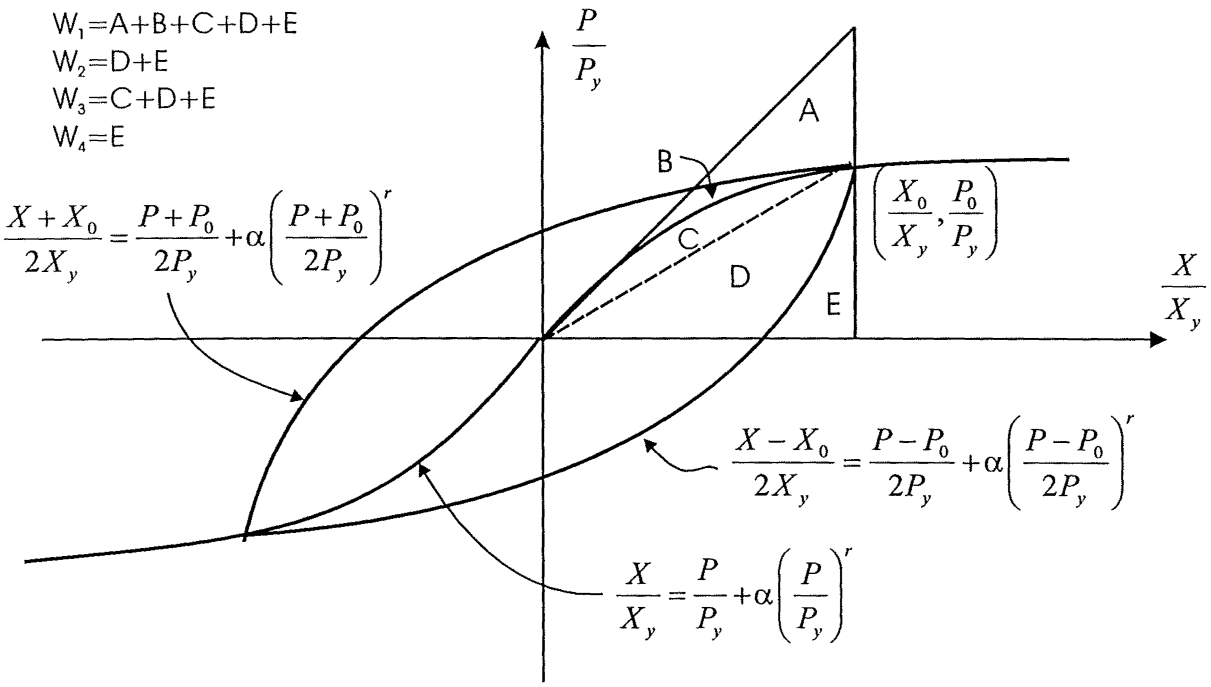


$$\varsigma = \frac{\Delta W}{4\pi W_n}$$

$$\varsigma_1 = \frac{2}{\pi}\left(\frac{r-1}{r+1}\right)\frac{X_y}{X_0}\frac{P_0}{P_y}\left[1-\left(\frac{X_y}{X_0}\right)\left(\frac{P_0}{P_y}\right)\right]$$

$$\varsigma_2 = \frac{2}{\pi}\left(\frac{r-1}{r+1}\right)\left[1-\left(\frac{X_y}{X_0}\right)\left(\frac{P_0}{P_y}\right)\right]$$

$$\varsigma_3 = \frac{\frac{2}{\pi}\left(\frac{r-1}{r+1}\right)\left[1-\frac{X_y}{X_0}\frac{P_0}{P_y}\right]}{2-\frac{X_y}{X_0}\frac{P_0}{P_y}\left[1+\frac{2}{r+1}\left(\frac{X_0}{X_y}\frac{P_y}{P_0}-1\right)\right]}$$

$$\varsigma_4 = \frac{\frac{2}{\pi}\left(\frac{r-1}{r+1}\right)\left[\frac{X_0}{X_y}\frac{P_y}{P_0}-1\right]}{1+\frac{1}{2^{r-2}(r+1)}\left(\frac{X_0}{X_y}\frac{P_y}{P_0}-1\right)}$$

Figure 7.2 Ramberg-Osgood type force-deformation relationship and different damping values (From Rea, 1969)

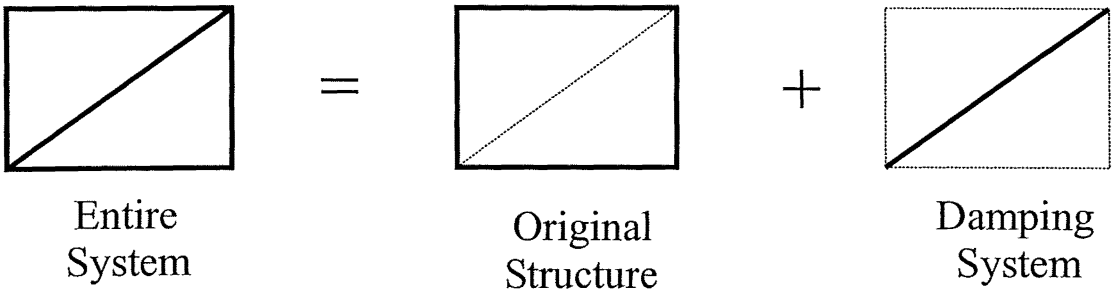


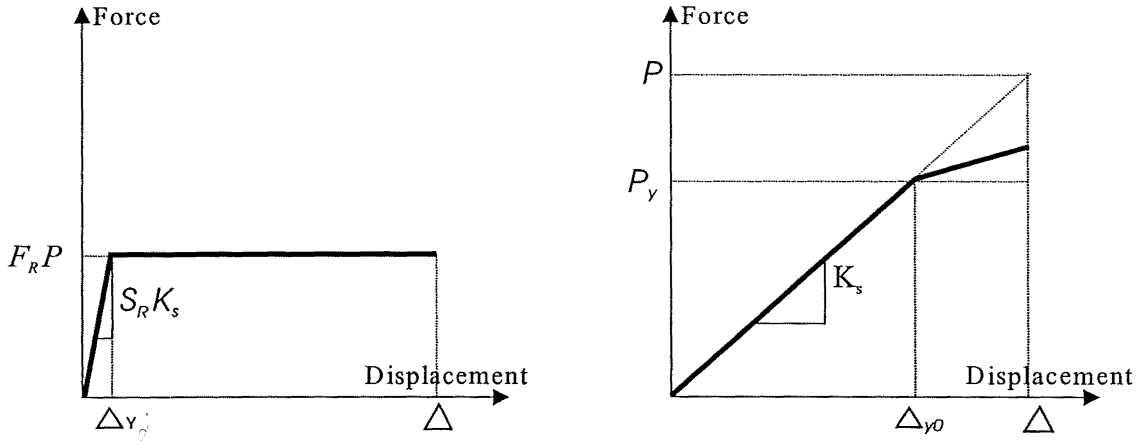


Figure 7.3. Force-displacement relationship for the dual system

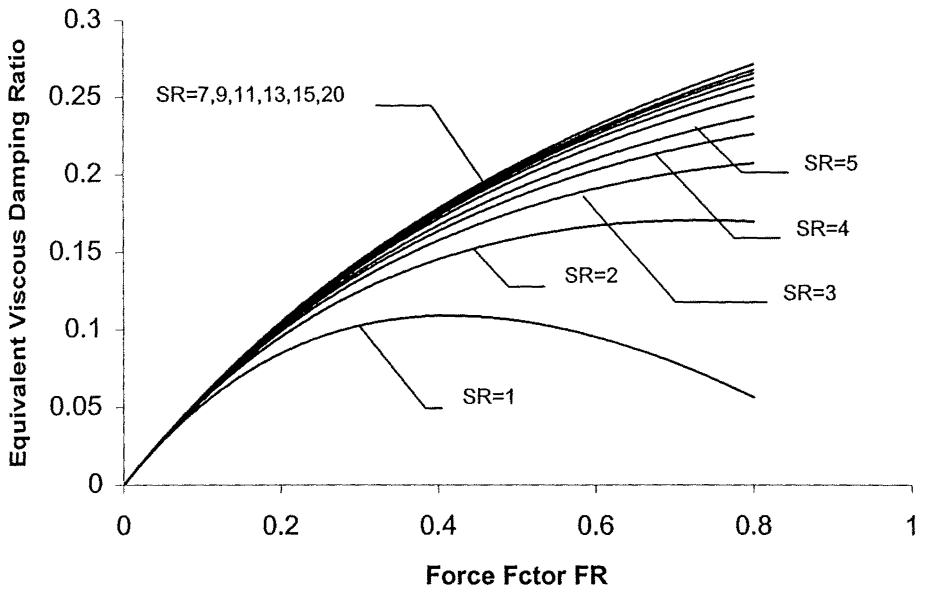


Figure 7.4 Equivalent viscous damping due to the supplemental damping system while the original structure remains elastic

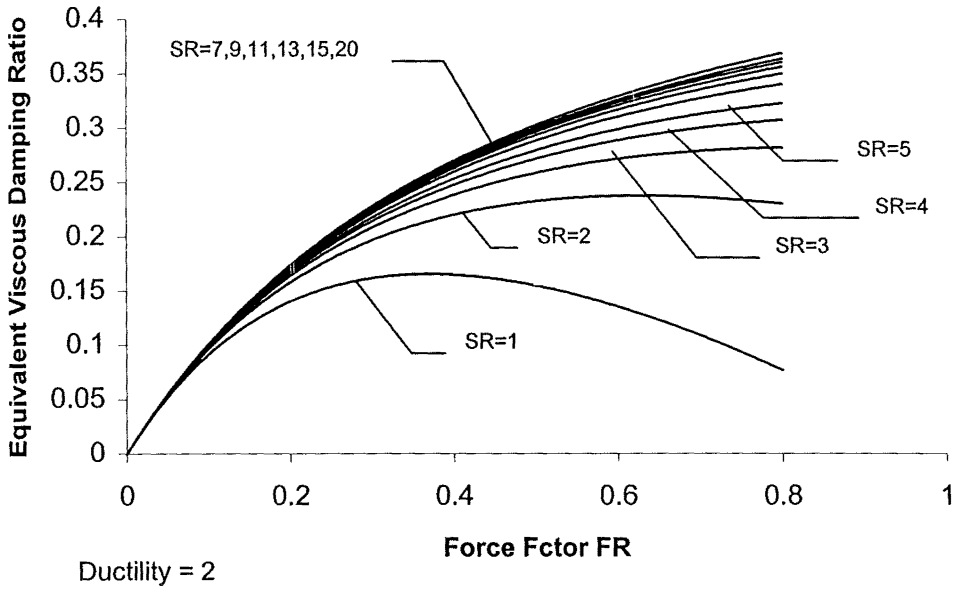


Figure 7.5 Equivalent viscous damping due to the supplemental damping system while the ductility of the original structure is equal to 2

# CHAPTER 8

# SIMPLIFIED NONLINEAR STATIC METHOD

## 8.1 INTRODUCTION

Modal analysis methods using response spectra are useful tools for estimating the peak response of elastic MDOF structures (Carr, 1994). The limitation of the modal analysis method using response spectra is that it can only be applied to linear elastic structures. This method may be extended to nonlinear inelastic structures as long as some approximations are made. The simplified nonlinear static method is based, in part, on the modal analysis using response spectra which are obtained by modifying the 5%-damped spectra to account for the damping provided by the supplemental dampers and the effects due to the inelastic deformation of the structure.

The procedure for approximating the inelastic response requires that two curves be determined: one curve represents the capacity of the structure; the other curve represents the demand from the ground motions.

Similar but slightly different procedures for the simplified nonlinear static method have been described by several investigators (Qi et al., 1991, Faifar et al., 1987, 1988, 1996, Reinhorn, 1997, 1995, Freeman, 1978, ATC-33.03, Rao et al., 1995).

Reinhorn (1997) presented methods based on a composite acceleration and inelastic displacement spectrum, which described the seismic demand, and inelastic capacity functions describing the structural behaviour. The inelastic response in terms of accelerations and displacements can be evaluated simultaneously from the relationship mentioned above. This is shown in Fig.8.1.

ATC-33.03 gave a similar procedure for the analysis of SDOF structures with supplemental dampers (Fig.8.2).

Freeman (1978) proposed a capacity spectrum approach to predict the inelastic response of structures (also see Deierlein et al., 1990). In this approach, the capacity curve and the ground

motion demand curve are described in terms of the spectral acceleration, $S_a$, and the response period of vibration, T. The capacity spectrum is a structural property which relates the fundamental period of free vibration to the level of deformation. This spectrum is also obtained from a pushover analysis. There is no essential difference between this method and ATC-33.03, except that the equivalent damping is calculated differently. This approach is shown in Fig.8.3.

The essential procedure of the simplified nonlinear static method should involve the following steps:

Step 1: Data

This data includes information for the structure (ie, moment-rotation relationship for members, force-deformation relationship for supplemental dampers) and the elastic response spectra. These elastic response spectra (pseudo acceleration spectrum and displacement spectrum) can be derived from a particular design earthquake or can use smoothed design spectra.

Step 2: Nonlinear pushover analysis of MDOF structures

The capacity curve for a MDOF structure can be obtained through a pushover analysis. This capacity curve is usually represented by the base shear-roof displacement relationship.

Step 3: Spectral capacity curve

The capacity curve obtained in Step 2 is transformed to that for the equivalent SDOF system which is referred to as spectral capacity curve. This transformation is described in Chapter 6.

Step 4: Seismic demand curve for the equivalent SDOF system

The demand curve can be obtained by modifying the elastic response spectra to account for the higher damping provided by the supplemental dampers and the effects due to the inelastic deformation of the structure.

Step 5: Estimate the peak response

The peak response of the equivalent SDOF system can be estimated by comparing these two curves – the spectral capacity curve and the seismic demand curve. Some iteration may be needed due to the fact that the unknown damping due to the supplemental dampers is a function of the displacement. The peak response of the MDOF structure can be calculated by transforming the results for the SDOF system back to those of the MDOF structure.

Some crucial items in this simplified nonlinear static method will be explained and discussed in the sections that follow.

## 8.2 PUSHOVER ANALYSIS

The pushover analysis of the structure with the supplemental dampers has been described in chapter 6. Some conclusions are stressed here.

### 8.2.1 Lateral Load Pattern

For regular framed structures with supplemental lead dampers that have a satisfactory distribution of yield strengths mentioned in Chapter 5, the inverted triangular lateral load pattern is a good choice for carrying out the pushover analysis. For irregular frame structures, the adaptive pushover analysis is recommended. Alternatively, the $\{P\}=[M]\{\Phi\}$ lateral load pattern can also be used, where $\{\Phi\}$ is the displacement shape at the target displacement.

### 8.2.2 Capacity Curve of a MDOF Structure

Usually the base shear – roof displacement relationship is adopted to represent the capacity curve of a MDOF structure. For the structure without supplemental dampers, the capacity curve can be approximated by a bi-linear relationship (Fig.8.4). The capacity curve of the supplemental damping system can be approximated by an elasto-plastic curve with very steep initial slope. The capacity curve of a MDOF structure with supplemental dampers can be considered as consisting of two curves – the capacity curve of the structure without damper and the one of the supplemental damping system (Fig.6.8).

### 8.2.3 Deflected Shape

For a regular structure with supplemental lead dampers, the deflected shape can be approximated by that for the structure without dampers at the same target displacement.

## 8.3 SPECTRAL CAPACITY CURVE

The spectral capacity curve is the capacity curve of the equivalent SDOF structure. It can be obtained from the capacity curve of the MDOF structure. It represents the force – displacement relationship, the strength and stiffness variation with respect to the displacement and the inelastic characteristics of the SDOF system. At the target displacement, the secant properties obtained from the spectral capacity curve are used to estimate structural response rather than using the elastic properties. This is one of the main differences between the simplified nonlinear static method and the linear static method.

From Eqs(6.8) and (6.14) the spectral displacement and the spectral acceleration can be obtained from:

$$S_d = \frac{M^*}{L^*} x_t = \frac{\sum_{i=1}^{N} m_i \phi_i^2}{\sum_{i=1}^{N} m_i \phi_i} x_t$$

$$S_a = \frac{\sum_{i=1}^{N} \phi_i \psi_i}{\sum_{i=1}^{N} \psi_i} \frac{Q}{L^*} = \frac{\sum_{i=1}^{N} \phi_i \psi_i}{\sum_{i=1}^{N} \psi_i} \frac{Q}{\sum_{i=1}^{N} m_i \phi_i} \qquad (8.1)$$

where $M^* = \sum_{i=1}^{N} m_i \phi_i^2$

$L^* = \sum_{i=1}^{N} m_i \phi_i$ = the effective mass of the equivalent SDOF system,

$x_t$ = target roof displacement of MDOF structure,

$Q$ = total base shear of the MDOF structure at the target displacement,

$\phi_i$ = normalised deflected shape at the target displacement,

$\psi_i$ = normalised vector of the lateral load pattern.

The procedure for obtaining the spectral capacity curve shown above is similar to that of modal spectral analysis for elastic structures (Carr, 1994).

The differences are: first, for the linear static analysis, the relationship between the spectral displacement $S_d$ and the spectral acceleration $S_a$ is:

$$S_d = \frac{1}{\omega^2} S_a = \frac{T^2}{4\pi^2} S_a \tag{8.2}$$

where $T$ = elastic period.

In this relationship of Eq(8.2), the elastic period is constant, but for the simplified nonlinear static analysis, the $S_d - S_a$ relationship is obtained from the capacity curve of the MDOF structure. This relationship is represented by the effective stiffness of the equivalent SDOF system that varies with respect to the target displacement.

Second, in the linear static method, the elastic mode shape for the ith mode of the structure is used to obtain the participation factor to show how much a given mode contributes to the response of the structure. For the nonlinear static method only the first mode is considered, the higher mode effects being neglected. The deflected shape is obtained from a pushover analysis at the target displacement at which state some inelastic deformation may occur.

Since the simplified nonlinear static method uses the results of the pushover analysis and involves the procedure of transforming the MDOF structure to the equivalent SDOF system, some assumptions are needed. These assumptions are that the response of the structure is dominated by the first mode and that the shape of this mode remains essentially constant throughout the time history response. Several investigators (Saiidi et al., 1981, Moehle, 1984, Fajfar et al., 1987, 1988, Qi et al., 1991, Lawson et al., 1994) have shown that these assumptions lead to a fairly good prediction of the peak seismic response of MDOF structures provided their response is dominated by the first mode. Where localised effects are to be considered (soft-storey effects, etc.), the adaptive pushover analysis is recommended. For the adaptive pushover analysis, the assumption of constant deflected shape is not necessary.

## 8.4 DESIGN DEMAND SPECTRA

### 8.4.1 Elastic Demand Spectra

For the elastic SDOF system, the relationship between the spectral acceleration and the spectral displacement is:

$$S_d(T,\xi) = \frac{T^2}{4\pi^2} S_a(T,\xi) \tag{8.3}$$

This relationship is valid only for small values of the viscous damping ratio (say $\xi < 30\%$).

For the simplified nonlinear static method, the design demand spectra can be obtained from a particular earthquake time history or from smoothed design spectra.

For this study, smoothed design spectra from NZS4203 (1992) are adopted. The variation of spectral acceleration versus period and the spectral displacement versus period are used to represent the design demand spectra.

The spectral acceleration for a 5%-damped elastic structure is given by NZS4203 (1992) as follows:

$$S_a(T,5\%) = C_h(T,1) S_p R Z L_u g \tag{8.4}$$

where $C_h(T,1)$ = basic seismic hazard acceleration coefficient for elastic structures (NZS4203: 1992)

$S_p$ = structural performance factor (= 0.67)

$R$ = risk factor for a structure (to be taken as 1 in this study)

$Z$ = zone factor (to be taken as 1 in this study)

$L_u$ = limit state factor for the ultimate limit state (= 1)

$g$ = acceleration due to gravity.

Kawashima et al. (1986) proposed a modification coefficient by which to multiply the 5%-damped earthquake response spectra in order to obtain the response spectra for an arbitrary damping ratio $\xi$ (up to 50%):

$$S_a(T,\xi) = S_a(T,5\%)\left[\frac{1.5}{40\xi+1}+0.5\right]$$
$$= C_h(T,1)S_pRZL_ug\left[\frac{1.5}{40\xi+1}+0.5\right]$$
$$= 6.5727C_h(T,1)\left[\frac{1.5}{40\xi+1}+0.5\right] \quad (8.5)$$

The spectral displacement for different damping ratios can be expressed as:

$$S_d(T,\xi) = \frac{T^2}{4\pi^2}C_h(T,1)S_pRZL_ug\left[\frac{1.5}{40\xi+1}+0.5\right]$$
$$= 9.81\times\frac{T^2}{4\pi^2}\times 0.67C_h(T,1)\left[\frac{1.5}{40\xi+1}+0.5\right]$$
$$= 0.1665T^2C_h(T,1)\left[\frac{1.5}{40\xi+1}+0.5\right] \quad (8.6)$$

For structures with supplemental dampers, the effect of the dampers can be included by considering the effective period and the equivalent viscous damping due to the supplemental dampers. As long as the equivalent viscous damping due to the supplemental dampers does not exceed 30% (ATC-33.03), the design demand spectra, including the effect of the supplemental dampers, can be obtained by the above procedure. In Eq(8.5) and (8.6), T is the effective period including the effect of the dampers. $\xi$ is the total viscous damping ratio including both the initial viscous damping of the structure and the equivalent viscous damping due to supplemental dampers plus the inelastic deformations of the structure.

### 8.4.2 Effect of Inelastic Deformation of Structures on Design Demand Spectra

If the structure without supplemental dampers has inelastic deformations, this effect also needs to be considered.

There are two ways for considering the effects of inelastic structural deformation. One way is to use the effective period and the equivalent viscous damping to represent the effect of inelastic deformation. The other way is to use a strength reduction factor that permits an estimation of the inelastic strength and displacement demands from the elastic strength and the displacement demands. These two methods are outlined in the following review.

Iwan (1980) proposed a simple empirical formula to estimate the mid-period range inelastic response spectrum of a general hysteretic structure given the linear response spectrum of the excitation. In his study, the effective linear period and damping ratio were defined as a function of ductility to represent the effects due to the inelastic deformation of the structure. Shibata et al. (1976) used the substitute-structure method to incorporate the effects of inelastic deformation to determine the design force using the ordinary linear response spectrum. Moehle (1984) proposed a simple procedure to obtain estimates of the maximum inelastic displacement response for a certain class of reinforced concrete building structures. The procedure was based on elastic response spectral analysis techniques, and the change in the vibration period and the equivalent viscous damping due to inelastic deformations were taken into account.

Miranda (1993a and 1993b) used strength reduction factors to reduce the linear elastic design spectra to account for the hysteretic energy dissipation of structures due to inelastic deformations. Miranda (1994) reviewed the results from various investigations of strength reduction factors carried out over the last 30 years. Some were those published by Newmark et al. (1980), Nasser et al. (1992), Lai et al. (1980) and Miranda (1993). In the paper published by Miranda (1994), the main parameters that affect the magnitude of the strength reductions were discussed. Simplified expressions for strength reduction factors to estimate inelastic design spectra were presented.

Bergman et al. (1989), Wu et al. (1989) and Hanson et al. (1993) all stated that the effect of high damping due to supplemental dampers and inelastic structural response on the spectral de-amplification factors can be considered separately. Thus, these reduction factors (ratios of inelastic response spectra to elastic response spectra) can be divided into those terms that include the supplemental damping system and those terms that include the structural inelastic deformations. The relatively small scatter in the data with changes in damping (from 10 to 50 percent) show that spectral modifications for high damping and for inelastic response can be considered separately (Hanson et al., 1993).

From the above-mentioned investigations, it can be seen that the effect of inelastic structural deformation and supplemental dampers on the design demand spectra can be taken into account by two methods.

Method 1

Both the effects due to inelastic deformations in the structure and the effect due to supplemental dampers can be taken into account by means of the equivalent viscous damping and the effective period shift. The total equivalent viscous damping ratio can be calculated as:

$$\xi_t = \xi_0 + \Delta\xi_0 + \xi_d \tag{8.7}$$

where $\xi_t$ = total equivalent viscous damping ratio of the structure with supplemental dampers

$\xi_0$ = original viscous damping ratio of the structure

$\Delta\xi_0$ = equivalent viscous damping ratio due to the inelastic deformation of the structure

$\xi_d$ = equivalent viscous damping ratio due to the supplemental damping system.

Eq(8.7) is an approximate relationship. Lobo et al. (1993) show that for a small stiffness increase due to supplemental dampers, the resultant damping is the sum of the added damping and the original damping. For a structure with the above-mentioned distribution of yield strengths of the supplemental dampers, once the supplemental dampers yield, the tangent stiffness increase due to the supplemental dampers is negligible, and the relationship in Eq(8.7) is still valid. $\Delta\xi_0$ in Eq(8.7) can be obtained from Eq(7.46), and $\xi_d$ can be calculated from Eq(7.22).

The effective period of the structure with the supplemental dampers can be calculated from Eq(7.32) at the target displacement.

The elastic demand spectra modified by the higher damping reduction given in Eqs(8.5) and (8.6) gives the demand spectra for the inelastic structure with supplemental dampers.

Method 2

The effects due to the inelastic deformation of structures and supplemental dampers on the de-amplification factors are considered separately. First it is assumed that the original structure remains elastic. The effect due to the supplemental dampers is taken into account. Eqs(8.5) and (8.6) are used to obtain elastic demand spectra for structures with the supplemental dampers (original structure remains elastic). Then appropriate strength reduction factors can

be used to obtain the inelastic demand spectra from the elastic demand spectra with the high damping effects.

Since the investigation of the inelastic demand spectra is not part of the scope of this study and also because of simplicity, method 1 is adopted in this study to carry out the simplified nonlinear static analyses and design of structures with supplemental dampers.

## 8.5 PROCEDURE FOR THE SIMPLIFIED NONLINEAR STATIC ANALYSIS OF STRUCTURES WITH SUPPLEMENTAL LEAD DAMPERS

The procedure for the simplified nonlinear analysis of structures with supplemental lead dampers is as follows (Lin et al., 1998b):

Step 1. Conduct a pushover analysis of the structure without supplemental dampers. The base shear and the roof displacement of the original structure at yield can be obtained. The ratio of the post-yield stiffness to the initial stiffness is also obtained.

Step 2. Make an initial estimate of the roof displacement ($x_{t0}$) of the structure with the supplemental dampers. The deflected shape $\{\phi\}$ can be obtained by the displacement profile corresponding to the estimated displacement from the results of step 1. The initial estimated target ductility $\mu$ is also obtained.

Step 3. The force factor $F_R$ of the structure with the supplemental dampers can be calculated. The equivalent viscous damping $\xi_d$ due to the supplemental dampers can be calculated from Eq(7.22). The equivalent viscous damping ratio ($\xi_0 + \Delta\xi_0$) due to the inelastic deformation and the initial damping can also be estimated by Eq(7.46) for the estimated displacement. The total equivalent viscous damping ratio $\xi_t$ is then known.

Step 4. The effective period $T_{eff}$ of the structure with the supplemental dampers can be obtained from Eq(7.32).

Step 5. The displacement for the equivalent SDOF system (or spectral displacement) $x^*$ for the effective period $T_{eff}$ and equivalent viscous damping ratio of $\xi_t$ can be obtained directly from the elastic displacement spectra.

Step 6. The target roof displacement $x_{t1}$ can be obtained by

$$x_{t1} = \frac{L^*}{M^*} x^*$$

where $x^*$ = spectral displacement

$$M^* = \sum_{i=1}^{N} m_i \phi_i^2$$

$$L^* = \sum_{i=1}^{N} m_i \phi_i$$

Let the new target roof displacement $x_t$ be:

$$x_t = \frac{x_{t1} + x_{t0}}{2}$$

Step 7. Compare $x_t$ with the initial estimated target displacement $x_{t0}$. If they are close enough, they are taken to be the target roof displacement. Then go to step 8. If the difference is large, iteration is needed. We need to use a new estimated roof displacement ($x_{t0} = x_t$) and go back to step 3.

Step 8. For the target displacement obtained in step 7, the effective period of the structure $T_{eff}$ and the total equivalent viscous damping ratio $\xi_t$ can be obtained. The spectral acceleration value $S_a$ can be obtained from the acceleration spectra for the $T_{eff}$ and $\xi_t$. The peak base shear of the structure with the supplemental dampers (MDOF) can be calculated from the spectral acceleration of its equivalent SDOF system as follows:

$$Q = L^* \frac{\sum_{i=1}^{N} \psi_i}{\sum_{i=1}^{N} \phi_i \psi_i} S_a(T_{eff}, \xi_t)$$

where $Q$ = the peak base shear

$S_a(T_{eff}, \xi_t)$= The spectral acceleration for the effective period $T_{eff}$ and the equivalent viscous damping ratio $\xi_t$.

The final deflected shape of the structure at the target displacement can be obtained from the result of the nonlinear analysis of the original structure in step 1. Then the peak interstory drift $IDI_{max}$ can be calculated as follows:

$$IDI_{\max} = \left[\frac{\phi_i - \phi_{i-1}}{h}\right]_{\max} x_t$$

## 8.6 EXAMPLE

For the 12-storey 3-bay frame structure used previously, the initial period of the structure without dampers is 1.99s. There is one damper placed in each storey. The strength of the damper at the 1st floor level is 211KN. The distribution of the strength of the dampers in every storey is proportional to the shear distribution developed due to a lateral load with an inverted triangular distribution. The stiffness ratio $S_R$ (the ratio of the initial stiffness of the damper to the initial stiffness of the original structure) is taken as 10. $\cos\theta = 0.91$, where $\theta$ is the angle of the braces with respect to the horizontal direction. From the results presented in earlier chapters, such a structure with supplemental dampers will respond predominantly in its first mode.

The procedure of the simplified nonlinear static analysis of the structure with the supplemental dampers is used to estimate the peak structural response:

Step 1: A pushover analysis of the structure without the supplemental dampers is conducted, using an inverted triangular lateral load pattern. The base shear-roof displacement curve is shown in Fig.8.4. From the base shear-roof displacement curve, roof displacement at yield is $\Delta_{y0}$ = 11.0cm, the base shear at yield is $F_{y0}$ = 780.0KN. The ratio of the post-yield stiffness to the initial stiffness of the original structure is $r$ = 0.05.

Step 2: An estimate of the roof displacement of the structure with the supplemental dampers is $x_{t0}$ =22.0cm, that is, the initial estimate of the target ductility of the original structure while incorporating the supplemental dampers is $\mu$ = 2.0. At this estimated roof displacement, the normalised deflected shape vector is

$\{0.03388,0.1077,0.2035,0.3145,0.4378,0.5635,0.6822,0.7868,0.8738,0.9375,0.9782,1\}$

Therefore:

$$L^* = \sum_{i=1}^{N} m_i \phi_i = 819.85,$$

$$M^* = \sum_{i=1}^{N} m_i \phi_i^2 = 627.99$$

$$\frac{M^*}{L^*} = 0.7660,$$

$$\frac{\sum_{i=1}^{N} \phi_i \psi_i}{\sum_{i=1}^{N} \psi_i} = 0.7533$$

Step 3: The force ratio of the structure with the supplemental dampers is:

$$F_R = \frac{211 \times 0.91}{780 \times \frac{22}{11}} = 0.1231$$

The equivalent viscous damping of the structure due to the supplemental dampers can be calculated from Eq(7.22) as $\xi_d$ = 12.09%. The equivalent viscous damping due to inelastic deformation and the original damping can also be calculated as $\xi_0 + \Delta\xi_0$ = 10.86%. So the total equivalent viscous damping of the structure with the supplemental dampers is $\xi_t = \xi_0 + \Delta\xi_0 + \xi_d = 22.95\%$.

Step 4: The effective period of the structure with the supplemental dampers at this target displacement is $T_{eff} = 2.496$s.

Step 5: The spectral displacement for the effective period $T_{eff}$ and the equivalent viscous damping $\xi_t$ can be read from the displacement spectra.

From NZS4203, $C_h(2.496,1) = 0.2$

Therefore

$$S_d(2.496,22.95\%) = 0.1665 \times 2.496^2 \times 0.2 \times \left[\frac{1.5}{40 \times 22.95\% + 1} + 0.5\right] = 0.1343$$

Step 6: The target roof displacement $x_t = 0.1343 \times \frac{1}{0.766} = 0.1753\text{m} = 17.53\text{cm}$

The new target displacement $x_t = \frac{22+17.53}{2} = 19.77\text{cm}$ $\mu = 1.80$

Step 7: Compare $x_t$ with $x_{t0}$

$\frac{x_t - x_{t0}}{x_t} = \frac{22-19.77}{19.77} = 11.28\%$ The difference is relatively large. More iteration is required.

Use the values of the target roof displacement and the ductility obtained in this step and go back to step 3.

Step 3-1: The force ratio $F_R = \frac{211 \times 0.91}{780 \times 1.8} = 0.1368$

$\xi_d = 12.189\%$, $\xi_0 + \Delta\xi_0 = 5\%+5.09\%=10.09\%$

$\xi_t = 22.279\%$

Step 4-1: $T_{eff} = 2.354\text{s}$

Step 5-1: From NZS4203, $C_h(2.354,1) = 0.2146$

$$S_d(2.354,22.279\%) = 0.1665 \times 2.354^2 \times 0.2146 \times \left[\frac{1.5}{40 \times 22.279\% + 1} + 0.5\right] = 0.1290$$

Step 6-1: The target roof displacement $x_t = 0.1290 \times \frac{1}{0.766} = 0.1684\text{m} = 16.84\text{cm}$

The new target displacement is $x_t = \frac{19.77+16.84}{2} = 18.31\text{cm}$ $\mu = 1.664$

Step 7-1: Compare $x_t$ with $x_{t0}$

$$\frac{x_t - x_{t0}}{x_t} = \frac{19.77-18.31}{18.31} = 7.39\%$$

Further iteration is needed.

Step 3-2: The force ratio $F_R = \frac{211 \times 0.91}{780 \times 1.664} = 0.1479$

$\xi_d = 12.247\%$, $\xi_0 + \Delta\xi_0 = 5\%+4.496\%=9.496\%$

$\xi_t = 21.743\%$

Step 4-2: $T_{eff} = 2.270$s

Step 5-2: From NZS4203, $C_h(2.270,1) = 0.223$

$$S_d(2.270,21.743\%) = 0.1665 \times 2.270^2 \times 0.223 \times \left[\frac{1.5}{40 \times 21.743\% + 1} + 0.5\right] = 0.1253$$

Step 6-2: The target roof displacement $x_t = 0.1253 \times \frac{1}{0.766} = 0.1635\text{m} = 16.35\text{cm}$

The new target displacement is $x_t = \frac{18.31+16.35}{2} = 17.33\text{cm}$ $\mu = 1.576$

Step 7-2: Compare $x_t$ with $x_{t0}$

$$\frac{x_t - x_{t0}}{x_t} = \frac{18.31-17.33}{17.33} = 5.66\%$$

The difference is relatively small and is taken as acceptable.

Hence,

$x_t = 17.33\text{cm}$

$\mu = 1.576$, $F_R = \frac{211 \times 0.91}{780 \times 1.576} = 0.1562$

$\xi_d = 12.29\%$

$$\xi_0 + \Delta\xi_0 = \frac{1 - \frac{1}{\sqrt{1.576}}}{5} + 0.05 = 0.907 = 9.07\%$$

$\xi_t = 21.359\%$

$T_{eff} = 2.213s$

$C_h(T_{eff} = 2.213, \mu = 1) = 0.2287$

Step 8: The spectral acceleration value $S_a$ can be calculated as:

$$S_a(\xi = 21.359\%, T = 2.213) = 6.5727 \times 0.2287 \times \left[\frac{1.5}{40 \times 21.359\% + 1} + 0.5\right] = 0.9879$$

For the target displacement $x_t$ = 17.33cm, the final deflected shape can be obtained from the result of the pushover analysis of the original structure (Step 1). The final deflected shape vector is

$\{0.03611, 0.1116, 0.2053, 0.3120, 0.4301, 0.5507, 0.6658, 0.7694, 0.8601, 0.9303, 0.9759, 1\}$.

Hence

$$L^* = \sum_{i=1}^{N} m_i \phi_i = 811.2066, \quad M^* = \sum_{i=1}^{N} m_i \phi_i^2 = 614.5893$$

$$\frac{M^*}{L^*} = 0.7576, \quad \frac{\sum_{i=1}^{N} \phi_i \psi_i}{\sum_{i=1}^{N} \psi_i} = 0.7458$$

$$[\phi_i - \phi_{i-1}]_{\max} = 0.1206$$

The peak base shear $Q$ of the structure with the supplemental dampers can be calculated as follows:

$$Q = L^* \frac{\sum_{i=1}^{N} \psi_i}{\sum_{i=1}^{N} \phi_i \psi_i} S_a(T_{eff}, \xi_t)$$

$$= 811.2066 \times \frac{1}{0.7458} \times 0.9879$$

$$= 1074.54 \quad \text{(KN)}$$

The peak interstory drift is

$$IDI_{\max} = \left[\frac{\phi_i - \phi_{i-1}}{h}\right]_{\max} x_t = 0.1206 \times 17.33 = 2.09(\text{cm})$$

A time history analysis of the structure with the supplemental dampers was also carried out. The El Centro 1940 NZS4203 compatible earthquake was used as the ground excitation. The comparisons of the structural response for the simplified nonlinear static analysis and the time history analysis is shown in Table 1.

The results of the simplified nonlinear static analysis are very close to those of the time-history analysis except for the peak base shears. This is because the base shear has a significant contribution from the higher modes while the simplified method is based on the first mode response. However, for the design of the structure with supplemental dampers the main concern is the displacement. For a preliminary design this method of analysis of the structure with the supplemental dampers is sufficiently accurate.

For comparison purposes, this simplified nonlinear static method is also used to analyse the structural response of the structure without the dampers for the NZS4203 design earthquake. The same procedure shown above is adopted except that there is no need to calculate the force ratio $F_R$ and the equivalent viscous damping due to the supplemental dampers ($F_R = 0$, $\xi_d = 0$).

The results for this simplified nonlinear static analysis of the structure without dampers are:

$x_t = 25.50\text{cm}, \mu = 2.318, T_{eff} = 2.9347\text{s}$

$\xi_t = 11.864\%$

$S_a = 0.87$

$$L^* = 821.5505, \quad \frac{\sum \phi_i \psi_i}{\sum \psi_i} = 0.7564, \quad [\phi_i - \phi_{i-1}]_{\max} = 0.1292$$

Hence,

$x_t = 25.50\text{cm}$

$Q = 944.935\text{KN}$

$ID_{\max} = 3.295\text{cm}$

The results from the simplified nonlinear static analysis and the time history analysis of the structure without dampers under the El Centro 1940 NZS4203 compatible earthquake are shown in Table 8.2. It can be seen that the peak roof displacements are very similar, but the difference of the peak interstorey drift and the peak base shear are relatively large. For the structure with the supplemental dampers, the difference in the peak interstorey drift is very small. Higher mode effects are more significant in the structure without dampers than in the structure with the supplemental dampers.

| | Roof displacement (cm) | Base shear (KN) | Interstorey drift (cm) |
|---|---|---|---|
| Simplified static analysis | 17.33 | 1074.54 | 2.09 |
| Time history analysis | 17.74 | 1262.7 | 2.087 |
| Difference | 2.37% | 17.51% | 0.14% |

Table 8.1 Comparison of the peak responses of the structure with the supplemental dampers for a simplified nonlinear static analysis and time history analysis under the El Centro 1940 NZS4203 compatible earthquake

| | Roof displacement (cm) | Base shear (KN) | Interstorey drift (cm) |
|---|---|---|---|
| Simplified static analysis | 25.50 | 944.935 | 3.295 |
| Time history analysis | 25.487 | 1178.8 | 3.799 |
| Difference | 0.05% | 24.75% | 15.3% |

Table 8.2 Comparison of the peak responses of the structure without dampers for a simplified nonlinear static analysis and time history analysis under the El Centro 1940 NZS4203 compatible earthquake

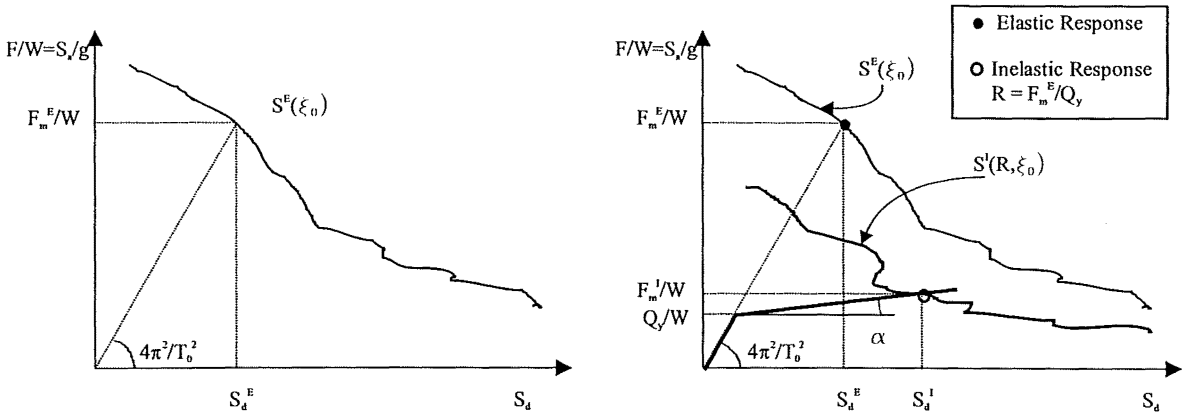


(a) Elastic

(b) Inelastic (elastic shown by dotted line)

Elastic and inelastic composite response spectra

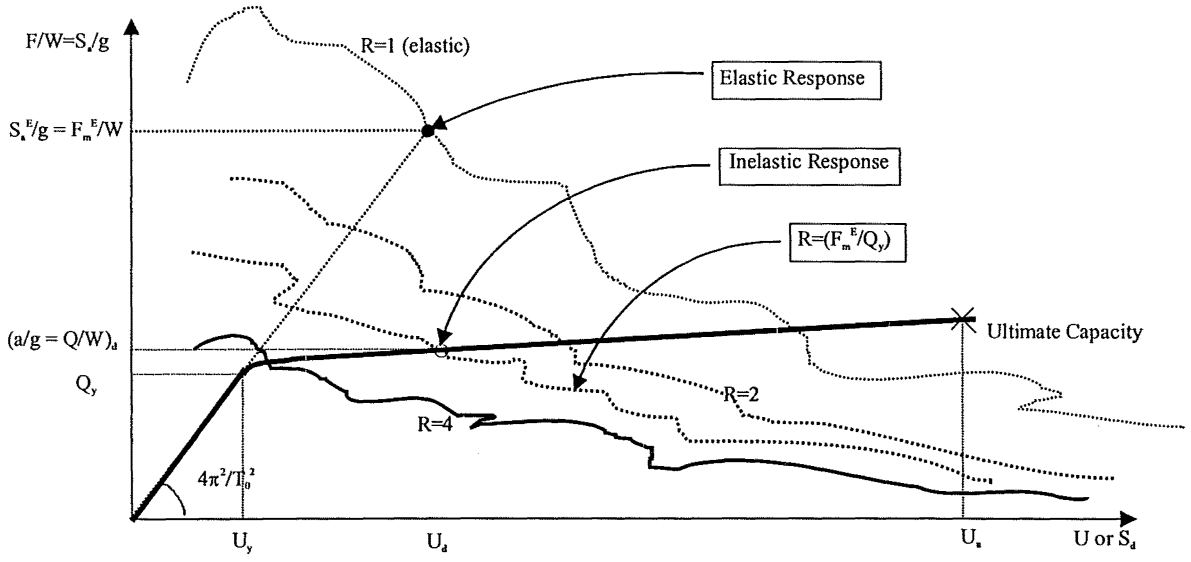


Estimate of maximum inelastic response

Figure 8.1 Composite spectra and estimated inelastic response (Reinhorn, 1997)

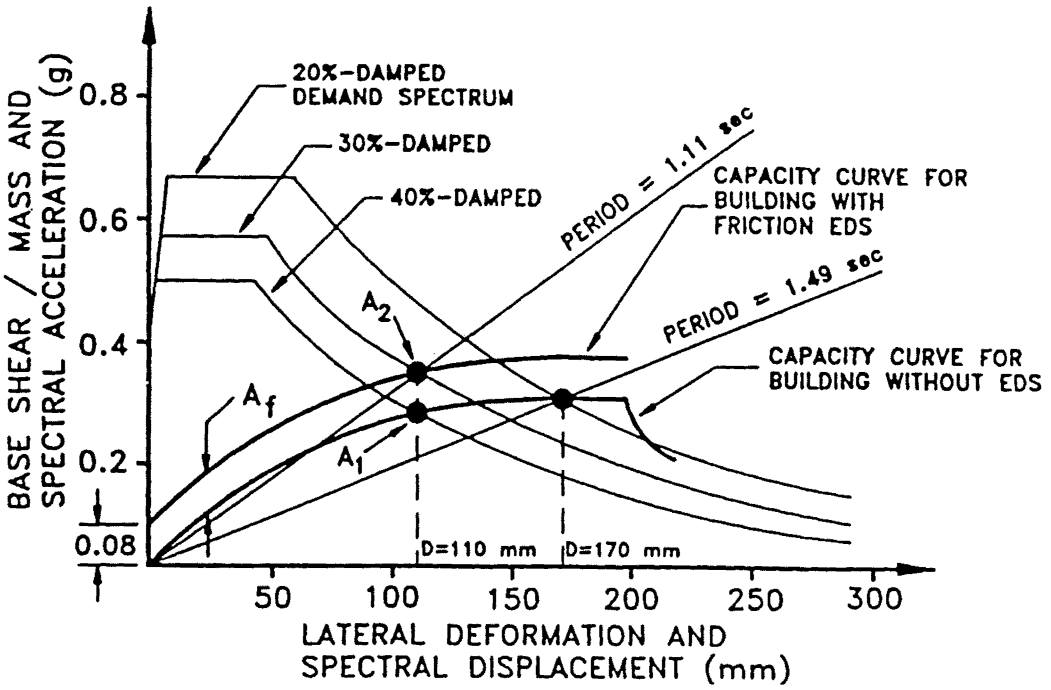


Figure 8.2 Capacity and demand curves for one-storey frame with friction dampers (from ATC-33, 75% submittal draft )

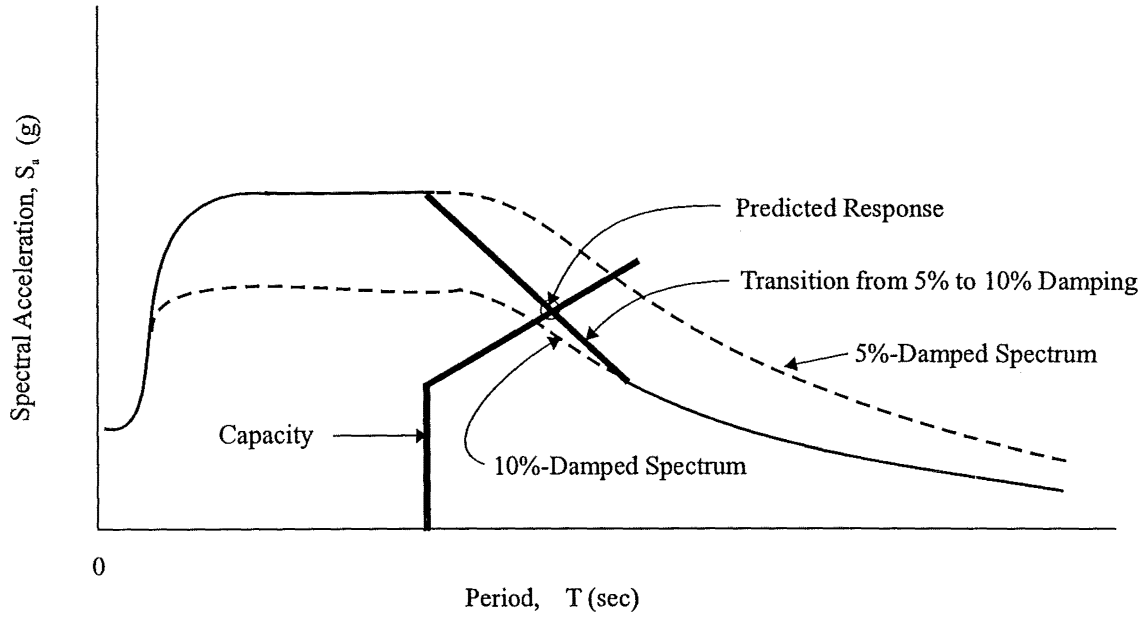


Figure 8.3 Capacity and demand, spectral acceleration versus period (Freeman, 1978)

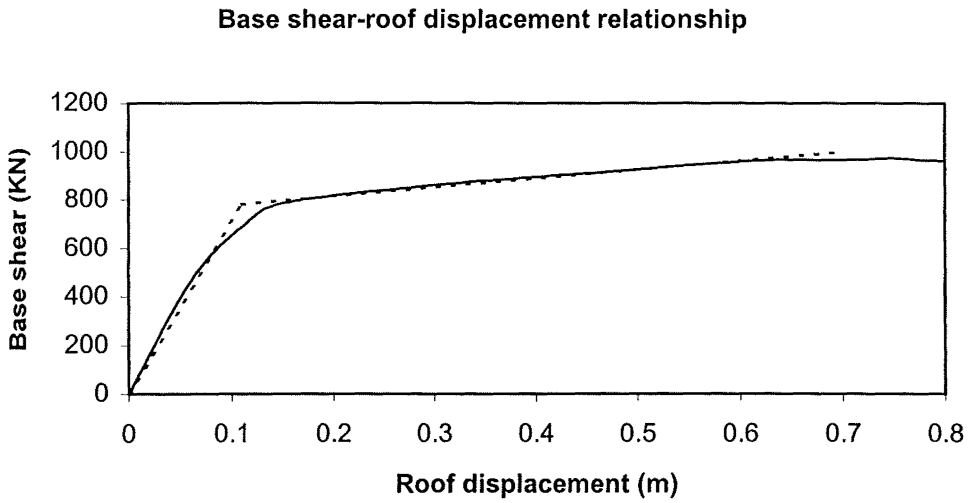


Figure 8.4 . Base shear-roof displacement relationship of the structure without dampers

# CHAPTER 9

# DISPLACEMENT-BASED DESIGN PROCEDURE FOR THE STRUCTURE WITH SUPPLEMENTAL LEAD DAMPERS

## 9.1 REVIEW OF EXISTING DESIGN METHODS FOR HYSTERETIC DAMPERS

Filiatrault et al. (1990) proposed a simplified seismic design procedure for structures with friction dampers. In the paper, the results of a parametric study on multi-storey friction-damped braced frames were used to construct a general design slip-load spectrum for a quick evaluation of the total optimum slip shear in a multi-storey building. The spectrum takes into account the properties of the structure and of the ground motion anticipated at the construction site. Time history analyses of 45 different structures under 5 scaled artificial earthquakes were performed to obtain this design slip-load spectrum. The dampers were placed in the stories, with the same bracing size and slip load in all the stories. A relative performance index ($RPI$) was defined as:

$$PRI = \frac{1}{2}\left(\frac{SEA}{SEA_{(0)}} + \frac{U_{\max}}{U_{\max(0)}}\right)$$

where $SEA$ = the area under the strain energy time-history for a friction damped structure,

$SEA_{(0)}$ = the area under the strain energy time-history for the identical structure, but without bracing (slip load = 0),

$U_{\max}$ = the maximum strain energy for a friction damped structure,

$U_{\max(0)}$ = the maximum strain energy for the identical structure, but without bracing (slip load = 0).

A series of dynamic time history analyses of friction damped braced frames of arbitrary configuration for specified distributions of slip load were performed. The optimum slip load distribution of the structure is defined to be the distribution slip load for which the $PRI$ is a minimum. For a given structure and a design ground motion, the slip load for the friction dampers can be selected from the design slip-load spectrum shown in Fig.9.1.

The proposed design equation is:

$$\frac{V_0}{ma_g} = \begin{cases} ((-1.24N - 0.31)T_b / T_0 + 1.04N + 0.43)T_g / T_0 & \text{for } 0 \le T_g/T_0 \le 1 \\ ((0.01N + 0.02)T_g / T_0 - 1.25N - 0.32)T_b / T_0 & \\ \quad + (0.002 - 0.002N)T_g/T_0 + 1.04N + 0.42 & \text{for } T_g/T_0 > 1 \end{cases}$$

where $V_0$ = the total optimum slip shear,

$N$ = number of stories in the structure,

$T_b$ = natural period of the braced structure (no slippage occurring)

$T_0$ = natural period of the unbraced frame,

$T_g$ = the predominant ground motion period,

$a_g$ = the peak ground acceleration.

A procedure for the seismic design of friction damped structures was also proposed in the same paper.

Su et al. (1990) proposed possible design criteria for a building structure with ADAS (Added Damping And Stiffness) devices as follows:

1. the ADAS devices carry more than 50% of the storey shear
2. the device ductility ratios are less than 6
3. The ductility ratios of building frame members are less than 1.75 for a severe earthquake
4. The maximum storey drift ratio does not exceed 1.5%

In a building designed to incorporate ADAS devices, the most important first step is to decide the appropriate design base shear. A design procedure was recommended by Su et al. (1990) to satisfy these design criteria. Because the spectral acceleration of buildings with ADAS devices are functions of the SR (stiffness ratio) and the device ductility μ, the design shear prescribed by the code may not be suitable for building design. In their study, the response spectra of a structure with ADAS devices related to five stiffness ratios (SR) and six device ductility ratios (μ=1,2,3,4,5,6) were established for the purpose of design. The Ramberg-Osgood model for the ADAS devices was adopted to obtain the response spectra. This procedure is suitable for a SDOF system.

Tsai et al. (1993) presented the research findings on the effectiveness of using steel Triangular-plate Added Damping And Stiffness (TADAS) devices for earthquake-resistant

structures. A design procedure, incorporating the structural response characteristics of structures with TADAS devices and the seismic-resistant design concept adopted in the Japanese Building Standard Law, was suggested as follows:

1. Establish the site-dependent service level design earthquake
2. Select a suitable SR value based on the fundamental period estimated for the frame
3. A moment-resisting frame capable of resisting at least 25% of the prescribed seismic force was recommended. A frame without the TADAS device in place can then be designed.
4. Compute the TADAS device stiffness and yield displacement
5. Perform lateral force analyses for the frame with the TADAS device in place, when necessary, repeat step 3 and 4 to meet member strength and frame drift requirements for the serviceability limit state.
6. Check the capacity of the braces, columns and beams.

This procedure is also basically suitable for a SDOF system.

Rao et al. (1995) presented a design procedure for retrofitting of RC frames using friction dampers. This procedure is as follows:

1. The structure is modelled for a nonlinear pushover analysis.
2. A pushover analysis is performed on the bare frame without dampers.
3. Perform a nonlinear time history analysis on the equivalent SDOF system.
4. If the response of the bare frame is more than the acceptable response, retroffiting is required. For different levels of increased initial stiffness, *IDS* (Inelastic Demand Spectrum) curves must be developed. By superimposing acceptable limits on the IDS curves, the required initial stiffness and yield level for the equivalent bilinear SDOF system can be estimated.
5. Knowing the required equivalent bilinear SDOF characteristics, a pushover analysis is performed on the frame with friction dampers added at the different storey levels. The properties of the dampers (i.e. initial stiffness and slip load) must be changed until the point when the pushover of the frame results in a capacity curve that matches the desired equivalent SDOF system. This damper setting is the design damper configuration.

Ciampi et al. (1992, 1995) also introduced a methodology that is based on inelastic response spectra for SDOF systems and can be used to design dissipative bracing systems for the

seismic protection of buildings. Two design problems were considered: retrofitting existing buildings which are not seismically safe and designing new buildings to provide higher degrees of seismic protection so that there is very little or no damage in the main structure, even for severe earthquakes. Two ductility indices were adopted to characterise the response of the frame: the maximum frame displacement ductility $\mu_f$ and the cumulative ductility $\mu_{fH}$.

In order to construct inelastic response spectra useful for designing dissipative bracings, a set of 5 artificial accelerograms compatible with the Code Proposal of the Italian Research Council, of 20 seconds duration, were generated. The constructed inelastic response spectra in terms of $\mu_f$ and $\mu_{fH}$ were obtained by averaging the corresponding response quantities over these 5 artificial accelerograms and were presented as functions of the parameters $T_f$, $\eta_f$, $\beta$ and $\alpha$. $T_f$ represents the natural period of free vibration of the original structure; $\eta_f$ is the normalised yield level of the frame; $\beta$ is the ratio of the storey displacement which induces yielding in the brace to that inducing yielding in the frame; $\alpha$ is the ratio of the elastic natural period of the braced frame to that of the original frame.

As mentioned in the paper (Ciampi et al., 1995), the application of this simple methodology to real MDOF structures requires the further effort of selecting proper distributions of stiffness and yield forces over the height of the building with the object of favouring uniform engagement of the bracings in the energy dissipation process and of avoiding a concentration of frame damage at specific locations.

The method proposed by Filiatrault et al. is not suitable for this study. This is due to the following reasons: first, the frames used in the analyses (by Filiatrault et al.) were assumed to be linear. However, inelastic deformations are allowed to occur in structures with supplemental lead dampers. Second, the design requirement can not be explicitly expressed by the design spectrum. Hence, it is not clear whether the design requirement (often displacements or deformations) can be achieved or not. The third reason is that the configuration of dampers adopted is not always the most economic one for all the cases.

The methods proposed by Su et al. and Tsai et al. respectively are based on ADAS devices. There are some differences between the ADAS devices and lead dampers. The hysteresis loop of lead dampers is very close to a rigid plastic behaviour. This will result in some differences in the structural response. Also, the start point for these methods is a force (base shear) which is the conventional concept in seismic design of building structures. The displacement

(deformation) requirement is checked later. The purpose of incorporating supplemental dampers into structures is to control the damage of the main structure caused by earthquake excitations. Damage is a consequence of deformation. The main concern here is no longer force or strength but displacement and deformation. Hence, a direct displacement-related design procedure is needed for the design of structures with supplemental dampers.

## 9.2 DISPLACEMENT-BASED DESIGN METHOD OVERVIEW

It is known that once structures yield, the base shear strength remains constant (for the elasto-plastic model), while the deformation can take any value, from its yielding value up to some maximum value. Hence, the base shear strength of a given structure is insensitive to variation of deformation and, therefore, to damage (Bertero et al., 1991).

Damage is a consequence of deformation. For any structure that is responding in the inelastic range under an approximately constant strength, the degree of damage depends on the level of the inelastic deformation that the structure undergoes. Thus, to control damage it is necessary to control deformation.

There are two displacement-related factors that can be used to describe the deformations and, therefore, the damage that structures might undergo. They are the displacement ductility factors and the interstorey drift indices. The displacement ductility factors provide good indications of structural damage but can not adequately reflect the damage to non-structural components. The interstorey drift indices are reasonably good indicators of the non-structural damage occurring during earthquake excitations (Bertero et al., 1991 and Sozen, 1981).

The displacement-based design is a seismic design methodology that uses displacements as the basis for the design procedure. Direct displacement-based design attempts to provide a more rational basis for seismic design by designing a structure for a specified level of displacement rather than force, under the design level earthquake. The design displacement may be a direct consequence of limit state criteria, such as non-structural damage drift limits. Strength and stiffness are not variables in the procedure – they are the end results.

The key element of the procedure is that stiffness and damping of the structure are characterised by secant properties at the maximum response, rather than based on initial elastic properties (Priestley et al., 1997).

Several investigators have presented their findings in this design methodology: Qi et al. (1991), Moehle (1992), Priestley (1995, 1997), Calvi et al. (1995) and Kowalsky et al. (1995).

From these research findings, the basic procedure for displacement-based design should be as follows:

Step 1. Define the design earthquake in terms of displacement response spectra.

Step 2. Specify the design target displacement and then the initial deflected shape. Initial displacement ductility demand can also be determined.

Step 3. Calculate structural properties for the equivalent SDOF system.

Step 4. From the characteristics of the equivalent SDOF system and the given displacement response spectra, determine the minimum stiffness required in terms of the maximum allowable fundamental period $T_{max}$, so that the desired target displacement can be satisfied. The equivalent static lateral force on the equivalent SDOF system can also be obtained.

Step 5. Calculate the distribution of applied forces acting on the MDOF structure.

Step 6. Conduct a structural analysis using the applied forces.

Step 7. Check and revise. If necessary, some iteration might be needed.

## 9.3 APPLY THE DISPLACEMENT-BASED DESIGN CONCEPT TO STRUCTURES WITH SUPPLEMENTAL LEAD DAMPERS

Before using the displacement-based design concept to determine parameters for supplemental lead dampers, some information necessary for carrying out this design procedure for the structure with the supplemental dampers must be investigated first. Such information includes the appropriate displacement spectra, the target displacement related to

the design criteria, the optimal damping level provided by the supplemental dampers, the deflected shape and characteristics of the equivalent SDOF system for a structure with the dampers.

### 9.3.1 Generation of Appropriate Displacement Spectra

In the simplified nonlinear static method, the structure with the supplemental dampers can be represented by its equivalent SDOF system. Hence, with the information of the total equivalent viscous damping (initial viscous damping, equivalent viscous damping due to the inelastic deformation of the structure and also due to the supplemental dampers) and of the effective period (including the influence of the inelastic deformations of the original structure and of the supplemental dampers) at the target displacement, the maximum relative displacement response can be estimated from elastic response spectra with different levels of damping. This agrees with the idea behind the displacement-based design concept, that is, the stiffness and damping of the structure are characterised by the secant properties at the maximum response.

Hence, for the use of the displacement-based method we need to choose appropriate displacement spectra for different levels of damping. In theory, these can be simply generated from acceleration spectra using the normal relationships between peak acceleration and displacement of elastic oscillators. However, as mentioned by Priestley (1995), it should be recognised that the design acceleration spectra are often unrealistically high in the long period range. The determination of spectral displacements from design acceleration spectra will result in displacements which continue to increase with period even at very large values of T. The realistic characteristics of the displacement spectra should be: spectral displacements increase with period until they reach a maximum and then decrease again at large periods, eventually reaching a stable value equal to the peak ground displacement, regardless of the ductility level or period of the structure.

The extensive investigation of the appropriate displacement spectra is beyond the scope of this study. The procedure for obtaining smoothed displacement spectra for different levels of damping shown in Chapter 8 is adopted here for design purposes. However, the suggestion of Eurocode8 concerning the displacement spectra is adopted for the modification of the long period cases ($T > 3s$). For periods longer than 3s, a moderate change in the slope of the

acceleration spectrum results in a plateau rather than linearly increasing displacement with increasing period (Calvi et al., 1995).

From Eq(8.6) and taking the above modification for long period cases into account, we have:

$$\begin{aligned} S_d(T,\xi) &= 0.1665T^2 C_h(T,1)\left[\frac{1.5}{40\xi+1}+0.5\right] \qquad (\text{for } T \le 3\text{s}) \\ S_d(T,\xi) &= 0.1665\times 3^2 C_h(T,1)\left[\frac{1.5}{40\xi+1}+0.5\right] \\ &= 1.4985 C_h(3\text{s},1)\left[\frac{1.5}{40\xi+1}+0.5\right] \qquad (\text{for } T \ge 3\text{s}) \end{aligned} \tag{9.1}$$

It also needs to be noted that the displacement spectra generated here and shown in Fig.9.2 are not suitable for the very short period range structures (< 0.4 seconds). Typical displacement spectra are shown in Fig.9.2.

### 9.3.2 Target Displacement and Deflected Shape

The structural ductility factor μ and the peak interstorey drift index (IDI) are used as parameters to control the damage. Once the deflected shape of the structure is determined, the relationship between the peak roof displacement $x_t$ and the peak interstorey drift index (*IDI*) can be expressed as (from Eq(6.17):

$$IDI_{\max} = \left(\frac{\phi_i - \phi_{i-1}}{h_i}\right)_{\max} x_t \tag{9.2}$$

where $h_i$ = the storey height at level $i$,

$\phi_i$ = value of the normalised deflected shape vector at level $i$.

For example, a 0.5% peak interstorey drift index is a reasonable drift limit for structures in which minor damage not requiring repair may occur under the design earthquake (Freeman, 1985). For a given peak interstorey drift index, the target roof displacement can be obtained from Eq(9.2). While considering the design peak interstorey drift requirement, the maximum displacement range which supplemental lead dampers are allowed to undergo also needs to be checked.

For structures with supplemental dampers, the desired ductility factors for the original structures are usually expected to be less than 2. It is intended that most of the inelastic deformations occur in the supplemental dampers while keeping the main structure within its elastic range.

From chapter 6 it can be seen that for a satisfactory distribution of yield strengths of supplemental lead dampers, the deflected shape of the structure with the supplemental dampers can be represented by that of the original structure without dampers. Hence, the deflected shape of the undamped structure at the target displacement is used for design.

### 9.3.3 Characteristics of the Equivalent SDOF System

The characteristics of the equivalent SDOF system for a MDOF structure with supplemental dampers have been described in detail in chapter 6. Some of the main points are:

1. The structure with supplemental dampers can be considered as a dual system – the original structure without dampers and the supplemental damping system.

2. The force – displacement characteristics of the original structure can be represented by its base shear – roof displacement relationship (bilinear curve) that can be obtained from a pushover analysis.

   The force – displacement characteristics of the supplemental damping system can be represented by an elasto-plastic curve whose properties are defined by Eqs(6.18) and (6.20).

3. Transformation of the properties of the equivalent SDOF system and its MDOF structure can be done through Eq(6.15).

### 9.3.4 Optimal Equivalent Viscous Damping Ratio due to the Supplemental Dampers

It was mentioned in chapter 7 that the equivalent viscous damping due to the inelastic deformations of the original structure can be estimated by Eq(7.46). For a satisfactory

distribution of yield strengths of the supplemental dampers, the equivalent viscous damping due to the dampers can be estimated by Eq(7.22).

From the equivalent SDOF system it can be seen that when the strength levels of the dampers increase, the effective period of the structure with the supplemental dampers will decrease and the equivalent viscous damping due to the dampers will increase. This will lead to a reduction of the spectral displacement. However, the influence of the strength levels of the dampers on the response spectral acceleration is not that straightforward. When the strength levels of the dampers increase on the one hand, the equivalent viscous damping will tend to increase, this will lead to lower value of the acceleration response; on the other hand, the effective period of the structure with the supplemental dampers will tend to reduce, this will result in a higher value of the acceleration response. The acceleration response of the structure reflects the response level of the base shear of the structure. It is desired that when the displacement response is reduced, the base shear response should not increase significantly. There exists a certain level of damping to minimise the acceleration response (Lin et al., 1998b).

The simplified formula of Kawashima et al. (1986) is used in order to obtain the response spectra for an arbitrary damping ratio $\xi$ (up to 50%).

From NZS4203 the elastic acceleration response spectra for a 5% damping ratio is taken as inversely proportional to period for structural periods greater than 1.0s.

$$S_a(T,0.05) = \frac{C_v}{T} g \tag{9.3}$$

where $C_v$ = site-dependent factor

$T$ = structural period

$g$ = acceleration of gravity.

Hence, the acceleration response spectra for an arbitrary value of damping is:

$$S_a(T,\xi) = \frac{C_v}{T} g \left[ \frac{1.5}{40\xi + 1} + 0.5 \right] \tag{9.4}$$

The equivalent viscous damping due to the supplemental damping system varies from $\xi_1$ to $\xi_2$. The viscous damping of the original structure is $\xi_s$ (=$\xi_0$+$\Delta\xi_0$), in which $\xi_0$ is the initial viscous damping of the original structure and $\Delta\xi_0$ is the equivalent viscous damping due to the inelastic deformations of the original structure. The force factor $F_R$ of the supplemental damping system corresponding to equivalent viscous damping $\xi_1$ and $\xi_2$ is $F_{R1}$ and $F_{R2}$ respectively. The effective periods of the structure with the supplemental dampers corresponding to force factor $F_{R1}$ and $F_{R2}$ are $T_1$ and $T_2$ respectively. $F_{R1}$ and $F_{R2}$ can be calculated through Eq(7.22a), and $T_1$ and $T_2$ can be calculated through Eq(7.32).

The difference in the acceleration response with respect to the change of the equivalent viscous damping from $\xi_1$ to $\xi_2$ can be taken as:

$$\frac{\Delta S_a}{S_a} = \frac{S_a(\xi_s+\xi_2, T_2) - S_a(\xi_s+\xi_1, T_1)}{S_a(\xi_s+\xi_1, T_1)} = \frac{S_a(\xi_s+\xi_2, T_2)}{S_a(\xi_s+\xi_1, T_1)} - 1 \tag{9.5}$$

From Eq(9.4) and Eq(7.32), Eq(9.5) can be written as:

$$\frac{\Delta S_a}{S_a} = \frac{\dfrac{1.5}{40(\xi_2+\xi_s)+1}+0.5}{\dfrac{1.5}{40(\xi_1+\xi_s)+1}+0.5}\sqrt{\frac{\mu F_{R2}+1+r(\mu-1)}{\mu F_{R1}+1+r(\mu-1)}} - 1 \tag{9.6}$$

where $\mu$ = ductility factor of the original structure

$r$ = ratio of the post-yield stiffness to the initial stiffness of the original structure.

The difference in the acceleration response with respect to the change in the equivalent viscous damping due to the supplemental dampers is shown in Table 9.1 and 9.2, in which the range of the variation of $\xi_1$ to $\xi_2$ is taken as 0-10%, 10-15%, 15-17%, 17-20% and 20-30% respectively. Two different ductility factors of the original structure, $\mu$=1 and 1.5, are considered.

It can be observed that the optimal equivalent viscous damping level due to the supplemental dampers is about 15 to 17%. In this range the displacement response can be reduced while the acceleration response will not be increased. This result agrees with the statement by Scholl

(1993b): "From a very broad and general perspective it can be concluded that providing supplemental damping in the range of 10 to 20 percent is a good design target."

It has to be noted that this is not the best damping level for all cases. This depends on the displacement requirements for a design. If the required displacement is not met for this damping level, higher strength levels of the dampers are needed even though this will lead to an increase in the acceleration response.

## 9.4 DISPLACEMENT-BASED DESIGN PROCEDURE FOR DETERMINING THE PARAMETERS FOR THE SUPPLEMENTAL DAMPERS FOR AN EXISTING STRUCTURE

It is known that of the two characteristic parameters of the supplemental dampers (the force factor $F_R$ and the stiffness factor $S_R$), the force factor $F_R$ dominates the dynamic behaviour of the structure with supplemental dampers as long as the stiffness factor $S_R$ exceeds a certain level. Hence in the displacement-based method we focus on the choice of the force factor $F_R$ for the supplemental dampers. It is assumed that the stiffness factor $S_R$ of the supplemental dampers meets the requirement of Eq(5.6). We already know that a satisfactory distribution of dampers is that in which the distribution of the yield strength of the dampers in every storey up the height of the structure is proportional to the storey shear developed due to an inverted-triangular lateral load pattern. It is assumed that the original structures are regular in mass and stiffness distribution. Hence the peak response of the MDOF structure with the supplemental dampers can be effectively predicted by its equivalent SDOF dual system. This gives good grounds for the displacement-based method to be adopted in the choice of the force factor $F_R$ of the supplemental dampers at the preliminary design stage.

The procedure for the displacement-based method can be established as follows (Lin et al., 1998a, 1998b):

Step 1. Check the original structure to see whether the maximum interstorey drift meets the requirements of the design or not (a time-history analysis or a pushover analysis can be used for this purpose). If it meets the design requirement, there is no need of any supplemental dampers. If it does not, go to step 2.

Step 2. Perform the pushover analysis of the original structure without dampers. The yield base shear $F_{y0}$ and the yield roof displacement of the original structure $\Delta_{f0}$ can be obtained. The initial deflected shape $\phi_0$ can be obtained from this pushover analysis (at the yield displacement of the original structure).

Step 3. Given the required design limit of the interstorey drift ratio (check the allowable maximum displacement range of the supplemental dampers is within this requirement), the first estimated target displacement at roof level ($x_t$) of the structure with the supplemental dampers can be obtained through Eq(9.2)(from the initial displacement shape). Generally, this target displacement might not coincide with the yield displacement at step 2. The deflected shape $\phi$ corresponding to this target displacement can then be obtained. A new target displacement can be obtained through the new deflected shape and the required design limit for the interstorey drift. Compare these two target displacements. If the difference is large, some iteration may be needed. Repeat the process in this step until these two target displacements are close enough (the design requirement of the interstorey drift has been met). Then the final target displacement and the constant deflected shape $\phi$ (at the target displacement) are known. The target ductility $\mu$ of the original structure can also be calculated. The elastic force of the original structure (if the original structure remained elastic), $P$, at the target displacement (converted to its equivalent SDOF system) can be calculated. The following equation can be obtained from Eq(6.15):

$$P = \mu F_{y0} \frac{\sum \phi_i \psi_i}{\sum \psi_i} \tag{9.7}$$

where $\frac{\sum \phi_i \psi_i}{\sum \psi_i}$ = the factor for converting the base shear in a MDOF structure to its equivalent SDOF system

$\psi_i$ = the ith term of the normalised lateral load distribution vector = $\frac{i}{N}$

$N$ = number of storeys.

The target spectral displacement can be obtained by Eq(6.15) (or Eq(8.1)) as

$$S_d == \frac{M^*}{L^*} x_t = \frac{\sum_{i=1}^{N} m_i \phi_i^2}{\sum_{i=1}^{N} m_i \phi_i} x_t \tag{9.8}$$

Step 4. Choose the optimal damping $\xi_d$ of 15 to 17% of critical viscous damping due to the supplemental dampers. Calculate the initial viscous damping and the equivalent viscous damping of the structure due to the inelastic deformation of the original structure ($\xi_0+\Delta\xi_0$) at the target ductility (from Eq(7.46)). The total equivalent viscous damping ratio $\xi_t$ (= $\xi_d$ $+\xi_0+\Delta\xi_0$) can be obtained.

Step 5. From the displacement spectra, knowing the equivalent viscous damping of $\xi_t$ and the target spectral displacement $S_d$ (obtained from the target displacement), the maximum effective period of the structure with supplemental dampers $T_{max}$ can be obtained (to meet the requirement of the design interstory drift ratio).

Step 6. For the given equivalent viscous damping ratio $\xi_d$ (15-17%) due to the supplemental dampers, the force factor $F_R$ can be obtained from Eq(7.22a) ($\xi$—$F_R$ relationship).

Step 7. The effective period of the structure with supplemental dampers $T_{eff}$ (corresponding to the $F_R$ factor from Step 6 and the target ductility $\mu$) can be calculated from Eq(7.32).

Step 8. Compare $T_{max}$ and $T_{eff}$. If $T_{eff} \le T_{max}$, it shows that the assumed optimal equivalent viscous damping ratio $\xi_d$ and the force factor $F_R$ obtained meet the design requirement.

If $T_{eff} > T_{max}$, it shows that the assumed optimal equivalent viscous damping ratio $\xi_d$ (thus the corresponding force factor $F_R$) is not high enough. Let $T_{eff} = T_{max}$, a new force factor $F_R$ and the corresponding equivalent viscous damping ratio $\xi_d$ can be calculated by Eq(7.32) and Eq(7.22a) respectively.

Step 9. From the force factor $F_R$ obtained in Step 8 and the elastic force $P$ at the target displacement of the original structure obtained in Step 3, the yield force of the damping mechanism for the equivalent SDOF system can be calculated as:

$$F_{yd}^{*} = F_R P \tag{9.9}$$

Thus the strength level of the damper at the 1st floor level ($F_{yd1}$) can be obtained from Eq(9.9) and Eq(7.18):

$$\begin{aligned} F_{yd1} &= \frac{F_{yd}^{*}}{\cos\theta}\frac{\sum\psi_i}{\sum\phi_i\psi_i} \\ &= \frac{F_R P}{\cos\theta}\frac{\sum\psi_i}{\sum\phi_i\psi_i} = \frac{\mu F_R F_{y0}}{\cos\theta} \end{aligned} \tag{9.10}$$

where $\theta$ = slope of the diagonal brace.

The strength level of the damper at the *ith*-story ($F_{ydi}$) can be obtained from Eq(7.17) as follows:

$$\begin{aligned} F_{ydi} &= \frac{2}{N(N+1)}\left(\sum_{j=i}^{N} j\right)F_{yd1} \\ &= \frac{2}{N(N+1)}\left(\sum_{j=i}^{N} j\right)\frac{\mu F_R F_{y0}}{\cos\theta} \end{aligned} \tag{9.11}$$

where $N$ = number of storeys.

**Example**:

The 12-storey 3-bay frame structure used in the earlier chapters is taken as an example. The design requirement is that the maximum interstorey drift ratio is limited to 0.5%. The procedure of the displacement-based method mentioned above is used to determine the strength parameters of the dampers in the structure.

Step 1: A time-history analysis of the original frame structure under the El Centro 1940 NZS4203 code compatible earthquake was conducted. The peak interstorey drift = 3.84cm (the peak interstorey drift index = $\frac{3.84}{3.65}\times 100\% = 1.05\% > 0.5\%$)

Hence supplemental dampers are needed to meet the design requirement on the interstorey drift.

Step 2: A pushover analysis of the original structure was conducted. The inverted-triangular lateral load pattern was used for this pushover analysis. The yield base shear and the yield roof displacement of the original structure were:

$F_{y0}$=780.0KN, $\Delta_{f0}$= 11.0cm

The ratio of post-yield stiffness to the initial stiffness $r$ = 5%.

Step 3: The required design maximum interstorey drift index is 0.5%. For determining the target roof displacement some iteration might be needed because the deflected shape at the target displacement is not known but is needed to obtain the target roof displacement from the required maximum interstorey drift. Firstly, the displacement profile at the yield of the original structure ($\mu$ =1) is taken as the initial deflected shape. This initial normalised deflected shape is

{0.04173,0.1234,0.2158,0.311,0.4133,0.521,0.6298,0.7356,0.8361,0.9171,0.9706,1}

Hence, we have:

$$\left(\frac{\phi_i-\phi_{i-1}}{h_i}\right)_{\max}=\frac{0.1088}{3.65}=2.981\times10^{-2}$$

For the maximum interstorey drift index 0.5%, the corresponding roof displacement is

$$x_{t0}=\frac{0.5\%}{2.981\times10^{-2}}=16.77(\text{cm})$$

The normalised deflected shape at this roof displacement is

{0.0316,0.1034,0.1998,0.3134,0.4402,0.5704,0.6936,0.8012,0.8868,0.9455,0.9814,1}

For this deflected shape we have:

$$\left(\frac{\phi_i-\phi_{i-1}}{h_i}\right)_{\max}=\frac{0.1234}{3.65}=3.381\times10^{-2}$$

For the maximum interstorey drift index 0.5%, the corresponding roof displacement is

$$x_{t1}=\frac{0.5\%}{3.381\times10^{-2}}=0.1479(\text{m})=14.79\text{cm}$$

The target displacement at roof level can be taken as:

$$x_t=\frac{x_{t0}+x_{t1}}{2}=\frac{16.77+14.79}{2}=15.78(\text{cm})$$

The deflected shape at the target displacement of $x_t$ = 15.78cm is

$\{0.0374,0.1141,0.2079,0.3138,0.4309,0.5504,0.6642,0.7663,0.8568,0.928,0.9747,1\}$

For this target displacement $\left(\frac{\phi_i - \phi_{i-1}}{h_i}\right)_{\max} = \frac{0.1195}{3.65} = 3.274\times10^{-2}$

For the maximum interstorey drift index 0.5%, the corresponding roof displacement is

$$x_t = \frac{0.5\%}{3.274\times10^{-2}} = 0.15272(\text{m}) = 15.272\text{cm}$$

The difference between these two values of $x_t$ is $\frac{15.78-15.272}{15.78} = 3.22\%$

So this target displacement at roof level ($x_t$ = 15.78cm) is sufficiently accurate.

Hence, $x_t$ = 15.78cm, the ductility of the original structure is $\mu$ = 1.435, the deflected shape at this target roof displacement is

$\{0.0374,0.1141,0.2079,0.3138,0.4309,0.5504,0.6642,0.7663,0.8568,0.928,0.9747,1\}$

The peak interstorey drift $ID_{\max} = 0.1195\times15.78 = 1.886\text{cm}$

The maximum displacement the dampers might undergo:

$ID_{\max}\cos\theta = 1.886\times0.91 = 1.716\text{cm} = 17.16\text{mm}$

The practical range of the supplemental lead dampers is taken as 17mm. The design requirement could be meet by means of the supplemental lead dampers.

For this deflected shape we have:

$$L^* = \sum m_i\phi_i = 810.917$$
$$M^* = \sum m_i\phi_i^2 = 612.707$$

The target spectral displacement (for the equivalent SD0F system) is:

$$S_d = \frac{M^*}{L^*}x_t = \frac{612.707}{810.917}\times15.78 = 11.923(\text{cm})$$

$$P = \mu F_{y0}\frac{\sum\phi_i\psi_i}{\sum\psi_i} = 1.435\times780.0\times0.7448 = 833.65(\text{KN})$$

Step 4: Choose the optimal damping $\xi_d$ due to the supplemental dampers to be 15% of critical. For the target displacement ($\mu$=1.435) the initial viscous damping and the effective damping of the structure due to inelastic deformation of the original structure is

$$\xi_0 + \Delta\xi_0 = \frac{1 - \frac{1}{\sqrt{1.435}}}{5} + 0.05 = 8.304\%$$

The total equivalent viscous damping ratio is $\xi_t$ =15%+8.304% = 23.304%.

Step 5: For the total equivalent viscous damping of 23.304% and the target spectral displacement 11.923cm. Eq(9.1) is used to generate a displacement spectrum for a damping ratio of 23.304%. To meet the maximum interstorey drift requirement (the spectral displacement not greater than 11.923cm) the maximum effective period of the structure with the supplemental dampers is $T_{max}$=2.219$s$.

Step 6: From Eq(7.22a) for the $\xi_d - F_R$ relationship, for the equivalent viscous damping of 15% due to the supplemental dampers and the ductility factor of the original structure $\mu$ = 1.435,the force factor can be obtained as follows:

$$F_R = \frac{\pi[1 + 0.05 \times (1.435 - 1)] \times 15\%}{(2 - \pi \times 15\%) \times 1.435} = 0.2195$$

Step 7: The effective period of the structure with the supplemental dampers corresponding to the force factor in step 6 is

$$T_{eff} = 1.99 \times \sqrt{\frac{1.435}{1.435 \times 0.2195 + 1 + 0.05 \times (1.435 - 1)}} = 2.062(\text{s})$$

Step 8: Compare $T_{eff}$ with $T_{max}$. It can be seen that $T_{eff} < T_{max}$ . The assumed optimal equivalent viscous damping due to the supplemental dampers can meet the design requirement. The force factor ($F_R$ = 0.2195) obtained is suitable.

Step 9: The strength level of the damper at the 1st floor level is

$$F_{yd1} = \frac{1.435 \times 0.2195 \times 780.0}{0.91} = 270(\text{KN})$$

The strength levels of the dampers over the height of the structure can be obtained (from 1st floor level to the roof level)

$\{270,266.54,259.61,249.24,235.39,218.08,197.32,173.07,145.4,114.24,79.62,41.55\}$ KN

Time-history analysis of the structure with the supplemental dampers that have such strength distribution was conducted under the El Centro NZS4203 code compatible earthquake. Some response results are:

The peak roof displacement = 16.15cm

The peak interstorey drift =1.815cm

The peak interstorey drift ratio = $\frac{1.815}{3.65}\times 100\% = 0.497\% < 0.5\%$, The design requirement is meet. It can be seen that the peak interstorey drift ratio is very close to the design target.

The total structural ductility factor $\mu = \frac{16.15\text{cm}}{11\text{cm}} = 1.468$.

Again it can also be observed that this simplified static method can give an accurate approximation of the response of the structure with the supplemental dampers.

The results from the time-history analysis of the original structure without dampers and the structure with the dampers are compared in Table 9.3. It can be seen from Table 9.3 that when compared to the original structure without dampers, the response of the structure with the supplemental dampers is greatly reduced except for the total peak base shear which is increased slightly (but the storey shear in the columns at the 1st floor level is still reduced). The peak roof displacement is reduced by 36.64%. The peak interstorey drift is reduced by 52.22%. The total peak base shear is only increased by 4.76%. The peak storey shear of columns at the 1st storey is reduced by 16.19% by incorporating supplemental dampers into the structure.

From the above comparison it can be seen that the dynamic response that the structure may undergo during the design earthquake is reduced significantly. The displacement-based procedure for determining the characteristic parameter of the supplemental dampers provides a straightforward and sufficiently accurate method for preliminary design.

The time-history response of the structure with such a distribution of the supplemental dampers and of the original structure without dampers is shown in Figs.9.3 and 9.4.

For a comparison of the ductility demands in the structure without dampers and the structure with dampers, time history analyses using 1.7 times the El Centro NZS4203 compatible earthquake were performed. The 1.7 times the El Centro NZS4203 compatible earthquake is close to the maximum credible earthquake. The comparison of the peak roof displacement and the peak interstorey drift is shown in Table 9.4. The comparison of the member ductility demands at each storey is shown in Table 9.5. It can be seen clearly that the member ductility demand is greatly reduced in the extreme earthquakes by the supplemental dampers.

## 9.5 DISPLACEMENT-BASED DESIGN PROCEDURE FOR DETERMINING PARAMETERS FOR THE SUPPLEMENTAL DAMPERS FOR A NEW STRUCTURE

The procedure mentioned above is for retrofit purposes. Now we consider how to determine suitable parameters for the dampers for a new structure. Whether for retrofitting an old building or for designing a new building, the purpose of utilising supplemental dampers is to control the displacements and to reduce the ductility demands of the structure. Before moving to the design procedure, some information necessary to the procedure needs to be considered first. They are the time-independent deflected shapes and the initial period of the original structure without dampers.

### 9.5.1 Time-Independent Deflected Shape

In design, if the purpose is to retrofit an existing structure by means of supplemental dampers, the deflected shape can be obtained through a pushover analysis of the original structure. If the purpose is to design a new structure, the time-independent deflected shape can not be obtained through a pushover analysis because the original structure does not exist yet. In this case an assumed deflected shape is necessary for carrying out the displacement-based design.

Fajfar et al. (1988,1996) after numerical experiments concluded that the results are relatively insensitive to small or moderate changes in the deflected shape $\{\phi\}$. Similar results have also been shown in previous chapters. Consequently, an estimate of the deflected shape can be

made. Fajfar et al. suggested deflected shapes of three typical systems shown in Fig.9.5. Type 1 refers to shear wall structure or frame-wall dual structure. Type 2 refers to the frame structure with a beam sidesway mechanism. Type 3 refers to a frame structure in which a column sidesway (soft storey) mechanism will occur.

For frame structures the beam sidesway mechanism is preferred and the type 3 deflected shape must be avoided. So the assumed deflected shape of type 2 is adopted here.

From Fig.9.5 we have

$$\begin{aligned} \phi_i &= \phi_{ie} + \phi_{ip} \\ \phi_{ie} &= \frac{1}{\mu}\frac{H_i}{H} \\ \phi_{ip} &= \left(1-\frac{1}{\mu}\right)\frac{H_i}{H_{N/2}} \qquad \cdots H_i \le H_{N/2} \\ \phi_{ip} &= 1-\frac{1}{\mu} \qquad \cdots H_i \ge H_{N/2} \end{aligned} \tag{9.12}$$

where $\phi_i$ = the ith term of the normalised deflected shape,

$\mu$ = assumed maximum global ductility,

$N$ = total storey number,

$H_i$ = the height of level i relative to the ground,

$H$ = the total height of the building structure.

### 9.5.2 The Initial Period of the Undamped Structure $T_0$

It is necessary to have a simple approximate expression for the first mode period as a function of the basic building parameters.

A BRANZ study report (1990) found that the period is well correlated with height and is reasonably insensitive to the other parameters. The following relationship between period and height was obtained from a regression analysis (BRANZ, 1990):

$$T(\text{sec}) = 0.13H^{0.71} \tag{9.13}$$

where $H$ = the total height of the building structure.

### 9.5.3 Design Procedure

Step 1. Assume the target ductility factor that the main frame structure may undergo during the design earthquake. Hence the deflected shape $\{\phi\}$ can be obtained by Eq(9.12).

Step 2. Estimate the initial period of the original structure $T_0$. The initial stiffness of the original structure $K_s$ (for its equivalent SDOF system) can then be calculated.

$$K_s = \frac{L^*}{\left(\frac{T_0}{2\pi}\right)^2} \tag{9.14}$$

where $L^* = m = \sum_{i=1}^{N} m_i \phi_i$ .

Step 3. Given the required maximum interstorey drift ratio, the target roof displacement $x_t$ can be obtained from Eq(9.2). The target spectral displacement $S_d$ for the equivalent SDOF can be calculated. Then the elastic restoring force of the original structure (SDOF) at the target displacement $S_d$ can also be calculated (if the original structure remained elastic) as follows:

$$S_d == \frac{M^*}{L^*} x_t = \frac{\sum_{i=1}^{N} m_i \phi_i^2}{\sum_{i=1}^{N} m_i \phi_i} x_t \tag{9.15}$$

where $S_d$ = the target spectral displacement for the equivalent SDOF system,

$x_t$ = the target roof displacement for MDOF structure.

$$P = K_s S_d \tag{9.16}$$

Step 4. Choose the optimal damping ratio $\xi_d$ = 15 to 17%. The total damping ratio can be calculated as $\xi_t = \xi_d + \xi_0 + \Delta\xi_0$ from Eq(7.46).

Step 6. The force factor $F_R$ corresponding to the equivalent viscous damping of $\xi_d$ due to the supplemental dampers can be obtained for the given $\xi_d$ from Eq(7.22a).

Step 7. $T_{eff}$ corresponding to the target ductility $\mu$ and the force factor $F_R$ can be calculated from Eq(7.32).

Step 8. $T_{max}$ can be obtained for the known total damping ratio $\xi_t$ and the target displacement $S_d$.

Step 9. Compare $T_{eff}$ with $T_{max}$.

If $T_{eff} \leq T_{max}$, go to step 10.

If $T_{eff} > T_{max}$, then let $T_{eff} = T_{max}$, for the desired ductility $\mu$ a new force factor $F_R$ can be calculated from Eq(7.32).

Step 10. The yielding force of the damping mechanism for the equivalent SDOF system can be calculated as:

$$F_{yd}^{*} = F_R P \tag{9.17}$$

Thus the strength level of the damper at the 1st floor level ( $F_{yd1}$) is:

$$\begin{aligned} F_{yd1} &= \frac{F_{yd}^{*}}{\cos\theta}\frac{\sum\psi_i}{\sum\phi_i\psi_i} \\ &= \frac{F_R P}{\cos\theta}\frac{\sum\psi_i}{\sum\phi_i\psi_i} \end{aligned} \tag{9.18}$$

where $\theta$ = slope of the diagonal brace.

The strength level of the damper at the *ith*-story ($F_{ydi}$) can be obtained from Eq(7.17)

$$\begin{aligned} F_{ydi} &= \frac{2}{N(N+1)}\left(\sum_{j=i}^{N} j\right)F_{yd1} \\ &= \frac{2}{N(N+1)}\left(\sum_{j=i}^{N} j\right)\frac{F_R P}{\cos\theta}\frac{\sum\psi_i}{\sum\phi_i\psi_i} \end{aligned} \tag{9.19}$$

Step 11. The restoring force of the original structure (SDOF) at yield force $P_y$ can be calculated as follows:

$$P_y = \frac{P}{\mu} \tag{9.20}$$

The design base shear for the original structure (not including the supplemental dampers) can be calculated as follows:

$$F_y = \frac{\sum_{i=1}^{N} \psi_i}{\sum_{i=1}^{N} \phi_i \psi_i} P_y \tag{9.21}$$

where $\psi_i = \frac{i}{N}$

**Example**:

The goal is to design a 12-storey 3-bay frame structure with supplemental dampers. The design requirement is that the peak interstorey drift ratio should not exceed 0.5%. The mass distribution of the structure is:

$\{124.67,124.67,124.67,124.67,121.23,121.23,121.23,121.23,117.98,117.98,117.98,109.04\}$

Step 1. It is assumed that the target global ductility of the original structure is 1.5. Hence the assumed deflected shape can be obtained through Eq(9.12).

The assumed deflected shape at a ductility of 1.5 is:

$\{0.1111,0.2222,0.3333,0.4444,0.5556,0.6667,0.7222,0.7778,0.8333,0.8889,0.9444,1\}$

Hence one can calculate:

$L^* = 892.178$ , $M^* = 663.454$

$\frac{M^*}{L^*} = 0.7436$

The distribution of the lateral loads is an inverted-triangular distribution. The vector $\{\psi\}$ is:

$\{0.0833,0.1667,0.250,0.3333,0.4167,0.50,0.5833,0.6667,0.75,0.8333,0.9167,1\}$

$$\frac{\sum \phi_i \psi_i}{\sum \psi_i} = 0.7714$$

Step 2. The initial period of the original structure can be calculated as:

$$T_0 = 0.13 \times 43.8^{0.71} = 1.903(s)$$

$$K_s = \frac{L^*}{\left(\frac{T_0}{2\pi}\right)^2} = \frac{892.178}{\left(\frac{1.903}{2\pi}\right)^2} = 9725.987(\text{KN/m})$$

Step 3.

$$x_t = 0.5\% \times \frac{3.65}{0.1111} = 0.1642\text{m}$$

$$S_d = x_t \frac{M^*}{L^*} = 0.1642 \times 0.7436 = 0.1221\text{m}$$

$$P = K_s S_d = 9725.987 \times 0.1221 = 1187.534(\text{KN})$$

Step 4. The equivalent viscous damping ratio due to the supplemental dampers is taken as $\xi_d$ = 15%. The equivalent viscous damping due to the inelastic deformation of the original structure is: $\Delta\xi_0 = \frac{1 - \frac{1}{\sqrt{1.5}}}{5} = 3.67\%$

So the total equivalent viscous damping ratio is $\xi_t$ = 5%+3.67%+15% = 23.67%.

Step 6. The force factor corresponding to the $\xi_d$ = 15% is:

$$F_R = \frac{\pi[1 + 0.05 \times (1.5 - 1)] \times 15\%}{(2 - \pi \times 15\%) \times 1.5} = 0.2106$$

Step 7. $T_{eff} = 1.903 \times \sqrt{\frac{1.5}{1.5 \times 0.2106 + 1 + 0.05 \times (1.5 - 1)}} = 2.01(\text{s})$

Step 8. For a target spectral displacement of 0.1221m and the equivalent viscous damping ratio of 23.67%, the maximum period can be obtained from the displacement spectra. $T_{max}$ = 2.27s.

Step 9. It can be seen that $T_{eff} < T_{\max}$. The assumed optimal equivalent viscous damping due to the supplemental dampers is appropriate and the force factor calculated can meet the design requirement.

Step 10. $F_{yd1} = \frac{0.2106 \times 1187.534}{0.91} \times \frac{1}{0.7714} = 356.27(\text{KN})$

The strength levels of the dampers over the height of the structure can be obtained as follows (from 1st floor level to the top level):

$\{356.27,351.71,342.55,328.87,310.6,287.76,260.36,228.37,191.85,150.74,105.06,54.83\}$

Step 11. The restoring force of the original structure (SDOF) at yield $P_y$:

$$P_y = \frac{1187.534}{1.5} = 791.69(\text{KN})$$

The design base shear for the original structure is:

$$F_y = 791.69 \times \frac{1}{0.7714} = 1026.3(\text{KN})$$

## 9.6 INFLUENCE OF THE DISTRIBUTION OF THE DAMPER YIELD STRENGTHS IN THE STRUCTURE IF A STEPPED RATHER THAN AN INVERTED-TRIANGULAR DISTRIBUTION IS ADOPTED

For designers, it is desired that instead of a change of the strength levels of the dampers for every storey, constant strength levels over some storeys are preferred. The influence of the distribution of the strength levels of the dampers which is not strictly the same as the one used in the previous example is investigated here.

The original structure is the same as the previous example, that is, a 12-storey 3-bay frame. There is one damper in each storey. Case-I refers to the case in which the distribution of the strength levels of the dampers is proportional to the storey shear due to the inverted-triangular lateral load pattern. In case-II the strength levels of the dampers are the same for every three storeys. The constant strength level for these three storeys is taken to be the average value of the strength levels of those three storeys in case-I. In case-III the strength levels of the dampers are the same for every four storeys. The constant strength level for every four storeys is taken to be the average value of the strength levels of those four storeys in case-I.

For case-I, the yield strengths of the supplemental dampers in the storeys are:

$\{270,266.54,259.61,249.24,235.39,218.08,197.32,173.07,145.4,114.24,79.62,41.55\}$ KN

For case-II,

The yield strengths of the dampers in storeys 1-3 are $\frac{270+266.54+259.61}{3}=265.38(\text{KN})$

The yield strengths of the dampers in storeys 4-6 are $\frac{249.24+235.39+218.08}{3}=234.24(\text{KN})$

The yield strengths of the dampers in storeys 7-9 are $\frac{197.32+173.07+145.4}{3}=171.93(\text{KN})$

The yield strengths of the dampers in storeys 10-12 are $\frac{114.24+79.62+41.55}{3}=78.47(\text{KN})$

For case-III the yield strengths in the storeys can be calculated in a similar manner. The distributions of the yield strengths of the supplemental dampers in the storeys for these three cases are shown in Table 9.6.

Responses for these three cases under the El Centro 1940 NZS4203 compatible earthquake are compared in Table 9.7 and the maximum interstorey drifts for all storeys are also compared in Fig.9.6. It can be found that the response is very similar for all three cases. Hence, for design purposes, after the designed yield strength of the supplemental damper at the 1$^{st}$ level is obtained, a reasonable stepped distribution of the dampers in the upper storeys can be obtained.

| | Range I | | Range II | | Range III | | Range IV | | Range V | |
|---|---|---|---|---|---|---|---|---|---|---|
| $\xi$ | $\xi_1$ = 0% | $\xi_2$ = 10% | $\xi_1$ = 10% | $\xi_2$ = 15% | $\xi_1$ = 15% | $\xi_2$ = 17% | $\xi_1$ = 17% | $\xi_2$ = 20% | $\xi_1$ = 20% | $\xi_2$ = 30% |
| $F_R$ | 0 | 0.1864 | 0.1864 | 0.3083 | 0.3083 | 0.3643 | 0.3643 | 0.4581 | 0.4581 | 0.8912 |
| $\frac{\Delta S_a}{S_a}$ | -22.20% | | -1.99% | | 0.03% | | 0.74% | | 7.38% | |

Table 9.1 Comparison of the difference of the acceleration response with respect to the variation in the equivalent viscous damping due to the supplemental dampers (The original structure remains elastic and the initial viscous damping is 5%.)

| | Range I | | Range II | | Range III | | Range IV | | Range V | |
|---|---|---|---|---|---|---|---|---|---|---|
| $\xi$ | $\xi_1$ = 0% | $\xi_2$ = 10% | $\xi_1$ = 10% | $\xi_2$ = 15% | $\xi_1$ = 15% | $\xi_2$ = 17% | $\xi_1$ = 17% | $\xi_2$ = 20% | $\xi_1$ = 20% | $\xi_2$ = 30% |
| $F_R$ | 0 | 0.1273 | 0.1273 | 0.2106 | 0.2106 | 0.2490 | 0.2490 | 0.3130 | 0.3130 | 0.6090 |
| $\frac{\Delta S_a}{S_a}$ | -11.75% | | -0.24% | | 0.51% | | 1.29% | | 8.52% | |

Table 9.2 Comparison of the difference of the acceleration response with respect to the variation in the equivalent viscous damping due to the supplemental dampers (The original structure has a limited inelastic deformation with a ductility of 1.5)

| | Peak roof displacement (cm) | peak interstorey drift (cm) | total peak base shear (KN) | peak storey shear of columns at 1st level (KN) |
|---|---|---|---|---|
| structure without dampers | 25.49 | 3.799 | 1178.8 | 1178.8 |
| structure with dampers | 16.15 | 1.815 | 1234.7 | 988.06 |
| Response Comparison | Reduced by 36.64% | Reduced by 52.22% | Increased by 4.74% | Reduced by 16.19% |

Table 9.3 Comparison of the structural response of the structure without dampers and of the structure with dampers under the El Centro 1940 NZS4203 compatible earthquake

| | Peak roof displacement (cm) | peak interstorey drift (cm) | Peak interstorey drift index |
|---|---|---|---|
| structure without dampers | 46.93 | 7.044 | 1.93% |
| structure with dampers | 32.54 | 4.424 | 1.21% |
| Response Comparison | Reduced by 30.66% | Reduced by 37.2% | Reduced by 37.2% |

Table 9.4 Comparison of the structural response of the structure without dampers and with dampers under 1.7 times the El Centro 1940 NZS4203 compatible earthquake

| | Maximum member ductility demand in the beams | |
|---|---|---|
| Storey level | structure without dampers | Structure with dampers |
| 1 | 8.396 | 6.97 |
| 2 | 13.00 | 7.24 |
| 3 | 14.44 | 7.75 |
| 4 | 21.45* | 9.41* |
| 5 | 19.94 | 8.25 |
| 6 | 16.63 | 6.68 |
| 7 | 18.90 | 6.06 |
| 8 | 15.22 | 6.28 |
| 9 | 12.82 | 3.73 |
| 10 | 10.28 | 2.86 |
| 11 | 4.437 | 1.88 |
| 12 | 2.967 | 1.01 |

Table 9.5 The comparison of the beam ductility demand in the structure without dampers and with dampers under 1.7 times the El Centro NZS4203 compatible earthquake (* indicates the maximum value for all members)

| Storey level | Distribution of yield strengths of the supplemental dampers in the storeys (KN) | | |
|---|---|---|---|
| | Case-I | Case-II | Case-III |
| 1 | 270 | 265.38 | 261.35 |
| 2 | 266.54 | | |
| 3 | 259.61 | | |
| 4 | 249.24 | 234.24 | 205.97 |
| 5 | 235.39 | | |
| 6 | 218.08 | | |
| 7 | 197.32 | 171.93 | |
| 8 | 173.07 | | |
| 9 | 145.4 | | 95.2 |
| 10 | 114.24 | 78.47 | |
| 11 | 79.62 | | |
| 12 | 41.55 | | |

Table 9.6 Distribution of yield strengths of the supplemental dampers in the storeys

| | Peak roof displacement (cm) | Peak interstorey drift (cm) |
|---|---|---|
| Case-I | 16.15 | 1.815 |
| Case-II | 16.13 | 1.814 |
| Case-III | 16.05 | 1.814 |

Tables 9.7 Influence of the stepped distribution of damper yield strengths in the storeys

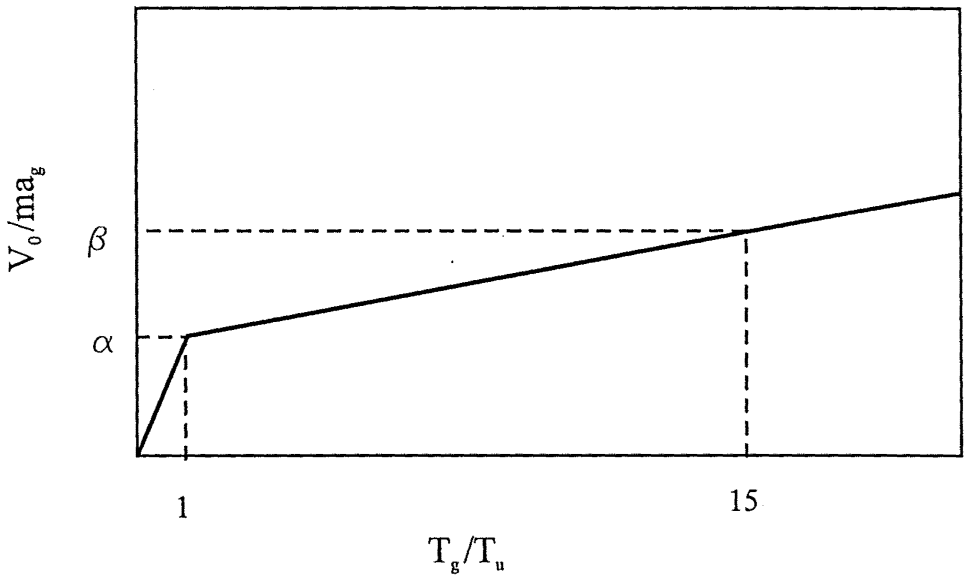


Figure 9.1 Construction of design slip-load spectrum (from Filiatrault et al., 1990)

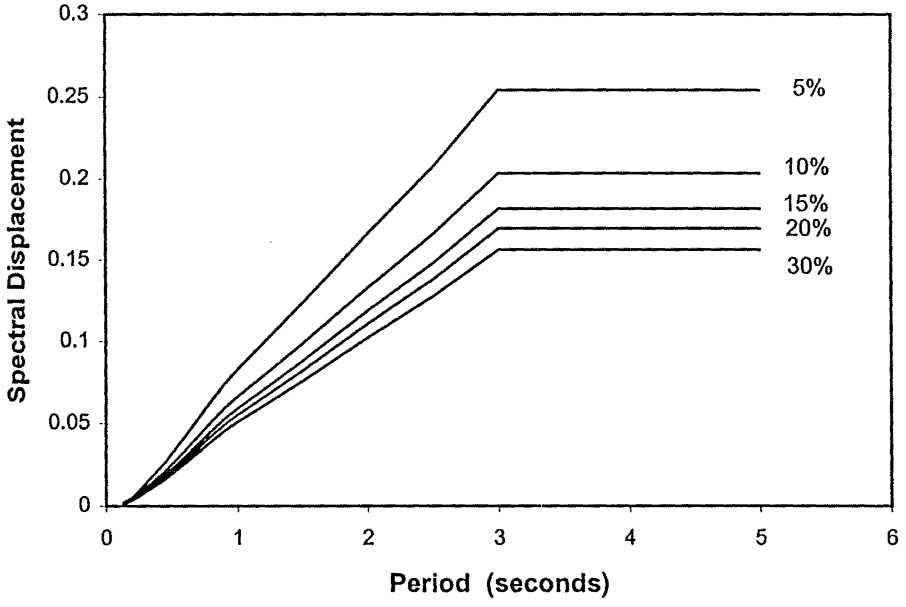


Figure 9.2 Displacement spectra for different levels of damping

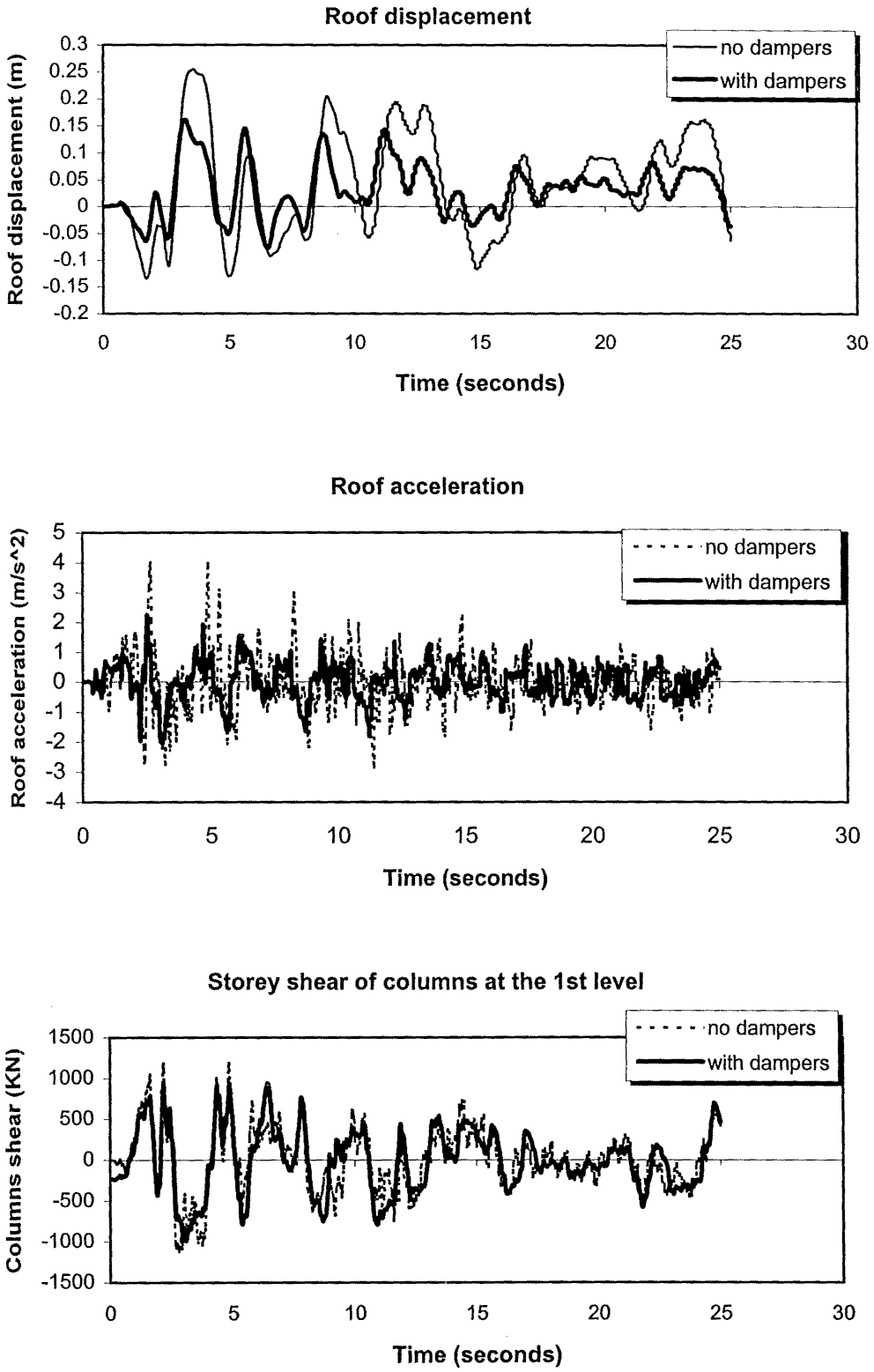


Figure 9.3 Comparison of responses for the structure with dampers and without dampers dunder the El Centro 1940 NZS4203compatible earthquake

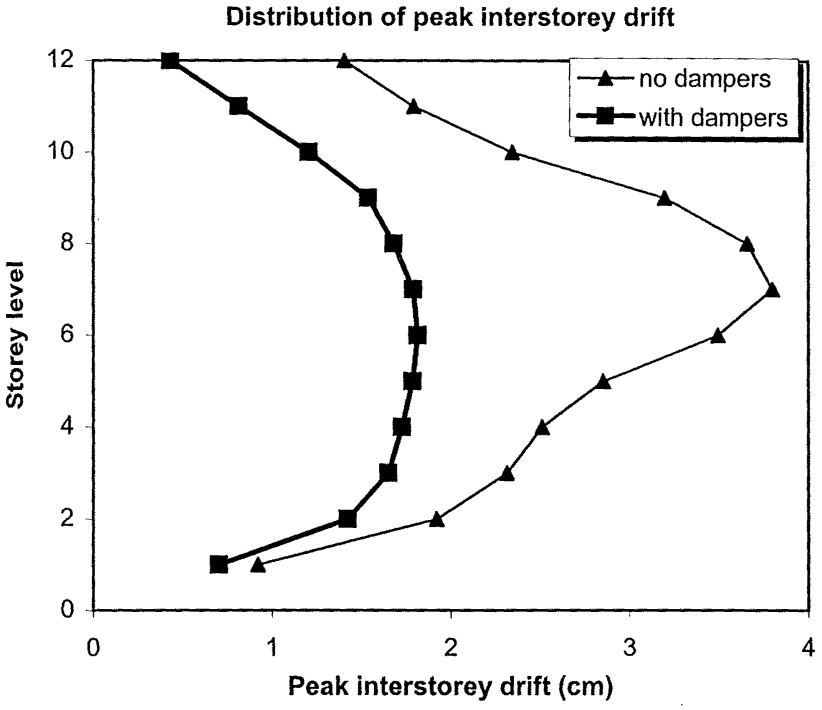


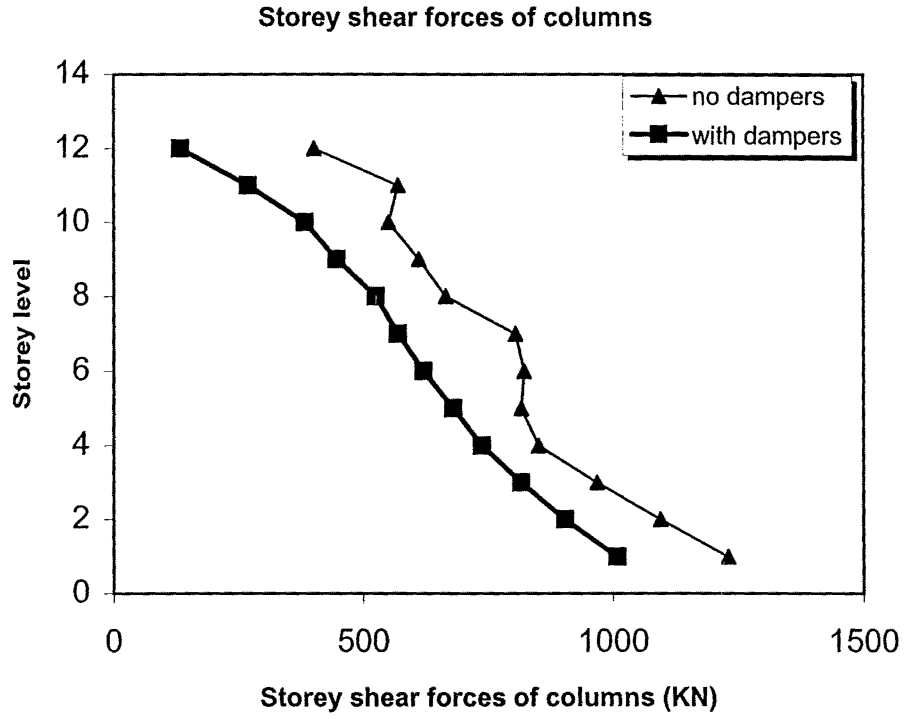


Figure 9.4 Distribution of maximum drifts and shear forces in the columns for the structure with dampers and without dampers under the El Centro 1940 NZS4203 compatible earthquake

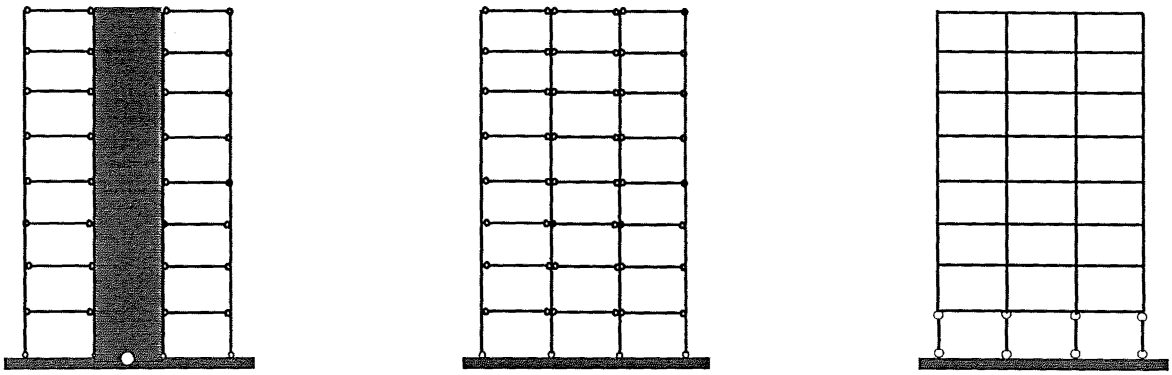


(A) Three types of building structures

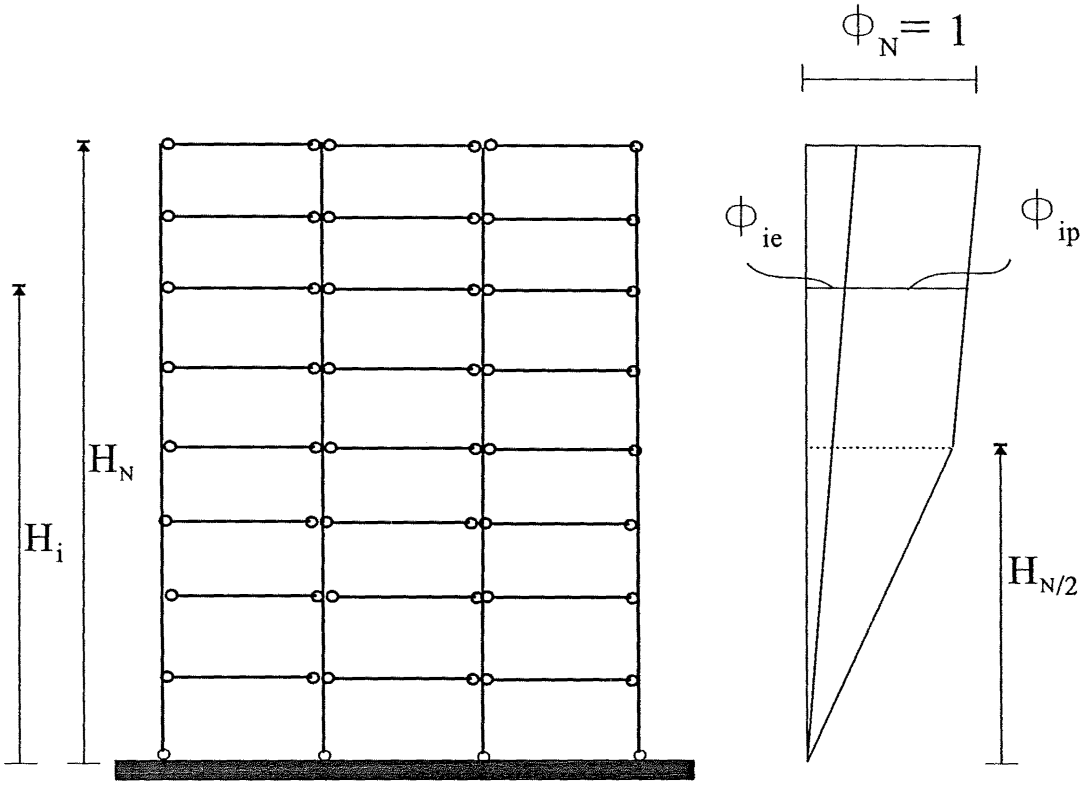


(B) Assumed displacement shape for type 2 building structures

Figure 9.5 Typical systems for building structures and the assumed deflected shape

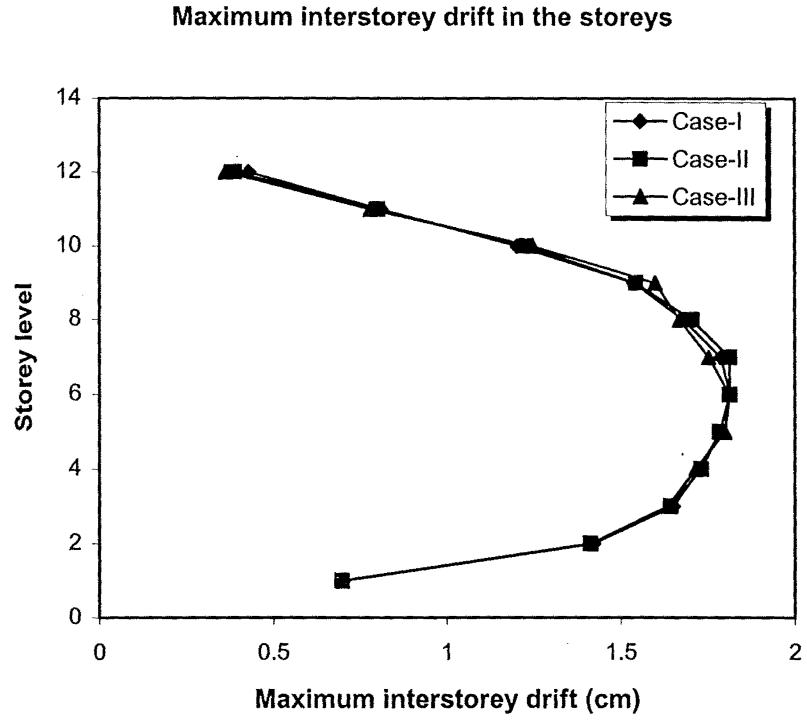


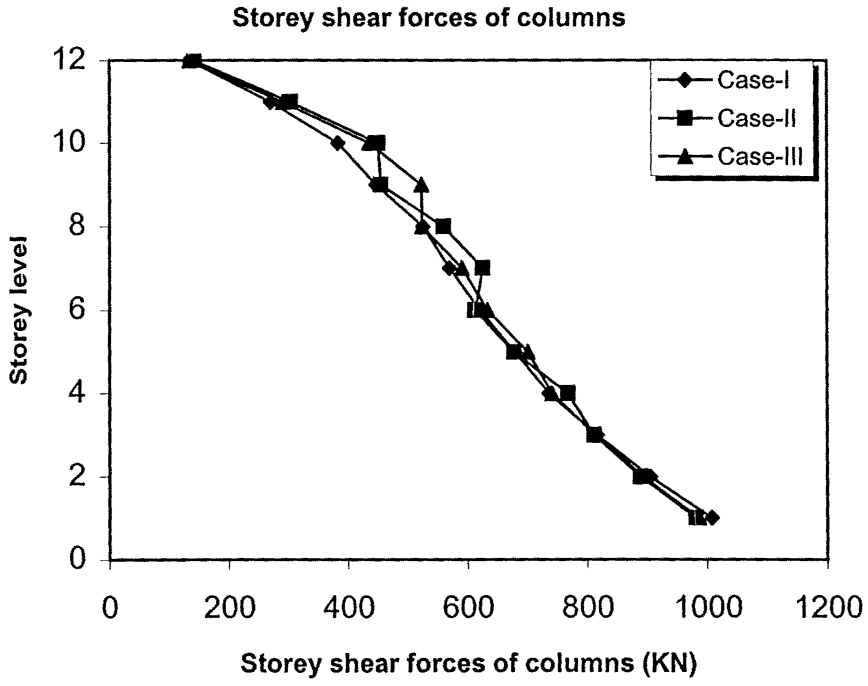


Figure 9.6 Comparison of distributions of drifts and shear forces in the columns in the storeys for the three cases under the El Centro 1940 NZS4203 compatible earthquake

# CHAPTER 10

# SIMULATION OF WIND SPEED AND WIND LOAD

## 10.1 INTRODUCTION

When a turbulent wind blows around a bluff structure, fluctuating pressures and loadings are induced on the surface of the structure that may cause it to vibrate. This motion due to the turbulence may be supplemented by phenomena such as vortex shedding from the sides of the structure and other aerodynamic instabilities such as galloping and flutter. Only the effect imposed on a flexible structure by the action of the fluctuating wind velocities in the mean wind direction (along-wind response) is taken into account in this study.

Until comparatively recently it has been common practice to simplify the direct along-wind loading calculations by assuming that the motion of the structure is small (i.e. dynamic effects are ignored). A quasi-static approach is often adopted in which a gust of a certain duration and velocity profile is assumed to act on the whole structure at a given instant of time. This is the basis of many code approaches (AS 1170 part 2). However, for many large structures this treatment is an over-simplification and, because the current trend in construction techniques often leads to structures of a comparatively smaller mass than previously, the dynamic effects due to the movement of the structure have become more important. The supplemental dampers have very little effect on those structures in which dynamic effects are insignificant because the supplemental damping is enhanced by dissipating energy through cyclic deformations of the dampers. But for the wind-sensitive buildings, the effect of the supplemental dampers may be significant.

The wind-induced response of structures is usually estimated through the analyses that are carried out on the basis of random vibration theories, as well as probabilistic and stochastic methods. In such a manner, response analysis is made mainly through conducting a modal spectral analysis within the frequency domain, and the response is computed statistically. This is due to the fact that the turbulence of the natural winds is random. This method is a generalisation of Fourier analysis and based on the superposition principle; therefore, strictly speaking, it can be applied only to linear time-variant systems. This method will be discussed in more detail in chapter 12.

On the other hand, in order to verify the efficiency of the supplemental dampers, or in order to analyse the response of a building in consideration of the nonlinear deformations of the structure, a step-by-step response analysis has to be carried out rather than an analysis in the frequency domain. Vaicaitis et al. (1975) studied the nonlinear problem of the response of tall buildings to wind loads in the time domain where the fluctuating wind velocity is simulated as a multi-dimensional and multi-variate random process using the Fast Fourier Transform (FFT) technique. The time domain analysis of the response of tall buildings to wind loads was also investigated by Saul et al. (1976). In their study, only along-wind response was considered and wind velocities were assumed to consist of three parts: mean wind, large and small gusts. The large gusts were simulated by generating random processes with specified auto-correlation and cross-correlation functions using a linear transformation. Small gusts were simulated by first generating uncorrelated random processes using a cosine series and then linearly transforming them into random processes with a specified cross-correlation function. Torkamani et al. (1985) have studied the dynamic response of tall buildings to wind excitation including torsional effects. In their study, a deterministic model of the wind (pseudo-turbulent) was assumed as harmonic in time and the results of the linearized and the nonlinear problems were compared. Tsukagoshi et al. (1993) discussed the application of a numerical simulation technique to estimate wind-induced vibrations of tall buildings. Fluctuating wind forces acting on a tall building in the along-wind and crosswind directions were simulated. Analyses of the response of a building installed with a Tuned Mass Damper (TMD) were also carried out to examine its efficiency. Das et al. (1990) presented a method for evaluating the lifetime risk of failure, in terms of probability of excessive inter-floor deflection, for a class of steel building frames subjected to dynamic wind loading. Wind loads were generated by a simulation technique using a power law profile and Davenport's gust spectrum model. In their simulation technique, wind speed time histories at floor levels were assumed to be perfectly correlated, hence only one set of the fluctuating wind speeds was generated.

## 10.2 STRUCTURE OF THE WIND

Several important characteristics of the wind have been summarised by Davenport et al. (1975) as follows:

1. The wind is not steady but fluctuating or gusty. It can be considered as consisting of a mean component and a fluctuating component.
2. The mean wind component does not vary significantly over the period of the record – about 10 minutes to 1 hour.
3. The mean wind increases with height.
4. The fluctuating component or gust amplitude is more or less constant with height.

Hence, wind speed can be written as:

$$V(z,t)=\overline{V}(z)+v(z,t) \tag{10.1}$$

where $\overline{V}(z)$ = the mean wind speed at height $z$,

$v(z,t)$ = turbulence (fluctuating) component.

### 10.2.1 Mean Wind Profiles

The mean wind profile throughout the height of interest to the structural engineers may be described by the well-known logarithmic profile (Davenport et al., 1975)

$$\overline{V}(z)=\frac{1}{k}v_* \ln\frac{z}{z_0} \tag{10.2}$$

where $\overline{V}(z)$ = the mean wind speed at height z above ground,

$k$ = von Karman coefficient (approximately 0.4)

$z_0$ = roughness length

$v_*$ = friction velocity.

The mean wind profile can also be represented by a power law model given by (Davenport, 1967):

$$\overline{V}(z)=\overline{V}_G\left(\frac{z}{z_G}\right)^{\alpha} \tag{10.3}$$

where $z_G$ = the gradient height

$\overline{V}_G$ = the mean gradient velocity

$\alpha$ = power law exponent.

Mean wind speeds averaged over a period of one hour are usually used in the design of tall buildings subjected to wind loading.

For this study the mean wind speeds are taken from NZS4203 part 5 – the hourly mean wind speeds.

The hourly mean site wind speed at height z can be determined from (NZS4203, 1992 part 5):

$$\overline{V}(z) = VM_{ls}\overline{M}_{(z,cat)}M_sM_tM_r \tag{10.4}$$

where $V$ = the basic directional wind speed

$M_{ls}$ = the limit state multiplier

$\overline{M}_{(z,cat)}$ = the site terrain/height multiplier

$M_s$ = the shielding multiplier

$M_t$ = the topographic multiplier

$M_r$ = the structure risk multiplier.

Assume the building to be located in Wellington region (Terrain Category 1 conditions) and

$M_s = M_t = M_r = 1$

$M_{ls} = 0.75$ (for serviceability limit state)

$V = 48$ m/s (nondirectional wind)

The 12-storey 3-bay reinforced concrete frame structure model described in chapter 3 is used for this study. The mean wind speeds at the floor levels of the structure are shown in Table 10.1

### 10.2.2 Structure of Turbulence (Fluctuating Component)

The structure of turbulence (fluctuating component) can be characterised by (Davenport et al., 1975):

- the power spectral energy distribution of the fluctuations in the wind;

- the correlation between velocity at different points in the flow;
- the probability distribution of the velocity fluctuations.

Spectra Of Longitudinal Components Of Turbulence

Several proposals for the expression for the longitudinal components of turbulence have been suggested. These can be seen in Davenport et al. (1975), Simiu et al. (1986), Harris (1971).

For this study, the power spectral density function of the turbulence component of the wind speed is taken from Australian Standard for Wind Loads AS1170 part 2 as follows.

$$E = \frac{\pi}{4}\frac{nS_v(n)}{\sigma_v^2} = \frac{0.47N}{\left(2+N^2\right)^{5/6}} \tag{10.5}$$

where $E$ = a spectrum of turbulence in the approaching wind stream

$N$ = an effective reduced frequency = $\frac{nL_h}{\overline{V}_h}$ (10.5a)

$n$ = the first mode along-wind frequency of the building, in Hertz

$L_h$ = a measure of the effective turbulence length scale, in metres

$= 1000\left(\frac{h}{10}\right)^{0.25}$

$h$ = the height of the building structure, in metres

$\overline{V}_h$ = the design hourly mean wind speed at height h, in metres per second

$\sigma_v$ = the standard deviation of turbulence component of along-wind velocity

$S_v(n)$ = the power spectral density function of the turbulence component.

Hence we have:

$$\frac{nS_v(n)}{\sigma_v^{\,2}} = \frac{0.6N}{\left(2+N^2\right)^{5/6}} \tag{10.6}$$

Cross Spectra of Wind Velocity (Simiu et al., 1986)

In random vibration analysis a cross-spectral density function is used to measure the correlation between two random quantities. This function is a complex quantity that is composed of two different parts: a real part, known as co-spectrum or in-phase component and an imaginary part, known as quadrature spectrum or out-of-phase component. For two fluctuating wind velocity components the cross spectrum can be written as:

$$S^{cr}_{v_1v_2}(r,n) = S^{C}_{v_1v_2}(r,n) + iS^{Q}_{v_1v_2}(r,n) \tag{10.7}$$

where $S^{cr}_{v_1v_2}(r,n)$ = the cross spectrum

$i = \sqrt{-1}$

$v_1, v_2$ = indicate that the two records are taken at points $M_1$ and $M_2$

$r$ = the distance between points $M_1$ and $M_2$

The coherence function is defined as:

$$\left[Coh(r,n)\right]^2 = c^2_{v_1v_2}(r,n) + q^2_{v_1v_2}(r,n) \tag{10.8}$$

where $\left[Coh(r,n)\right]^2$ = the coherence function

$$c^2_{v_1v_2}(r,n) = \frac{\left[S^{C}_{v_1v_2}(r,n)\right]^2}{S_v(z_1,n)S_v(z_2,n)}$$

$$q^2_{v_1v_2}(r,n) = \frac{\left[S^{Q}_{v_1v_2}(r,n)\right]^2}{S_v(z_1,n)S_v(z_2,n)}$$

in which $S_v(z_1,n), S_v(z_2,n)$ = the power spectral density function of the along-wind components of turbulence at points $M_1$ and $M_2$.

It is assumed that the power spectral density is invariant with height (Harris, 1971). Hence

$$S_v(z_1,n) = S_v(z_2,n) = S_v(n) \tag{10.9}$$

In Eq(10.7) the imaginary part can be neglected when analysing wind engineering problems. Therefore, the coherence function and the cross spectra can be written as:

$$[Coh(r,n)]^2 = \frac{[S^C_{v_1v_2}(r,n)]^2}{S_v(z_1,n)S_v(z_2,n)} \tag{10.10}$$

$$S^C_{v_1v_2}(r,n) = \sqrt{S_v(z_1,n)}\sqrt{S_v(z_2,n)}Coh(r,n) \tag{10.11}$$

$Coh(r,n)$ is the square root of the coherence function (also known as narrow-band cross-correlation). An expression for this function can be written as:

$$Coh(r,n) = e^{-\hat{f}}$$

where $\hat{f} = \dfrac{n\left[C_z^2(z_1-z_2)^2 + C_x^2(x_1-x_2)^2\right]^{1/2}}{\frac{1}{2}\left[\overline{V}(z_1)+\overline{V}(z_2)\right]}$

In which $x_1$, $x_2$ and $z_1$, $z_2$ are the coordinates of points $M_1$, $M_2$, the line $M_1$, $M_2$ is assumed to be perpendicular to the direction of the mean wind. The exponential decay coefficients $C_x$, $C_z$ are determined experimentally.

Probability Distribution of the Velocity Turbulence Components

Generally speaking, it may be assumed that the probability distribution of the velocity turbulence components is Gaussian (Davenport et al., 1975). Thus it has a distribution of the familiar form:

$$p(v) = \frac{1}{\sqrt{2\pi}\sigma_v} e^{-\frac{v^2}{2\sigma_v^2}} \tag{10.12}$$

where $v$ = the turbulence component of velocity = $V - \overline{V}$

$p(v)$ = the probability density of $v$

$\sigma_v^2$ = the variance of v.

The variance is equal to the area under the spectrum, that is:

$$\sigma_v^2 = \int_0^\infty S_v(n)dn = \int_0^\infty nS_v(n)d\ln n \tag{10.13}$$

For the expression of the along-wind components of turbulence proposed by Davenport, the intensity of turbulence at height $z$ is (Davenport et al., 1975):

$$\frac{\sigma_v}{\overline{V}(z)} = 2.45\sqrt{k}\left(\frac{z}{10}\right)^{-\alpha}$$

where $\frac{\sigma_v}{\overline{V}(z)}$ = the intensity of turbulence at height $z$.

For this study, the intensity of turbulence $\frac{\sigma_v}{\overline{V}(z)}$ at height z is taken from NZS4203 (1992) part 5. The results are shown in Table 10.1.

## 10.3 EQUIVALENT WIND SPECTRUM (Solari, 1988)

The equivalent wind spectrum technique is a mathematical model according to which the wind is schematised as a stochastic stationary Gaussian process made up of a mean-speed profile on which an equivalent turbulence fluctuation, perfectly coherent in space, is superimposed (Solari, 1988). This equivalent wind structure is expressed as:

$$V_{eq}(z,t) = \overline{V}(z) + \sigma_v(z)v_{eq}^*(t) \tag{10.14}$$

where $V_{eq}(z,t)$= the velocity field of an "equivalent wind structure"

$\sigma_v(z)$ = the standard deviation of $V(z,t)$

$v_{eq}^*(t)$ = a non-dimensional stochastic stationary Gaussian process, called the "reduced equivalent velocity fluctuation", a random function of time only.

The power spectral density function for this "reduced equivalent velocity fluctuation", $S^*_{veq}(n)$, is called the "reduced equivalent wind spectrum". This "reduced equivalent wind spectrum" is defined so that the modal spectra of external fluctuating forces associated with the equivalent wind configuration (Eq(10.14)) approximate, in an optimal way, the corresponding spectra related to the actual velocity field (Eq(10.1)).

Solari showed that the "reduced equivalent wind spectrum" can be expressed as:

$$S^*_{veq}(n) = \frac{S_v(h_1,n)}{\sigma_v^2(h_1)} \ell\left[K_x \frac{nC_x b}{\overline{V}(h_1)}\right]\left\{1+\gamma\ell\left[\frac{nC_y d}{\overline{V}(h_1)}\right]-\gamma\right\}\ell\left[K_z \frac{nC_z h}{\overline{V}(h_1)}\right] \qquad (10.15)$$

where $\ell(\eta) = \frac{1}{\eta} - \frac{1}{2\eta^2}\left(1-e^{-2\eta}\right)$ (10.16)

$\gamma = 2C_w C_l / C_D^2$

$C_w$, $C_l$ = the absolute values of mean pressure coefficients on the windward and leeward side of the structure, respectively

$C_D = C_w + C_l$ = the drag coefficient

$C_x$, $C_y$, $C_z$ = the exponential decay coefficients

$$K_x = \frac{0.24\frac{b}{h_1}}{0.6\frac{b}{h_1}+0.1}, K_z = 0.38 \qquad (10.17)$$

in which $b$, $h$ = the width and height of the structure

$h_1$ = $0.607h$ = the reference height

In this study, the partial correlation between the windward and leeward wind speed is neglected. Hence in Eq(10.15)

$$\left\{1+\gamma\ell\left[\frac{fC_y d}{\overline{V}(h_1)}\right]-\gamma\right\} = 1 \qquad (11.18)$$

From Solari (1988)

$C_x = 16$, $C_z = 10$

It can be shown that for the particular 12-storey building being considered,

$h_1 = 0.607h = 26.587\text{m}$, $b = 6\text{m}$

$\bar{V}(26.587) = 28.433\text{m/s}$

From Eq(10.17), $K_x = 0.23$, $K_z = 0.38$

and

$$K_x \frac{nC_x b}{\bar{V}(h_1)} = \frac{0.23 \times 16 \times 6}{28.433} n = 0.7766n$$

$$K_z \frac{nC_z h}{\bar{V}(h_1)} = 0.38 \times \frac{10 \times 43.8}{28.433} n = 5.8538n$$

From Eq(10.16)

$$\ell\left(K_x \frac{nC_x b}{\bar{V}(h_1)}\right) = \ell(0.7766n) = \frac{1.2877}{n} - \frac{0.8291}{n^2}\left(1 - e^{-1.5531n}\right)$$

$$\ell\left(K_z \frac{nC_z h}{\bar{V}(h_1)}\right) = \ell(5.8538n) = \frac{0.17083}{n} - \frac{0.01459}{n^2}\left(1 - e^{-11.7077n}\right)$$

It is known that $L_h = 1446.67$, from Eq(10.5a)

$$N = n\frac{1446.67}{28.433} = 50.88n$$

From Table 10.1 it can be found that:

$$\frac{\sigma_v}{\bar{V}(h_1)} = 0.1424, \quad \sigma_v = 0.1424 \times 28.433 = 4.0486$$

Hence

$$\frac{nS_v(h_1, n)}{\sigma_v^2} = \frac{0.6 \times 50.88n}{\left[2 + (50.88n)^2\right]^{5/6}} = \frac{30.528n}{\left(2 + 2588.774n^2\right)^{5/6}}$$

Then

$$\frac{S_v(h_1, n)}{\sigma_v^2} = \frac{30.528}{\left(2 + 2588.774n^2\right)^{5/6}}$$

From Eq(10.15) we have:

$$S^{*}_{veq}(n)=\frac{30.528}{\left(2+2588.774n^{2}\right)^{5/6}}\left[\frac{1.2877}{n}-\frac{0.8291}{n^{2}}\left(1-e^{-1.5531n}\right)\right]\left[\frac{0.17083}{n}-\frac{0.01459}{n^{2}}\left(1-e^{-11.7077n}\right)\right] \tag{10.19}$$

From the above-mentioned procedure, it can be seen that to represent the wind structure over the height of the building, only one set of turbulence wind speeds is needed. The coherence function has already been considered in the spectrum. Hence, this equivalent wind spectrum technique can render the time-domain approach extremely simple, avoiding the high computational burden of generating families of cross-correlated velocity histories.

## 10.4 WIND LOAD DISTRIBUTION

Aerodynamic forces of wind on tall buildings are mainly due to the complex nature of the unsteady flow about a bluff body. This is a source of uncertainty in modelling unsteady aerodynamic forces on structures. Quasi-steady and strip assumptions are used in this study (Vickery et al., 1972, Kawai, 1983). This implies that the aerodynamic forces, due to the flow geometry, would develop instantaneously without accounting for the usual force deficiency and phase lag encountered in unsteady fluid dynamics. These assumptions have been adopted by several researchers in time-domain analysis (Torkamani et al., 1985, Das et al., 1990, Torkamani et al., 1994).

The drag load force per unit length (along the height of a structure) in a turbulent flow can be represented as follows (Vickery et al., 1972, Torkamani et al., 1985):

$$D(z,t)=\frac{1}{2}\rho V(z,t)^{2}C_{D}(z)+\rho b^{2}\dot{V}(z,t)C_{m}(z) \tag{10.20}$$

where $b$ = width of the structure

$\rho$ = air mass density

$V(z,t)$ = wind speed at a height $z$ at time $t$

$C_D(z)$ = drag coefficient

$C_m(z)$ = added mass coefficient at height $z$.

In most applications, the term containing the coefficient $C_m(z)$ in Eq(10.20), the inertial force associated with the mass of the fluid displaced by the body, is disregarded because in wind applications the contribution of this term to the overall response is small.

Hence, the drag load force acting at the level i (of a height z) of a building at time t can be expressed as:

$$F_i(z,t)=\frac{1}{2}\rho V(z,t)^2 C_D A_i \tag{10.21}$$

where $A_i$ = tributary area perpendicular to the wind loading for the level $i$

$C_D = C_w + C_l$

in which

$C_w$ = windward drag coefficient

$C_l$ = leeward drag coefficient

In the case of tall buildings with a rectangular shape in plan, it may be assumed that $C_w = 0.8$, $C_l = 0.5$ and then $C_D = C_w + C_l = 1.3$ (Simiu et al., 1986)

For the equivalent wind structure, the drag force acting at the level $i$ (of a height $z$) of a building can be written as (from Eq10.14 and Eq10.21):

$$\begin{aligned} F_i(z,t) &= \frac{1}{2}\rho V_{eq}(z,t)^2 C_D A_i \\ &= \frac{1}{2}\rho\left[\overline{V}(z)+\sigma_v(z)v^*_{eq}(t)\right]^2 C_D A_i \\ &= \frac{1}{2}\rho\overline{V}(z)^2 C_D A_i + \rho C_D A_i \sigma_v(z)\overline{V}(z)v^*_{eq}(t)+\frac{1}{2}\rho C_D A_i \sigma_v(z)^2 v^*_{eq}(t)^2 \\ &= \overline{F}_i(z)+F'_i(z,t) \end{aligned} \tag{10.22}$$

where $\overline{F}_i(z)$ = the mean drag at level $i$

$$= \frac{1}{2}\rho\overline{V}(z)^2 C_D A_i$$

$F'_i(z,t)$ = the fluctuating drag = $\rho C_D A_i \sigma_v(z)\overline{V}(z)v^*_{eq}(t)+\frac{1}{2}\rho C_D A_i \sigma_v(z)^2 v^*_{eq}(t)^2$

The mean drag at the various levels of the structure is shown in Table 10.1. A time history of the equivalent velocity fluctuation can be simulated by the technique to be introduced below.

## 10.5 SIMULATION OF ARTIFICIAL WIND SPEED TIME HISTORY

The use of time-domain analysis requires the artificial wind to be realistic and the simulation technique efficient. A number of methods for simulating stationary random fields, with specified spectral density, have been proposed so far. The simulation methods more generally used can be divided into two classes: (1) methods based on the use of series of sine and/or cosine function (wave superposition); and (2) methods based on the application of linear filters to sequences of random numbers (linear filtering). Iannuzzi et al. (1987) investigated the merits and drawbacks of some of the most commonly used simulation techniques when applied to the field of structural aerodynamics. In their study, methods for the simulation of single and multiple time series were reviewed and compared when applied to the simulation of natural winds.

It has been known that for the equivalent wind spectrum technique, an equivalent turbulence fluctuation, perfectly coherent in space, is used to represent the actual turbulence component. Also it is assumed that the power spectral density is invariant with height (Harris, 1971) for the actual turbulence component. Hence, only one set of the turbulence wind speed needs to be simulated.

For simulation of single artificial wind time history, the weighted amplitude wave superposition method is adopted. The reduced equivalent velocity turbulence component can be simulated as a one-variate, one-dimensional, homogeneous, Gaussian random process with a zero mean and a power spectral density function $S^*_{veq}(n)$ given by the following expression:

$$v^*_{eq}(t) = \sqrt{2}\sum_{i=1}^{N}\left[S^*_{veq}(n_i)\Delta n\right]^{1/2}\cos(2\pi n_i t + \theta_i) \tag{10.23}$$

where $\theta_i$ = random phase angles uniformly distributed between 0 and $2\pi$

$N$ = the number of frequency intervals

$n_i$ = frequency

The amplitude of each cosine function is chosen so that its contribution to the total mean square value is equivalent to the area under the target spectral density curve within the chosen frequency interval Δn, that is, $S^*_{veq}(n)\Delta n$. In this study, the upper cut-off frequency, n, is set at 2.0 Hz. The lower value of the frequency is 0.005 Hz. The time steps selected for generating the turbulence component in the time domain are equal to 0.02 second. The time duration is equal to 600s.

The 12-storey 3-bay reinforced concrete frame structure shown in chapter 3 is used for the time-domain analysis. Equivalent along-wind turbulence component time histories are generated using this technique.

The "reduced equivalent velocity fluctuation" time history is shown in Fig.10.1. The wind velocity time history at the roof level is shown in Fig.10.2.

## 10.6 COMPARISON OF THE RESPONSE FROM TIME-HISTORY ANALYSIS WITH THE ONE FROM CODE METHOD

### 10.6.1 Method Given By Australian Standard For Wind Loads AS 1170 Part2

The gust factor $G$ can be calculated as:

$$G = 1 + r\sqrt{\left[ g_v{}^2 B(1+w)^2 + \frac{g_f{}^2 SE}{\xi} \right]} \tag{10.24}$$

where $g_v$ = a peak factor for the upwind velocity fluctuation

= 3.7

$g_f$ = a peak factor, the ratio of the expected peak value which occurs once per hour to the standard deviation of the resonant part of the fluctuating response

$$= \sqrt{2\ln(3600 n_1)} \tag{10.25}$$

$B$ = a background factor, which is a measure of the slowly varying background component of the fluctuating response caused by the lower frequency wind speed variations

$$= \frac{1}{1+\frac{\sqrt{(36h^2+64b^2)}}{L_h}} \tag{10.26}$$

$h$ = the height of the building structure, in metres

$b$ = the horizontal breadth of a vertical structure normal to the windstream

$n_1$ = the first mode along-wind frequency of the building, in Hertz

$L_h$ = a measure of the effective turbulence length scale, in metres

$$= 1000\left(\frac{h}{10}\right)^{0.25}$$

$w$ = a factor to account for the second order effects of the turbulence intensity

$$= \frac{g_v r\sqrt{B}}{4} \tag{10.27}$$

$r$ = a roughness factor, twice the longitudinal turbulence intensity at height $h$

$$= \frac{2\left(\frac{\sigma_v}{\overline{V}}\right)}{M_t} \text{ evaluated for } z = h \tag{10.28}$$

$\xi$ = the structural damping capacity as a fraction of the critical damping ratio

$S$ = a size factor to account for the correlation of pressures over a structure

$$= \frac{1}{\left[1+\left(\frac{3.5n_1h}{\overline{V}_h}\right)\right]\left[1+\left(\frac{4n_1b}{\overline{V}_h}\right)\right]} \tag{10.29}$$

$$E = \frac{0.47N}{(2+N^2)^{5/6}}$$

where $E$ = a spectrum of turbulence in the approaching wind stream

$N$ = an effective reduced frequency = $\frac{nL_h}{\overline{V}_h}$

$\overline{V}_h$ = the design hourly mean wind speed at height h, in metres per second

$\sigma_v$ = the standard deviation of the turbulence component of the along-wind velocity.

By means of this gust factor $G$, the expected peak response can be obtained as follows:

$$\hat{x} = G\overline{x}$$
$$\hat{M} = G\overline{M} \tag{10.30}$$

where $\hat{x}, \hat{M}$ = expected peak displacement and peak overturning moment respectively,

$\overline{x}, \overline{M}$ = mean displacement and mean overturning moment due to the mean wind load.

The peak along-wind acceleration at the top of the building can be calculated from (Cenek et al., 1990, Holmes et al., 1990):

$$a_x\,(\mathrm{m/s^2}) = g_f \frac{3\overline{M}}{M_b h}\sqrt{\frac{r^2 SE}{\xi}} \tag{10.31}$$

where $\overline{M}$ = the mean along-wind overturning moment, N-m

$h$ = building height, m

$M_b$ = the total building mass, kg.

### 10.6.2 Numerical Results

For the 12-storey structure under the above-mentioned wind conditions, the gust factor can be calculated as follows:

$g_v = 3.7$,

$n_1 = 0.5\mathrm{Hz}$, $g_f = \sqrt{2\ln(3600 n_1)} = 3.8718$

From Table 10.1: $\frac{\sigma_v(h)}{\overline{V}(h)} = 0.1311$, So $r = 0.2622$

$$L_h = 1000\left(\frac{h}{10}\right)^{0.25} = 1446.67$$

$$N = \frac{n_1 L_h}{\overline{V}_h} = 24.036$$

$$E = \frac{0.47N}{\left(2+N^2\right)^{5/6}} = 0.05627$$

$$B = \frac{1}{1 + \frac{\sqrt{(36h^2 + 64b^2)}}{L_h}} = 0.8441$$

$$w = \frac{g_v r\sqrt{B}}{4} = 0.2228$$

$$S = \frac{1}{\left[1 + \left(\frac{3.5 n_1 h}{\overline{V}_h}\right)\right]\left[1 + \left(\frac{4 n_1 b}{\overline{V}_h}\right)\right]} = 0.2016$$

For the serviceability limit state, it is assumed that the structural damping capacity as a fraction of the critical damping ratio $\xi = 1\%$

The gust factor $G$ can be calculated as:

$$G = 1 + r\sqrt{\left[g_v^{\,2} B(1+w)^2 + \frac{g_f^{\,2} SE}{\xi}\right]}$$

$$= 1 + 0.2622 \times \sqrt{3.7^2 \times 0.8441 \times (1 + 0.2228)^2 + \frac{3.8718^2 \times 0.2016 \times 0.05627}{0.01}}$$

$$= 2.535$$

The mean forces acting at the floors due to the mean wind are listed in Table 10.1.

The mean along-wind overturning moment can be calculated for known mean forces at the floors.

$$\overline{M} = 3662.7947 \text{ KN-m}$$

$$M_b = 1446.58 \times 10^3 \text{ kg}$$

$$\overline{x} = 1.416 \times 10^{-2} \text{ m}$$

$$a_x = 3.8718 \times \frac{3 \times 3662.7947}{1446.58 \times 43.8}\sqrt{\frac{0.2622^2 \times 0.2016 \times 0.05627}{0.01}} = 0.1875 \text{ (m/s}^2\text{)}$$

$$\hat{x} = G\overline{x} = 2.535 \times 1.416 \times 10^{-2} = 3.59 \times 10^{-2} \text{ m}$$

$$\hat{M} = G\overline{M} = 2.535 \times 3662.7947 = 9285.18 \text{KN-m}$$

These results are shown in Table 10.2.

A time-domain analysis of the 12-storey model structure under the artificial wind load has been performed. Some of the structural responses are also shown in Table 10.2. Roof displacement and roof acceleration time histories are shown in Figs.10.3 and 10.4.

The differences of the results from these two methods are also shown in Table 10.2. It can be seen that the differences between these two methods are very small. Hence, it can be concluded that the simulation technique adopted here and the time-domain analysis give good results.

| Level | Height (m) | $\overline{M}_{(z,cat)}$ | $\overline{V}(z)$ (m/s) | $\frac{\sigma_v(z)}{\overline{V}(z)}$ | $\sigma_v(z)$ | $\overline{F}_D(z)$ |
|---|---|---|---|---|---|---|
| 1 | 3.65 | 0.623 | 22.428 | 0.1691 | 3.7926 | 8.5925 |
| 2 | 7.3 | 0.6776 | 24.394 | 0.1613 | 3.9348 | 10.1650 |
| 3 | 10.95 | 0.7157 | 25.765 | 0.1561 | 4.0219 | 11.3396 |
| 4 | 14.6 | 0.7376 | 26.554 | 0.1524 | 4.0468 | 12.0448 |
| 5 | 18.25 | 0.7595 | 27.342 | 0.1488 | 4.0685 | 12.7703 |
| 6 | 21.9 | 0.7757 | 27.925 | 0.1457 | 4.0687 | 13.3206 |
| 7 | 25.55 | 0.7867 | 28.321 | 0.1431 | 4.0527 | 13.7011 |
| 8 | 29.2 | 0.7976 | 28.714 | 0.1406 | 4.0372 | 14.084 |
| 9 | 32.85 | 0.8086 | 29.11 | 0.1380 | 4.0172 | 14.4752 |
| 10 | 36.5 | 0.8195 | 29.502 | 0.1355 | 3.9975 | 14.8676 |
| 11 | 40.15 | 0.8303 | 29.891 | 0.1329 | 3.9725 | 15.2623 |
| 12 | 43.8 | 0.8376 | 30.154 | 0.1311 | 3.9532 | 7.7660 |

Table 10.1 Mean wind velocity and mean wind forces at the storeys of the structure

| | Peak roof displacement (cm) | Peak roof acceleration (m/s^2) | Peak overturning moment (KN-m) |
|---|---|---|---|
| AS 1170 part2 code method | 3.59 | 0.1875 | 9285.18 |
| Time-domain analysis method | 3.67 | 0.1909 | 9174.9 |
| Difference | 2.23% | 1.81% | 1.19% |

Table 10.2 Comparison of structural response for two analyses

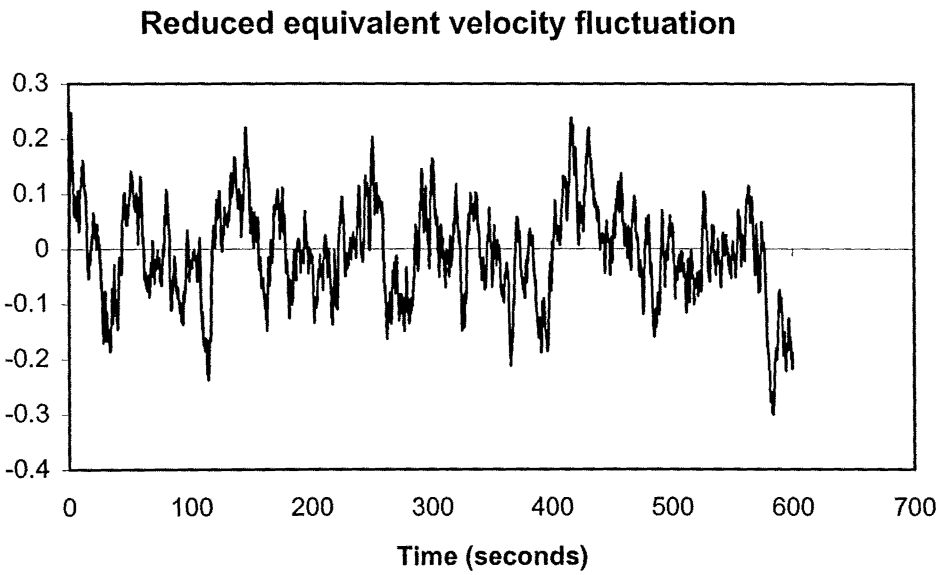


Figure 10.1 Reduced equivalent velocity fluctuation time history

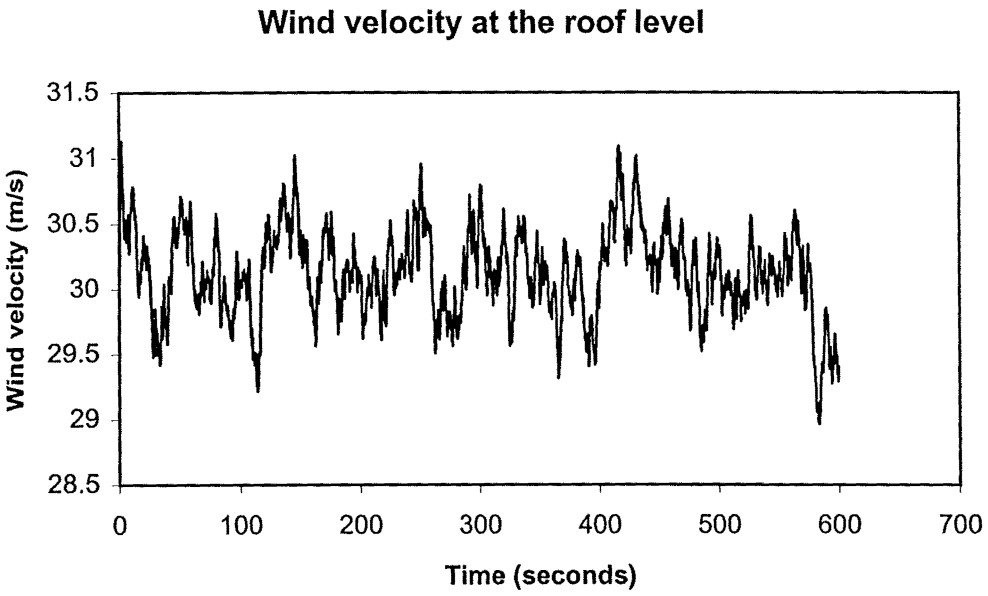


Figure 10.2 Roof level wind velocity time history

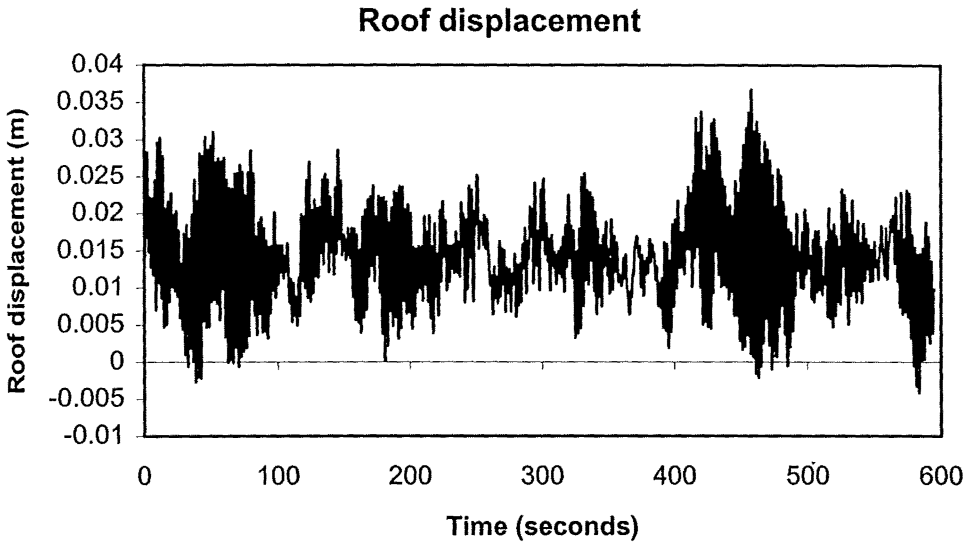


Figure 10.3 Roof displacement time history

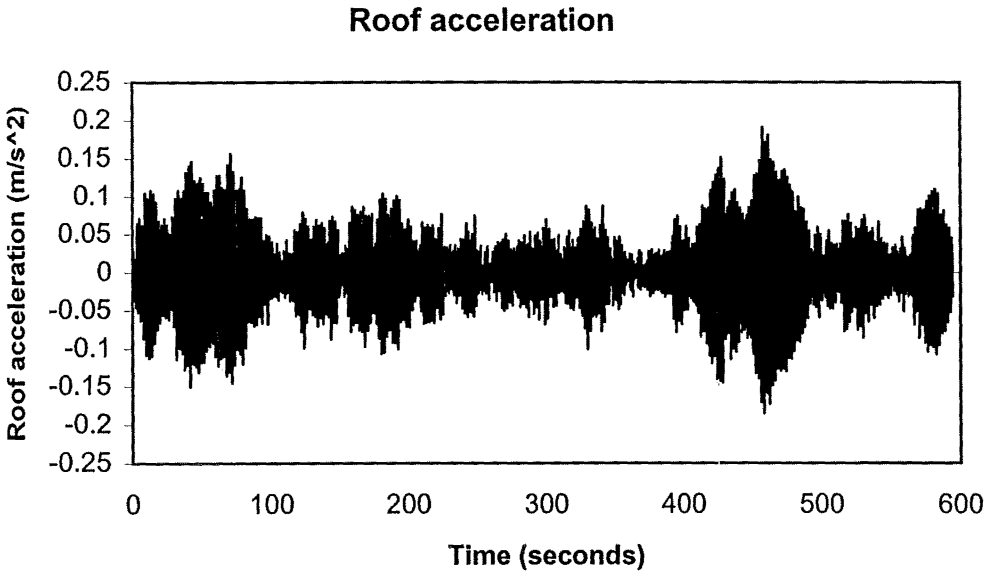


Figure 10.4 Roof acceleration time history

# CHAPTER 11

# PLACEMENT AND STRENGTH LEVELS OF THE SUPLEMENTAL DAMPERS IN THE STRUCTURE

## 11.1 PLACEMENT OF THE SUPPLEMENTAL DAMPERS IN THE STRUCTURE

It is assumed that all the supplemental dampers in the structure are identical. Three types of placement of the dampers throughout the structure are discussed here. They are: one damper at the 1st floor level only; one damper at every second level; and one damper at every level (Fig.11.1). The number of dampers for these three types of distribution is 1, 6, and 12 respectively. Different strength levels (or yielding force) of the dampers are considered for each case ($F_{yd}$=2.5, 5, 10, 20KN). It is assumed that yield deformations of the dampers for different strength levels are 0.09mm. The peak roof displacement and the peak roof acceleration are taken to represent the dynamic response of the structure under wind gusts. For the structure with supplemental dampers, under wind gusts the peak roof acceleration response is the main concern (this will be discussed in chapter 12). The results from these different placements and yield strength levels of the dampers are compared with the response of the structure without dampers and are shown in Tables 11.1and 11.2.

Firstly the case when there is one damper at the 1st floor level only is considered. From Tables 11.1and 11.2 it can be observed that only one damper at the 1st floor level is not sufficient. The reduction in the response is small. For the four strength levels of the dampers, the reduction of the peak roof acceleration due to the damper is in the range of 9.49 to 18.56%.

When the dampers are incorporated in every second storey or every storey, the effect of dampers becomes significant. For the structure with the dampers in every second storey, the reduction in the peak roof acceleration due to the dampers is in the range of 22.24 to 66.6% for the different yield strengths of the dampers. For the structure with the dampers in every storey, the reduction in the peak roof acceleration due to the dampers is in the range of 46.25 to 62.7%.

The difference between the case in which the dampers are in every second storey and the case in which the dampers are in every storey varies with respect to the yield strength levels of the

dampers. For low damper yield strengths, this difference is great (as for the yield strength of the dampers of 2.5KN, the reduction factor of the roof acceleration varies from 22.24% to 46.25%). For a higher damper strength, this difference becomes smaller (for the yield strength of 20KN, the reduction factor of the roof acceleration varies from 66.6% to 62.7%).

Comparing the cases in which the dampers are in every second storey and in which the dampers are in every storey but with only half of the yield strength of the first case. The results of such comparison are shown in Tables 11.3, 11.4. It can be seen from Tables 11.3 and 11.4 that for each pair of cases the peak roof response and the peak roof displacement are all very close to each other. It can be concluded that the structure with dampers in every second storey can be replaced by the case in which the dampers are in every storey but with half the value of yield strength. In the remainder of this study the dampers are incorporated into the structure in every storey.

## 11.2 INFLUENCE OF THE DAMPER YIELD STRENGTHS

The structure with the supplemental dampers in every storey but with different yield strength levels is investigated here. Four different damper yield strengths are adopted: they are 2.5KN, 5KN, 10KN and 20KN. The peak roof acceleration and the peak roof displacement for these four cases are shown in Fig.12.2 and 12.3. It can be seen that even for low levels of damper yield strength, an increase in the damper strength levels has a significant effect on the structural response under wind gusts (yield strength varies from 0 to 2.5KN or 5KN). When the damper yield strengths varies from 5KN to 20KN, the change in the structural response is not significant. Yet comparing the peak roof acceleration of the structure with the 10KN-yield strength dampers and the one with 20KN-yield strength dampers, it is found that the former is more effective than the latter (Table 11.1).

Damper force time histories for the structure with three different damper yield strengths are shown in Figs.11.4, 11.5 and 11.6. These three different yield strength levels are 5KN, 10KN and 20KN. Dampers in the $1^{st}$, $6^{th}$ and the top levels are taken to represent the lower, middle and the upper section with dampers. It can be seen from the figures that for the structure with 5KN yield-strength dampers, almost all the dampers yield during the wind gust excitation. Dampers in the structure can effectively dissipate cyclic energy. For the structure with 20KN yield-strength dampers, the dampers in the upper levels hardly yield. Even for the dampers in the lower levels, there are many cycles in which the dampers have not yielded. This reduces

the effectiveness of the energy dissipation of the dampers. Hence, the yield strength of the dampers needs to be chosen carefully.

It is known that the acceleration response of structures can be reduced by increasing the damping capacity, the mass or the stiffness (Vickery et al., 1983). For the structure with supplemental dampers under wind gusts, the role of the dampers is mainly to add damping to the structure. If the damper yield strength is too low, the energy dissipated by the dampers is also small, hence the supplemental damping induced by the dampers is low and the effectiveness of the dampers is not significant. However, if the damper yield strength is too high, many dampers do not yield during the response time history and the energy dissipated by the dampers is again not significant. This explains the fact that the dampers with the 10KN-yield strength are more effective than the dampers with the 20KN-yield strength.

The roof acceleration time histories for the structure without dampers and the structure with four different damper yield strengths (2.5KN, 5KN, 10KN and 20KN) are shown in Figs.11.7, 11.8 and 11.9. Comparing the responses in Figs.11.7 and 11.8, it is clear that the supplemental dampers have a significant effect on the reduction of the acceleration response. From Fig.11.9, it can be seen that for the different damper yield strengths (from 5KN to 20KN) the roof acceleration responses are very similar.

## 11.3 NATURAL FREQUENCY AND NORMAL MODE SHAPE OF THE STRUCTURE WITH THE SUPPLEMENTAL DAMPERS

Identical dampers are incorporated into the structure at all storey levels. The influence on the natural frequency and normal mode shape of the structure caused by the dampers were investigated. Four different yield strength levels of the dampers (2.5KN, 5KN, 10KN and 20KN) were used for this discussion. Only the first mode effect was taken into account, the higher mode effect being ignored. Natural frequencies and normal mode shapes of the $1^{st}$ mode for the structure without and with dampers are shown in Table 11.5 and Fig.11.10. These modal properties are associated with the state in which the structures are subject to mean wind forces and the vertical static loads, and the tangent characteristics of the main structure and the supplemental dampers at that state are used for calculating the modal properties.

It can be seen that the difference of the 1st mode shape between the original structure and the structure with the supplemental dampers is quite small. When the yield strength of the dampers is smaller than 10KN, the difference is extremely small (in this case there is no need for the yield strength of the dampers to exceed 10KN). This is due to the fact that the forces in the dampers are small compared with the internal forces in the original structure. The dampers tend to yield in a very small displacement range and the force – displacement relationship of the dampers is elasto-plastic with no stiffening effect on the main structure. It can be observed that the supplemental dampers for wind-resisting buildings have very little influence on the modal properties of the structures. For the analysis and design of building structures with the supplemental dampers under wind gusts, the modal properties of the structures can be taken to be those of the undamped structures and the stiffening effect due to the supplemental dampers can be ignored.

## 11.4 SUPPLEMENTAL DAMPING LEVEL DUE TO THE DAMPERS

It has been shown that the stiffening effect on the main structure due to the supplemental dampers can be ignored for wind-resisting structures. Thus the only effect which the supplemental dampers exert on the structure is supplemental damping. There is one question to be answered: what is the appropriate range of this supplemental damping for structures with dampers under wind gusts to ensure a balance of efficiency and economy?

The main concern for wind-sensitive buildings under the serviceability Limit State conditions is the acceleration response. This will be discussed in more detail in chapter 12. The peak roof acceleration response is used as the parameter to measure the optimum range of supplemental damping.

The relationship between the peak acceleration and the stiffness, mass, damping capacity can be given as (Vickery et al., 1983):

$$a_x \approx CK^{-5/8}M^{-3/8}\xi_t^{-1/2} \tag{11.1}$$

where $C$ = a constant of proportionality

$K$ = stiffness of the structure

$M$ = mass of the structure

$\xi_t$ = damping capacity of the structure

The damping capacity of the structure with the dampers is composed of the original viscous damping of the structure $\xi_0$ and the equivalent viscous damping due to the supplemental dampers $\xi_d$:

$$\xi_t = \xi_0 + \xi_d \tag{11.2}$$

It has been mentioned that the modal frequency of the structure does not vary significantly due to the presence of the supplemental dampers. Hence, the mass and stiffness will be approximately the same for both the structure without dampers and the structure with dampers. From Eqs(11.1) and (11.2), the ratio of the peak acceleration $r_a$ of the structure with the dampers to that of the original structure without dampers can be expressed as:

$$r_a = \frac{a_{x,d}}{a_{x,0}} = \sqrt{\frac{\xi_0}{\xi_0 + \xi_d}} \tag{11.3}$$

where $a_{x,d}$ = the peak acceleration of the structure with the supplemental dampers

$a_{x,0}$ = the peak acceleration of the original structure without dampers

$\xi_0$ = the viscous damping of the original structure

= 0.01 (for reinforced concrete building structures under the serviceability limit state)

The relationship between the acceleration ratio $r_a$ and the supplemental damping ratio $\xi_d$ is shown in Fig.11.11 and Table 11.6. Consider the range of the damping level due to the supplemental dampers $\xi_d$ from 0 – 50%. It can be observed that during the range 0 – 5% of supplemental damping, the reduction of the peak acceleration is most significant. Once the damping ratio due to the supplemental dampers is larger than 10%, continued increase in the damping ratio due to the supplemental dampers has very little effect on the acceleration response. For $\xi_d$ equal to 5%, the peak acceleration can be reduced by about 60%. For $\xi_d$ equal to 50%, the peak acceleration can be reduced by about 86%. About 70% of the possible reduction of peak acceleration that may occur for 50% supplemental damping can be achieved by providing only 5% supplemental damping. About 80% of the possible reduction of peak acceleration that may occur for 50% supplemental damping can be achieved by providing

only 10% supplemental damping. From economic considerations, usually 0% to 5% supplemental damping is provided.

| | Damper Yield Strength | | | |
|---|---|---|---|---|
| | $F_{yd}$ = 2.5 KN | $F_{yd}$ = 5 KN | $F_{yd}$ = 10 KN | $F_{yd}$ = 20 KN |
| Original structure | 19.475 | 19.475 | 19.475 | 19.475 |
| One damper at the 1st level only | 17.627 (reduced by 9.49%) | 15.958 (reduced by 18.06%) | 16.482 (reduced by 15.37%) | 15.860 (reduced by 18.56%) |
| One damper for every second storey | 15.144 (reduced by 22.24%) | 10.733 (reduced by 44.89%) | 8.892 (reduced by 54.34%) | 6.505 (reduced by 66.6%) |
| One damper for every storey | 10.468 (reduced by 46.25%) | 8.789 (reduced by 54.87%) | 7.263 (reduced by 62.71%) | 7.334 (reduced by 62.34%) |

Table 11.1 Comparison of the peak roof acceleration (milli-g) of the structure with different placements and damper yield strengths under wind gust loading

| | Damper Yield Strength | | | |
|---|---|---|---|---|
| | $F_{yd}$ = 2.5 KN | $F_{yd}$ = 5 KN | $F_{yd}$ = 10 KN | $F_{yd}$ = 20 KN |
| Original structure | 3.676 | 3.676 | 3.676 | 3.676 |
| One damper at the 1st level only | 3.595 (reduced by 2.2%) | 3.513 (reduced by 4.43%) | 3.352 (reduced by 8.81%) | 3.171 (reduced by 13.74%) |
| One damper for every second storey | 3.284 (reduced by 10.66%) | 2.821 (reduced by 23.26%) | 2.748 (reduced by 25.25%) | 2.662 (reduced by 27.58%) |
| One damper for each storey | 2.810 (reduced by 23.56%) | 2.745 (reduced by 25.33%) | 2.657 (reduced by 27.72%) | 2.477 (reduced by 32.62%) |

Table 11.2 Comparison of the peak roof displacement (cm) of the structure with different placements and damper yield strengths under wind loading

| | Peak roof acceleration (milli-g) | Peak roof displacement (cm) |
|---|---|---|
| Damper at every second storey $F_{yd}$ = 5KN | 10.733 | 2.821 |
| Damper at every storey $F_{yd}$ = 2.5KN | 10.468 | 2.810 |
| Difference | 2.53% | 0.39% |

Table 11.3 Comparison of the peak response of the structure with two different distributions of the dampers

| | Peak roof acceleration (milli-g) | Peak roof displacement (cm) |
|---|---|---|
| Damper at every second storey $F_{yd}$ = 10KN | 8.892 | 2.748 |
| Damper at every storey $F_{yd}$ = 5KN | 8.789 | 2.745 |
| Difference | 1.17% | 0.11% |

Table 11.4 Comparison of the peak response of the structure with two different distributions of the dampers

| | Without Dampers | With Dampers ($F_d$=2.5KN) | With Dampers ($F_d$= 5KN) | With Dampers ($F_d$= 10KN) | With Dampers ($F_d$= 20KN) |
|---|---|---|---|---|---|
| Natural frequencies | 0.5009 | 0.5009 | 0.5009 | 0.5024 | 0.5072 |
| Level | | | | | |
| 1 | 0.0499 | 0.04994 | 0.04995 | 0.05118 | 0.05412 |
| 2 | 0.1445 | 0.1445 | 0.1445 | 0.1481 | 0.1565 |
| 3 | 0.2485 | 0.2485 | 0.2485 | 0.2546 | 0.2690 |
| 4 | 0.3531 | 0.3531 | 0.3531 | 0.3618 | 0.3821 |
| 5 | 0.4639 | 0.4639 | 0.464 | 0.4752 | 0.5017 |
| 6 | 0.5742 | 0.5742 | 0.5743 | 0.5881 | 0.6203 |
| 7 | 0.6756 | 0.6756 | 0.6757 | 0.6917 | 0.7290 |
| 8 | 0.7658 | 0.7658 | 0.7658 | 0.7837 | 0.8247 |
| 9 | 0.8498 | 0.8498 | 0.8498 | 0.8691 | 0.9111 |
| 10 | 0.9202 | 0.9202 | 0.9202 | 0.9394 | 0.9721 |
| 11 | 0.9702 | 0.9702 | 0.9702 | 0.9843 | 0.9914 |
| 12 | 1 | 1 | 1 | 1 | 1 |

Table 11.5 1$^{st}$ mode natural frequencies and mode shape for the structure without dampers and the structure with different damper yield strength

| | $\xi_d = 5\%$ | $\xi_d = 10\%$ | $\xi_d = 15\%$ | $\xi_d = 20\%$ | $\xi_d = 50\%$ |
|---|---|---|---|---|---|
| Acceleration ratio $r_a$ | 0.4083 | 0.3015 | 0.25 | 0.2182 | 0.14 |
| Reduction of acceleration $(1- r_a)\times 100\%$ | 59.17% | 69.85% | 75% | 78.18% | 86% |
| Compare with respect to $\xi_d$ =50% | 68.8% | 81.22% | 87.21% | 90.91% | 100% |

Table 11.6 Comparison of the reduction of acceleration response with respect to supplemental damping level

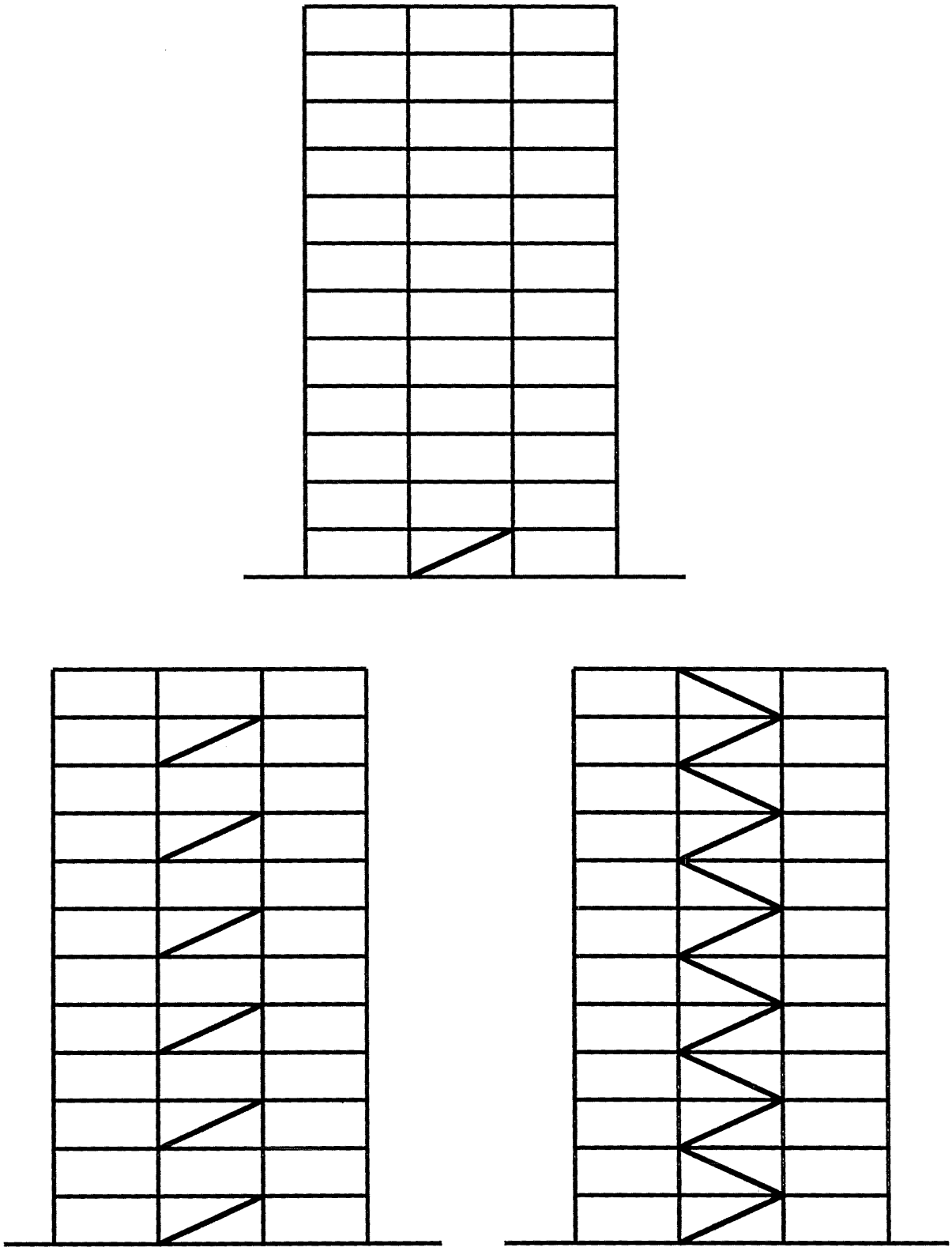

Figure 11.1 Three types of the placement of the supplemental dampers in the structure

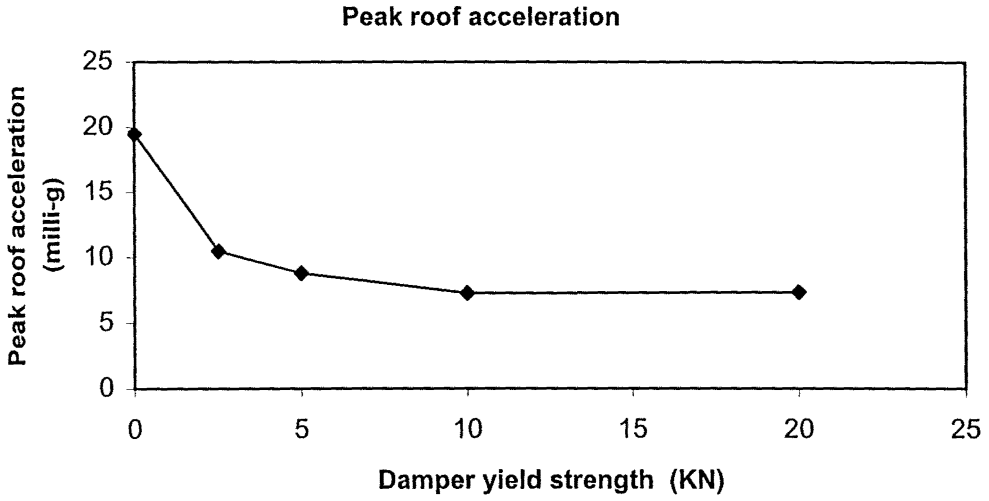


Figure 11.2 Variation of the peak roof acceleration with respect to the different damper yield strengths

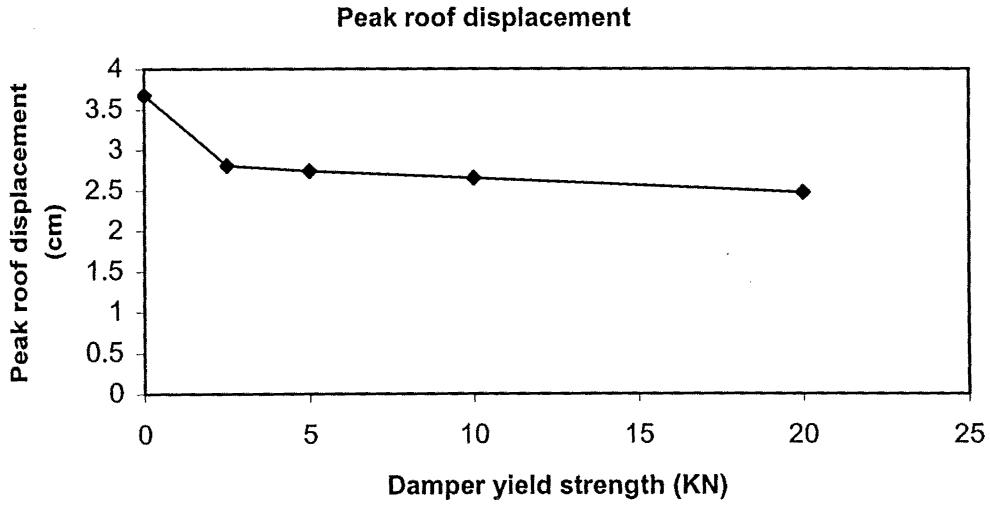


Figure 11.3 Variation of the peak roof displacement with respect to the different damper yield strengthss

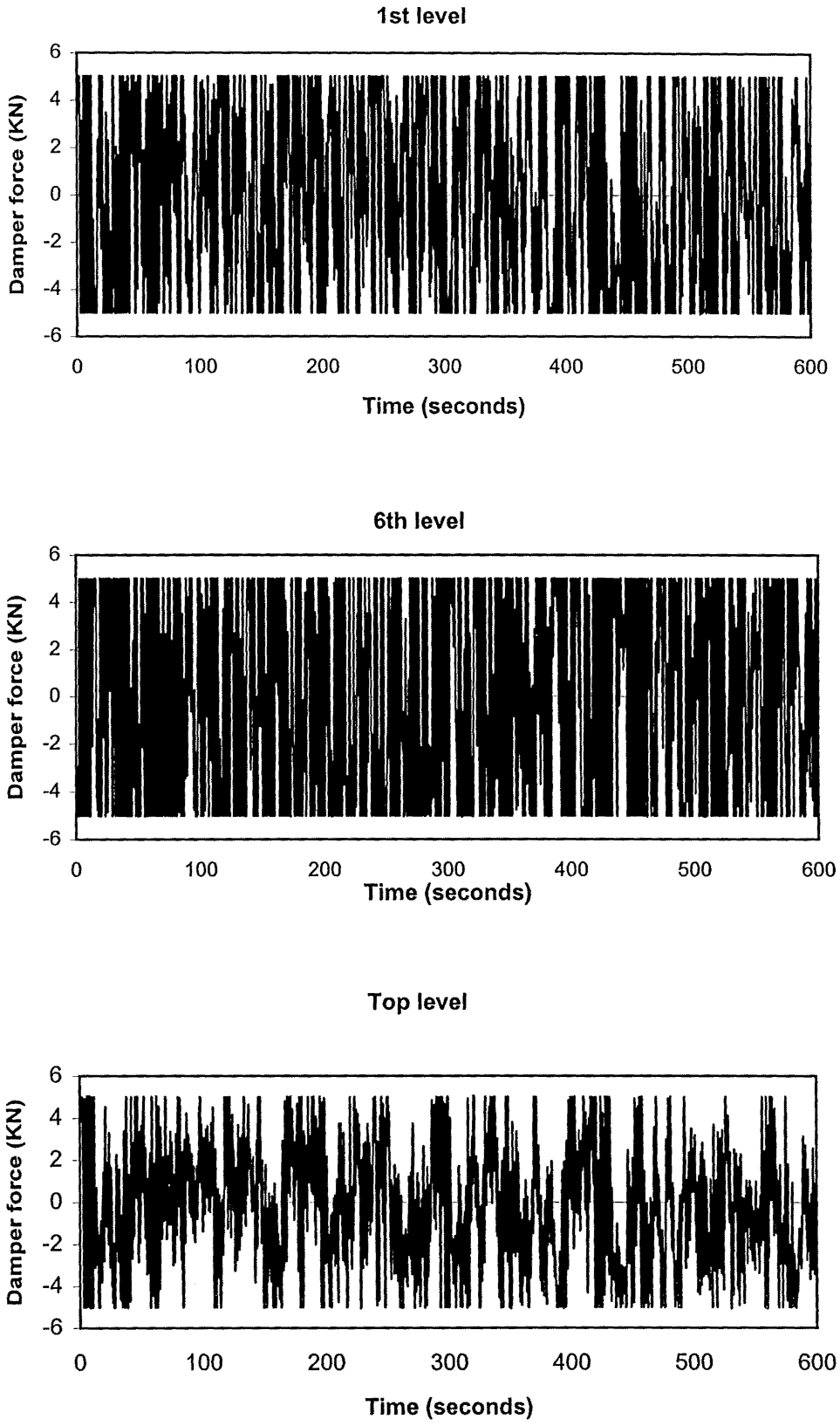


Figure 11.4 Damper force time histories for the structure with the dampers of 5KN yield strength

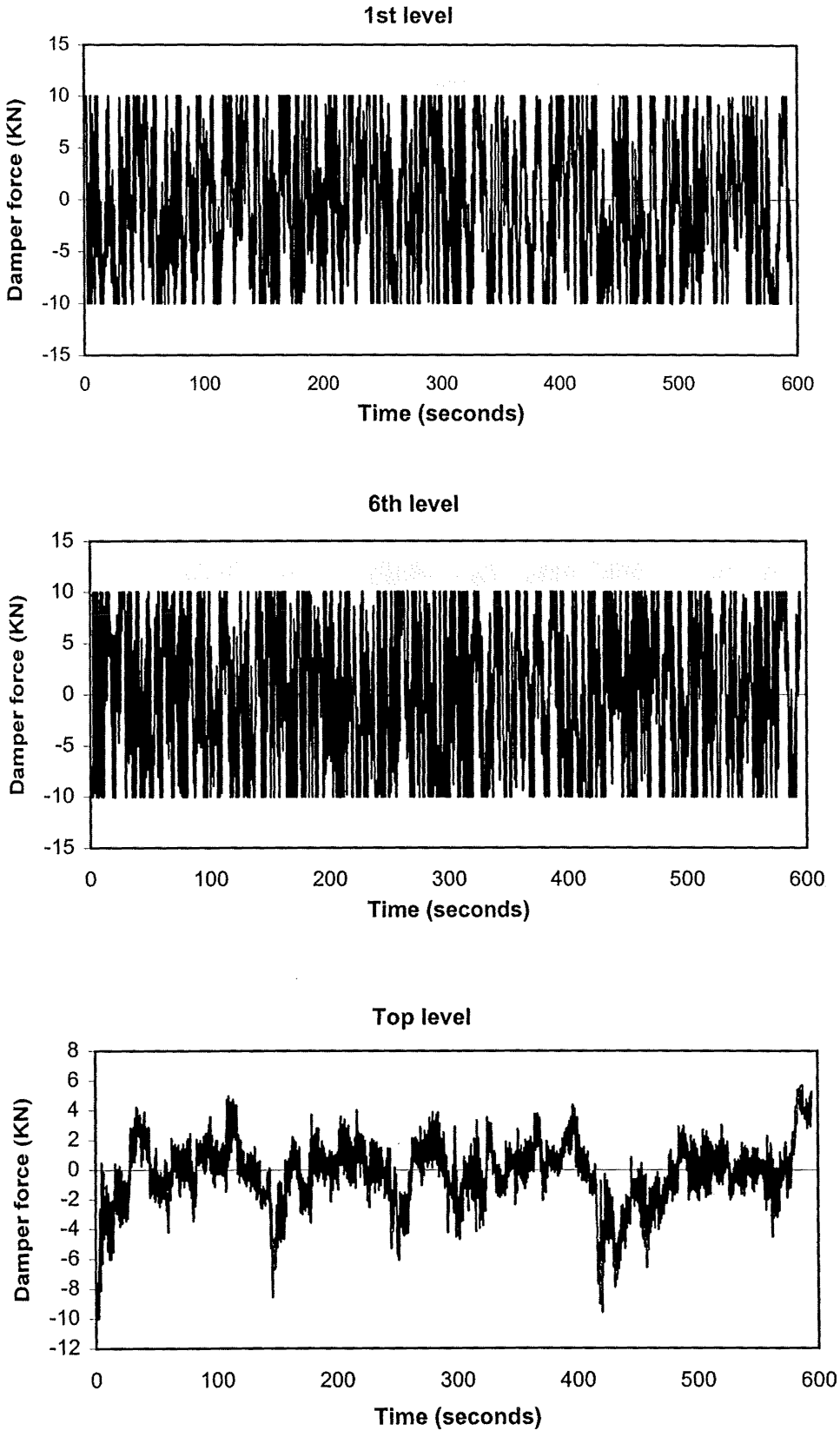


Figure 11.5 Damper force time histories for the structure with the dampers of 10KN yield strength

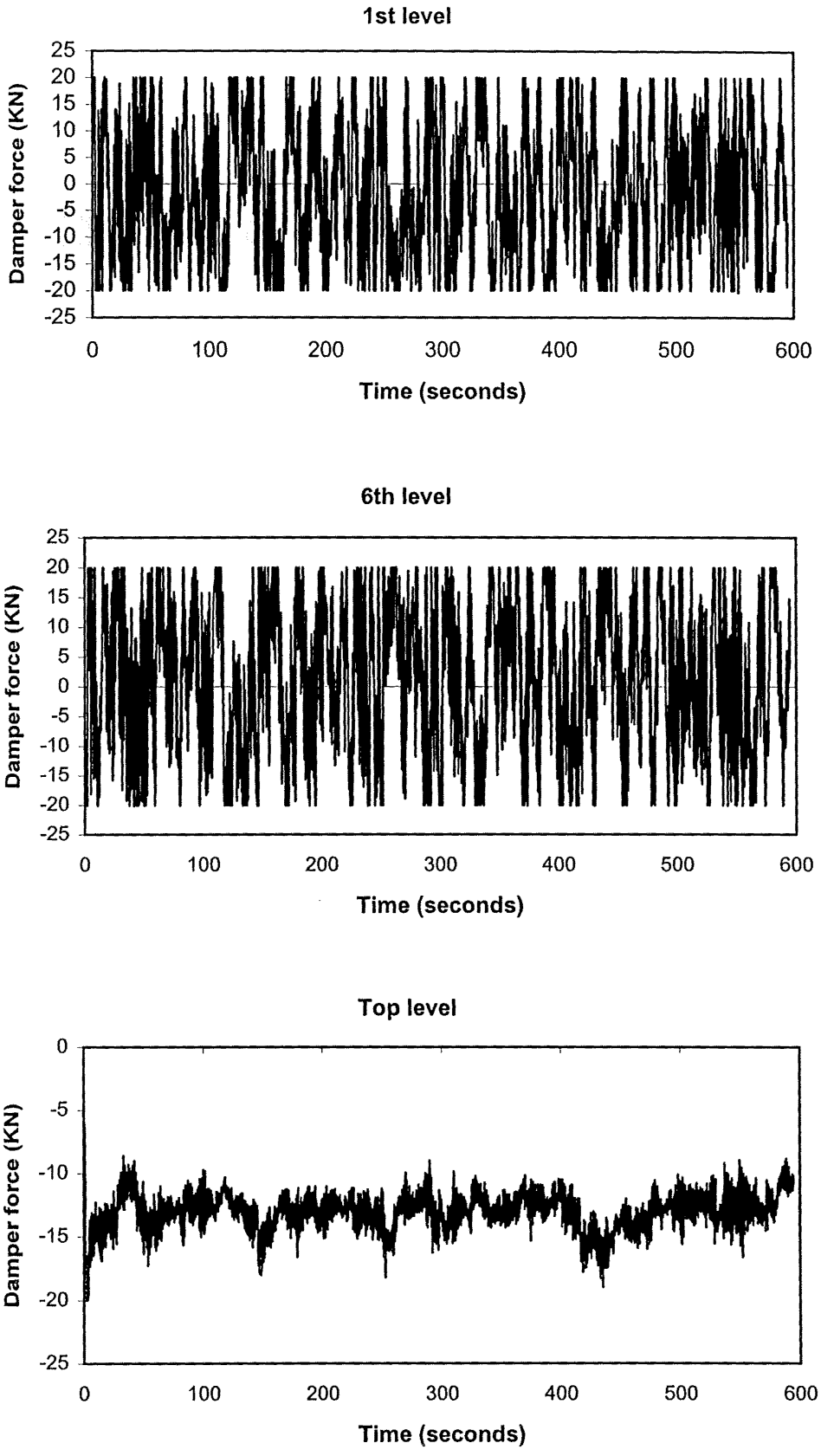


Figure 11.6 Damper force time histories for the structure with the dampers of 20KN yield strength

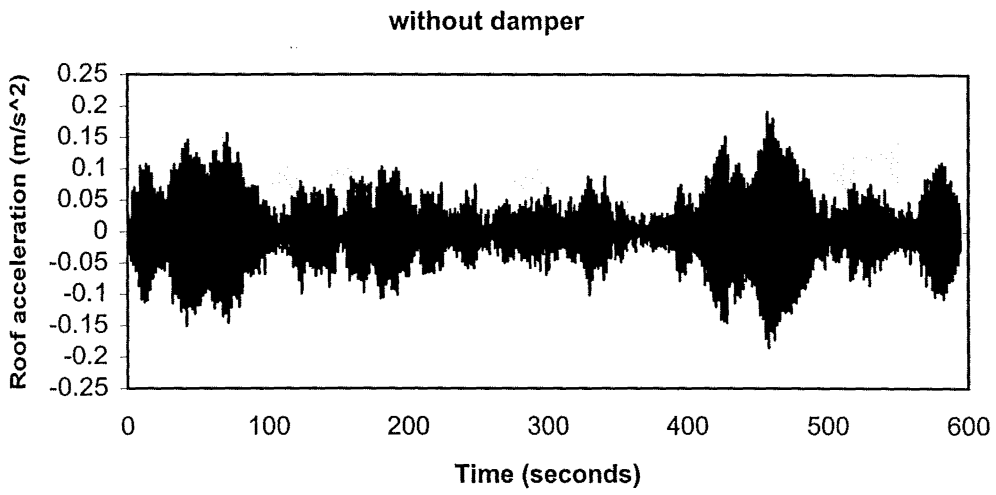


Figure 11.7 Roof acceleration time history for the structure without dampers

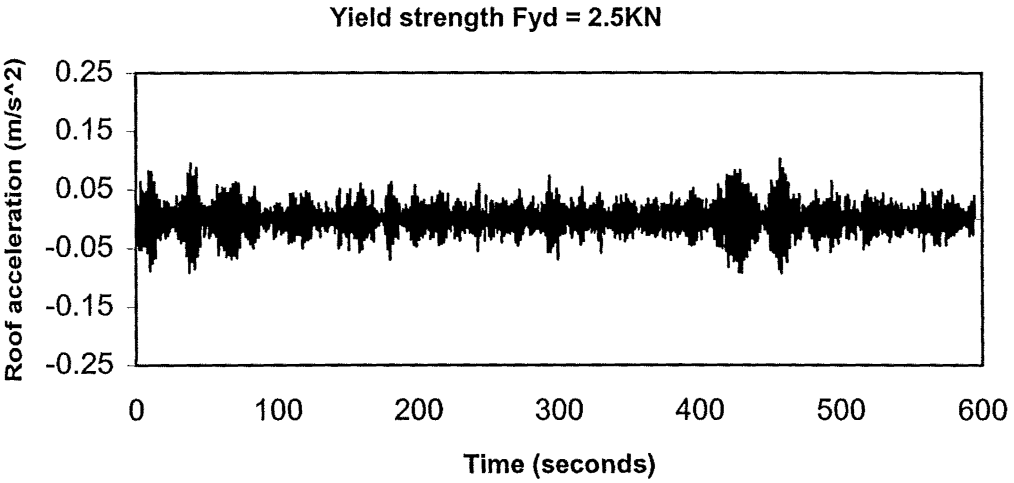


Figure 11.8 Roof acceleration time history for the structure with the 2.5KN-yield strength dampers

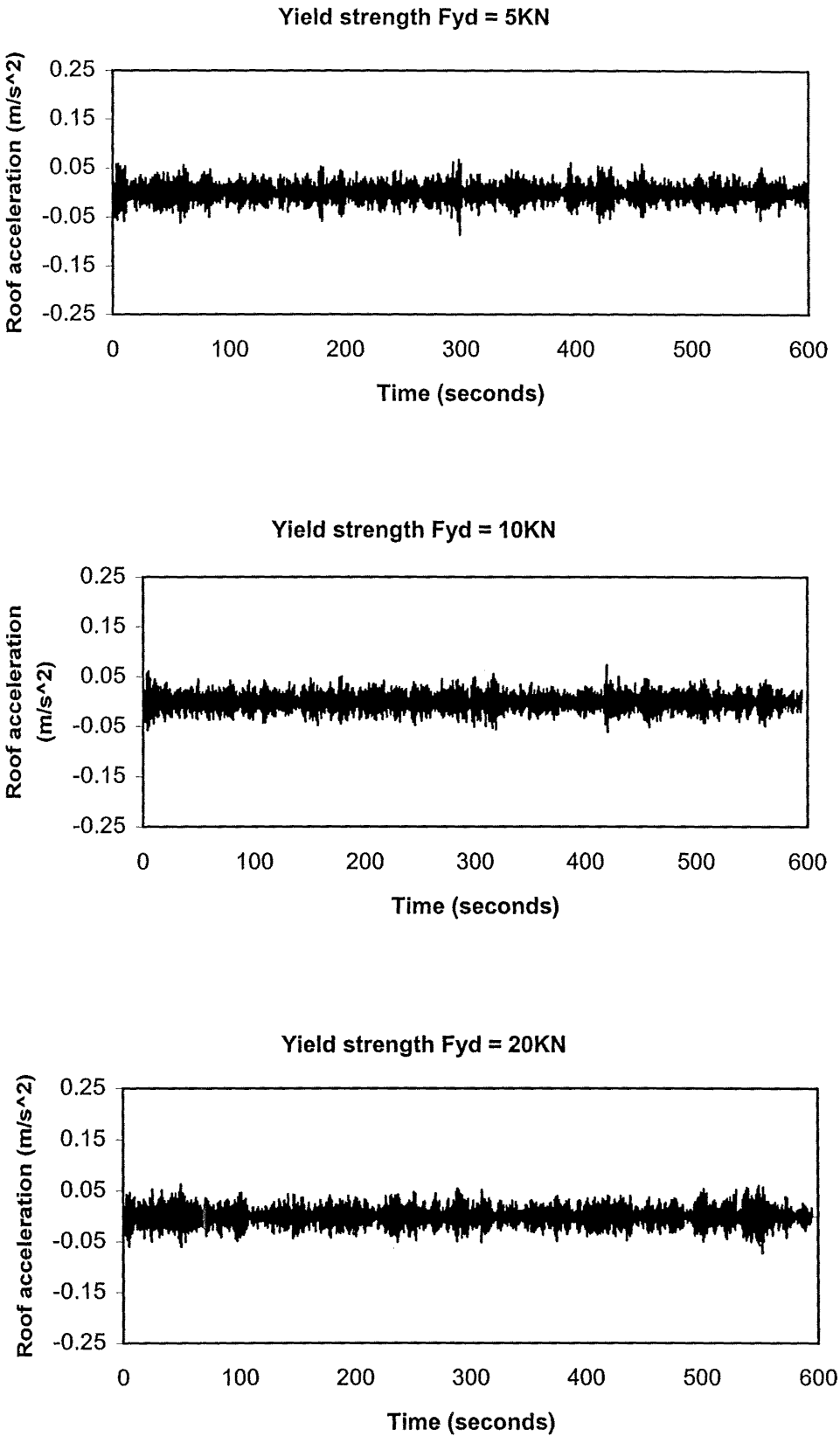


Figure 11.9 Roof acceleration time histories for the structure with 5KN, 10KN and 20KN-yield strength dampers

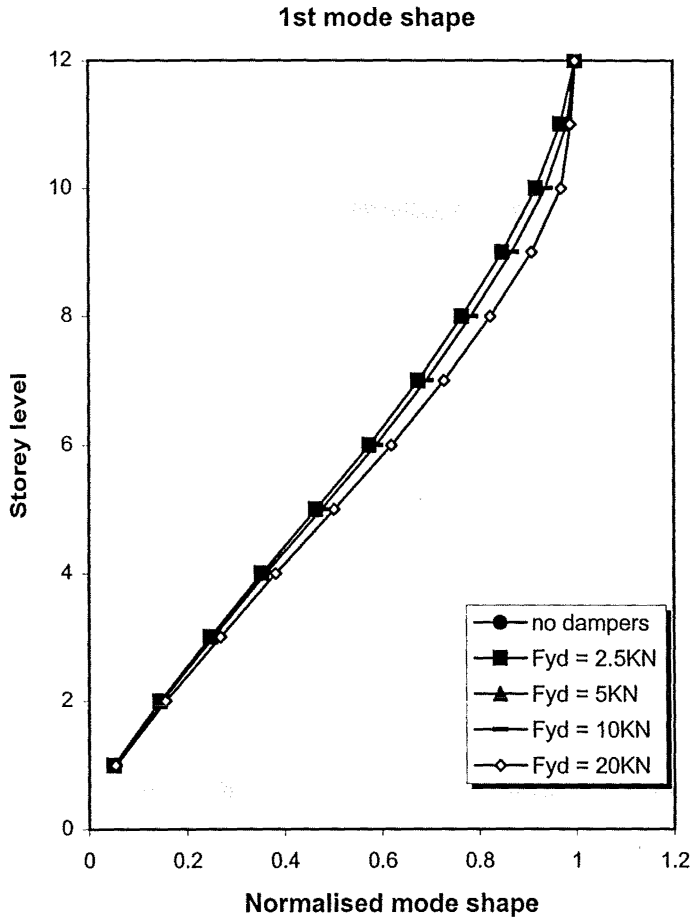


Figure 11.10 Normalised 1st mode shape for the structure without dampers and the structure with different yield-strength dampers

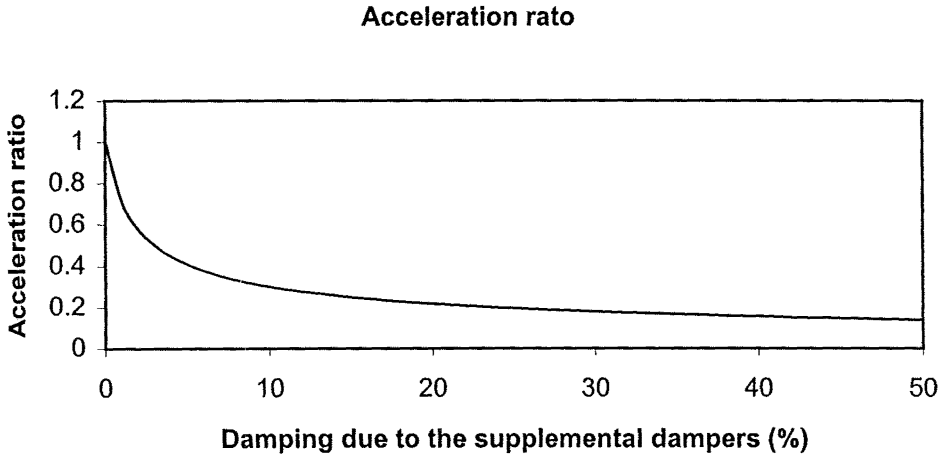


Figure 11.11 Acceleration ratio with respect to damping due to the supplemental dampers

# CHAPTER 12

# SIMPLIFIED ANALYSIS AND DESIGN OF THE STRUCTURE WITH THE SUPPLEMENTAL DAMPERS UNDER WIND GUSTS

Time-domain analyses of the structure with supplemental dampers using the artificial wind time history have been shown in last two chapters. In engineering practice, the frequency-domain method is widely used for analytical and design purposes. This chapter investigates the frequency-domain analysis method for the structure with supplemental dampers under wind loads. This leads to a simplified code-type method for design purposes.

## 12.1 CALCULATION OF ALONG-WIND DEFLECTION AND ACCELERATION

For a very small structure of area A placed in the atmospheric boundary layer, the bulk of the turbulent gust energy is at wavelengths much greater than a typical dimension of the structure (Davenport et al., 1975). The drag force experienced by the structure can be expressed as:

$$F(z,t) = \frac{1}{2}\rho C_D A V^2(z,t) \tag{12.1}$$

where $V(z,t) = \overline{V}(z) + v(z,t)$ = wind speed at a height $z$

$\rho$ = air mass density

$C_D$ = drag coefficient

Hence, Eq(12.1) becomes:

$$F(z,t) = \frac{1}{2}\rho C_D A\left[\overline{V}^2(z) + 2\overline{V}(z)v(z,t) + v^2(z,t)\right]$$

The drag force consists of the mean drag and the fluctuating drag:

$$F(z,t) = \overline{F}_D(z) + F'_D(z,t)$$

Ignoring terms of order $\left(\frac{v(z,t)}{\overline{V}(z)}\right)^2$, the mean drag is

$$\overline{F}_D(z)=\frac{1}{2}\rho C_D A\overline{V}^2(z) \tag{12.2}$$

and the fluctuating drag is

$$F'_D(z,t)=\rho C_D A\overline{V}(z)v(z,t) \tag{12.3}$$

The power spectrum of $F'_D(z,t)$ can be related to the velocity spectrum as follows (Davenport et al., 1975):

$$\begin{aligned} S_F(n) &= (\rho C_D A\overline{V})^2 S_v(n) \\ &= \frac{4\overline{F}^2}{\overline{V}^2} S_v(n) \end{aligned} \tag{12.4}$$

where $S_F(n)$, $S_v(n)$ = power spectrum of the fluctuating drag and velocity respectively.

The influence of the size of the disturbance in relation to the size of the structure is introduced through an 'aerodynamic admittance function' $\chi^2(\frac{f\sqrt{A}}{\overline{V}})$, so that the power spectrum of the fluctuating drag can be modified as (Davenport et al., 1975)

$$S_F(n)=\frac{4\overline{F}^2}{\overline{V}^2}\chi^2(\frac{f\sqrt{A}}{\overline{V}})S_v(n) \tag{12.5}$$

For AS1170, a size reduction factor $S$ is introduced as

$$S=\chi^2(\frac{n\sqrt{A}}{\overline{V}})=\frac{1}{\left[1+\frac{3.5nh}{\overline{V}_h}\right]\left[1+\frac{4nb}{\overline{V}_h}\right]} \tag{12.6}$$

where $h$, $b$ are the height and width of the structure respectively,

$\overline{V}_h$ is the mean velocity at height $h$.

From Eq(12.6), it can be seen that if $h$ and $b\rightarrow 0$, $S\rightarrow 1$; if $h$ and $b\rightarrow\infty$, $S\rightarrow 0$.

### 12.1.1 SDOF Structure

First, consider a linear single-degree-of-freedom structure with a natural frequency $n_1$, damping $\xi_0$ and a stiffness $k$. The equation of motion for the idealised SDOF structure under wind gust loading can be written as

$$m\ddot{x}(t) + c\dot{x}(t) + kx = \overline{F}_D + F'_D(t)$$

The displacement response of the structure due to loading by wind gusts is

$$x(t) = \bar{x} + x'(t) \tag{12.7}$$

where

$\bar{x}$ = mean component

$x'(t)$ = fluctuating component.

The mean or static component of the response is

$$\bar{x} = \frac{\overline{F}_D}{k} \tag{12.8}$$

The spectrum of the displacement response can be expressed as (Davenport et al., 1975)

$$S_x(n) = \frac{|H(n)|^2}{k^2} S_F(n) \tag{12.9}$$

in which $H(n)$ is the mechanical admittance function and

$$|H(n)|^2 = \frac{1}{\left[1 - \left(\frac{n}{n_1}\right)^2\right]^2 + 4\xi^2\left(\frac{n}{n_1}\right)^2} \tag{12.10}$$

The variance of the fluctuating component of the displacement (or rms, root-mean-square, response of the displacement) is

$$\sigma_x^2 = \frac{1}{k^2}\int_0^\infty S_F(n)\left|H(n)\right|^2 dn \tag{12.11}$$

Since the effect of $|H(n)|^2$ is significant only at resonance, the above integral in Eq(12.11) can be simplified by dividing it into two parts: a background (or broad band or quasi-static) response and the resonant (or narrow band) response. Eq(12.11) can be approximated by

$$\begin{aligned}\sigma_x^2 &= \frac{1}{k^2}\left[\int_0^{n_1} S_F(n)dn + S_F(n_1)\int_0^\infty |H(n)|^2 dn\right] \\ &= \frac{1}{k^2}\left[\int_0^{n_1} S_F(n)dn + \frac{\pi n_1 S_F(n_1)}{4\xi_0}\right] \\ &= \frac{1}{k^2}\left[\sigma_{BF}^2 + \sigma_{DF}^2\right] = \sigma_{Bx}^2 + \sigma_{Dx}^2\end{aligned} \tag{12.12}$$

where $\sigma_{BF}$, $\sigma_{DF}$ = the standard deviation (rms) of the background (non-resonant) component and the resonant component of the fluctuating force respectively

$\sigma_{Bx}$, $\sigma_{Dx}$ = the standard deviation (rms) of the background (non-resonant) component and the resonant component of the displacement respectively

The resonant component of the rms displacement corresponds to the contribution from the dynamic amplification of frequency components near $n_1$ and the background component corresponds to excitation by low frequencies.

Substitute Eq(12.5) into Eq(12.12) and express the velocity spectrum in the normalised form:

$$\sigma_x^2 = 4\frac{\overline{F}_D^2}{k^2}\frac{\sigma_v^2}{\overline{V}^2}\left[\int_0^{n_1} \chi^2\left(\frac{n\sqrt{A}}{\overline{V}}\right)\frac{S_v(n)}{\sigma_v^2}dn + \chi^2\left(\frac{n_1\sqrt{A}}{\overline{V}}\right)\frac{S_v(n_1)}{\sigma_v^2}\frac{\pi n_1}{4\xi_0}\right] \tag{12.13}$$

Let

$$
\begin{aligned}
B &= \int_0^{n_1} \chi^2\left(\frac{n\sqrt{A}}{\bar{V}}\right)\frac{S_v(n)}{\sigma_v^2}dn \\
E &= \frac{\pi}{4}\frac{n_1 S_v(n_1)}{\sigma_v^2} \\
S &= \chi^2\left(\frac{n_1\sqrt{A}}{\bar{V}}\right) \\
r &= 2\frac{\sigma_v}{\bar{V}}
\end{aligned}
\tag{12.14}
$$

Eq(12.13) becomes

$$
\frac{\sigma_x^2}{\bar{x}^2} = r^2\left(B + \frac{SE}{\xi_0}\right) \tag{12.15}
$$

and

$$
\begin{aligned}
\sigma_{Bx} &= r\bar{x}\sqrt{B} \\
\sigma_{Dx} &= r\bar{x}\sqrt{\frac{SE}{\xi_0}}
\end{aligned}
\tag{12.16}
$$

$$
\begin{aligned}
\frac{\sigma_{BF}^2}{\bar{F}_D^2} &= r^2 B \\
\frac{\sigma_{DF}^2}{\bar{F}_D^2} &= r^2\frac{SE}{\xi_0}
\end{aligned}
\tag{12.17}
$$

Then the ratio of the rms to the mean displacement is

$$
\frac{\sigma_x}{\bar{x}} = r\left(B + \frac{SE}{\xi_0}\right)^{\frac{1}{2}} \tag{12.18}
$$

The expected peak displacement is

$$\begin{aligned} x_{\max} &= \hat{x} \\ &= \bar{x} + x'_{\max} \\ &= \bar{x} + g_f \sigma_x \\ &= \bar{x}\left[1 + r g_f \left(B + \frac{SE}{\xi_0}\right)^{\frac{1}{2}}\right] \end{aligned} \tag{12.19}$$

where $g_f$ = a peak factor.

The gust factor $G$ is

$$G = \frac{\hat{x}}{\bar{x}} = 1 + r g_f \left(B + \frac{SE}{\xi_0}\right)^{\frac{1}{2}} \tag{12.20}$$

The accelerations of the structure under wind excitations are due almost entirely to the "resonant peak" (Vickery et al., 1983). Hence the rms acceleration can be obtained from the resonant component of the rms displacement as follows (Davenport et al., 1975, Cenek et al., 1990):

$$\sigma_{\ddot{x}} = (2\pi n_1)^2 \sigma_{Dx} = (2\pi n_1)^2 \bar{x} \sqrt{\frac{r^2 SE}{\xi_0}} \tag{12.21}$$

where $\sigma_{\ddot{x}}$ = rms acceleration

And the peak acceleration $a_x$ is given by

$$\begin{aligned} a_x &= g_f \sigma_{\ddot{x}} \\ &= g_f (2\pi n_1)^2 \bar{x} \sqrt{\frac{r^2 SE}{\xi_0}} \end{aligned} \tag{12.22}$$

### 12.1.2 MDOF Structure

The analysis described above can be extended to MDOF structures. Mode superposition is necessary to calculate the along-wind response for MDOF structures. ESDU (1976) presented

a frequency-domain method for flexible structures using the modal superposition method. In the following section, the time-domain modal analysis of the structure will be performed to see how great the higher mode effect is.

Modal Analysis

For an elastic multi-degree-of-freedom structure, the equation of motion is

$$[M]\{\ddot{u}(t)\}+[C]\{\dot{u}(t)\}+[K]\{u(t)\}=\{\overline{F}_D(z)\}+\{F'_D(z,t)\} \tag{12.23}$$

where

$\{u(t)\},\{\dot{u}(t)\},\{\ddot{u}(t)\}$ = displacement, velocity and acceleration vectors respectively,
$[M],[C],[K]$ = mass, damping and stiffness matrices respectively,
$\{\overline{F}_D(z)\},\{F'_D(z,t)\}$ = the mean drag and the fluctuating drag force vector respectively.

In the wind resistant design, structural members should not be in the inelastic region in a strong wind of long duration, especially at the Serviceability Limit State. Therefore, the structure is assumed to respond within the elastic region (supplemental dampers are not included here) and the modal superposition method is valid. The displacement of the structure can be expressed as

$$\{u(t)\}=\sum_{r=1}^{N_r} x_r(t)\{\phi_r\} \tag{12.24}$$

where

$\{\phi_r\}$ = the $r$th mode-shape vector
$x_r(t)$ = generalized displacement of the $r$th mode

Pre-multiply both sides of Eq(12.23) by $\{\phi\}^T$ and substitute Eq(12.24) into Eq(12.23). From the orthogonality properties of the normal modes of free vibration, Eq(12.23) can be uncoupled into a set of SDOF equations of motion.

$$m_r^*\ddot{x}_r(t)+c_r^*\dot{x}_r(t)+k_r^*x_r(t)=\{\phi_r\}^T\{\overline{F}_D(z)\}+\{\phi_r\}^T\{F'_D(z,t)\} \qquad (r=1,2,\cdots\cdots,N_r) \tag{12.25}$$

where

$m_r^* = \{\phi_r\}^T [M]\{\phi_r\} = \sum m_i \phi_{ri}^2$ (for lumped masses)

$c_r^* = \{\phi_r\}^T [C]\{\phi_r\}$

$k_r^* = \{\phi_r\}^T [K]\{\phi_r\}$

Eq(12.25) can also be expressed as

$$\ddot{x}_r(t) + 2\xi_r \omega_r \dot{x}_r(t) + \omega_r^2 x_r(t) = \left[\{\phi_r\}^T \{\overline{F}_D(z)\} + \{\phi_r\}^T \{F_D'(z,t)\}\right] / m_r^* \quad (r = 1,2,\cdots\cdots, N_r) \tag{12.26}$$

where

$$\omega_r^2 = \frac{k_r^*}{m_r^*} \tag{12.27}$$

From Eq(12.25) we can see that the solution for the MDOF structure involves no more than the solution of a set of equations each corresponding to a SDOF structure as discussed above.

A MDOF time-history analysis of the 12-storey 3-bay frame structure subjected to wind gust excitation was carried out together with a set of SDOF time-domain modal analyses. Two modes were considered and their properties are listed in Tables 12.1 and 12.2. The comparison of the results for the modal analysis and the MDOF structure is shown in Table 12.3.

From Table 12.3 it can be seen that in this structure the higher mode effect is not significant. It is expected that for the structure with supplemental dampers, the first mode effect becomes more predominant. For this study, it was assumed that the higher modes make a negligible contribution to the total response, hence only the first mode response is taken into account.

It is known that the supplemental dampers have nonlinear characteristics. Strictly speaking, the modal analysis method may not be valid for the structure with the supplemental dampers. However, under the Serviceability Limit State the main structure will remain elastic. It has been shown that for a wind-resistant structure, the supplemental dampers have very little effect on the modal characteristics of the structure. The forces in the dampers are very small compared with the internal forces in the structure. The effect of the supplemental dampers may be taken into account by means of the equivalent viscous damping ratio and the total response can be analysed with a modal analysis. During this modal analysis, only the first mode is considered. The frequency-domain method in Australia Standard AS 1170 part 2 is adopted.

With reference to Australia Standard AS 1170 Part 2, since the Australia code gust factor is based on moment, rather than force spectra, Eq(12.17) becomes (Cenek et al., 1990):

$$\frac{\sigma_{BM}^2}{\overline{M}^2} = r^2 B(1+w)^2$$
$$\frac{\sigma_{DM}^2}{\overline{M}^2} = r^2 \frac{SE}{\xi_0} \tag{12.28}$$

where $\overline{M}$ = mean overturning moment of the structure

$w$ = a factor to account for the second order effects of turbulence.

The relationship between the spectral modal force and the spectral overturning moment is (Cenek et al., 1990):

$$n_1 S_F(n_1) = \frac{n_1 S_M(n_1)}{h^2} \tag{12.29}$$

where $h$ = the height of the structure.

Hence,

$$\sigma_{DF} = \frac{\sigma_{DM}}{h} \tag{12.30}$$

where $\sigma_{DM}$ = the standard deviation of the resonant dynamic component of overturning moment.

From Eqs(12.12), (12.28) and (12.30), we have:

$$\sigma_{Dx} = \frac{\sigma_{DF}}{k} = \frac{\overline{M}}{kh}\sqrt{\frac{r^2 SE}{\xi}} \tag{12.31}$$

This corresponds to Eq(12.16).

Eq(12.21) becomes:

$$\sigma_{\ddot{x}} = (2\pi n_1)^2 \sigma_{Dx} = (2\pi n_1)^2 \frac{\overline{M}}{kh}\sqrt{\frac{r^2 SE}{\xi_0}} \tag{12.32}$$

The peak roof acceleration is:

$$a_x = g_f \sigma_{\ddot{x}} = g_f (2\pi n_1)^2 \frac{\overline{M}}{kh}\sqrt{\frac{r^2 SE}{\xi_0}} \tag{12.33}$$

Assuming a linear mode shape and uniform mass distribution, the modal mass (for the 1st mode) can be expressed as:

$$M^* = \int_0^h m(z)\phi(z)^2 dz = \overline{m}\int_0^h \left(\frac{z}{h}\right)^2 dz = \frac{1}{3}\overline{m}h = \frac{1}{3}M_b$$

where $\overline{m}$ = mass per unit height,

$\phi(z)$ = mode shape,

$M_b$ = total mass of the structure.

Hence,

$$k = \omega^2 M^* = (2\pi n_1)^2 \frac{1}{3}M_b \tag{12.34}$$

Substituting Eq(12.34) into Eq(12.33) gives:

$$a_x = g_f \sigma_{\ddot{x}} = g_f \frac{3\overline{M}}{M_b h}\sqrt{\frac{r^2 SE}{\xi_0}} \tag{12.35}$$

This is the equation already given in chapter 10 (Eq(10.31)).

The gust factor G has been given in chapter 10 (Eq(10.24)). The expected peak response for displacement and overturning moment can be obtained through Eq(10.30).

## 12.2 EQUIVALENT VISCOUS DAMPING OF THE MDOF STRUCTURE

The modal strain energy method introduced in chapter 7 is adopted here to estimate the equivalent viscous damping ratio provided by the supplemental dampers.

The strain energy of the structure with the supplemental dampers can be expressed as:

$$E_s^r = \frac{1}{2}\{u_r\}^T [K]\{u_r\} \tag{12.36}$$

where $E_s^r$ = strain energy of the $r$th mode of the structure with the dampers,

$\{u_r\}$ = the $r$th mode displacement vector of the structure at the target displacement,

$[K]$ = stiffness matrix of the structure.

$$\{u_r\} = \{\phi_r\} x_{t,r} \tag{12.37}$$

in which $x_{t,r}$ = the roof displacement of the structure at the $r$th mode,

$\{\phi_r\}$= the $r$th mode shape of the structure.

Substitute Eq(12.37) into Eq(12.36) and use the orthogonality properties of the mode shape:

$$\begin{aligned} E_s^r &= \frac{1}{2}\{\phi_r\}^T [K]\{\phi_r\} x_{t,r}^2 \\ &= \frac{1}{2} K_r^* x_{t,r}^2 \\ &= \frac{1}{2}\omega_r^2 m_r^* x_{t,r}^2 = \frac{1}{2}\omega_r^2 \left(\sum_{i=1}^{N} m_i \phi_{ir}^2\right) x_{t,r}^2 \end{aligned} \tag{12.38}$$

where $\omega_r$ = circular frequency of the $r$th mode,

$N$ = total number of storeys of the structure,

$m_i$ = the mass at level $i$,

$m_r^* = \{\phi\}_r^T [M]\{\phi\} = \sum_{i=1}^{N} m_i \phi_{ir}^2$ = the effective mass at the $r$th mode.

All the supplemental dampers have an elasto-plastic force-deformation relationship. Hence, the energy dissipated by the dampers per cycle for the rth mode can be expressed as:

$$\begin{aligned} E_{di}^{r} &= 4F_{di}\left(\Delta_i - \Delta_{yi}\right) \\ \Delta_i &= \left(\phi_{i,r} - \phi_{i-1,r}\right)x_{t,r}\cos\theta \end{aligned} \tag{12.39}$$

where $E_{di}^{r}$ = energy dissipated by the dampers per cycle for the $r$th mode,

$\Delta_i$ = deformation of the dampers at level $i$ at the target displacement,

$\Delta_{yi}$ = yield deformation of the damper at level $i$,

$\phi_{i,r}$ = value of the $r$th normalised mode shape at level $i$,

$\theta$ = slope of the damper-brace with respect to the floor.

It is assumed that the same dampers are placed at each storey. Hence

$$\begin{aligned} F_{di} &= F_d \\ \Delta_{yi} &= \Delta_y \end{aligned}$$

Then, Eq(12.39) becomes:

$$\begin{aligned} E_d^r &= \sum_{i=1}^{N} E_{di}^r \\ &= \sum_{i=1}^{N} 4F_d\left(\Delta_i - \Delta_y\right) \\ &= 4F_d \sum_{i=1}^{N}\left[\left(\phi_{i,r} - \phi_{i-1,r}\right)x_{t,r}\cos\theta - \Delta_y\right] \end{aligned} \tag{12.40}$$

The equivalent viscous damping ratio due to the supplemental dampers can be estimated through Eq(7.8). Substitute Eq(12.40) and (12.38) into Eq(7.8):

$$\begin{aligned} \xi_r &= \frac{E_d^r}{4\pi E_s^r} \\ &= \frac{2}{\pi}\frac{F_d\sum_{i=1}^{N}\left[\left(\phi_{i,r} - \phi_{i-1,r}\right)x_{t,r}\cos\theta - \Delta_y\right]}{\omega_r^2\left(\sum_{i=1}^{N} m_i\phi_{i,r}^2\right)x_{t,r}^2} \end{aligned} \tag{12.41}$$

where $\xi_r$ = the equivalent viscous damping ratio due to the supplemental dampers for the $r$th vibration mode.

For the equivalent viscous damping for the 1st mode, Eq(12.41) can be further simplified as:

$$\xi_1 = \frac{2}{\pi} \frac{F_d \left[\phi_{N,1} x_t \cos\theta - N\Delta_y\right]}{\omega_1^2 \left(\sum_{i=1}^{N} m_i \phi_{i,1}^2\right) x_{t,r}^2} \tag{12.42}$$

where $\phi_{N,1}$ = value of the normalised first mode shape at the roof level ( = 1),

$N$ = number of storeys,

$\omega_1$ = circular frequency of the structure at the first mode.

It is assumed that the supplemental dampers in the structure will not change the modal characteristics of the main structure. Hence, the mode shapes and circular frequencies are taken as those of the original structure without the dampers.

Eq(12.41) depends on the roof displacement, $x_t$. Since the displacement response is mainly in the first mode, Eq(12.41) may be used for estimating the first mode damping ratio only. In the higher modes, the displacement response becomes very small. When dividing an extremely small number by another extremely small number, large errors may occur. This is the case in Eq(12.41) when applying it to the higher modes. In trying this, it was found that the iteration would not even converge. Hence, only the first mode equivalent damping ratio may be estimated by Eqs(12.41) or (12.42).

## 12.3 SIMPLIFIED ANALYSIS OF THE STRUCTURE WITH SUPPLEMENTAL DAMPERS UNDER WIND GUST LOADING

The equivalent viscous damping ratio due to the supplemental dampers can be estimated using Eq(12.42). Once the equivalent viscous damping ratio is known, the total damping ratio (due to the original damping of the structure and the supplemental dampers) can be calculated. By means of Eqs(12.32), (12.35), (10.24) and (10.30) the response of the structure with the dampers can be estimated. However, the equivalent viscous damping due to the supplemental dampers is dependent upon the target roof displacement, $x_t$, and this is not

known prior to the analysis. Iteration is needed to estimate the equivalent damping ratio due to the supplemental dampers.

It is known that displacement of the structure subjected to wind gust excitations consists of three components: the mean displacement, the background (or quasi-static) component and the resonant component. The mean value is a static value and is not affected by the damping at all. The background (or quasi-static) component varies slowly during excitations and is only slightly influenced by the dynamic characteristics of the structure and is virtually quasi-static. The component that may be influenced by the supplemental dampers is the resonant component. The target displacement in Eq(12.42) should be the peak resonant component of roof displacement.

From Eq(12.19) we have:

$$x_t = g_f \sigma_{Dx} \tag{12.43}$$

where $g_f$ = a peak factor defined by Eq(10.25).

Substituting Eq(12.31) into Eq(12.43):

$$x_t = g_f \sigma_{Dx} = g_f \frac{\overline{M}}{kh}\sqrt{\frac{r^2 SE}{\xi}} = g_f \frac{3\overline{M}}{(2\pi n_1)^2 M_b h}\sqrt{\frac{r^2 SE}{\xi}} \tag{12.44}$$

From the preceding development, the simplified analytical procedure can be established as follows:

Step 1: Assume an equivalent viscous damping ratio due to the supplemental dampers $\xi_d$. The initial damping ratio of the original structure is $\xi_0$. The total damping ratio is therefore $(\xi_0+\xi_d)$.

Step 2: The peak resonant dynamic roof displacement can be estimated through Eq(12.44)

Step 3: The equivalent viscous damping ratio due to the supplemental dampers $\xi'_d$ can be estimated from Eq(12.42).

Step 4: Compare $\xi'_d$ with $\xi_d$. If the difference is large, let $\xi_d = \xi'_d$ and go back to Step 2. If the difference is small enough, go to Step 5.

Step 5: Calculate the structural response through Eqs(12.35), (10.24) and (10.30).

Example:

A 12-storey 3-bay frame structure (as shown in chapter 3) with supplemental dampers at all storeys using diagonal braces is analysed using the simplified procedure as follows. Only the 1st mode effect is considered.

From Chapter 10, it is known that:

the 1st mode natural frequency is: $n_1 = 0.50\text{Hz}$, $\omega_1 = 2\pi n_1 = 3.1473$

the height of the structure is: $h = 43.8\text{m}$

the total building mass is: $M_b = 1446.58\times10^3\text{kg}$

the mean along-wind overturning moment and the mean displacement is:

$\overline{M} = 3662.7947\text{KN-m}$, $\bar{x} = 1.326\times10^{-2}\text{m}$

the effective mass for the 1st mode is:

$\sum m_i\phi_i^2 = 623.839(\times10^3\text{kg})$

The damper yield strength is taken as $F_d$ = 5KN; the initial stiffness of the dampers is $K_d$ = 398KN/mm, then, $\Delta_y = \dfrac{F_d}{K_d} = 1.256\times10^{-5}\text{m}$.

The Serviceability Limit State is under consideration, the initial viscous damping of the structure is $\xi_0 = 1\%$ .

From chapter 10:

$$L_h = 1000\left(\frac{h}{10}\right)^{0.25} = 1446.67$$

$$N = \frac{n_1 L_h}{\bar{V}_h} = 24.036$$

$$E = \frac{0.47N}{\left(2+N^2\right)^{5/6}} = 0.05627$$

$$B = \frac{1}{1 + \frac{\sqrt{(36h^2 + 64b^2)}}{L_h}} = 0.8441$$

$$w = \frac{g_v r\sqrt{B}}{4} = 0.2228$$

$$S = \frac{1}{\left[1 + \left(\frac{3.5n_1 h}{\overline{V}_h}\right)\right]\left[1 + \left(\frac{4n_1 b}{\overline{V}_h}\right)\right]} = 0.2016$$

Step 1: Assume $\xi_d = 5\%$.

Step 2:

$$x_t = g_f \frac{3\overline{M}}{(2\pi n_1)^2 M_b h} r\sqrt{\frac{SE}{\xi_0 + \xi_d}}$$

$$= 3.8718 \times \frac{3 \times 3662.7947}{(2\pi \times 0.5009)^2 \times 1446.58 \times 43.8} \times 0.2622\sqrt{\frac{0.2016 \times 0.05627}{1\% + 5\%}}$$

$$= 7.729 \times 10^{-3}\,\text{m}$$

Step 3:

$$\xi_d' = \frac{2}{\pi} \times \frac{5 \times \left(7.729 \times 10^{-3} \times 0.91 - 12 \times 1.256 \times 10^{-5}\right)}{3.1473^2 \times 623.839 \times \left(7.729 \times 10^{-3}\right)^2} = 5.94\%$$

Step 4: $\frac{\xi_d' - \xi_d}{\xi_d} \times 100\% = \frac{5.94 - 5}{5} \times 100\% = 18.8\%$ The difference is large.

Let $\xi_d = 5.94\%$ and go to Step 2.

Step 2-1: $x_t = 7.186 \times 10^{-3}$m

Step 3-1: $\xi_d' = 6.37\%$

Step 4-1: The difference = 7.24%. Hence carry out further iteration. Let $\xi_d = 6.37\%$ and go to Step 2.

Step 2-2: $x_1 = 6.974\times10^{-3}$m

Step 3-2: $\xi_d' = 6.56\%$

Step 4-2: The difference is 2.98%. Small enough! Let $\xi_d = 6.56\%$ Go to Step 5

Step 5:

$$a_x = 3.8718\times\frac{3\times3662.7947}{1446.58\times43.8}\sqrt{\frac{0.2622^2\times0.2016\times0.05627}{1\%+6.56\%}} = 0.0682\,(\text{m/s}^2)$$

$$G = 1+r\sqrt{\left[g_v^{\,2}B(1+w)^2+\frac{g_f^{\,2}SE}{\xi}\right]}$$

$$= 1+0.2622\times\sqrt{3.7^2\times0.8441\times(1+0.2228)^2+\frac{3.8718^2\times0.2016\times0.05627}{1\%+6.56\%}}$$

$$= 2.1587$$

$$\hat{x} = G\overline{x} = 2.1587\times1.326\times10^{-2} = 2.862\times10^{-2}\,\text{m}$$

The time-domain analysis of the structure with the dampers was also performed using the artificial wind time history. Comparison of the results from the simplified analysis and the time-domain analysis is also shown in Table 12.4. It can be seen that the simplified analysis can give good estimates of the peak response of the structure with the supplemental dampers.

## 12.4 DESIGN OF THE YIELD STRENGTHS OF THE DAMPERS IN THE STRUCTURE

### 12.4.1 Design Criteria For Wind-Sensitive Buildings

For the 12-storey reinforced concrete structure model studied, wind load will not normally control the Ultimate Limit State. Hence only the serviceability of the structure under wind loads needs to be investigated. Generally buildings should be designed to limit drift and/or acceleration under wind loads for the Serviceability Limit State.

Drift Limits

The reasons for requiring drift limits in buildings are (Cenek et al., 1990):

(a) to limit damage to the cladding on the building facade and to partitions and interior finishes
(b) to reduce the effects of motion perceptibility
(c) to limit the P-delta or secondary loading effects

Drift damage limits for cladding and partitions should be specified in terms of serviceability wind speeds, and the limit should be related to the type of non-structural materials used and the methods of fixing. Because there is a lack of information available on the performance of partitions and cladding systems under racking loads, it is difficult to establish a rational basis for specifying drift limits. In practice, values of $H/300$ to $H/600$, in which $H$ is the overall height of the building, are commonly used. Interstorey drifts typically are limited to $0.0015h$ – $0.0025h$, in which $h$ is storey height (Tallin et al., 1984). Cooney et al. (1988) also provided some guidance for drift limits.

Acceleration Limits

Modern buildings that satisfy the static lateral drift requirements may still vibrate excessively during windstorms. While such dynamic motion usually is insufficient to cause any structural damage, it may disturb the building occupants who expect the building to remain stationary under normal conditions (Tallin et al., 1984). Static lateral drift criteria do not address explicitly the relation between the fluctuating component of the structural response and the structural performance necessary to ensure that the building remains serviceable.

The levels at which structural motion becomes perceptible or intolerable to a building occupant depend on whether the motion is transient or steady-state, the frequency and duration of the motion, the occupant's activity and body position at the time the motion occurs, etc. Numerous studies concerned with human response to structural motion, reviewed by Galambos (1973), have concluded that building acceleration is the best indicator of potential discomfort to building occupants.

The perception threshold for steady-state acceleration may be as low as 0.02 m/s$^2$, while the limit for psychological well being and the ability to perform routine tasks is about 0.39 m/s$^2$. Studies of the response of tall buildings to wind have suggested thresholds of perception and annoyance of approximately 0.05 m/s$^2$ and 0.15 m/s$^2$ respectively (Tallin et al., 1984).

Most data on motion perception and tolerance have been obtained at frequencies greater than 1 Hz (Galambos, 1973). The data are more limited in longer periods associated with tall buildings. With reference to Melbourne et al. (1988), it appears that at building sway and twisting frequencies, the lower threshold (10 percentile) of human perception to horizontal motion, in terms of horizontal peak acceleration, is 0.007 m/s$^2$, whereas most people (90 percentile) would perceive an acceleration 10 times greater, i.e. 0.07 m/s$^2$. Melbourne et al. (1988) recommended a peak horizontal acceleration limitation of 0.1 m/s$^2$ once every year for frequencies in the range 0.1 – 0.3 Hz, with the implication that motions perceptible by most people would occur during storms once or twice per annum.

Melbourne et al. (1988) show that different criteria of acceleration limitations (Reed, 1971, Melbourne et al., 1988, North American) are all in reasonable agreement with the following equation (Eq(12.45)). This equation shows the horizontal acceleration criteria in terms of the standard deviation of acceleration for the worst 10 consecutive minutes in a 5-year return period for buildings as a function of frequency:

$$\sigma_{\ddot{x}} = \exp\left(-3.65 - 0.41 \ln n\right) \tag{12.45}$$

where $\sigma_{\ddot{x}}$ = the standard deviation of acceleration in the horizontal plane,

$n$ = the frequency of oscillation with an approximately normal distribution.

On the assumption that it relates to a normally distributed process, the peak acceleration for a 5-year return period can be expressed as (from Eq(12.35)):

$$\begin{aligned} a_x &= g_f \sigma_{\ddot{x}} \\ &= \sqrt{2 \ln nT}\, \exp\left(-3.65 - 0.41 \ln n\right) \end{aligned} \tag{12.46}$$

where $a_x$ = the peak acceleration

$g_f$ = a peak factor, the ratio of the expected peak value which occurs once per hour to the standard deviation of the resonant part of the fluctuating response

$= \sqrt{2\ln(nT)}$

$T$ = duration, seconds.

Combining the influence of an arbitrary return period, Melbourne et al. (1992) proposed the peak acceleration criteria for occupancy comfort in buildings as:

$$a_x = \sqrt{2\ln nT}\left(0.68 + \frac{\ln R}{5}\right)\exp(-3.65 - 0.41\ln n) \qquad (12.47)$$

where $R$ = return period in years.

These acceleration criteria are also shown in Fig.12.1.

The structural forces and the displacement caused by wind are composed of three parts: the mean part, the background component and the resonant component. The benefits to be gained for the structural forces and the displacement by increasing the damping capacity are generally not great since the resonant response is only one component of the whole. The mean part and the background component (induced by low frequency gusts) are not affected by damping and these together generally constitute a large part of the peak response (Vickery et al. 1983). The resonant component plays a dominant role only when the first mode frequency falls below about 0.1 Hz.

As far as wind induced accelerations are concerned, the benefits due to the increase of damping become great. The accelerations are due almost entirely to the "resonant peak" and the peak acceleration is given by Eq(12.35). It can be seen that acceleration levels can be reduced by increasing the damping capacity.

Based on the above discussion, the peak acceleration criterion shown in Eq(12.47) is adopted as the design criterion for determining the yield strengths of the dampers in the structure.

### 12.4.2 Design Procedure for Determining the Yield Strengths of the Dampers

For the structure without dampers, the peak acceleration can be obtained through Eq(12.35). For the structure with the supplemental dampers, the peak acceleration can be calculated as:

$$\begin{aligned} a_{x,d} &= g_f \sigma_{\dot{x}} \\ &= g_f \frac{3\overline{M}}{M_b h} \sqrt{\frac{r^2 SE}{\xi_0 + \xi_d}} \end{aligned} \tag{12.48}$$

where $\xi_d$ = the equivalent viscous damping ratio due to the supplemental dampers.

It is assumed that the modal characteristics of the structure change very little due to the presence of the supplemental dampers. Comparing Eq(12.35) with Eq(12.48), the only difference is the equivalent viscous damping ratio due to the supplemental dampers $\xi_d$.

The design criteria can be obtained from Eq(12.47). For a given design requirement, the target equivalent viscous damping ratio $\xi_d$ due to the supplemental dampers can be calculated from Eq(12.48). From Eq(12.44) the peak resonant component of the roof displacement can be obtained as:

$$x_t = g_f \sigma_{Dx} = g_f \frac{3\overline{M}}{(2\pi n_1)^2 M_b h} \sqrt{\frac{r^2 SE}{\xi_0 + \xi_d}} \tag{12.49}$$

From Eq(12.42), for the equivalent viscous damping due to the dampers, $\xi_d$, and the target peak resonant component of the roof displacement, $x_t$, the yield strength of the supplemental dampers can be determined. For the supplemental lead dampers, the yield displacement $\Delta_y$ is usually very small when compared with the resonant component of the interstorey drift response. Hence the $\Delta_y$ term in Eq(12.42) may be neglected. Eq(12.42) can be simplified as:

$$F_d = \frac{\pi}{2} \frac{\omega_1^2 \left( \sum_{i=1}^{N} m_i \phi_{i,1}^2 \right) x_t}{\cos\theta} \xi_d \tag{12.50}$$

It is assumed that there is one damper for each storey in the structure and the yield strengths of the dampers in all the storeys are identical. The design procedure for determining the yield strength of the dampers can be established as follows:

Step 1: Estimate the peak roof acceleration of the original structure without dampers under the design wind load through Eq(12.35). Obtain the design required peak roof acceleration through Eq(12.47). Compare these two values to determine whether the design requirement is met or not. If it is, then there is no need for any supplemental dampers. If it is not satisfied, go to step 2.

Step 2: Calculate the desired equivalent viscous damping ratio due to the supplemental dampers, $\xi_d$, using Eq(12.48) and (12.35).

Step 3: Calculate the target resonant component of the roof displacement through Eq(12.49) for the desired equivalent viscous damping ratio obtained in step 2.

Step 4: Calculate the strength level of the dampers from Eq(12.50).

Step 5: Use the simplified method or the time-domain method to verify that the criteria for the peak roof acceleration is satisfied.

**Example**

Again, consider the 12-storey structure used previously. The parameters needed for this structure have been given earlier.

Step 1: the peak roof acceleration of the structure under the design wind load has been obtained in chapter 10, that is, $a_x = 0.1875\ \text{m/s}^2$.

The peak roof acceleration criteria can be obtained as follows (for a return period of 20 years):

$$a_x = \sqrt{2\ln nT}\left(0.68+\frac{\ln R}{5}\right)\exp(-3.65-0.41\ln n)$$

$$= \sqrt{2\ln(0.5009\times 3600)}\left(0.68+\frac{\ln 20}{5}\right)\exp(-3.65-0.41\ln 0.5009)$$

$$= 0.1709\ (\text{m/s}^2)$$

The peak response roof acceleration is quite close to the acceleration criterion. There is actually no need for the dampers.

For this example, it is arbitrarily assumed that the design requirement is to reduce the peak roof acceleration by 50%, i.e. $a_{x,d} = 0.09375\text{m/s}^2$.

Step 2: Divide Eq(12.35) by Eq(12.48) to obtain:

$$\frac{\xi_0 + \xi_d}{\xi_0} = \left(\frac{a_x}{a_{x,d}}\right)^2 = \left(\frac{0.1875}{0.09375}\right)^2 = 4$$

It is known that $\xi_0 = 1\%$. Hence, the required supplemental damping is $\xi_d = 3\%$.

Step 3:

$$x_t = g_f \frac{3\overline{M}}{(2\pi m_1)^2 M_b h}\sqrt{\frac{r^2 SE}{\xi_0 + \xi_d}}$$

$$= 3.8718 \times \frac{3 \times 3662.7947}{(2\pi \times 0.5009)^2 \times 1446.58 \times 43.8} \times 0.2622\sqrt{\frac{0.2016 \times 0.05627}{1\% + 3\%}}$$

$$= 9.4657 \times 10^{-3}(\text{m})$$

Step 4:

$$F_d = \frac{\pi}{2}\frac{\omega_1^2\left(\sum_{i=1}^{N} m_i \phi_{i,1}^2\right)x_t}{\cos\theta}\xi_d$$

$$= \frac{\pi}{2}\frac{3.1473^2 \times 623.839 \times 9.4657 \times 10^{-3}}{0.91} \times 3\% = 3.03\text{KN}$$

The yield strength of the dampers is taken to be 3.1KN. It is assumed that the yield displacement of the damper is about $7.54 \times 10^{-5}\text{m}$.

The simplified analysis of the structure with the supplemental dampers designed above is shown as follows:

Step 1: Assume that $\xi_d = 3\%$.

Step 2:

$$x_t = g_f \frac{3\overline{M}}{(2\pi n_1)^2 M_b h} r \sqrt{\frac{SE}{\xi_0 + \xi_d}}$$

$$= 3.8718 \times \frac{3 \times 3662.7947}{(2\pi \times 0.5009)^2 \times 1446.58 \times 43.8} \times 0.2622 \sqrt{\frac{0.2016 \times 0.05627}{1\% + 3\%}}$$

$$= 9.466 \times 10^{-3} \text{m}$$

Step 3: $\xi_d' = \frac{2}{\pi} \times \frac{3.1 \times \left(9.466 \times 10^{-3} \times 0.91 - 12 \times 7.54 \times 10^{-5}\right)}{3.1473^2 \times 623.839 \times \left(9.466 \times 10^{-3}\right)^2} = 2.749\%$

Step 4: $\frac{\xi_d' - \xi_d}{\xi_d} \times 100\% = \frac{2.749 - 3}{3} \times 100\% = -8.4\%$. The difference is relatively large. Iteration is needed. Let $\xi_d = 2.749\%$ and go back to Step 2.

Step 2-1: $x_t = 9.778 \times 10^{-3}$m

Step 3-1: $\xi_d' = 2.67\%$

Step 4-1: The difference = -2.87%. The difference is small enough. Let $\xi_d = 2.67\%$ and go to step 5.

Step 5:

$$a_x = 3.8718 \times \frac{3 \times 3662.7947}{1446.58 \times 43.8} \sqrt{\frac{0.2622^2 \times 0.2016 \times 0.05627}{1\% + 2.67\%}} = 0.09788 \, (\text{m/s}^2)$$

Time-domain analysis of the structure with the designed supplemental dampers was also conducted. The peak roof acceleration response is:

$a_x = 0.1032 \, (\text{m/s}^2)$ Close to the design requirement.

The difference between the simplified method and the time-domain method for the peak roof acceleration is 5.4%.

Roof displacement time histories for the structure without dampers and the structure with the supplemental dampers are shown in Figs.12.2 and 12.3 respectively. Roof acceleration time histories for the structure without dampers and the structure with the supplemental dampers are shown in Figs.12.4 and 12.5 respectively. It can be seen that the roof acceleration response is significantly reduced by the supplemental dampers.

| | Mode 1 | Mode 2 |
|---|---|---|
| Modal frequency | 0.5009 | 1.447 |
| Mode shape | | |
| Level 1 | 0.0499 | -0.1485 |
| 2 | 0.1445 | -0.4095 |
| 3 | 0.2485 | -0.6493 |
| 4 | 0.3531 | -0.8159 |
| 5 | 0.4639 | -0.8817 |
| 6 | 0.5742 | -0.8184 |
| 7 | 0.6756 | -0.6295 |
| 8 | 0.7658 | -0.3397 |
| 9 | 0.8498 | 0.04821 |
| 10 | 0.9202 | 0.4569 |
| 11 | 0.9702 | 0.7906 |
| 12 | 1 | 1 |

Table 12.1 Mode shape of the structure for the 1st and 2nd modes

| | Mode 1 | Mode 2 |
|---|---|---|
| M* (x 1000kg) | 623.839 | 604.364 |
| $\omega^*$ | 3.1473 | 9.0918 |
| K* (KN/m) | 6179.23 | 49956.889 |
| $\{\phi\}^T\{\overline{F}\}$ (KN) | 91.139 | -30.876 |

Table 12.2 Modal properties for the 1st and 2nd modes

| | Mean Roof Displacement (mm) | Roof Displacement (mm) | | Roof Acceleration ( milli-g) | |
|---|---|---|---|---|---|
| | | Peak | σ | Peak | σ |
| 1st Mode | 14.749 | 37.438 | 5.973 | 17.946 | 4.938 |
| 2nd Mode | -0.618 | -1.332 | 0.1854 | 2.315 | 0.691 |
| Total | 14.16 | 36.755 | 5.89 | 19.475 | 5.068 |
| Difference between 1st mode and total response | 4.15% | 1.86% | 1.41% | 7.85% | 2.56% |

Table 12.3 Comparison of the results for the modal analysis and the MDOF analysis

| | Peak roof displacement (cm) | Peak roof acceleration (m/s^2) |
|---|---|---|
| Simplified analysis | 2.862 | 0.0682 |
| Time-domain analysis method | 2.739 | 0.0662 |
| Difference | 4.49% | 3.02% |

Table 12.4 Comparison of the results from the simplified analysis and the time-domain analysis

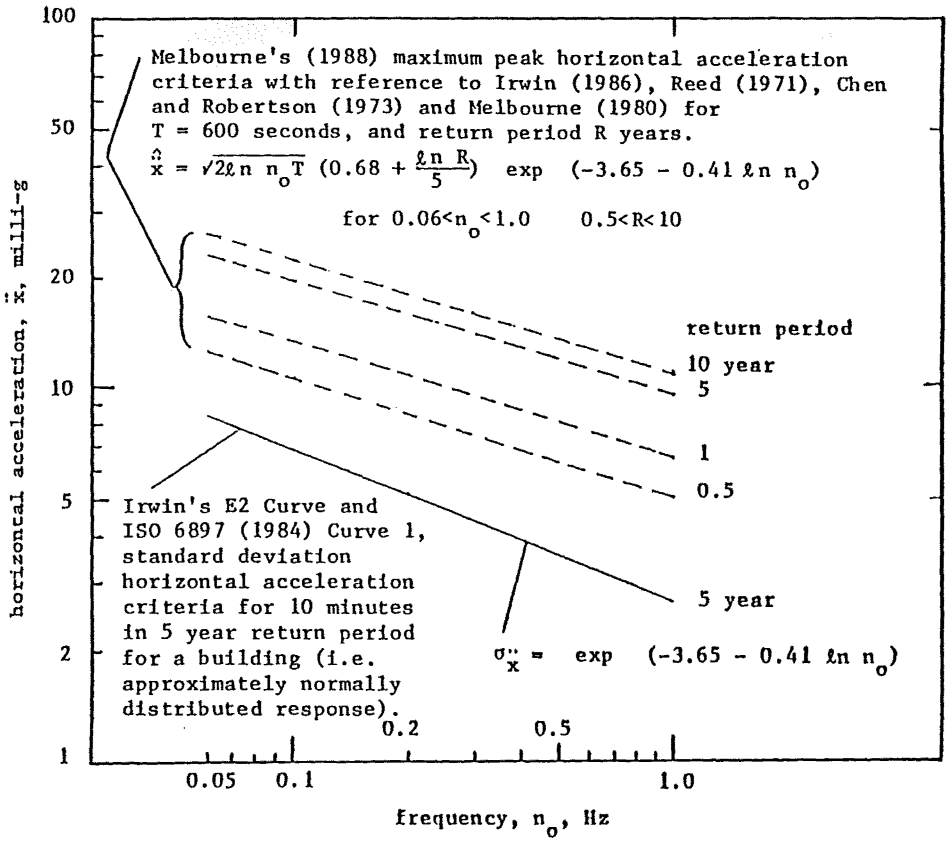


Figure 12.1 Horizontal acceleration criteria for occupancy comfort in buildings (from Melbourne et al., 1992)

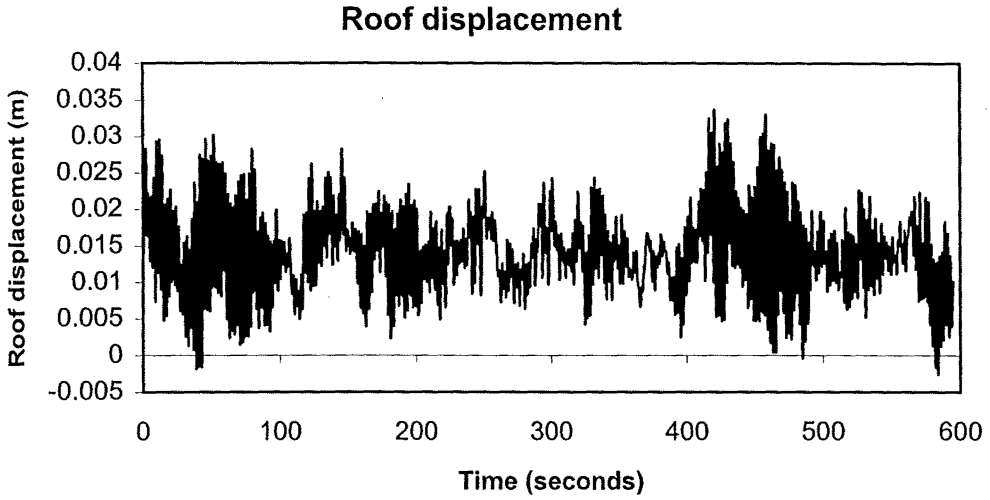


Figure 12.2 Roof displacement time history for the structure without dampers

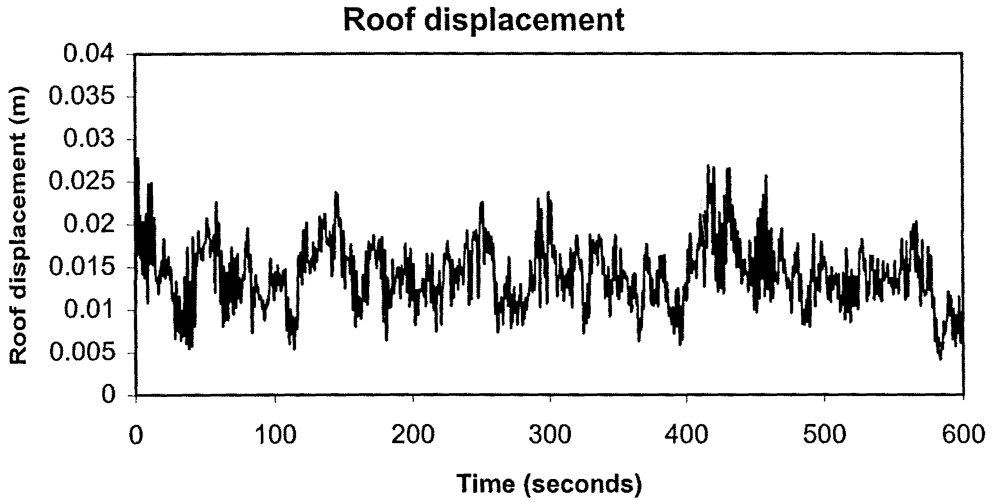


Figure 12.3 Roof displacement time history for the structure with the designed supplemental dampers

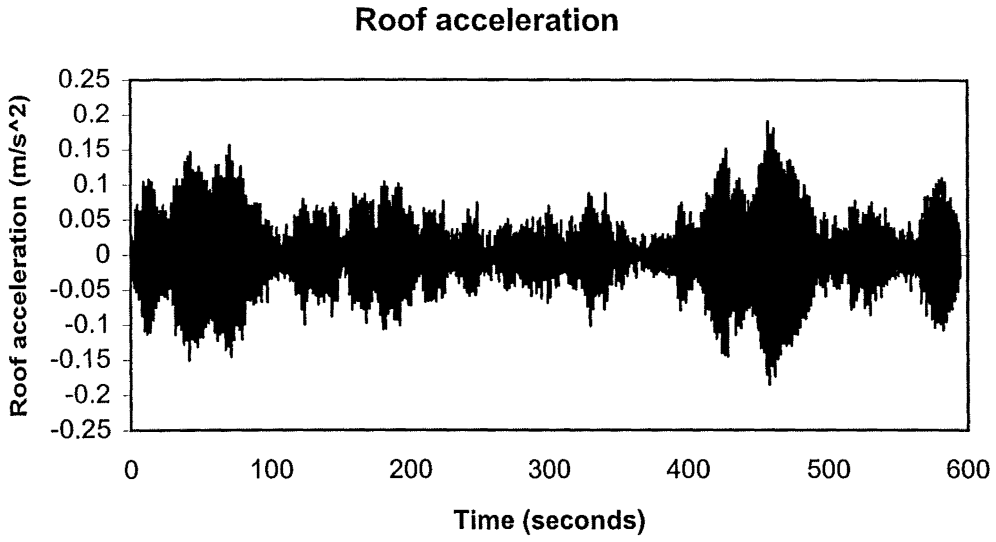


Figure 12.4 Roof acceleration time history for the structure without dampers

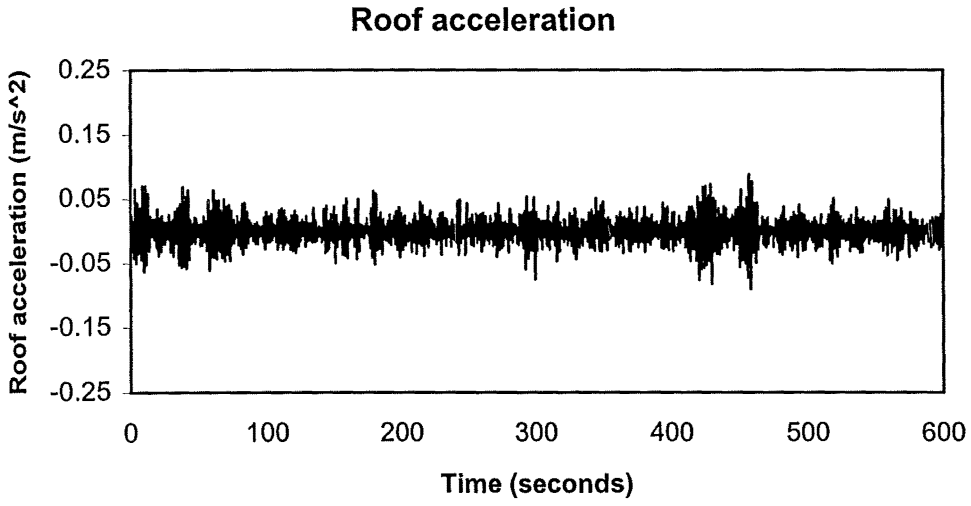


Figure 12.5 Roof acceleration time history for the structure with the designed supplemental dampers

# CHAPTER 13

# SUMMARY, CONTRIBUTIONS, CONCLUSIONS AND RECOMMENDATIONS

## 13.1 SUMMARY

The seismic response of a 12-storey reinforced concrete structure with supplemental lead dampers has been investigated. For regular framed structures under earthquake excitations, a satisfactory distribution of damper yield strengths in the storeys has been found using the criteria of minimising interstorey drift, base shear and cost of the dampers. The displacement, acceleration and the interstorey drift responses for the structure with supplemental dampers can be reduced significantly. Pushover analyses of the structure with supplemental dampers have been performed to investigate the effect of different distributions of dampers on the deflected shape. It was found that for a structure with supplemental dampers having a satisfactory distribution, its deflected shape could be accurately represented by that of the original structure without dampers. An equivalent SDOF system for the MDOF structure with dampers has been obtained through an appropriate transformation by means of using the deflected shape of the structure at the target displacement. For such a distribution of dampers, the structure with supplemental dampers will behave predominantly in its first mode. A MDOF structure with dampers can be considered as a dual system and be effectively represented by its equivalent SDOF system consisting of both original structural spring and damping system. The equivalent viscous damping ratio due to dampers and the effective period for the MDOF structure with supplemental dampers can be simply calculated from its equivalent SDOF system (both have almost exactly the same form). The equivalent SDOF system can be used to predict the response of the MDOF structure with dampers with good accuracy. A simplified nonlinear static method, taking into account the effect of the supplemental dampers, has been investigated to conduct the seismic analysis of the structure with dampers. While comparing with the nonlinear time history analysis method, it has been found that this simplified method can give a very good approximation to the response. By investigating the effects on the displacement and acceleration response associated with the supplemental dampers under earthquake excitations, optimal damping levels of the dampers have been found. Based on the simplified nonlinear static method and the optimal damping ratio of the dampers, displacement-based design procedures have been established to

determine the damper yield strengths in the storeys both for retrofitting an existing structure and designing a new building structure.

Dynamic analyses and design of the structure with supplemental dampers under wind loads were also investigated. Time-domain analyses of the structure with supplemental lead dampers have been performed using the artificial wind time history that was simulated by means of an equivalent wind spectrum technique. The effects of the dampers on the structural displacement response are not as significant as on the acceleration response for wind loading. For structures under the serviceability Limit State subject to wind loading, the acceleration response is the main concern. Considerable benefit can be gained by incorporating lead dampers into the structures. A simplified analytical method, using a code-type frequency-domain approach that takes the effect of dampers into account, has been established. A design procedure for determining the yield strength of the dampers in a structure subject to wind loading has been established.

## 13.2 MAIN CONTRIBUTIONS OF THIS RESEARCH

1. For a structure under earthquake excitations, a satisfactory distribution of damper yield strengths in the storeys has been found using the criteria of minimising interstorey drift, base shear and cost of the dampers (Chapter 5). The influence of the initial stiffness of dampers and the flexibility of braces were also investigated. (Chapter 5)

2. Pushover analyses of the structure with supplemental dampers have been performed to investigate the effect of different distributions of dampers on the deflected shape. It was found that for the structure with the supplemental dampers having a satisfactory distribution, its deflected shape could be accurately represented by that of the original structure without dampers. This makes analysis and design much easier since pushover analysis only need to be performed once to get the information concerning the deflected shape. (Chapter 6)

3. For a satisfactory distribution of dampers, the structure with supplemental dampers will behave predominantly in its first mode. A MDOF structure with dampers can be considered as a dual system and be effectively represented by its equivalent SDOF system consisting of both original structural spring and damping system. (Chapter 6)

4. A theoretical verification of the equivalence of the MDOF structure with supplemental dampers having a satisfactory distribution and its equivalent SDOF system has been performed. It was found that both the MDOF structure and the equivalent SDOF system give the same results of the equivalent viscous damping ratio due to dampers and the effective period. Hence, the equivalent viscous damping ratio due to dampers and the effective period for the MDOF structure with supplemental dampers can be simply calculated from its equivalent SDOF system. (Chapter 7)

5. Based on the results from 2, 3, 4, simplified methods of nonlinear static analysis can be extended to structures with supplemental dampers. Analytical procedures were also established. (Chapter 8)

6. By investigating the effects on the displacement and acceleration response associated with supplemental dampers under earthquake excitations, optimal damping levels of the dampers have been found. (Chapter 9)

7. For a structure with supplemental dampers under earthquake excitations, the main concern is displacement. Hence, a displacement-based design concept was adopted. Displacement-based design procedures for determining yield strengths of dampers in the structure both for retrofitting an existing structure and designing a new building structure have been established. By following these procedures, dampers can be directly designed to meet the design requirements. (Chapter 9)

8. For a structure under wind load, placement and yield strength levels of dampers have been investigated. A suitable supplemental damping ratio provided by dampers has been suggested. (Chapter 11)

9. For analysing a structure with supplemental dampers under wind load, a simplified analytical method has been established. The approach is based on the Australian Standard AS 1170 code method by modifying the overall structural damping capacity to take the effect of the dampers into account. (Chapter 12)

10. An acceleration-based design procedure for determining the yield strength of dampers in a structure subject to wind has been established. (Chapter 12)

## 13.3 CONCLUSIONS FOR THE ANALYSIS AND DESIGN OF THE STRUCTURE WITH SUPPLEMENTAL LEAD DAMPERS UNDER EARTHQUAKE LOADS

1. A type of newly developed supplemental lead damper (Penguin Vibration Damper) is a metallic yielding device, for which the Ramberg-Osgood model and the Elasto-plastic model can be used to represent the force-deformation relationship of this damper. The structural dynamic responses of these two models are very close to each other. For the sake of simplicity, the elasto-plastic model was used to represent the characteristics of this type of supplemental damper.

2. For regular framed structures, a satisfactory strength distribution of the supplemental lead dampers in the structure is for the yield strengths of the dampers in the storeys to be proportional to the storey shears due to an inverted-triangular lateral load pattern.

3. For the effectiveness of supplemental dampers in the structure, the stiffness ratio of the dampers to the undamped structure should not be less than 4. The stiffness of the braces connecting the dampers to the structure should be such that the stiffness ratio of the brace-damper assemblies is not less than 4, otherwise, the influence of the stiffness ratio must be considered.

4. For regular framed structures with a satisfactory distribution of supplemental lead dampers, the lateral load pattern for performing a pushover analysis can be taken as an inverted-triangular pattern with good accuracy.

5. For a satisfactory distribution of the supplemental lead dampers, the deflected shape (profile) of the structure with the dampers is very close to that for the structure without dampers. This means that the deflected shape of the structure with supplemental dampers can be estimated using that of the undamped structure by means of a pushover analysis.

6. For regular framed structures with a satisfactory distribution of supplemental lead dampers, the dynamic response of the structure is dominated by the first mode. The peak response of a MDOF structure can be estimated from the results of the equivalent SDOF system with good accuracy.

7. A regular framed structure with a satisfactory distribution of supplemental lead dampers can be considered as a dual system – the undamped structure and the damping system. The properties of the equivalent SDOF system can be obtained from the results of a pushover analysis by means of a transformation of the properties of the original MDOF structure.

8. The equivalent viscous damping and the effective stiffness of a structure with the supplemental lead dampers can be calculated from its equivalent SDOF system using simple equations.

9. A simplified nonlinear static analysis method can be adopted for analysing the structure with dampers with good accuracy. The method is to use response spectra that are obtained by modifying the 5%-damped spectra to account for the damping provided by the supplemental dampers and the effect due to the inelastic deformation of the structures. The effective period shift due to the supplemental dampers and the inelastic deformation of the structures is also taken into account.

10. The optimal equivalent viscous damping ratio that the supplemental dampers can provide to the structure can be taken as 15% to 17%.

11. The displacement-based design concept can be adopted for the design of the structure with supplemental lead dampers for both retrofitting existing buildings and new-building design purposes. The starting point is no longer the forces or strengths, but the interstorey drift ratio. The proper yield strengths of the dampers in the storeys can be determined to meet the design limitation of the interstorey drift under the design earthquake by following the given design procedure.

12. For practical design, after the yield strengths of the supplemental dampers in the storeys have been obtained, a stepped distribution of the damper strengths, in which the same yield strengths of the dampers for group of 3 or 4 storeys can be used, making the design more practical.

13. For structures with supplemental lead dampers, the displacement, acceleration and interstorey drift response can be reduced significantly.

14. The ductility demand of the main structure under the design earthquake can be greatly reduced by incorporating supplemental dampers into the structure.

15. The total base shear of the structure with supplemental lead dampers may be increased slightly due to the additional force of the dampers in the storey. The storey shears of the main structure (not including dampers) are still reduced due to the dampers.

Structural control by supplemental dampers provides a new way of controlling structural deformation and damage under earthquake excitations. Such dampers can be easily incorporated into a structure or replaced if needed without touching the primary structural system. This type of structural control is particularly suitable for retrofitting a non-ductile structure, in which ductility demand will be largely reduced by incorporating supplemental dampers. The displacement and deformation of the structure can be greatly reduced without the need of increasing the stiffness (member sizes) of the primary structure. This type of structural control also provide a good alternative solution for designing new building structures under earthquake excitations – especially for those structures in which non-structural damage is limited under Serviceability Limit State or large inelastic deformations of primary structures are not allowed under Ultimate Limit State. It providing a design which may possibly preclude the necessity of allowing for inelastic deformations in the primary structure without the penalty of increasing lateral forces acting on the structure caused by earthquake excitations – due to the enhanced damping capacity in the structure.

## 13.4 CONCLUSIONS FOR THE ANALYSIS AND DESIGN OF THE STRUCTURE WITH SUPPLEMENTAL LEAD DAMPERS UNDER WIND LOADS

1. Time-domain analyses of the structure with the supplemental lead dampers have been performed using the artificial wind time history that was simulated by means of an equivalent wind spectrum technique.

2. For the structure with the supplemental dampers acted on by wind loads, identical strength dampers may be placed in all storey levels. This will result in an efficient and simple solution.

3. For the structure with the proper yield-strength lead dampers acted on by wind loads, the stiffening effect of the dampers on the structure is negligible. The dampers provide the structure with supplemental damping only.

4. The effect caused by the dampers on the structural displacement response is not as significant as on the acceleration response. For structures under the serviceability Limit State subject to wind loads, the acceleration response is the main concern. Considerable benefit can be gained by incorporating the dampers into the structures.

5. Usually there is no need to provide more than 5% supplemental damping in the structures for economic considerations.

6. The simplified analytical method, which is based on the Australian Standard AS 1170 code method by modifying the structural damping capacity to take the effect of the dampers into account, has been established. In this analytical method, only the first mode is considered and higher mode effects are ignored.

7. Peak acceleration criteria are adopted as design criteria. A design procedure for determining the yield strength of the dampers has been established.

Structural control by supplemental dampers provides a new and cost-effective way of reducing wind-induced vibration of buildings. Accelerations in a building structure can be greatly reduced by incorporating such dampers into the structure without the need of increasing its stiffness (member sizes) or changing building shape.

## 13.5 RECOMMENDATIONS FOR FURTHER RESEARCH

Further research of the following issues is needed:

1. The effectiveness of supplemental lead dampers for different periods (or different heights) of structures needs to be investigated. The applicability of the simplified analytical methods and design procedures presented for different period range of structures needs to be examined.

2. For tall building structures with supplemental dampers, higher mode effects need to be investigated. Especially for tall buildings under wind loads, it may not be possible to ignore higher mode effects because the acceleration response is more sensitive to higher mode effects.

3. Further analyses with 3D-models are needed to investigate the effect of supplemental dampers on structural response taking torsional effects into account.

4. For a designed structure with supplemental dampers, the effectiveness of the dampers under different intensities of earthquake excitations needs to be investigated in more detail. For example, how will a structure with dampers designed for a strong earthquake behave under a minor earthquake?

5. The effect of combining the two typical supplemental dampers, one for earthquake with large yield strength and the other with small yield strength for wind load, how does this building respond to a large earthquake and wind load?

6. More earthquake time histories are needed to examine whether the results shown in this study are applicable to other input motions.

7. In order to successfully implement lead dampers into real structures, it is recommended that large-scale experimental work needs to be undertaken in the future. This could be in the form of either shaking table tests on structural frames with several degrees of freedom, and/or strong floor/wall testing of near full-size frames under high speed forced lateral loading.

# REFERENCES

Aiken, I.D. and Kelly, J.M. (1990) "Earthquake simulator testing and analytical studies of two energy-absorbing system for multistorey structures", Report No. UCB / EERC-90 / 03, University of California at Berkely.

Aiken, I.D., Nims, D.K. and Kelly, J.M. (1992) "Comparative study of four passive energy dissipation systems", Bulletin of the New Zealand National Society for Earthquake Engineering, Vol.25, No.3, Sept., pp.175-192.

AS1170.2 (1989) SAA Loading Code, Part 2: Wind Loads, Australian Standard.

ATC-33.03 (75% submittal) (1995) Guidelines and Commentary for the Seismic Rehabilitation of Buildings, Applied Technology Council.

Bergman, D.M. and Hanson, R.D. (1989) "Consequences and achievement of supplemental damping for improved seismic performance", Seismic Engineering: Research and Practice, Proceedings of the Sessions related to seismic engineering at Structures Congress'89, San Francisco, CA, May 1-5.

Bergman, D.M. and Hanson, R.D. (1993) "Viscoelastic mechanical damping devices tested at real earthquake displacement", Earthquake Spectra, Vol.9, No.3, Aug., pp.389-417.

Bertero, V.V., Anderson, J.C., Krawinkler, H. and Miranda, E. (1991) "Design guidelines for ductility and drift limits", Report No. UCB / EERC – 91 / 15, University of California at Berkeley.

Bishop, R.E.D. (1955) "The treatment of damping forces in vibration theory", Journal of the Royal Aeronautical Society, Vol.59, Nov. p738-742.

Brebbia, C.A., Tottenham, H., Warburton, G.B., Wilson, J.M. and Wilson, R.P. (1985) "Vibrations of engineering structures", Lecture Notes in Engineering, 10, Springer-Verlag, Berlin.

Calvi, G.M. and Kinsley, G.R. (1995) "Displacement-based seismic design of multi-degree-of-freedom bridge structures", Earthquake Engineering and Structural Dynamics, Vol.24, pp.1247-1266.

Carr, A.J. (1994) "Dynamic analysis of structures", Bulletin of the New Zealand National Society for Earthquake Engineering, Vol.27, No.2, June, pp.129-146.

Carr,A.J. (1996) "RUAUMOKO - inelastic dynamic analysis program", Computer Program Library, Department of Civil Engineering, University of Canterbury, Christchurch, New Zealand.

Carr,A.J. (1996) "DYNAPLOT – post-processor for RUAUMOKO", Computer Program Library, Department of Civil Engineering, University of Canterbury, Christchurch, New Zealand.

Carr,A.J. (1996) "SIMQKE - generation of artificial earthquakes program", Computer Program Library, Department of Civil Engineering, University of Canterbury, Christchurch, New Zealand.

Caughey, T.K. (1962) "Vibration of dynamic systems with linear hysteretic damping (linear theory)", Proc. of the Fourth U.S. National Congress of Applied Mechanics, Vol.1, pp.87-97.

Cenek, P.D. and Wood, J.H. (1990) "Designing multi-storey buildings for wind effects", BRANZ Study Report, No.25.

Chang, K.C. Soong, T.T., Oh, S-T and Lai, M.L. (1991) "Seismic response of a 2/5 scale steel structure with added viscoelastic dampers", Technical Report NCEER-91-0012, National Centre for Earthquake Engineering Research, SUNY/Buffalo.

Chang, K.C., Lai, M.L., Soong, T.T., Hao, D.S. and Yeh, Y.C. (1993) "Seismic behaviour and design guidelines for steel study of building frames with added energy-absorbing devices", Technical Report NCEER-93-0009, National Center for Earthquake Engineering Research, SUNY/Buffalo.

Ciampi, V., De Angelis, M. and Paolacci, F. (1995) "Design of yielding or friction-based dissipative bracings for seismic protection of buildings", Engineering Structures, Vol.17, No.5, pp.381-391.

Ciampi, V., Paolone, A. and De Angelis, M. (1992) "On the seismic design of dissipative bracings", Tenth World Conference on Earthquake Engineering, Balkema, Rotterdam, pp.4133-4138.

Clough, R.W. and Penzien, J. (1975) Dynamics of Structures, McGraw-Hill, New York.

Constantinou, M.C. and Symans, M.D. (1992) "Experimental and analytical investigation of seismic response of structures with supplemental fluid viscous dampers", Technical Report NCEER-92-0032, National Center for Earthquake Engineering Research, SUNY/Buffalo.

Cooney, R.C. and King, A.B. (1988) "Serviceability criteria for buildings", BRANZ Study Report, SR14, Building Research Association of New Zealand.

Cousins, W.J. and Porritt, T.E. (1993) "Improvements to lead-extrusion damper technology", Bulletin of the New Zealand National Society for Earthquake Engineering, Vol.26, No.3, Sept., pp.342-348.

Das, N.K. and McDonald, J.R (1990), "Lifetime risk of failure of steel building frames subjected to dynamic wind loading", Journal of Wind Engineering and Industrial Aerodynamics, Vol.36, pp549-558.

Davenport, A.G. (1967) "Gust loading factors", Journal of the Structural Division, ASCE, Vol.93, No.ST3, June, pp.11-34.

Davenport, A.G., Vickery, B.J. and Melbourne, W.H. (1975), The Structure & Environmental Effects of Wind on Buildings & Structures, Post-graduate Course Notes, Department of Mechanical Engineering, Monash University.

Deierlein, G.G. and Hsieh, S-H (1990) "Seismic response of steel frames with semi-rigid connections using the capacity spectrum method", Proceedings of the 4$^{th}$ U.S. National

Conference on Earthquake Engineering, Palm Springs, California, May 20-24, Vol.2, pp.863-872.

Dorka, U.E. (1994) "Hysteretic device systems for earthquake protection of buildings", Fifth U.S. National Conference on Earthquake Engineering, July 10-14, 1994, Chicago, Illinois, Vol.I, pp.775-785.

Engineering Sciences Data Unit (1976) "The response of flexible structures to atmospheric turbulence", ESDU 76001, London.

Fajfar, P. and Fischinger, M. (1987), "Non-linear seismic analysis of RC buildings: implications of a case study", European Earthquake Engineering, Vol.1, pp31-43.

Fajfar, P. and Fischinger, M. (1988), "N2 – a method for non-linear seismic analysis of regular structures", Proceedings of the 9th World Conference on Earthquake Engineering, Tokyo – Kyoto, Japan, pp.V-111-116.

Fajfar, P. and Gašperšic, P. (1996), "The N2 method for the seismic damage analysis of RC buildings", Earthquake Engineering and Structure Dynamics, Vol.25, pp31-46.

Filiatrault, A. and Cherry, S. (1987) "Performance evaluation of friction damped braced steel frames under simulated earthquake loads", Earthquake Spectra, Vol.3, No.1, p57-81.

Filiatrault, A. and Cherry, S. (1990) "A simplified seismic design procedure for friction damped structures", Proc. Of Fourth U.S. National Conference on Earthquake Engineering, May 20-24, 1990, Palm Springs, California, Vol.3, pp.479-488.

Freeman, S.A. (1978) "Prediction of response of concrete buildings to severe earthquake motion", Donglas McHenry International Symposium on Concrete and Concrete Structures, SP-55, ACI, Detroid, Michigan, pp.589-605.

Freeman, S.A. (1985) "Structural moments number 4 – drift limits: are they realistic", Earthquake Spectra, Vol.1, No.2, Feb. pp.355-362.

Hanson, R.D., Aiken, I.D., Nims, D.K., Richter, P.J. and Bachman, R.E. (1993) "State-of-the-art and state-of-the-practice in seismic energy dissipation", Proceedings of a Seminar on Seismic Isolation, Passive Energy Dissipation and Active Control, ATC-17-1, Applied Technology Council, Redwood City, California, March, pp.449-471.

Harris, R.I. (1971), "The nature of the wind", The Modern Design Of Wind-Sensitive Structures, CIRIA Publication.

Hill, K.E. (1995) "The utility of ring springs in seismic isolation systems", Ph.D Thesis, Department of Mechanical Engineering, University of Canterbury, Christchurch, New Zealand, December.

Holmes, J.D, Melbourne, W.H. and Walker, G.R. (1990), A Commentary on the Australian Standard for Wind Loads, AS 1170 Part 2.

Holmes, J.D. (1978), "Computer simulation of multiple, correlated wind records using the inverse fast fourier transform", Civil Engineering Transactions, The Inst. of Engineers, Australia.

Hudson, D.E. (1965) "Equivalent viscous friction for hysteretic systems with earthquake-like excitations", Proc. 3rd World Conference on Earthquake Engineering, Auckland and Wellington, New Zealand.

Iannuzzi, A. and Spinelli, P. (1987) "Artificial wind generation and structural response", Journal of Structural Engineering, ASCE, Vol.113, No.12, December, pp.2382-2398.

Inaudi, J.A., Nims, D.K., Kelly, J.M. (1993) "On the analysis of structures with energy dissipating restraints", Report No. UCB / EERC – 93 / 13, University of California at Berkeley.

Iwan, W.D. (1980) "Estimating inelastic response spectra from elastic spectra", Earthquake Engineering and Structure Dynamics, Vol.8, pp.375-388.

Iwan, W.D. and Gates, N.C. (1979) "Estimating earthquake response of simple hysteretic structures", Journal of the Engineering Mechanics Division, ASCE, Vol.105, No.EM3, June, pp.391-405.

Jacobsen, L.S. (1930) "Steady forced vibrations as influenced by damping", Trans. ASME, Vol. 51, p227.

Jacobsen, L.S. (1960) "Damping in composite structures", Proc. Second World Conference on Earthquake Engineering, Tokyo,Japan, pp.1029-1044.

Jennings, P.C. (1968) "Equivalent viscous damping for yielding structures" Journal of the Engineering Mechanics Division, ASCE, Vol.94, No.EM1, February, p103-115.

Johnson, C.D. and Kienholz, D.A. (1982) "Finite element prediction of damping in structures with constrained viscoelastic layers", AIAA Journal, American Institute of Aeronautics and Astronautics, Vol.20, No.9, pp.1284-1290.

Kaldjian, M.J. (1967) "Moment-curvature of beams as Ramberg-Osgood functions", Journal of the Structural Division, ASCE, Vol.93, No.ST5, Oct., pp.53-65.

Kanai, H. (1983) "Pressure fluctuations on square prisms – applicability of strip and quasi-steady theories", Journal of Wind Engineering and Industrial Aerodynamics, Vol.13, pp.197-208.

Kawashima, K. and Aizawa, K. (1986) "Modification of earthquake response spectra with respect to damping ratio", Proceedings of the Third U.S. National Conference on Earthquake Engineering, Charleston, South Carolina, Vol. II, pp.1107-1116.

Keel, C.J. and Mahmoodi, P. (1986) "Design of viscoelastic dampers for the Columbia Centre building", Building Motion in Wind, edited by Isyumov, N. and Tschanz, T., ASCE, New York.

Kelly, J.M., Skinner, R.I. and Heine, A.J. (1972) "Mechanisms of energy absorption in special devices for use in earthquake-resistant structures", Bulletin of the New Zealand National Society for Earthquake Engineering, Vol.5, No.3, Sept., pp.63-88.

Kowalsky, M.J., Priestley, M.J.N. and Macrae, G.A. (1995) "Displacement-based design of RC bridge columns in seismic regions", Earthquake Engineering and Structural Dynamics, Vol.24, pp.1623-1643.

Lai, S.-P. and Biggs, J.M. (1980) "Inelastic response spectra for seismic building design", Journal of the Structural Engineering Division, ASCE, Vol.106, No.ST6, pp.1295-1310.

Lawson, R.S., Vance, V. and Krawinkler, H. (1994) "Nonlinear static pushover analysis – Why, When and How? ", Proceedings of the 5th U.S. National Conference on Earthquake Engineering, Chicago, Earthquake Engineering Research Institute, Oakland, CA, Vol.1, pp.283-292.

Li, C. and Reinhorn, A.M. (1995) "Experimental and analytical investigation of seismic retrofit of structures with supplemental damping— friction devices", Technical Report NCEER-95-0009, National Centre for Earthquake Engineering Research, SUNY /Buffalo.

Lin, R.C., Liang, Z., Soong, T.T. and Zhang, R.H. (1988) "An experimental study of seismic structural response with added viscoelastic dampers", Technical Report NCEER-88-0018, National Centre for Earthquake Engineering Research, SUNY /Buffalo.

Lin, X., Moss, P.J. and Carr, A.J. (1998a) "Analysis and seismic design of building structures with supplemental lead dampers", Technical Conference for New Zealand National Society for Earthquake Engineering, Wairakei, Taupo, New Zealand, March, pp.167-174.

Lin, X., Moss, P.J. and Carr, A.J. (1998b) "Seismic analysis and design of building structures with supplemental lead dampers", Proceedings of Australasian Structural Engineering Conference, Auckland, New Zealand, 30 September- 2 October, Vol. 2, pp.735-742.

Lobo,R.F., Bracci,J.M., Shen,A.M., Reinhorn,A.M., and Soong,T.T. (1993) "Inelastic response of reinforced concrete structures with viscoelastic braces", Technical Report NCEER-93-0006, National Center for Earthquake Engineering Research, SUNY /Buffalo.

Mahmoodi, P. (1969) "Structural dampers", Journal of the Structural Division, ASCE, Vol.95, No.ST8, August, pp.1661-1672.

Mahmoodi, P. and Keel, C.J. (1986) "Performance of viscoelastic structural dampers for the Columbia Centre building", Building Motion in Wind, edited by Isyumov, N. and Tschanz, T., ASCE, New York.

Melbourne, W.H. and Palmer, T.R. (1992) "Acceleration and comfort criteria for buildings undergoing complex motions", Journal of Wind Engineering and Industrial Aerodynamics, Vol. 41-44, 1992, pp.105-116.

Miranda, E. (1993a) "Evaluation of site-dependent inelastic seismic design spectra", Journal of Structural Engineering, ASCE, Vol.119, No.5, May, pp.1319-1338.

Miranda, E. (1993b) "Site-dependent strength-reduction factors", Journal of Structural Engineering, ASCE, Vol.119, No.12, December, pp.3503-3519.

Miranda, E. (1994) "Evaluation of strength reduction factors for earthquake-resistant design", Earthquake Spectra, Vol.10, No.2, pp.357-379.

Miyazaki, M. and Mitsusaka, Y. (1992) "Design of a building with 20% or greater damping", Proc. of 10th World Conference on Earthquake Engineering, Madrid, Spain, July, pp.4143-4148.

Moehle, J.P. (1984) "Strong motion drift estimates for R/C structures", Journal of Structural Engineering, ASCE, Vol.110, No.9, pp.1988-2001.

Moehle, J.P. (1992) "Displacement-based design of RC structures subjected to earthquakes", Earthquake Spectra, EERI, Vol.3, No.3, pp.403-427.

Monti, M.D. and Robinson, W.H. (1996) "A lead shear damper suitable for reducing the motion induced by wind and earthquake", 11th World Conference on Earthquake Engineering, June 23-28, Acapulco, Mexico.

Monti, M.D., Ferguson, W.G. and Robinson, W.H. (1995) "Lead as a cyclic motion damper", Pacific Conference on Earthquake Engineering, Vol.3, pp.323-330.

Moss, P.J. and Carr, A.J. (1999) "Generation of design earthquake records", unpublished paper, Department of Civil Engineering, University of Canterbury, Christchurch, New Zealand.

Nassar, A.A., Osteraas, J.D. and Krawlinker, H. (1992) "Seismic design based on strength and ductility demands", Tenth World Conference on Earthquake Engineering, pp.5861-5866.

Newmark, N.M. and Hall, W.J. (1982) "Earthquake spectra and design", Earthquake Engineering Research Institute, Berkeley, California.

NZS4203 (1992) Code of Practice for General Structural and Design Loading for Building, NZS4203: 1992 and Commentary, Standard New Zealand, Wellington.

Otani, S. (1974) "SAKE, A computer program for inelastic response of R/C frames to earthquakes", Report UILU-Eng-74-2029, Civil Engineering Studies, University Of Illinois at Urbana-Champaign, November.

Otani, S. (1981) "Hysteresis models of reinforced concrete for earthquake response analysis", Journal of Faculty Of Engineering, University Of Tokyo, Tokyo, Vol. XXXVI, No.2, pp.125-159.

Pall, A.S. and Marsh, C. (1982) "Response of friction damped braced frames", Journal of the Structural Division, ASCE, Vol.108, No.ST6, June, pp.1313-1323.

Pall, A.S., Verganelakis, V. and Marsh, C. (1987) "Friction dampers for seismic control of Concordia University library building", 5th Canadian Conference on Earthquake Engineering, Ottawa, p191-200.

Park, R. (1992) "Capacity design of ductile RC building structures for earthquake resistance", The Structural Engineer, Vol.70, No.16, August, pp.279-289.

Pong,W.S., Tsai,C.S. and Lee,G.C. (1994) "Seismic study of building frames with added energy-absorbing devices", Technical Report NCEER-94-0016, National Center for Earthquake Engineering Research, SUNY/Buffalo

Priestley, M.J.N. (1995) "Displacement-based seismic assessment of existing reinforced concrete buildings", Pacific Conference on Earthquake Engineering, Australia, 20-22 Nov., Vol.2, pp.225-244.

Priestley, M.J.N. and Calvi, G.M. (1997) "Concepts and procedures for direct displacement-based design and assessment", Proceedings of the International Workshop on Seismic Design Methodologies for the Next Generation of Codes, edited by Fajfar, P. and Krawinkler, H., Bled, Slovenia, 24-27 June, pp.171-181.

Qi, X. and Moehle, J.P. (1991) "Displacement-based approach for reinforced concrete structures subject to earthquakes", Report No.UCB/EERC/91-02, Earthquake Engineering Research Centre, University of California at Berkely.

Rao R.S., Gergely P. and White R.N. (1995) "Retrofit of non-ductile reinforced concrete frames using friction dampers ", Technical Report NCEER-95-0020, National Center for Earthquake Engineering Research, SUNY, Buffalo.

Rea, D. and Clough, R.W. (1969) "Damping capacity of a model steel structure", Earthquake Engineering Research Center at Berkeley, PB-187 906, Jan. p45-61.

Reid, T.J. (1956) "Free vibration and hysteretic damping", Journal of the Royal Aeronautical Society, Vol.60, pp.283.

Reinhorn, A.M. (1997) "Inelastic analysis techniques in seismic evaluation", Proceedings of the International Workshop on Seismic Design Methodologies for the Next Generation of Codes, edited by Fajfar, P. and Krawinkler, H., Bled, Slovenia, 24-27 June, pp.277-287.

Reinhorn, A.M., Li, C. and Constantinou, M.C. (1995a) "Experimental and analytical investigation of seismic retrofit of structures with supplemental damping — fluid viscous damping devices", Technical Report NCEER-95-0001, National Center for Earthquake Engineering Research, SUNY/Buffalo.

Reinhorn,A.M. and Li,C. (1995b) "Experimental and analytical investigation of seismic retrofit of structures with supplemental damping— viscous damping walls", Technical Report NCEER-95-0013, National Center for Earthquake Engineering Research , SUNY/Buffalo.

Robinson, W.H. and Greenbank, L.R. (1976) "An extrusion energy absorber suitable for the protection of structures during an earthquake", Earthquake Engineering and Structure Dynamics, Vol.4, pp.251-259.

Saiidi, M. and Sozen, M.A. (1981) "Simple nonlinear seismic analysis of R/C structures", Journal of the Structural Engineering Division, ASCE, Vol.107, No.ST5, May, pp.937-951.

Satyarno, I., Carr, A.J. and Restrepo, J. (1998) "Refined pushover analysis for the assessment of older reinforced concrete buildings", Technical Conference for New Zealand National Society for Earthquake Engineering, Wairakei, Taupo, New Zealand, March, pp.75-82.

Saul, W.E., Jayachandran, P. and Peyrot, A.H. (1976) "Response to stochastic wind of N-degree tall buildings", Journal of the Structural Division, ASCE, Vol.102, No.ST5, May, pp.1059-1075.

Scholl, R.E. (1990) "Improve the earthquake performance of structures with added damping and stiffness elements", Proc. of Fourth U.S. National Conference on Earthquake Engineering, May 20-24, Palm Springs, California, Vol.3, pp.489-498.

Scholl, R.E. (1993a) "Design criteria for yielding and friction energy dissipations", Proc. of Seminar on Seismic Isolation, Passive Energy Dissipation, and Active Control, Applied Technology Council Report, No. ATC-17-1, Redwood City, CA., pp.485-495.

Scholl, R.E. (1993b) "Fundamental design issues for supplemental damping application", Earthquake Spectra, Vol.9, No.3, pp.627-636.

Seleemah, A.A. (1997) Technical Report NCEER-97-0004, National Center for Earthquake Engineering Research, SUNY/Buffalo.

Sharpe, R.D. (1974) "The seismic response of inelastic structures", Ph.D Thesis, Department of Civil Engineering, University Of Canterbury, November.

Shibata, A. and Sozen, M. (1976) "Substitute-structure method for seismic design in R/C", Journal of the Structural Engineering Division, ASCE, Vol.102, No.ST1, January, pp.1-18.

Simiu, E. (1975), "Equivalent static wind loads for tall building design", Proc. of the Fourth International Conference on Wind Effects on Buildings.

Simiu, E. and Scanlan, R.H. (1986) Wind Effects on Structures – An Introduction to Wind Engineering, 2nd Edition, John Wiley & Sons.

Skinner, R.I., Kelly, J.M. and Heine, A.J. (1975) "Hysteretic dampers for earthquake-resistant structures", Earthquake Engineering and Structural Dynamics, Vol.3, pp.287-296.

Skinner, R.I., Robinson, W.H. and McVerry, G.H. (1993) An Introduction to Seismic Isolation, John Wiley & Sons Ltd, West Sussex, England.

Sladek, J.R. and Klingner, R.E. (1980) "Using tuned-mass dampers to reduce seismic response", Seventh World Conference on Earthquake Engineering, Turkey, Vol.7, pp.265-271.

Solari, G. (1988), "Equivalent wind spectrum technique: theory and applications", Journal of Structural Engineering, ASCE, Vol.114, No.6, June.

Soong, T.T. and Dargush, G.F. (1997) Passive Energy Dissipation Systems in Structural Engineering, John Wiley & Sons.

Sozen, M.A. (1981) "Review of earthquake response of RC buildings with a view to drift control", State-of-the-Art in Earthquake Engineering – 1981, edited by Ergunay, O. and Erdik, M., Ankara, October, pp.383-418.

Su, Y.F. and Hanson, R.D. (1990) "Comparison of effective supplemental damping: equivalent viscous and hysteretic", Proc. of the Fourth U.S. National Conference on Earthquake Engineering, May 20-24, 1990, Palm Springs, California, Vol.3, p507-516.

Tabuchi, M. (1992) "Design of 12-storey ductile frame model", part of PhD Project, Department of Civil Engineering, University of Canterbury, Christchurch, New Zealand.

Tallin, A. and Ellingwood, B. (1984) "Serviceability limit states: wind induced vibrations", Journal of Structural Engineering, ASCE, Vol.110, No.10, October, pp.2424-2437.

Torkamani, M.A.M. and Murad, R.S. (1994) "A probabilistic approach to the response of tall buildings to wind loadings", Structural Congress XII, pp.1439-1444.

Torkamani, M.A.M. and Pramono, E. (1985) "Dynamic response of tall building to wind excitation", Journal of Structural Engineering, ASCE, Vol.111, No.4, April, pp.805-825.

Tsai, K.C., Chen, H.W., Hong, C.P. and Su, Y.F. (1993) "Design of steel triangular plate energy absorbers for seismic-resistant construction", Earthquake Spectra, Vol.9, No.3, pp.505-528.

Tsukagoshi, H., Tamura, Y., Sasaki, A. and Kanai, H. (1993) "Response analyses on along-wind and cross-wind vibrations of tall buildings in time domain", Journal of Wind Engineering and Industrial Aerodynamics, Vol. 46 - 47, pp.497-506.

Turkington, D.H., Carr, A.J., Cook, N. and Moss, P.J. (1989) "Seismic design of bridges on lead-rubber bearings", Journal of Structural Engineering, Vol.115, No.12, December, pp.3000-3016.

Tyler, R.G. (1978) "Tapered steel energy dissipators for earthquake resistance structure", Bulletin of the New Zealand National Society for Earthquake Engineering, Vol.11, No.4, pp.282-294.

Tyler, R.G. (1985) "Further notes on steel energy-absorbing element for braced frameworks", Bulletin of the New Zealand National Society for Earthquake Engineering, Vol.18, No.3, pp.270-279.

Vaicaitis, R., Shinozuka, M. and Takeno, M. (1975) "Response analysis of tall buildings to wind loading", Journal of the Structural Division, ASCE, Vol.101, No.ST3, March, pp.585-600.

Vickery, B.J. and Kao, K.H. (1972) "Drag or along-wind response of slender structures", Journal of the Structural Division, ASCE, Vol.98, No.ST1, January, pp.21-35.

Vickery, B.J., Isyumov, N. and Davenport, A.G. (1983) "The role of damping, mass and stiffness in the reduction of wind effects on structures", Journal of Wind Engineering and Industrial Aerodynamics, Vol.11, pp285-294.

Whittaker, A., Bertero, V., Alonso, J. and Thompson, C. (1989) "Earthquake simulator testing of steel plate added damping and stiffness elements", Report No. UCB / EERC – 89 / 02, University of California at Berkeley.

Witting, P.R. and Cozzarelli, F.A. (1992) "Shape memory structural dampers: material properties, design and seismic testing", Technical Report NCEER-92-0013, National Centre for Earthquake Engineering Research, SUNY/Buffalo.

Wu, J. and Hanson, R.D. (1989) "Study of inelastic spectra with high damping", Journal of Structural Engineering, ASCE, Vol.115, No.6, June 1989, pp.1412-1431.

Xia, C. and Hanson, R.D. (1992) "Influence of ADAS element parameters on building seismic response", Journal of Structural Engineering, ASCE, Vol.118, No.7, July, p1903-1917.

Zhang, R-H, and Soong, T.T. (1989) "Seismic response of steel frame structures with added viscoelastic dampers", Earthquake Engineering and Structural Dynamics, Vol.18, pp.389-396.

**ADDITIONAL READING:**

Pekcan, G., Mander, J.B., and Chen, S.S. (1995) "The seismic response of a 1: 3 scale model R.C. structure with elastomeric spring dampers", Earthquake Spectra, Vol. 11, No.2, May, 1995, pp.249-267.

Pekcan, G., Mander, J.B., and Chen, S.S. (1995) "Experimental performance and analytical study of a non-ductile reinforced concrete frame structure retrofitted with elastomeric spring dampers", Technical Report NCEER-95-0010, National Centre for Earthquake Engineering Research, SUNY/Buffalo.

Gluck, N., Reinhorn, A.M., Gluck, J. and Levy, R. (1996) "Design of supplemental dampers for control of structures", Journal of Structural Engineering, ASCE, Vol.122, No.12, Dec. 1996, pp.1394-1399.

Lobo, R.F., Bracci,J.M., Shen, K., Reinhorn, A.M., and Soong,T.T. (1993) "Inelastic response of R/C structures with viscoelastic braces", Earthquake Spectra, Vol. 9, No.3, August, 1993, pp.419-446.

FEMA 273, "NEHRP guidelines for the seismic rehabilitation of buildings", Federal Management Emergency Agency, Washington D.C.

ATC40 (1996) "Seismic evaluation and retrofit of concrete buildings", Report SSC96-01, Seismic Safety Commission, State of California.

Proceedings of Structural Engineering Association of California (SEAOC) Annual Convention, Maui, October 1-3, 1996.

# APPENDIX

A 12-storey 3-bay two-way frame structure was designed by a former PhD student M. Tabuchi in 1992 to the New Zealand Loading Code, NZS4203. The frame configuration is illustrated in Fig.A-1. The important information concerning this frame for time-history analysis is summarised as follows. All details in the frame design can be obtained from the reference (Tabuchi, 1992).

| | | | |
|---|---|---|---|
| Fundamental period | = | 1.99 | seconds |
| Seismic coefficient $C_d$ | = | 0.048 | |
| Total frame weight | = | 11864.4 | KN |
| Modulus of elasticity, E | = | 25.0 | Gpa |
| Shear modulus, G | = | 10.4 | Gpa |
| Concrete compressive strength $f_c'$ | = | 30 | Mpa |
| Beam hysteresis | = the modified TAKEDA, no axial load-moment Interaction | | |
| The 1st level column hysteresis | = the degrading Bi-linear | | |
| Other column hysteresis | = Linear elastic | | |

Sign Convention

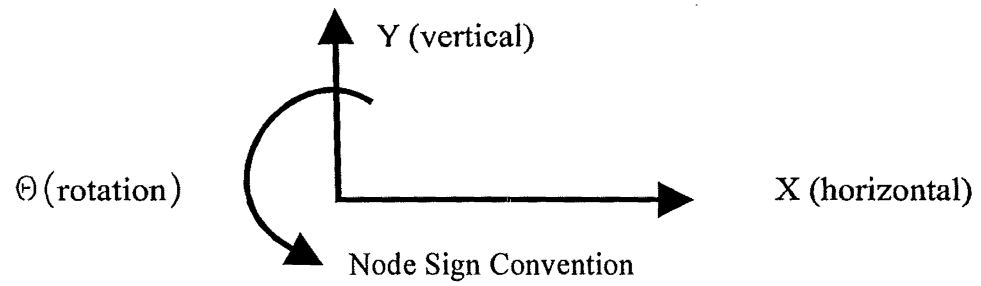


Node Sign Convention

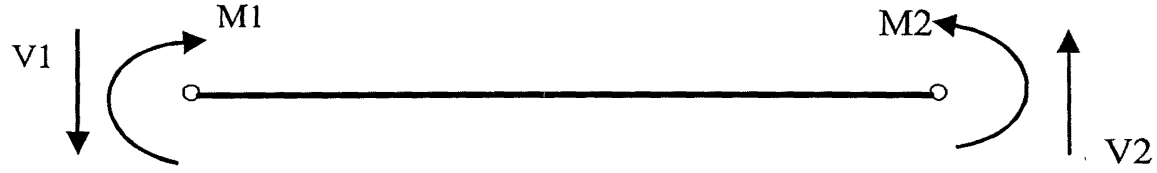


Beam Member Sign Convention

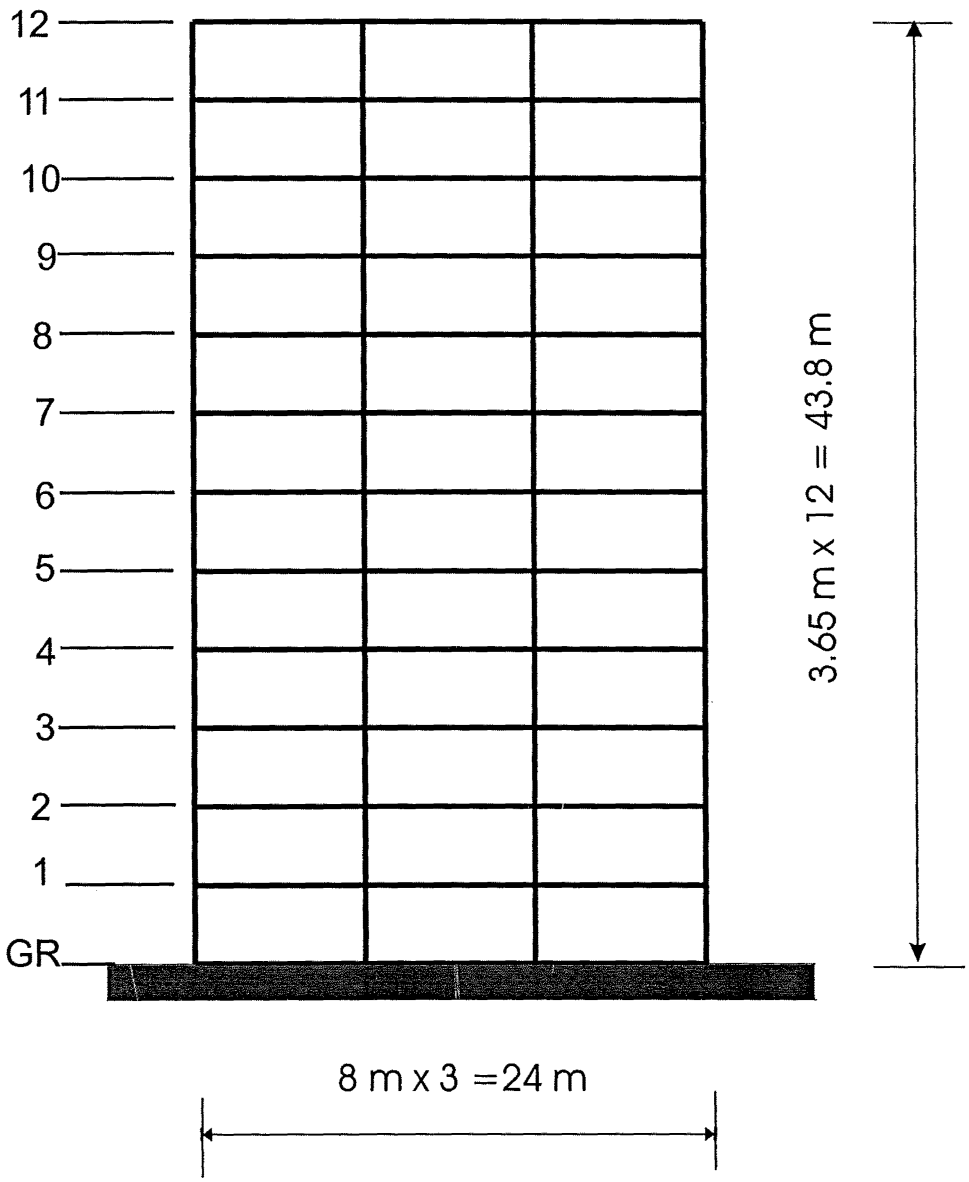


Figure A-1. A 12-storey 3-bay reinforced concrete frame structure

Member Dimensions

| Level | Beam (mm) | Column (mm) |
|---|---|---|
| 9-12 | 350 × 700 | 600 × 600 |
| 5-8 | 350 × 750 | 650 × 650 |
| 1-4 | 350 × 800 | 700 × 700 |

Member Properties

| Member | Levels | Axial area ($m^2$) | Shear area ($m^2$) | Moment of inertia ($\times 10^{-3} m^4$) | Plastic hinge length (m) |
|---|---|---|---|---|---|
| Beams | 1-4 | 0.28 | 0.14 | 8 | 0.56 |
| | 5-8 | 0.2626 | 0.1312 | 6.64 | 0.525 |
| | 9-12 | 0.245 | 0.1226 | 5.4 | 0.49 |
| External Columns | 1-4 | 0.49 | 0.245 | 12.02 | 0.49 (level 1) |
| | 5-8 | 0.4226 | 0.211 | 8.92 | — |
| | 9-12 | 0.36 | 0.18 | 6.48 | — |
| Internal columns | 1-4 | 0.49 | 0.245 | 16.02 | 0.49 (level 1) |
| | 5-8 | 0.4226 | 0.211 | 11.9 | — |
| | 9-12 | 0.36 | 0.18 | 8.64 | — |

| Member | Levels | Length of rigid end-block (m) | |
|---|---|---|---|
| | | End1 | End2 |
| Beams | 1-4 | 0.35 | 0.35 |
| | 5-8 | 0.325 | 0.325 |
| | 9-12 | 0.3 | 0.3 |
| External Columns | 1-4 | 0.4 | 0.4 |
| | 5 | 0.4 | 0.375 |
| | 6-8 | 0.375 | 0.375 |
| | 9 | 0.375 | 0.35 |
| | 10-12 | 0.35 | 0.35 |
| Internal columns | 1-4 | 0.4 | 0.4 |
| | 5 | 0.4 | 0.375 |
| | 6-8 | 0.375 | 0.375 |
| | 9 | 0.375 | 0.35 |
| | 10-12 | 0.35 | 0.35 |

Beam Initial Fixed End Moments and Shears

| Beam initial fixed end forces | | | | |
|---|---|---|---|---|
| Levels | Moment (KN-m) End 1 | Moment (KN-m) End 2 | Shear (KN) End 1 | Shear (KN) End 1 |
| 1-4 | -193 | -193 | -117 | 117 |
| 5-8 | -190.8 | -190.8 | -115.4 | 115.4 |
| 9-12 | -188.6 | -188.6 | -113.7 | 113.7 |

Beam Yield Data

| Beam yield moments (KN-m) | | | | |
|---|---|---|---|---|
| Levels | End 1 positive | End 1 negative | End 2 positive | End 2 negative |
| 1 | 263 | -439 | 263 | -439 |
| 2-3 | 321 | -493 | 321 | -493 |
| 4 | 263 | -493 | 263 | -493 |
| 5 | 244 | -457 | 244 | -457 |
| 6 | 244 | -407 | 244 | -407 |
| 7 | 231 | -357 | 231 | -357 |
| 8 | 231 | -314 | 231 | -314 |
| 9-12 | 186 | -290 | 186 | -290 |

Nodal Loads and Weights

| Levels | Nodal weights (KN) | | Nodal loads (KN) | |
|---|---|---|---|---|
| | External node | Internal node | External node | Internal node |
| 1 | 203.6 | 407.3 | -111.7 | -223.4 |
| 2 | 203.6 | 407.3 | -111.7 | -223.4 |
| 3 | 203.6 | 407.3 | -111.7 | -223.4 |
| 4 | 203.6 | 407.3 | -111.7 | -223.4 |
| 5 | 198 | 396 | -107 | -214 |
| 6 | 198 | 396 | -107 | -214 |
| 7 | 198 | 396 | -107 | -214 |
| 8 | 198 | 396 | -107 | -214 |
| 9 | 192.7 | 385.4 | -102.7 | -205.5 |
| 10 | 192.7 | 385.4 | -102.7 | -205.5 |
| 11 | 192.7 | 385.4 | -102.7 | -205.5 |
| 12 | 178.1 | 356.2 | -86.3 | -172.7 |

Note : Based on Dead Load + 1/3 * Live Load.